

Ph.D. Thesis.

UNIVERSITY OF CAPE TOWN.

A COMPACT SHORT-WAVE RECEIVING ANTENNA  
FOR USE IN HIGH-NOISE AREAS.

by

L.M. Muggleton.

The copyright of this thesis vests in the author. No quotation from it or information derived from it is to be published without full acknowledgement of the source. The thesis is to be used for private study or non-commercial research purposes only.

Published by the University of Cape Town (UCT) in terms of the non-exclusive license granted to UCT by the author.

## C O N T E N T S.

List of diagrams and photographs.	F 1. to F 2.
Summary.	
Chapter 1 : Introduction to the problem and the proposed approach.	1.1.
Chapter 2 : The incoming signal from London at noon, September 1956, on 21.47 Mc/s.	2.1. to 2.10.
Chapter 3 : The minimum antenna gain necessary.	3.1. to 3.3.
Chapter 4 : Noise in short-wave circuits in tropical countries.	4.1. to 4.16.
Chapter 5 : Disadvantages of the Rhombic Receiving Antenna.	5.1. to 5.2.
Chapter 6 : The search for an improved design.	6.0. to 6.18.
Chapter 7 : The parasitic Antenna.	7.0. to 7.14.
Chapter 8 : The V.H.F. Scale Model.	8.0. to 8.22.
Chapter 9 : The 4-director test array at 21.47 Mc/s.	9.0. to 9.12.
Chapter 10 : The 6-director design.	10.0. to 10.29.
Chapter 11 : Indication of applicability.	11.1. to 11.6.
Acknowledgements.	
Bibliography.	1.to 8.
Appendix A : Antenna Theory.	A.0 to A.24.
Appendix B : The incoming signal : London - Salisbury	B.1 to B 50.
Appendix C : Results of scale model tests.	C.1. to C.6.
Appendix D : Results of tests at 21.47 Mc/s.	D.1. to D.2.
Appendix E : Frequency run on two, 6-director arrays.	E.1.

---

LIST OF DIAGRAMS AND PHOTOGRAPHS.

<u>Number</u>	<u>Subject</u>	<u>Page</u>
F 4.4.1.1.	Calculated noise field strength variation with $\Delta$ .	4.9.
F 4.4.1.2.	Noise Map, C.C.I.R. Noise predictions.	4.10.
F 4.4.3.1.	Power density diagram, Rhombic Antenna.	4.13.
F 4.4.3.2.	Power density diagram, Koomans H/4/4/1 Array.	4.14.
F 4.4.3.3.	Comparison curves, antenna signal-to-noise performance.	4.15.
F 6.3.3.1./2.	Polar diagrams, vertical monopole on perfect grnd.	6.4.
F 6.3.4.0.1.	Polar diagrams, $\lambda/2$ dipole grnd. of finite $\sigma$ .	6.7.
F 6.3.4.1.3.	Derived vertical polar diagrams at 21.47 Mc/s for various types of ground plane.	6.18.
F 7.1.1.	$Z_{12}$ and $\phi$ for $\lambda/2$ radiators in terms of spacing.	7.2.
F 7.1.2.	Reactance of parasitic radiators.	7.4.
F 7.2.1.	Yagi antenna, transmission line analogy.	7.5.
F 7.2.2.-4.	Spector's curves, phase vel., Q factor, beam width.	7.7.
F 7.3.2./1.	Reid's optimum "a" value for Yagi antennas.	7.11.
F 8.2.1.	Circuit diagram, V.H.F. transmitter.	8.2.
F 8.3.0.1.	Model antenna, micrometer screw adjustment of rod.	8.4.
F 8.3.0.2.	Model antenna, matching arrangements.	8.5.
F 8.3.1.1.	Shelkunoff's curves for $X_1$ and $R_1$ for cyl. dipole.	8.6.
F 8.3.3.1.	Model antenna, receiving loop.	8.8.
F 8.3.3.2.	Model antenna, control cabin.	8.9.
F 8.3.3.3.	Model antenna, method of measuring polar diagram.	8.10.
F 8.3.3.4.	Model antenna, calib. curve for VHF signal detect.	8.12.
F 8.3.5.1.1.	Polar diagrams, measured and expected, $\lambda/4$ monopole.	8.16.
F 8.3.5.2.1.	Array designs for one to six directors.	8.18.
F 8.3.5.3.1.1.	Measured and derived polar diagrams for 4-director and 6-director arrays.	8.21.
F 9.2.1.	Full-scale design, antenna matching unit.	9.2.
F 9.2.2.	Ditto.	9.3.
F 9.4.1.	Test transmitter for 21.47Mc/s experiments.	9.5.
F 9.4.2.	Measurement of vert. polar diag. at 21.47 Mc/s.	9.6.
F 9.5.1.	Calibration curve, Eddystone Receiver.	9.7.
F 9.6.1.	The 4-director Test array.	9.8.
F 9.6.2.	Polar diagram ( vertical plane) for Test array.	9.9.
F 9.6.3.	Polar diagram ( horizontal plane) for Test array.	9.10.
F 6.3.4.1.3.	Derived polar diagrams at 21.47 Mc/s.	10.4(a)
F 8.3.5.3.1.1.	Measured and derived polar diag.s for 4-director and 6-director arrays. (Repeated for convenience).	10.4(b)
F 10.2.1.1.	6-director array, derived polar diag.s for various ground planes.	10.5.
F 10.3.2.1.	Antenna performance curves, 6-dir. vs Rhombic and Koomans signal-to-noise performance.	10.12.
F 10.3.3.1.	Calibration curve, CR 88 Receiver.	10.14.
F 10.3.4.1.	R.F. Input vs. A.F. Output for large range of sig.	10.17.
F 10.4.0.1.	The double 6-director design ( photograph).	10.18.
F 10.4.1.1.	The phasing of the double 6-director antenna.	10.20.
F 10.5.1.1.1.	Practical details of parasitic elements.	10.24.
F 10.5.1.1.2.	Base of parasitic element.	10.25.
F 10.5.1.1.3.	Dismantled view of element.	10.26.
F 10.5.1.2.1.	Base design of driven element.	10.27.
F 10.5.1.2.2.	The driven element ( photograph).	10.28.
F 11.4.1.	Amplitude distribution for fading S.W. signals.	11.3.
F 11.5.1.1.	Power density diagram, 6-director design.	11.6.
A 7.0.1.	Mechanism of reflection at a discontinuity.	A.5.
A 8.1.	Field components of a doublet.	A.10.
A 10.1.1.	Element of area on a spherical surface.	A.13.
A 11.1.1.	Radiation from a $\lambda/2$ dipole.	A.14.
A 11.3.0.1.	Image antennas.	A.16.
A 11.4.0.1.	The phasing of two antennas.	A.17.
A 11.4.0.2./3.	Height factors for negative and positive images.	A.18.
A 12.0.1.	Straight wire carrying travelling wave.	A.19.
A 12.1.1.	Elements of the Rhombic Antenna.	A.20.
A 12.1.2.	Radiation from Rhombic Antenna.	A.21.



<u>Number</u>	<u>Subject</u>	<u>Page</u>
B 4.0.1.	Estimated variation of N,v, and Nv, Sept. 1956	B.7.
B 5.1.2.	Curves relating $\Delta$ , hop length, and layer height	B.12.
B 5.3.1.	Illustration of great-circle bearing.	B.14.
B 5.4.1.	Power density diagram, Kocmans H 4/4/1 array.	B.16.
B 5.4.2.	Power density diagram. Kocmans H 2/4/1 array.	B.17.
B 6.2.1.1.	Illustration of virtual height of reflection.	B.21.
B 6.2.5.1.	Illustration used in development of Breit and Tuve's theorem.	B.29.
B 6.2.9.1.	Piggott's curves relating dip and declination as a function of position in equatorial zone.	B.34.
B 6.2.9.2.	Piggott's curves relating $\Delta$ and distance, and unabsorbed field strength and distance.	B.35.
B 6.2.9.3.	Absorption factor "K".	B.36.
B 6.2.9.4/5	Piggott's nomograms for absorption loss.	B.37.
B 6.2.9.6.	Curves by Hacke and Kelso, absorption in a deviating medium.	B.41.

---

## A COMPACT SHORT-WAVE RECEIVING ANTENNA FOR USE IN HIGH-NOISE AREAS.

### SUMMARY

An antenna has been developed with a signal-to-noise performance that is better than that of a typical Rhombic antenna during local thunder storms. Although the design is of general application to the reception, in high-noise areas, of long distance transmissions, this work deals in particular with the London-Salisbury circuit, at September noon, 1956, on 21.47 Mc/s.

A basis of theoretical comparison between the performances of different antennas has been proposed. It relies on the technique of replacing a thunder storm by an "equivalent radio transmitter" set up on the frequency to which the receiver is tuned and for which the antenna is designed.

A V.H.F. scale model has been used to produce an optimum design for the proposed antenna which is an end-fire array of parasitic elements. The polar diagrams and signal-to-noise performance of the proposed design are derived for several different types of earth mat. The method used for these derivations is substantiated by correlation with practical sampling measurements.

A specification for the final configuration is given and its applicability is indicated by applying the design to the problem of improving the expected performance on the London-Salisbury transmissions from September to December, 1960.

Appendices A to E deal with the following :-

- Appendix A Antenna Theory, which includes the derivation of gain and polar equations for the  $\lambda/2$  dipole,  $\lambda/4$  monopole, the Rhombic antenna, and the mechanism of reflections.
  - Appendix B The Incoming Signal, which includes a summary of modern propagation theory, and details the calculations made in respect of the field strength and wave arrival angle of the incoming signal.
  - Appendix C The results of Scale Model tests.
  - Appendix D The results of tests at 21.47 Mc/s.
  - Appendix E A frequency run on an array of two, six-director designs.
-

CHAPTER I.

INTRODUCTION TO THE PROBLEM AND THE PROPOSED APPROACH.

At Hatcliffe receiving station, Salisbury, S. Rhodesia, it has been the practice to use Rhombic Antennas, with open-wire feeders, for the reception of B.B.C. sound transmissions to Central Africa. During those portions of the year when tropical thunder storms are prevalent the signal-to-noise ratio of the Rhombic antennas was observed to be poor. In an attempt to improve this, work was commenced in 1955 on the production of an antenna consisting of an end-fire arrangement of parasitic elements. In 1956 a suitable day frequency was 21.47 Mc/s and this has been taken as the design frequency for the purpose of the investigation.

The approach to the problem in this presentation will be as follows:

- (a) The London to Salisbury propagation path mechanism will be studied and an estimate made concerning wave arrival angle, signal strength, and probable variations. Even if considerable care is exercised when making the calculations, and modern methods used, it cannot be expected that the result will do more than to indicate the correct order of magnitude but this is sufficient for the present purpose.
- (b) The causes of noise interference will be investigated and a method sought of expressing the variation of noise field strength with wave arrival angle. This information is needed so as to compare the calculated signal-to-noise performance of one antenna with that of another if the antenna polar diagrams are known.
- (c) Using Yagi theory an antenna will be proposed which uses parasitic elements but is not a Yagi antenna. The optimum element lengths and spacings will be obtained experimentally by means of a scale model.
- (d) In a vertically polarized arrangement such as that proposed the reflecting ground plane is of major importance. The effect of the heavy clay soil at Hatcliffe, and of a wire grating laid on that soil, on the polar diagram of a vertical grounded  $\lambda/4$  monopole, will be investigated theoretically and used to derive the expected polar diagram of the full scale antenna.
- (e) The calculated performance of the proposed antenna will be verified by making sampling measurements in connection with the full-scale antenna.

- - - - -

## CHAPTER 2.

THE INCOMING SIGNAL FROM LONDON AT NOON, SEPTEMBER, 1956, on 21.47 Mc/s.

2.1.0 General: Before attempting to improve the design of a receiving antenna system it is necessary to have information concerning wave arrival angle, median field strength, and probable variations.

Signal strength measurements on long distance circuits are so variable that it has been decided to obtain the median signal strength and wave arrival angle from theoretical considerations.

From Radio Propagations Predictions<sup>(99)</sup>, for the epoch being considered, 21.47 Mc/s is slightly below the noon optimum frequency thereby providing a traffic channel for a useful portion of the day.

It has been considered necessary to deal with the propagation mechanism, calculations of path attenuation, and ionospheric perturbations in greater detail than space will permit in the main text. Therefore the fuller treatment is given in Appendix B and in this present Chapter the subject is dealt with only briefly in the knowledge that Appendix B is available should more detail be required regarding any particular aspect of the treatment. As a cross reference the relevant sections of Appendix B are quoted in each section heading in this Chapter.

### 2.2.0 WAVE ARRIVAL ANGLE AND ITS RELATION TO DISTANCE OVER A CURVED EARTH. (B.5.1)

Suppose two points A and B on the earth's surface are L km. apart, that the earth's radius is r km., the virtual height of reflection is h km., the wave arrival angle is  $\Delta^\circ$ , and the angle of incidence at height h is  $i^\circ$ . Then by triangulation it can be shown that: (See Appendix B section 5.1)

$$L = \frac{\pi r}{90} (90 - \Delta - i) \quad (2.2.0.1)$$

$$\cos \Delta = (1 + h/r) \sin i \quad (2.2.0.2)$$

For frequencies near the optimum frequency the value of h is often taken as 350 km.<sup>(102)</sup> The value of r is about 6730 km. Substitution in equations 2.2.0.1 and 2.2.0.2 of these values, and the value of L for a given circuit, yields the value of  $\Delta$ .

### 2.3.0 THE MAXIMUM DISTANCE FOR A SINGLE HOP. (B. 5.2)

For  $\Delta = 0$  the corresponding value of L, for h = 400 km., is 4400 km. For h = 200 km. the value of L is 3100 km.

In practice ground absorption for values of  $\Delta$  less than  $5^\circ$  is prohibitive. Allcock<sup>(38)</sup> has shown that, over a transequatorial path, the practical limit of a single hop is 3560 km. Observations by Shearman<sup>(39)</sup> and Allan<sup>(40)</sup> support this view.

2.4.0 GREAT CIRCLE DISTANCE AND BEARING OF LONDON TO SALISBURY. (B. 5.3).

The great circle distance is obtained from the relationship: <sup>(12,16)</sup>

$$\cos D_{AB} = \sin L_A \sin L_B + \cos L_A \cos L_B \cos LO_{AB} \quad (2.4.0.1).$$

where  $D_{AB}$  = great circle distance in degrees and minutes between points A and B ( 1 minute = 1.853 km.).

$L_A, L_B$  = latitude of station A,B, (positive for N and negative for S latitude).

$LO_{AB}$  = difference in longitude between A and B.

The great circle bearing of B from A is obtained from the relationship:

$$\sin B_{AB} = \cos L_B \operatorname{cosec} D_{AB} \sin LO_{AB} \quad (2.4.0.2).$$

where  $B_{AB}$  = the bearing of B from A.

As a high degree of accuracy is not necessary the latitude and longitude of the two terminals may be taken as:

London  $52^\circ$  N.,  $0^\circ$ .

Salisbury  $18^\circ$  S.,  $31^\circ$  E.

Substitution in equations 2.4.0.1 and 2.4.0.2 yields:-

Distance Salisbury-London =  $75^\circ = 8300$  km.

Bearing London from Salisbury =  $19^\circ$  W. of N.

2.5.0 THE NUMBER OF HOPS LONDON TO SALISBURY AND CALCULATED WAVE ARRIVAL ANGLE. (B. 5.4).

One hop of 8300 km. or two hops of 4150 km. are impracticable for the reasons given in section 2.3.0.

Three hops of about 2770 km. via the F layer will represent the dominant mode of propagation.

Substitution in equations 2.2.0.1 and 2.2.0.2 yields the value of  $\Delta$  as  $8^\circ$  to the nearest degree.

For frequencies near the optimum it is not expected that h will vary beyond the limits of 400 km. and 300 km. i.e. it is not expected that  $\Delta$  will vary by more than  $2^\circ$  from that calculated above.

Thus: Dominant mode London/Salisbury = 3 hops F.

Wave arrival angle  $\Delta = 8 \pm 2$  degrees.

2.6.0 THE HEIGHT OF THE TRAJECTORY. ( B. 6.2.2).

Neglecting collisions and the effect of the earth's curvature and magnetic field, Baker and Rice <sup>(37)</sup> have shown that the refractive index  $n$  of an ionized layer is given by (See B. 5.0.):-

$$n^2 = 1 - 81 N/f^2 \quad (2.6.0.1).$$

where  $n$  = refractive index at level of density  $N$ .

$N$  = electrons/ $\text{cm}^3$ .

$f$  = wave frequency in kilocycles/sec.

From Snell's Law <sup>(4)</sup>, a wave entering a horizontally stratified medium at angle of incidence  $i^\circ$  will reach the top of its trajectory at point  $x$  when the following condition is satisfied:-

$$n_x = \sin i = \left( 1 - 81 N_x / f^2 \right)^{\frac{-2.3-}{2}} \quad (2.6.0.2).$$

where  $n_x$  = refractive index at point  $x$ .

$N$  = electrons/cm<sup>3</sup> at point  $x$ .

For vertical incidence  $\sin i = 0$  and, from equation 2.6.0.2.

$$f_c^2 = 81 N_{\max} \quad (2.6.0.3).$$

Also from eqn. 2.6.0.2:-

$$1 - \sin^2 i = 81 N_{\max} / f_{ci}^2 = \cos^2 i. \quad (2.6.0.4).$$

where  $N_{\max}$  = max. electron density of the layer.

$f_c$  = critical frequency (vertical incidence) in kc/s.

$f_{ci}$  = oblique incidence critical frequency in kc/s.

Combining 2.6.0.3 and 2.6.0.4:

$$f_{ci} = f_c \sec i. \quad (2.6.0.5)$$

But when the wave arrival angle  $\Delta$  is small the earth cannot be assumed flat and Millington<sup>(97)</sup> has shown that Snell's Law should be written thus (See B. 6.2.2):-

$$n_x (r + h_x) \sin \theta_x = (r + h) \sin i = r \cos \Delta. \quad (2.6.0.6).$$

where  $r$  = earth's radius = 6370 km.

$h_x$  = height of point  $x$ .

$h$  = height of the underboundary of the medium.

$\theta_x$  = angle between wave and the vertical at point  $x$ .

The top of the trajectory is now no longer given by  $n_x = \sin i$  but depends somewhat upon the way  $n$  (and hence  $N$ ) varies with height and, among other things, will vary with the time of day. The value of  $n_x$  at the point where the wave direction becomes horizontal, instead of defining the height of the trajectory, is itself a function of that height:

$$n_x = \frac{r+h}{r+h_x} \sin i. \text{ (from eqn. 2.6.0.6).}$$

Further, the value  $h$  and corresponding value of  $i$  are not easy to decide upon. Probably one of the best practical solutions is to assume a flat earth and to obtain  $i$  by substituting the values of  $f_c$  and  $f_{ci}$  from frequency prediction curves in equation 2.6.0.5. In this case  $f_{ci}$  will be in respect of 2770 km.

Substituting now for  $i$  in equation 2.6.0.2 should lead to a result which has taken into account some of the errors at least.

The noon values of  $0.85 f_{ci}$  and  $0.85 f_i$  (i.e. of the optimum frequencies) for 2770 km and 0 km respectively in September 1956 at the equator, are obtained from Radio Propagation Predictions<sup>(99)</sup> as 11.3 Mc/s and 29.0 Mc/s respectively. Thus  $i$  is calculated (equation 2.6.0.5) to be 67°.

Substitution in equation 2.6.0.2 yields:

$$N_x, \text{ at the top of the trajectory, } = 8.7 \times 10^5 \text{ electrons/cm}^3.$$

To proceed further it is necessary to know the approximate variation of  $N$  with height. From rocket soundings quoted by Friedman<sup>(79)</sup> and critical frequency soundings taken by Thomas<sup>(82)</sup> and, after incorporating certain adjustments suggested by Piggott resulting from an exchange of correspondence with him<sup>(177)</sup>, the ionospheric model of Table T. 2.6.0.1 has been formulated for September 1956, which is about midway between a sunspot maximum and a sunspot minimum. For other times of day and/or other seasons, and/or other latitudes in the same sunspot epoch, find the solar zenith angle  $X$ : then  $N$  is approximately proportional to  $(\cos X)^{\frac{1}{2}}$  in the  $F_1$  region and  $(\cos X)$  in the  $F_2$  region. The variation of  $N_{\max}$  for other sunspot epochs may be derived from the fact that  $N_{\max}$  is proportional to  $(f_c)^2$

height km.	$N$ electrons/cm <sup>3</sup>	$v$ collision/sec.
70	0	-
75	$3 \times 10^3$	$7 \times 10^6$
80	$10^4$	$3 \times 10^6$
85	$2 \times 10^4$	$10^6$
90	$2 \times 10^4$	$6 \times 10^5$
95	$3 \times 10^4$	$3 \times 10^5$
100	$10^5$	$10^5$
110	$2.5 \times 10^5$	$3 \times 10^4$
120	$2.5 \times 10^5$	$5 \times 10^3$
150	$4 \times 10^5$	$1.5 \times 10^3$
180	$5 \times 10^5$	$10^3$
230	$6 \times 10^5$	$6 \times 10^2$
250	$8 \times 10^5$	$5 \times 10^2$
300	$14 \times 10^5$	$3 \times 10^2$
350	$20 \times 10^5$	$1.5 \times 10^2$
400	$21 \times 10^5$	$10^2$

TABLE T. 2. 6.0.1.

The collision frequency between an electron and ions,  $v_{ei}$ , and between an electron and neutral particles,  $v_{en}$ , may be calculated from the following formulae due to Chapman<sup>(89)</sup>:-

$$v_{ei} = (34 + 4.18 \log_{10} T^{\frac{3}{N}}) N T^{\frac{3}{2}} \quad (2.6.0.7).$$

$$v_{en} = 5.4 + 10^{10} N_n T^{\frac{1}{2}} \quad (2.6.0.8).$$

where  $N_n$  = neutral particles/cm<sup>3</sup>. The particle densities quoted by Terman<sup>(4)</sup>, page 715, may be used for the values of  $N_n$ .

$N$  = electrons/cm<sup>3</sup>.

$T$  = the absolute temperature. This is given by Nicolet<sup>(90)</sup> for heights from 50 km. to 100 km. Martin<sup>(86)</sup>, from satellite results quoted by Schilling and Stern<sup>(96)</sup>, indicates that  $T$  rises fairly uniformly from 560° K at 160 km. ( $F_1$ ) to about 1400° K at 300 km. ( $F_2$ ).

The collision frequency,  $\nu$ , is taken as the sum of  $\nu_{ei}$  and  $\nu_{en}$  and is quoted in the third column of Table T. 2.6.0.1.

If  $N$  versus  $h$  is plotted graphically the height of the trajectory for the example quoted (where  $N = 8.7 \times 10^5$  electrons/cm<sup>3</sup>) is found to be 255 km.

#### 2.7.0 LOSSES AT REFLECTION POINTS. (B. 6.1)

The two reflection points in the path considered are:

- (a) in the Sahara Desert at roughly 10°E, 28°N; and
- (b) in equatorial Africa at roughly 20°E, 5°N.

The ground constants are expected to be: (16)(8)  
in respect of (a)  $\epsilon_r = 10$ ,  $\sigma = 2 \times 10^{-3}$  mho/metre and  
in respect of (b)  $\epsilon_r = 14$ ,  $\sigma = 10^{-2}$  mho/metre.

The ground-level angle of incidence =  $90 - \Delta = 82^\circ$ .

Expressing the ground constants in e.s.u., and using curves produced by Burrows<sup>(43)</sup> and McPetrie<sup>(44)</sup>, quoted by Terman<sup>(4)</sup>, the reflection coefficients  $R_v$  and  $R_h$  for vertical and horizontal polarization are found to be:-

for (a)  $R_v = 0.38$  (4.2 db);  $R_h = 0.92$  (0.3 db)

and for (b)  $R_v = 0.36$  (4.4 db);  $R_h = 0.93$  (0.3 db).

#### 2.8.0 VALUES OF GYRO-MAGNETIC FREQUENCY AT CONTROL POINTS. (B. 6.2.9.0).

The three control points correspond to the mid-points of the three hops. Control Point 1 occurs at about 26°E, 6°S; Control Point 2 at about 16°E, 16°N; Control Point 3 at about 6°E, 48°N.

The equatorial declination of the horizontal component of the earth's magnetic field is roughly in line with the horizontal direction of propagation (19°W of N). From a method indicated by Piggott<sup>(102)</sup> the effective longitudinal component of the magnetic field, averaged for ascent and descent of the wave, taking into account the angle of dip of the magnetic field, leads to an effective longitudinal gyro-frequency equal to 0.78, 0.79, and 0.67 Mc/s respectively for the three control points.

#### 2.9.0 NON-DEVIATIVE ABSORPTION IN THE IONOSPHERE. (B.2.6.2.0/4 and B.2.6.2.9.2.)

Appleton and others,<sup>(47,48,49 and 57)</sup> following the magneto-ionic theory and allowing for collisions and the earth's magnetic field, indicate that the absorption coefficient is given by the following relationship:-

$$\alpha = \frac{2 \pi e^2}{m c} \times \frac{1}{n} \times \frac{N \nu}{\nu^2 + (\omega \pm \omega_1)^2} \quad (2.9.0.1).$$

where  $\alpha$  = absorption coefficient (nepers/cm if units are in e.s.u.).

$e$  = electron charge =  $4.77 \times 10^{-10}$  e.s.u.

$m$  = electron mass =  $9.1 \times 10^{-28}$  grams (e.s.u.)

$c$  = velocity of light in vacuo =  $3 \times 10^{10}$  cm/sec. (e.s.u.)

$\nu$  = collisions /sec.

$\omega$  = angular frequency of wave, radians/sec.

$\omega_1 = 2 \pi f_1$ .



$f_1$  = effective gyro-frequency.

$n$  = refractive index ( equations 2.6.0.1/2).

Later work by Piggott<sup>(56)</sup> has taken into account more complex ionization conditions and he has shown that the total absorption suffered in travelling "1" cm through the ionized medium is given by the relation:

Total absorption (nepers) =

$$\int_0^1 \alpha \, dl = B \cos^X X \quad (2.9.0.2).$$

where  $\alpha$  is given by equation 2.9.0.1.

$B$  is a constant for a given path in a given sunspot epoch.

$X$  is the solar zenith angle (degrees).

$x$  is a constant proposed as 0.75 by Piggott<sup>(56)</sup> and Allcock<sup>(59)</sup>.

Equation 2.9.0.2 yields the diurnal variation of absorption. In the D and E Regions a wave of frequency of the same order as the optimum frequency is bent a negligible amount. The absorption suffered in such circumstances is called non-deviative absorption. It may be calculated by performing a numerical integration, with the aid of the ionospheric model (Table T. 2.6.0.1) for each 10 km. difference in layer height. In the non-deviating region  $n = 1$ . As transmission is taking place over a curved earth, each height considered will correspond to a different angle of incidence  $i$ . By plotting the product  $Nv$  against height the average value, for the 10 km. being considered, is obtained. Substituting in equation 2.9.0.1 and calculating for ascending and descending waves yields the result that the value of  $B$  in equation 2.9.0.2 for Control Point 1 = 1.48 nepers ( i.e. 13 db).

The result obtained from a nomogram method (based on the above theory but weighted by practical measurements taken) and produced in 1959 by Piggott<sup>(102)</sup> is 15 db for C.P. 1, 15 db for C.P. 2, and 11.6 db for C.P.3.

Total non-deviative absorption for the path = 41.6 db.

## 2.10.0 DEVIATIVE ABSORPTION IN THE IONOSPHERE.

In the region where  $n$  is not unity, but varies with  $N$ ,  $v$ , and  $\omega$ , the wave is continually bending and the absorption is referred to as the deviative absorption:

$$V = c n. \quad (2.10.0.1).$$

where  $V$  = group velocity of wave.

$c$  = velocity of light in vacuo.

$n$  = refractive index.

In regions where  $n$  is small the reduction in group velocity has the effect of causing the energy to take a longer time to traverse a given distance in the medium than it would have taken in a non-deviating region. Bearing in mind that absorption is caused by energy lost during collisions produced by an alternating field, it is seen that group retardation produces additional absorption. The theorem of Breit and Tuve<sup>(68)</sup> makes provision for group retardation by substituting a mirror reflection

at the virtual height in place of the curved trajectory. The deviative absorption is thus obtained by calculating the absorption for a wave travelling a distance  $(h_v - h_x)$  sec  $i$  in a medium where  $N$  and  $v$  are the values corresponding to the height  $h_x$ , where  $h_v$  is the virtual height of reflection, and  $h_x$  is the height of the trajectory.

Substitution in equation 2.9.0.1, with  $n = \text{unity}$ , yields the result that the deviative absorption for the whole path is very small (about 2 db).  
2.11.0 SPATIAL ATTENUATION. (B.6.2.6 and B. 6.2.9.1).

In free space the field strength at a point  $r$  km. from the transmitter is equal to  $1/r$  of the field strength at 1 km. from the transmitter. Basic antenna theory indicates that if a dipole, situated in free space, is radiating  $P$  kilowatts the field strength, in  $\text{mV/m}$  in the equatorial plane, one km. from the dipole, is  $222/(P)^{1/2}$ .

The total distance London-Salisbury travelled by the wave, assuming mirror reflections at the height of 350 km. (angle of incidence  $69.6^\circ$ , and angle subtended at centre of earth =  $24.8^\circ$  per hop) is 8760 km. Thus if  $P$  kilowatts were radiated from London by a dipole, the field strength expected in Salisbury would be  $\frac{222}{8760 \times (P)^{1/2}} \text{ mV/m}$ .

The spatial attenuation =  $20 \log_{10} 8760 = 78.9 \text{ db}$ .

Curved earth propagation, when the hop length exceeds 1500 km. (E mode) and 2200 km. (F mode), introduces a certain amount of focussing and curves supplied by Piggott<sup>(102)</sup> indicate this focussing reduces the spatial attenuation by 4 db. for 2770 km. hop. Therefore spatial attenuation =  $79 - 4 = 75 \text{ db}$  for the whole path.

#### 2.12.0 POLARIZATION LOSS.

A wave emerging from the ionosphere will usually be elliptically or circularly polarized<sup>(66)</sup>. If the receiving antenna is only sensitive to one plane of polarization it is necessary to make allowance for the resultant loss. The C.R.P.L.<sup>(101)</sup> recommend an allowance of - 1.6 db for phasing and (-3 db) for polarization loss at the receiver. Total 4.6 db.

#### 2.13.0 TOTAL PATH ATTENUATION AND ESTIMATED RECEIVED SIGNAL STRENGTH. (B.6.28., B.6.2.9.5).

On the path considered:-

- |  |                                      |
|--|--------------------------------------|
| (a) Losses at reflection points  | - 8.6 db.                            |
| (b) Non-deviative absorption   | -41.6 db.                            |
| (c) Deviative absorption   | - 2.2 db.                            |
| (d) Spatial attenuation.   | -75.0 db.                            |
| (e) Polarization and phasing loss  | - 4.6 db.                            |
| <u>Total path loss:</u>  | <u>- 132.0 db.</u>                   |
| (f) Signal strength at 1 km. from half wave dipole radiating 1 kw<br>= $20 \log 222 \times 10^3$                             | = + 107 db above 1 $\mu\text{V/m}$ . |
| (g) Power gain when 100 kw is radiated instead of 1 kw   | = + 20 db.                           |
| (h) Directivity gain of H 4/4/1 Koomans <sup>(11)</sup> in direction $\Delta = 8^\circ$ relative to free space dipole ... .. | = + 17 db.                           |

Calculated field strength in Salisbury at noon, September 1956, due to 100 kw radiated at  $\Delta = 8^\circ$  in direction  $161^\circ$  E of S on 21.47 Mc/s from London =  $144 - 132 = 12$  db above  $1\mu\text{V/m}$ , i.e.  $4\mu\text{V/m}$ .

2.14.0 EXPECTED VARIATIONS IN SIGNAL STRENGTH. (B. 6.2.10).

The field strength of the incoming signal may vary due to the following causes each of which is covered more fully in Appendix B:-

- (a) Interference between signal components which are out of phase (B. 6.2.10.1) e.g. extraordinary component phasing against ordinary component and signals which arrive via different propagation modes phasing against each other.
- (b) Wave frequency approaching the value of path M.U.F. (B. 6.2.10.2). Such a condition will give rise to very deep fades and for this reason the optimum transmission frequency is regarded as  $0.85 \times \text{M.U.F.}$  to allow a safe margin.
- (c) Dallinger fades (B. 6.2.10.3.1.1). These are sometimes referred to as "Sudden Ionospheric Disturbances", (S.I.D.)  
Simultaneously with the appearance of unusually large eruptions on the solar disc the D layer becomes heavily ionized so that the product  $N v$  in this region, and hence the short wave absorption, is usually such as to disrupt communications. Such a condition may last anything from a few minutes to a few hours and the effect is greatest in equatorial regions.
- (d) Prolonged Ionospheric Disturbances (P.I.D.) (B. 6.2.10.3.1.2). These are similar in cause and nature to the S.I.D. but are usually not so severe, usually commence and end more gradually, and last a longer period.
- (e) Ionospheric storms (B. 6.2.10.3.1.3).  
These are the main cause of the variability of the  $F_2$  layer; <sup>(111)</sup> are closely linked with sunspot activity <sup>(112-116)</sup>; show a maximum incidence at the equinoxes each year <sup>(117)</sup>; have a short term maximum every 27 days <sup>(118-119)</sup>, (i.e. being linked with emission from sunspots there is maximum activity when that emission normal to the sun's surface is in the direction of the earth); and there is a marked correlation between increased auroral activity and magnetic and ionospheric storms. <sup>(120-125)</sup>  
Beginning with a "turbulent" phase which lasts about 2 hours and affects ionization in the F layers particularly at high latitudes, the storm then enters the "moderate" phase in which virtual heights of  $F_1$  and  $F_2$  are unusually high, critical frequencies of the F layers are unusually low and deviative absorption is unusually high. The "recovery" phase which follows the "moderate" phase usually lasts several days and is the period in which the ionosphere gradually returns to normal.

Ionospheric storms usually produce very little effect at the magnetic equator but their importance increases with increasing latitude. Several theories have been offered to explain the cause of ionospheric storms. (e.g. Birkeland - Störmer<sup>(127-129)</sup>; Chapman-Ferraro<sup>(132-134)</sup>; Martyn's Extension<sup>(135)</sup> to Chapman-Ferraro theory; Ultra-Violet light theory<sup>(136-138)</sup>) but the Solar wind theory<sup>(140,141,126)</sup> appears to fit the observed facts more closely than the older theories. The theories are summarized in Appendix B.

- (f) Sporadic E ionization ( $E_s$ ) (B. 6.2.10.3.2). Patches of abnormally high ionization, intruding into the body of the E layer, cause it to exhibit high critical frequencies sporadically. In equatorial regions  $E_s$  is weak but present throughout daylight hours with a maximum at noon.<sup>(146)</sup> In temperate and sub-tropical latitudes  $E_s$  occurs most frequently in the early morning and evening and it occurs more in local summer than at any other time of the year<sup>(146-147)</sup>. It is not related to the sunspot cycle<sup>(76)</sup>. It has been suggested (a) that  $E_s$  stems from the trails of ionization left in the wake of meteors<sup>(147-151)</sup>; (b) that  $E_s$  is associated with thunder activity<sup>(154,160,76)</sup>. It is probable that it is due to both (a) and (b).

(g) Winds and tides in the ionosphere (B. 6.2.10.3.3).

Observations on noctilucent clouds<sup>(161,162)</sup> at 72-92 km. in height, meteor trails<sup>(163)</sup> at 80-120 km. in height, and echo patterns of  $E_s$  patches<sup>(164-165)</sup> have led to the conclusion that wind velocities in the D and E region are of the order 50-100 m/sec. Motions of an oscillatory nature in the F region have also been reported.<sup>(165-167)</sup> Martyn suggests that at latitudes above about  $35^\circ$  there is an upward ionic drift and below  $35^\circ$  there is a corresponding downward drift<sup>(168-171)</sup>.

- (h) Scatter Phenomena (B. 6.2.10.4). Osborne<sup>(205)</sup> has reported that in tropical countries the incidence of scatter is common but insufficient data has been collected to define the phenomenon adequately<sup>(102)</sup>. It can cause large changes in the sky-wave field strength.

Paras (a) to (h) indicate (1) that the field strength of the received signal will be subject to considerable short-and long-term variation; (2) that it will be difficult to obtain a measured result for the median field strength of the received signal because such a measured result would have to be in respect of a long observation period and natural seasonal changes will cause significant changes within that period; (3) that the calculated median field strength, because of the complex nature of the propagation mechanism, will be, at best, only an approximation.

In spite of the fact that it is an approximation, the calculated median field strength will be used throughout this work because of the difficulties indicated in (2) above. The variations, however, are best based on practical measurements and in this respect it has been noted that, on magnetically quiet days, short-term fades of up to 10 db are common.

Long-term fades need not be considered as these represent abnormal conditions. The wave arrival angle is not expected to deviate from the median value of  $8^\circ$  by more than  $\pm 2^\circ$  because the  $F_2$  virtual height is seldom greater than 400 km. and seldom less than 300 km.

As the calculated median strength of the incoming signal is to be used mainly for the purpose of comparing the signal to noise performance of various antennas, the inevitably approximate nature of the calculations is considered to be relatively unimportant.

-----

CHAPTER 3.

THE MINIMUM ANTENNA GAIN NECESSARY.

3.0.1 Terminal voltage at receiving antenna.

The field traversing a receiving antenna induces emfs in the antenna that are distributed along its length. This behaves as a generator of emf  $e = E l \cos \phi \cos \theta$  where  $E$  is the field strength of the wave in volts/metre and  $l$  is the effective length of the antenna in metres,  $\phi$  is angle between plane of polarization and the antenna conductor, and  $\theta$  is the angle between the wave front and the direction of the antenna. The generator has an internal resistance equal to the radiation resistance  $R_r$  plus the loss resistance  $R_l$  of the system. It delivers power to the load  $R_L$  connected across the antenna terminals. The condition of maximum power transfer is when  $R_L + R_l = R_r$ . In this event the terminal voltage is  $e/2$  and the maximum power delivered to the load from the receiving antenna =  $\frac{E^2 l^2}{4 R_r}$ .

The power density contained in the wave front

$$= \frac{E^2}{Z_{\infty}} = \frac{E^2}{377} \text{ watts/m}^2$$

where  $Z_{\infty} = 377 =$  impedance of free space (see Appendix A eqn. 4.13)

If the receiving antenna is a doublet (an infinitesimal dipole) the effective length and actual length are the same ( $=l$ )

Power delivered to load across the doublet terminals

$$= W = \frac{E^2 l^2}{4 R_r} \quad 3.0.1$$

Now, from Appendix A, eqn. 10.9, the radiation resistance of a doublet is given by:

$$R_r = \frac{2\pi}{3} \cdot Z_{\infty} \cdot \frac{l^2}{\lambda^2} \quad 3.0.2$$

where  $\lambda$  is the wavelength in same units as  $l$ .

$$\begin{aligned} \text{Therefore } W &= E^2 l^2 / \frac{8\pi}{3} \cdot Z_{\infty} \cdot \frac{l^2}{\lambda^2} \\ &= A_D \cdot \frac{E^2}{Z_{\infty}} \end{aligned}$$

where  $A_D$  is the effective area of absorption i.e. the area of wave-front, in the direction of maximum pick-up, over which complete absorption of the wave energy must take place to extract a power equal to that which is available at the antenna terminals.

$$\text{Therefore } A_D = \frac{3\lambda^2}{8\pi} \quad 3.0.3$$

The gain of a doublet over an isotropic radiator is 1.5; therefore the effective area of absorption of an isotropic radiator  $A_o$  is given by:

$$A_o = \frac{\lambda^2}{4\pi} \quad 3.0.4$$

Any antenna of power gain  $G_o$  over an isotropic radiator will have an effective area of absorption ( $A_e$ ) given by:

$$A_e = \frac{G_o \lambda^2}{4 \pi} \quad 3.0.5$$

3.1 Terminal Voltage for a half wave receiving dipole in free space.

Here  $G_o = 1.64$   
and  $A_e = \frac{1.64 \lambda^2}{4 \pi} = 0.13 \lambda^2 \quad 3.1.1$

$$W = A_e \frac{E^2}{Z_{oo}} \\ = \frac{0.13 \lambda^2 E^2}{377} \quad 3.1.2$$

Terminal voltage  $V$  developed across a 73 ohm load is given by:

$$V = (73 W)^{\frac{1}{2}} \\ = E \lambda (.13 \times 73/377)^{\frac{1}{2}} \\ = E \lambda / 2 \pi.$$

Assuming  $E = 12$  db above  $1 \mu V/m$  as calculated in section

2.6.2.9 ,  
 $= 4 \mu V/m$  and  $\lambda = 300/21.47 = 13.97$  m.

Then  $V = 4 \times 13.97/2 \pi = \underline{8.9 \mu V}$  or 19 db above  $1 \mu V$ .

3.2 Terminal voltage for any receiving antenna.

- a) If the antenna gain is  $G_o$  relative to an isotropic antenna then from eqn. (3.0.5):

$$A_o = \frac{G_o \lambda^2}{4 \pi} \\ W = \frac{G_o \lambda^2 E^2}{4 \pi \times 377} = \frac{G_o \lambda^2 E^2}{4730} \quad 3.2.1$$

Terminal voltage  $V$  across load  $Z_o$  is given by:

$$V = (Z_o W)^{\frac{1}{2}} \\ = E \lambda (Z_o G_o / 4730)^{\frac{1}{2}} \quad 3.2.2$$

- b) If the antenna gain is  $G$  relative to a half wave dipole in free space then from eqn. 3.2.1 and 3.2.2 :

$$W = 1.64 G \lambda^2 E^2 / 4730 \text{ and} \\ V = E \lambda (Z_o G \times 1.64/4730)^{\frac{1}{2}} \\ = E \lambda (Z_o G/2890)^{\frac{1}{2}} \quad 3.2.3$$

### 3.3. Minimum terminal voltage required at the input of a typical communications receiver.

This figure will vary considerably from one receiver to the next. A good communications receiver, such as the Marconi CR 150 (noise factor quoted as 5 - 9 db<sup>(215)</sup>), may be taken as fairly representative.

Accepting that the signal output level to the loudspeaker must be at least 20 db above the noise generated in the receiver,<sup>(195,215)</sup> the following minimum terminal voltages were obtained in tests conducted by the writer on a Marconi CR 150 receiver when the bandwidth was set to 10 Kc/s and the receiver was tuned to about 21 Mc/s.

Modulation depth	Minimum input at 70 ohm terminals for 20 db signal-to-noise ratio.
40%	12.6 $\mu$ V
30%	15.9 $\mu$ V
20%	22.4 $\mu$ V

TABLE T. 3.3.1.

The 30% modulated carrier is probably a good representation of the average modulation on a broadcast transmission. For an antenna to supply the terminal voltage necessary in this circuit it must have a gain, G, such that equation 3.2.3. is satisfied when  $E = 4 \mu\text{V/m}$  and  $V = 16 \mu\text{V}$ .

$$\text{Thus } G = \frac{V^2 \times 2890}{E^2 \lambda^2 Z_0} = \frac{16^2 \times 2890}{4^2 \times 14^2 \times 70} = 3.37$$

i.e. In this circuit G must be at least 5.4 db better than a free-space dipole for the audio signal output level to be 20 db higher than the set noise.

### 3.4. Minimum signal-to-noise ratio required at R.F. input to receiver.

Double sideband speech transmissions are considered to be just usable if the time-averaged signal-to-noise ratio of the input to the receiver is 18 db.<sup>(182,186)</sup>

It was indicated in section 3.3. that the minimum input voltage to the receiver must exceed 16  $\mu$ V for a 30% modulated signal if the receiver apparatus noise is to have negligible effect. In addition it is now required that the 16  $\mu$ V minimum input must possess an average signal-to-noise content of 18 db or more if reception is to be satisfactory.

Before attempting to design an antenna which will discriminate against noise in favour of the signal, it is necessary to investigate the probable nature, field strength, and expected wave arrival angle, of noise in the short wave band.



# CHAPTER 4.

## NOISE IN SHORT WAVE CIRCUITS IN TROPICAL COUNTRIES.

### 4.1.0 GENERAL.

Assuming that the radio receiving station is far removed from sources of man-made noise the interference to the signal is due to: <sup>(181)</sup>

- (a) Noise generated in the receiver.
- (b) Thermal noise in antenna and feeder conductors.
- (c) Extraterrestrial noise.
- (d) Atmospheric noise.
- (e) and (b) together represent the controlling factor at frequencies above 30 Mc/s according to Laver <sup>(182)</sup>.

North <sup>(183)</sup> has shown that an antenna can be regarded as a generator of thermal agitation emf  $e_n$  volts, where:

$$e_n = (4 k T R_a B)^{\frac{1}{2}} \quad (4.1.0.1)$$

where  $R_a$  = radiation resistance of antenna in ohms.

$k$  = Boltzmann's constant =  $1.37 \times 10^{-16}$  erg. sec/degree.

$T$  = absolute temperature of the conductors.

$B$  = bandwidth of the receiver (c/s).

This generator, of internal resistance  $R_a$ , is capable of delivering maximum power to a load if the load resistance is equal to  $R_a$  and this power is called the available noise power,  $W_{ni}$  watts, where:

$$W_{ni} = \left( \frac{e_n}{R_a + R_a} \right)^2 \times R_a = \frac{e_n^2}{4 R_a} = k T B \quad (4.1.0.2).$$

Thus if antenna A ( $R_a = 630$  ohms) and antenna B ( $R_a = 70$  ohms) were each connected to a matched load, each will deliver the same thermal agitation noise power to that load. If, however, each were connected to a load of high impedance, the agitation voltage of A would be  $(630/70)^{\frac{1}{2}} = 3$  times greater than that of B. The value of  $T$  is usually taken as about 290 K for objects near the ground.

Extraterrestrial noise (c) is due <sup>(184)</sup> to radiations at radio frequencies emanating from the sun, from stars, from interstellar gas, and from invisible concentrations called "radio stars". This noise is mainly significant between 30 Mc/s and 100 Mc/s.

The main interference that concerns short wave circuits, particularly when the receiving station is in the tropics, is atmospheric noise. This is dealt with more fully below. In passing it will be observed that if the antenna is always matched to the receiver input, (b) will be the same no matter what antenna is used and (c) is minimised if the antenna sensitivity is concentrated in a narrow beam as near the horizon as possible.

#### 4.2.0 ATMOSPHERIC NOISE.

It is generally accepted that atmospheric noise is caused by lightning discharges<sup>(182)</sup> which, due to their transient nature, radiate energy over a wide band of frequencies. As the amplitude decreases with frequency, noise from this source is relatively unimportant above 30 Mc/s.

Tremellen and Cox<sup>(185)</sup> have supplied charts which show the levels of atmospheric noise over the globe but the data on which they are based is meagre<sup>(186)</sup> and more recent publications by the C.C.I.R., e.g. their report No. 6<sup>(187)</sup>, are more reliable. However, as usual, the report gives median values of radio noise power available from a short vertical grounded monopole and, as such an antenna is insensitive to energy arriving at high angles, the picture it gives is incomplete. In order to obtain a better understanding of how to combat atmospheric noise in the quest for improved signal-to-noise ratios it is necessary to formulate a rough picture of how that noise is generated and propagated and also of what noise field strength may be expected at various arrival angles.

##### 4.2.1.0 GENERATION OF ATMOSPHERIC NOISE.

Srivastava<sup>(186)</sup>, regarding a lightning discharge as a one-millisecond pulse, has demonstrated how the energy contained in the Fourier components could be propagated in the wave guide formed by the earth and the under-boundary of the ionosphere. However, his theory does not take account of the important individual discharges that go to make up a lightning stroke and it would appear to be helpful only in the case of very low frequency interference.

Although it is only possible to obtain a rough estimate of the effect of a lightning flash, it is worthwhile attempting to express the probable effect of a storm in terms of an equivalent transmitter.

##### 4.2.1.1 THE PHYSICAL NATURE OF A STROKE.

The microstructure of a lightning stroke is complex but Schonland<sup>(189-194)</sup>, by his investigations, has made it possible to obtain a fairly clear understanding of what actually happens during a stroke.

When the electric field, at some point in a cloud, exceeds the dielectric strength there is first produced a "pilot streamer" which advances slowly and in which the currents are small. This produces negligible radiation. Superimposed in space on this pilot there follows a succession of "leader streamers" which advance in steps and which together constitute a "stepped leader". On average there are four stepped leader strokes per lightning flash.

Aiya<sup>(95)</sup> Studying data produced by Schonland<sup>(192)</sup> has deduced that the median length of each step in a stepped leader is 67 metres; the duration (t) of each step is less than one microsecond; the median interval (t<sub>i</sub>) between steps is about 74 microseconds and therefore the recurrence frequency = 1/t<sub>i</sub> = 13.5 kc/s. Appleton and Chapman<sup>(196)</sup> and, later, Watson-Watt, Hird and Lutken<sup>(197)</sup> concur that the duration (t<sub>i</sub>) of a complete "stepped leader" is about one millisecond. The experiments of Aiya<sup>(200)</sup> indicate that the median value of the duration (t<sub>f</sub>) of a complete flash is 0.2 sec. The median value of the separation (t<sub>s</sub>) between any two of the leader strokes is therefore about 65 milliseconds.

In their studies of the electrostatic field of a stepped leader, Appleton and Chapman<sup>(196)</sup> have agreed with the figure of 74 microseconds given above for (t<sub>i</sub>) and the microstructure of the stepped leader, deduced from their photographs of field strength fluctuations, indicates that the rate of rise of current in each step is very nearly the same in all discharges and is exponential. Berger<sup>(198)</sup> indicates that the maximum rate of change of current is 10<sup>10</sup> amps/sec and this is supported by Thomas and Burgess<sup>(199)</sup> who express the current in the form:

$$i = I_0 \left( e^{-at} - e^{-bt} \right) \quad (4.2.1.1.3).$$

$$\text{Thus } \frac{di}{dt} \text{ max.} = (b - a) I_0$$

From their<sup>(199)</sup> observations the median values may be taken as:

$$I_0 = 24 \times 10^3 \text{ amps.}$$

$$a = 4.4 \times 10^4 \text{ per sec.}$$

$$b = 4.6 \times 10^5 \text{ per sec.}$$

Substitution in equation (2.1.1.4) leads to the result:

$$\left( \frac{di}{dt} \right)_{\text{max.}} = 10^{10} \text{ amps per sec.}$$

#### SUMMARY OF DATA (approximate median values).

Length of step	: 67 metres.
Duration (t) of each step	: 1 microsecond.
Interval (t <sub>i</sub> ) between steps	: 74 microseconds.
Recurrence frequency of steps	: 13.5 Kc/s.
Duration (t <sub>L</sub> ) of stepped leader	: 1 millisecond.
Number of stepped leaders per flash	: 4
Duration (t <sub>f</sub> ) of flash	: 0.2 sec.
Separation (t <sub>s</sub> ) between stepped leaders	: 65 milliseconds.
Maximum value of discharge current	: 24 × 10 <sup>3</sup> amps.
Maximum rate of change of current	: 10 <sup>10</sup> amps/sec.

Discharges may occur (a) within the cloud, (b) from the cloud to upper atmosphere, and (c) from the cloud to earth. Discharges within the cloud are more numerous in the tropics than the other two types, and, according to Aiya<sup>(195,201)</sup>, it is this type which is primarily responsible for noise on short-wave circuits. His observations<sup>(195)</sup> indicate that these discharges occur at an average height of about 6 km. in the tropics.

#### 4.3.0 RECEPTION OF NOISE.

Radiation occurs during each step discharge of the stepped leader. The step, about 70 metres long, may be regarded as an antenna carrying current, the value of which is changing at the rate of  $10^{10}$  amps/second and the speed of which is about one tenth of the speed of light<sup>(195)</sup>. The different components in the frequency spectrum are propagated as would be ordinary radio waves by ground wave, optical ray, tropospheric wave, or via the ionosphere.

#### 4.3.1 ACOUSTIC EFFECTS OF A STROKE.

The acoustic effect on the listener depends on the characteristics of his ear and the characteristics of the receiver used.

The ear acts as an integrating device. Davis<sup>(202)</sup> maintains that its response to single impulsive sounds depends upon the maximum value of those impulses averaged over about a millisecond. Thus the apparent loudness of the interference produced by a stepped leader ( $t_L$  = one millisecond) depends on the average amplitude of the train of individual steps. Davis<sup>(202)</sup> indicates that subsequent repetitions of the impulsive sound have a cumulative effect tending to increase the apparent loudness but leakage of intensity occurs during the interval between impulses and this leakage is almost complete if the interval exceeds one second.

Aiya<sup>(201)</sup> has likened the ear to a circuit with a charging time constant of about 10 milliseconds and a discharging time constant of 500 milliseconds. Thus the apparent loudness of the impulses, produced by a flash consisting of four stepped leaders, as judged at the end of a flash, will be:

Average due to stepped leader no. "1"  
minus leakage between leaders "1" and "2",  
plus average of leader "2",  
minus leakage between leaders "2" and "3",  
plus average of leader "3",  
minus leakage between leaders "3" and "4",  
plus average of leader "4".

Aiya<sup>(200)</sup> has observed that impulsive noise only causes annoyance to listeners when its recurrence frequency exceeds 10 times per minute and that noise in the presence of a signal interferes with the programme if the difference in level between the signal and the apparent loudness is less than 20 db.<sup>(203)</sup> The average tropical thunderstorm produces 10 or more flashes per minute at peak activity.

#### 4.3.2 OUTPUT FROM THE RECEIVER.

Thomas and Burgess<sup>(199)</sup> have shown that the time integral (referred to in section 4.3.1) of the output envelope is independent of the damping and number of the tuned circuits in the R.F. and I.F. stages of the receiver. Lever<sup>(182)</sup> and others have indicated

that the loudspeaker noise power output is proportional to the receiver bandwidth (e.g. equations 4.1.0.1 and 4.1.0.2 refer).

#### 4.3.3.0. EFFECTIVE RADIATED POWER IN LIGHTNING FLASH.

When a doublet in free space carries current of sinusoidal waveform, the field strength  $E$   $\mu$  V/m at the point  $r$  km. from the doublet in the direction  $\theta$  from the axis of the doublet, is given by the relationship

$$E = \frac{212 \times 10^3 \times (P)^{\frac{1}{2}} \sin \theta}{r} \quad (4.3.3.1).$$

where  $P$  is the radiated power in kW, Appendix A refers.

Assuming that the human ear will respond to a lightning flash as described in section 4.3.1 and also assuming the median values quoted in section 4.2.1.1, Aiy<sup>(21)</sup> has calculated that an average tropical lightning flash will produce approximately the same acoustic effect, in a receiver of 6 kc/s bandwidth, tuned to a frequency of  $f$  Mc/s, as a doublet antenna, at a height of 6 km., radiating  $P$  kW, of sinusoidal waveform, 30% modulation, where:

$$P = 0.045/f^2 \quad (4.3.3.2).$$

If the receiver bandwidth is 10 kc/s instead of 6 kc/s then:

$$P = 0.07/f^2 \text{ (approx.)} \quad (4.3.3.3).$$

For any other bandwidth,  $B$  kc/s,  $P$  is multiplied by  $(B/10)$ .

Substituting for  $P$  in equation (4.3.3.1) the field strength  $E_2$  produced by the equivalent transmitter is given by:

$$E_2 = \frac{5.6 \times 10^4 \sin \theta}{r f} \text{ (approx.)} \quad (4.3.3.4).$$

where  $E_2$  = noise field strength in  $\mu$  V/m.

$r$  = distance between storm and receiver measured in km.

$f$  = frequency in Mc/s.

This is the unabsorbed field strength. If the energy is propagated via the ionosphere it will suffer deviative and non-deviative absorption and this attenuation will be in addition to the spatial attenuation taken into account in equation 4.3.3.4.

#### 4.3.3.1 LIMITATIONS ON ACCURACY.

It must be stressed that the method of deriving the value of  $P$  relies, to a large extent, on approximations. Therefore the value quoted for  $P$  (equation 4.3.3.3) and hence that quoted for  $E_2$  (equation 4.3.3.4) must be regarded as approximations only. If the value of  $E_2$  is required for the purpose of comparison between the signal-to-noise performance of two antennas then the absolute value of  $E_2$  (if this exists) is not needed so long as equations 4.3.3.3 and 4.3.3.4 represent the correct order of magnitude.

4.4.0

APPLICATION TO THE ASSESSMENT OF ANTENNA PERFORMANCE.

Circuit parameters.

It is assumed (a) that it is desired to compare the signal-to-noise performance of several antennas to be used at the Salisbury end of the London-Salisbury circuit;

(b) that the period under investigation is midday, September, 1956;

(c) that the operating frequency is 21.47 Mc/s;

(d) that the receiver bandwidth is 10 Kc/s;

(e) that, as calculated in Chapter 2, the dominant mode of the signal is 3 hop F, the median wave arrival angle of the signal is  $8^\circ$  approximately, on a bearing  $19^\circ$  W of N and of median strength  $4 \mu$  V/m (12 db above  $1 \mu$  V/m) for 100 kW radiated at  $\Delta = 8^\circ$  from London using a Kocmans H/4/4/1 array.

The C.C.I.R. noise predictions<sup>(187)</sup> indicate that the time averaged noise power, available from a short, vertical, grounded monopole, located at Salisbury for the conditions: quoted above, is such as to correspond to a noise field strength of 11 db below  $1 \mu$  V/m (median) and 8 db below  $1 \mu$  V/m (upper decile). The vertical polar diagram of such an antenna is defined by<sup>(11)</sup>

$$E = \frac{300 P^{\frac{1}{2}} \cos \Delta}{d} \quad (4.4.0.1)$$

where E is the field strength in mV/m at distance d km in the direction  $\Delta$  to the horizontal for a radiated power of P kW.

It follows that the vertical grounded monopole is sensitive primarily to the noise arriving at a low angle. But the signal will also arrive at a low angle. If the signal and the noise both arrive from the same direction, the receiving antenna cannot discriminate in favour of the signal. In this case the signal-to-noise ratio is simply the ratio between the received field strength of the signal and of the noise. The C.C.I.R. noise predictions<sup>(187)</sup>, therefore, do not make it possible, in a circuit such as this, to compare the expected signal-to-noise performance of one low-angle antenna with another: they merely assist in the prediction of the grade of service that may generally be expected. Evidence supplementary to that provided by the C.C.I.R. predictions is therefore needed before an effective comparison can be made between antennas proposed for this circuit. Of assistance in this connection is the equivalent transmitter concept developed in the preceding sections which makes it possible to plot the expected instantaneous values of  $E_2$  for various angles of arrival for distant

CHAPTER 5.

DISADVANTAGES OF RHOMBIC RECEIVING ANTENNA.

5.0 General.

The Test Rhombic antenna, in which the dimensions are:-

side length =  $5 \lambda$ .

height =  $1 \lambda$ .

angle of tilt =  $70^\circ$ ,

represents a fairly large version because it is frequently not considered economically sound to make the antenna larger than this. For example this is the largest of the designs considered in the C.C.I.R. publications "Antenna Diagrams"<sup>(11)</sup>. Though the Rhombic antenna has so much to commend it for point-to-point working it is considered to have the following serious disadvantages in the Salisbury-London circuit as a receiving antenna at Salisbury:-

5.1 Maximum gain in wrong direction.

As shown in Chapter 2 the wanted signal, of median strength  $4 \mu \text{ V/m}$ , will arrive at  $8^\circ \pm 2^\circ$  whatever the season and whatever the year, on transmissions when  $f = f(\text{optimum})$ . The Test Rhombic antenna has maximum gain at  $\Delta = 12.5^\circ$  and the power gain at  $\Delta = 8^\circ$  is down to 50% of the maximum. (See fig. F.4.4.3.1).

In Appendix A equations 12.29 to 12.32 it was shown that for maximum gain at an angle  $\Delta$  to the horizontal the following dimensions are necessary:-

$$H = \frac{\lambda}{4 \sin \Delta} \quad 5.1.1$$

$$\psi = 90 - \Delta \quad 5.1.2$$

$$l = \frac{0.371 \lambda}{\sin^2 \Delta} \quad (\text{for reception}) \quad 5.1.3$$

For  $\Delta = 8^\circ$  the Rhombic antenna would require the following dimensions:-

$$H = 1.8 \lambda \quad (\text{approx. 82 feet at } 21.47 \text{ Mc/s})$$

$$\psi = 82^\circ.$$

$$l = 19.15 \lambda \quad (\text{approx. 1175 feet at } 21.47 \text{ Mc/s}).$$

This would be a structure so large as to be uneconomical, usually.

5.2 Sensitive to high-angle noise.

As shown in Chapter 4 the noise field strength increases with wave arrival angle for both distant-zone and near-zone activity and the Rhombic antenna was shown to have a poor signal-to-noise ratio during periods of higher thunder activity because of its sensitivity to noise coming in at high angles. The noise voltage fed to the receiver was shown to be greater for noise picked up by the 6.1% lobe ( $\Delta = 46^\circ$ ) than by, say, the 100% lobe ( $\Delta = 12.5^\circ$ ) because of the greater value of  $E_2$ , the noise signal strength, at the higher values of  $\Delta$ .

5. 3 Sensitive to high-angle unwanted signals.

The high angle lobes give rise, not only to serious noise interference, but also to interference from:

- (a) transmissions on frequencies near to the wanted frequency with fairly high wave arrival angles. (The antenna should assist the receiver in discriminating against these transmissions);
- (b) unwanted components of the wanted transmission, e.g. signal energy arriving out of phase with that employing the dominant 3-hop F mode because it has used some other mode. This unwanted energy will come in at the following angles of arrival ( $\Delta$ ):  $13^\circ$  (4 hop),  $16^\circ$  (5 hop),  $22^\circ$  (6 hop),  $25^\circ$  (7 hop),  $30^\circ$  (8 hop),  $42^\circ$  (12 hop) but as each hop introduces considerable additional attenuation it is probable that the only noticeable reaction will come from the 4 hop mode which will suffer about 8 db more absorption than the 3 hop mode but enjoys a gain of 3 db in receiving antenna sensitivity at  $13^\circ$  compared with  $8^\circ$ . However at the transmitting antenna (see fig. F.4.4.3.2) it will lose 3 db at  $13^\circ$  compared with the transmission at  $8^\circ$ . Therefore the voltage at the receiver terminals produced by the 4 hop mode will be of the order of 8 db below that due to the 3 hop mode and, because of the phase difference between the two components, will cause much of the distortion and fading which are characteristic of long distance reception on this type of antenna.

- - - - -



CHAPTER 6.

THE SEARCH FOR AN IMPROVED DESIGN.

6. 0 SUMMARY OF THIS CHAPTER.

- (a) The following antennas are investigated by means of the "worst-condition signal-to noise ratio" concept proposed in Chapter 4:
- (a) Horizontal half-wave dipole (3.5 db).
  - (b) Koomans Array (8.7 db).
  - (c)  $\lambda/4$  Vertical rod antenna (2.3 db).

The figures in brackets represent the calculated "worst-condition signal-to-noise ratio" (distant storms) for the conditions specified in Chapters 2 and 4. A vertically polarised array promises maximum sensitivity in the desired direction if the directivity is made high.

- (b) The reflecting ground plane is important in the case of vertically polarized antennas and curves are derived representing the vertical polar diagram of a grounded  $\lambda/4$  monopole on:
- i) sea water.
  - ii) soil of good conductivity.
  - iii) soil of poor conductivity.
  - iv) grid of copper wires spaced at 15" centres laid on heavy clay soil.
  - v) grid of copper wires spaced at 12" centres laid on heavy clay soil.
  - (vi) grid of copper wires spaced at  $7\frac{1}{2}$ " centres laid on heavy clay soil.

These curves appear in figure F. 6.3.4.1.3.

#### 6.0.1 Summary of malady inherent in Rhombic antenna.

The weight of evidence amassed in Chapters 2, 3 and 4 led to the conclusion, stated in Chapter 5, that the defects of the Test Rhombic (accepted as being as large as is usually economically sound in the circumstances) are as follows:

- (a) Maximum gain in wrong direction.
- (b) Sensitive to high-angle noise.
- (c) Sensitive to high-angle unwanted signals.

#### 6.1 The cure prescribed.

A broadcast transmitting antenna (A) must have a fairly blunt polar diagram so as to give coverage of a fairly large area in the country to which the energy is beamed. A receiving antenna, (B) designed specifically for reception of transmissions from (A) should have, on the other hand, maximum sensitivity in the direction of median wave arrival angle ( $\Delta$ ) and, as narrow a beam as possible provided that the expected limits of variation of  $\Delta$  can be accommodated within the half-power points of the maximum lobe.

In the circuit under consideration the receiving antenna sensitivity must be concentrated in a narrow beam centred on  $8^\circ$  to the horizontal and with half-power points at  $6^\circ$  and  $10^\circ$  (from Chapter 2). The sensitivity should fall away as rapidly as possible to zero above  $10^\circ$  and below  $6^\circ$ .

#### 6.2 High gain versus absence of side lobes.

It is possible that in the quest for an antenna which satisfies the requirements of section 6.1 there may be found one which has a lower gain than that of the test Rhombic antenna. However, if the reduction in noise (db) is greater than the deficiency in sensitivity (db), an improvement will have been achieved provided that the signal output from the receiver is still large compared with the noise generated in the receiving apparatus and the thermal agitation in the antenna system.

#### 6.3 The search for an improved design.

Having taken the type of antenna which is usually accepted as the one giving best results for reasonable capital outlay and, suspicion having been aroused by observed noisy reception during the months of high thunder activity, it has been investigated and the causes are as summarised in section 6.0.1. In the search for a design which will not have these inherent defects the following possibilities are considered:

##### 6.3.1 The horizontal half wave dipole.

It is well known that the polar diagram in the equatorial plane consists (a) for height ( $H$ ) =  $\lambda/4$ , one lobe with maximum sensitivity at  $\Delta = 90^\circ$ ; (b) for  $H = \lambda/2$ , two lobes, each giving equal maximum sensitivity at  $\Delta = 30^\circ$  and  $\Delta = 150^\circ$ ; (c) for  $H = 3\lambda/4$ , three lobes, each giving equal

maximum sensitivity at  $\Delta = 20^\circ$ ,  $\Delta = 90^\circ$  and  $\Delta = 160^\circ$ ; (d) for  $H = \lambda$ , four lobes, each giving equal maximum sensitivity at  $\Delta = 15^\circ$ ,  $\Delta = 50^\circ$ ,  $\Delta = 130^\circ$ ,  $\Delta = 165^\circ$ .

To obtain one of the lobes at  $8^\circ$  it would be necessary for  $H$  to be  $2\lambda$  according to Terman<sup>(4)</sup>, there being 8 lobes, each giving equal maxima at  $\Delta = 8^\circ, 23^\circ, 40^\circ, 60^\circ, 120^\circ, 140^\circ, 157^\circ, 172^\circ$ . From Fig. F. 4.3.2.5.1 in Chapter 4 it is clear that the high-angle lobes will pick up a great deal of noise. Making the same assumptions as in Chapter 4, the "worst condition signal-to-noise ratio" for distant storms would be:

$$\frac{(4)^2}{(6.0)^2} \text{ for } 60^\circ : \text{ a noise-to-signal ratio of } 2.25 \text{ (3.5 db)}$$

which, being 10.7 db worse than the Test Rhombic, is quite unsuitable for the purpose even if the  $2\lambda$  (92') masts were available to support such an antenna.

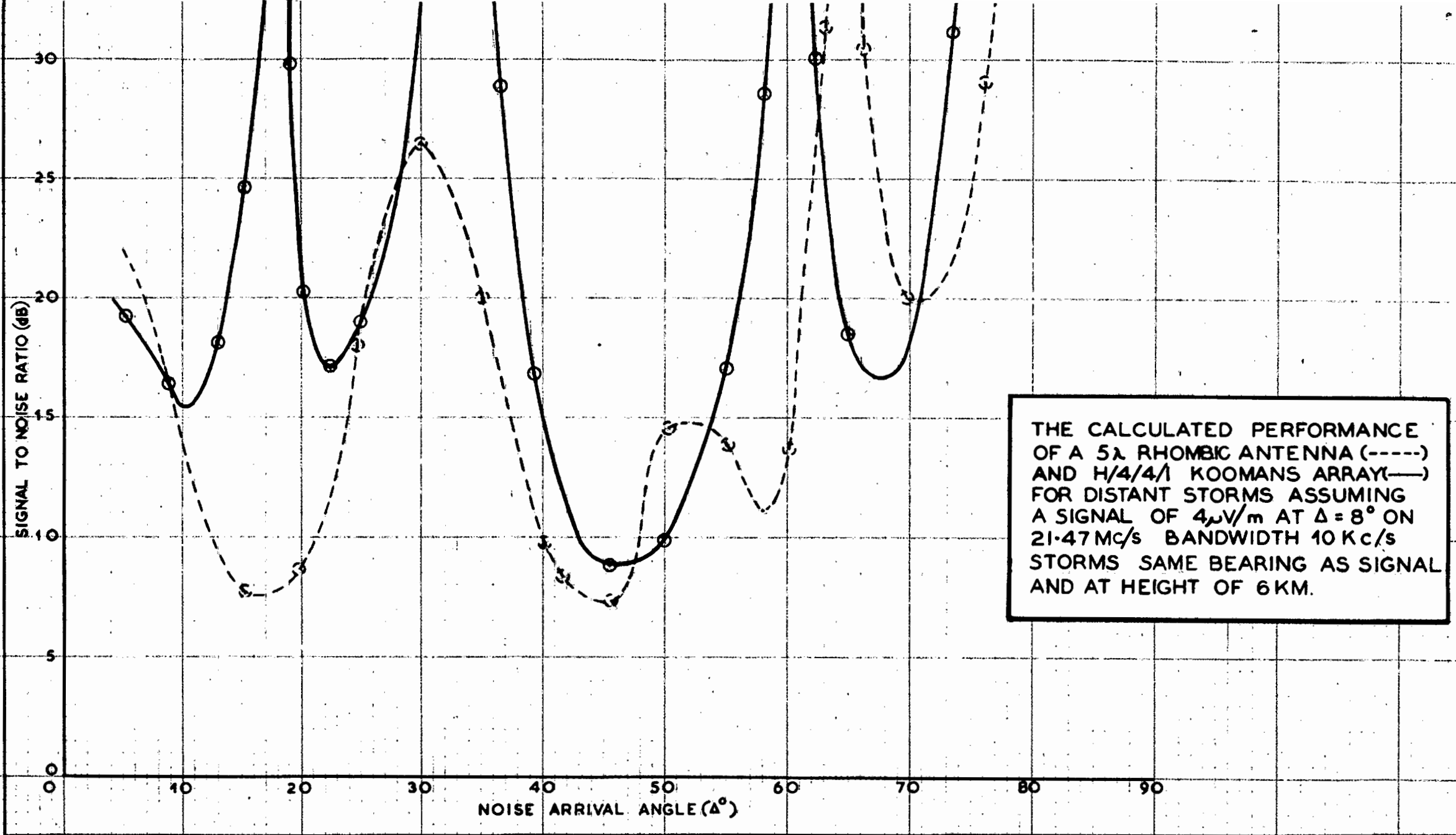
### 6.3. 2 THE KOOMANS ARRAY.

This array is used by the B.B.C. as the transmitting antenna in this circuit and it is logical to consider the use of a similar design as a receiving antenna. In Chapter 4 the signal-to-noise performance of the Koomans  $H/4/4/1$  design was compared with that of the Test Rhombic and the curves of fig. F. 4.4.3.3 reveal that the over-all performance of the Koomans array for distant storms is better than that of the Test Rhombic.

However, the  $H/4/4/1$  design is an expensive structure: the top row of dipoles is  $2.5\lambda$  above the ground and the masts supporting the triatics would be about  $3.5\lambda$  high (about 160 feet at 21.47 Mc/s). The masts would have to be surmounted by a boom of length greater than  $\lambda/4$  so that the reflecting curtain and "radiating" curtain can be separated by  $\lambda/4$ . The correct phasing of the four stacks of four co-linear dipoles is a major problem. In the circumstances the extra expense of the Koomans design does not appear to be warranted for the sake of the calculated improvement (Chapter 4) of 1.5 db in the "worst-condition signal-to-noise ratio" for distant storms.

The power density diagram of an  $H/4/4/1$  design is given in fig. F. 4.4.3.2 or B. 5.4.1 and that of an  $H/2/4/1$  design (four stacks of two co-linear dipoles plus reflector curtain) is given in figure B. 5.4.2.

FIG F 4.4-3.3



From the noise map it is seen that, on average, the noise level in an area corresponding to a value of  $\Delta$  of about  $67^\circ$  is about 4 db lower than in one corresponding to  $\Delta$  equal to about  $45^\circ$  which in turn is about 20 db lower than for an area corresponding to a value of  $\Delta$  equal to about  $10^\circ$ . Therefore figures F. 4.4.1.2 and F. 4.4.3.3 should be read in conjunction with each other but it is of more value, probably, to read figure F.4.4.3.3 in conjunction with known weather conditions for a certain area. For example if it is known that at the time of the year being considered an area corresponding to  $\Delta = 10^\circ$  to  $25^\circ$  is subjected to heavy thunder activity and that noise arriving at all other values of  $\Delta$  is negligible then, for these conditions, the signal-to-noise performance of the Koomans Array is greatly superior to that of the Test Rhombic Antenna. Similarly from  $\Delta = 29^\circ$  to  $47^\circ$  and  $54^\circ$  to  $62^\circ$ . But if the storms were to become so close that  $\Delta$  exceeds  $62^\circ$  the position would be reversed.

At  $\Delta = 46^\circ$  the signal-to-noise ratio for each of the antennas is at its lowest (7.2 db for the Rhombic, 8.7 db for the Koomans). It is proposed calling this the "worst condition signal-to-noise ratio" for distant storms. A similar treatment can be given in respect of local storms. The "worst condition signal-to-noise ratio" is a useful figure of merit when assessing the performance of antennas.

If the radiated power of the equivalent transmitter had been taken as something other than 0.16 watts the performance figures of the two antennas would still have borne the same relationship to one another as in figure F.4.4.3.3 but it is preferable to use a value of P which is of the correct order of magnitude because this increases the usefulness of the figure obtained for the "worst condition signal-to-noise ratio".

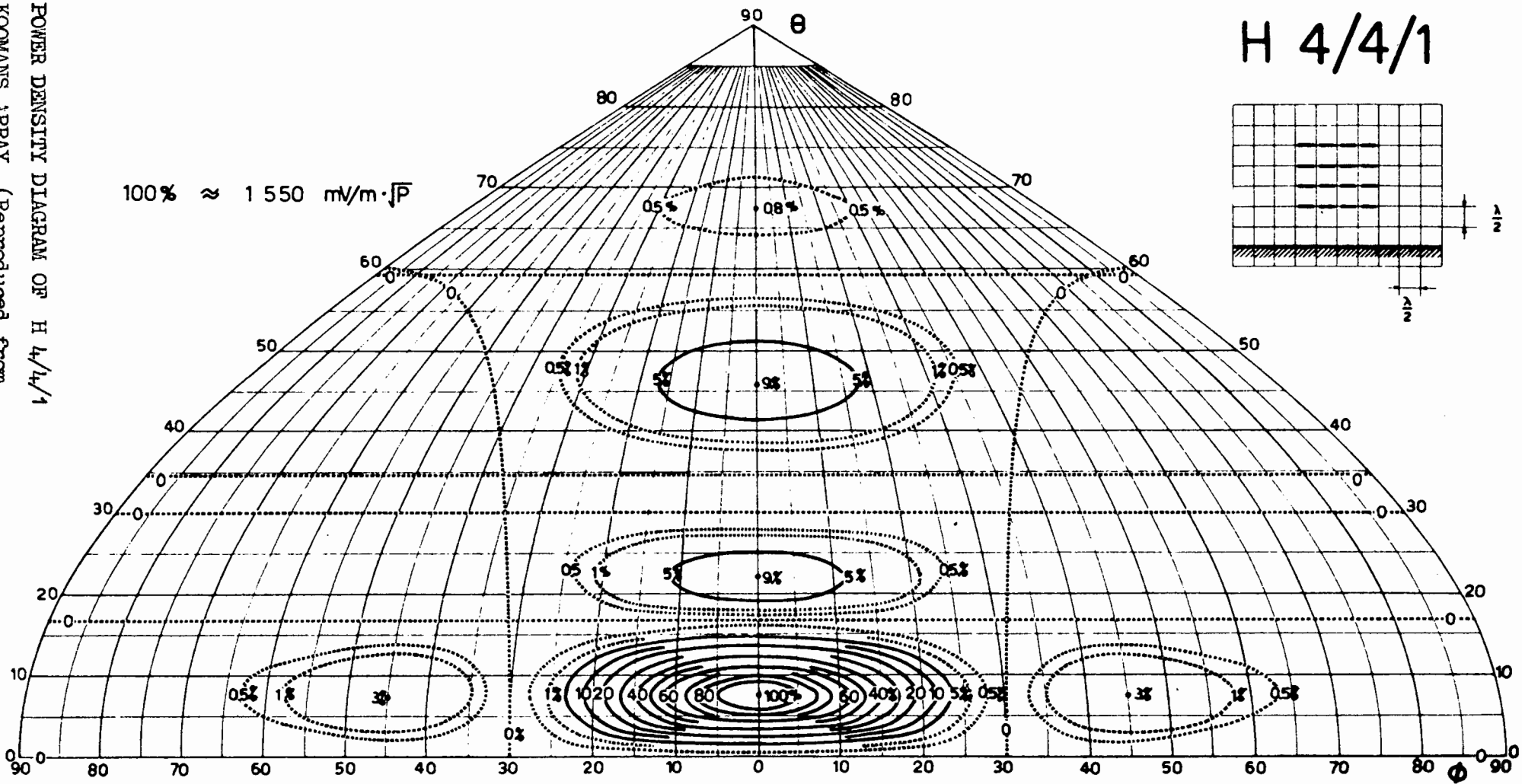
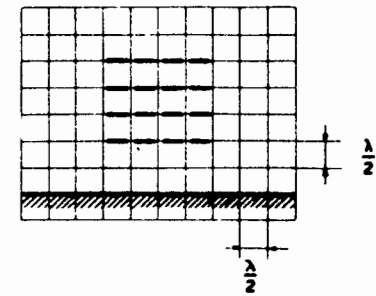
#### 4.5.0. Conclusions

When investigating the relative merits of two antennas, one approach is to compare the average grade of service by using the time-averaged C.C.I.R. predictions. This approach does not yield a satisfactory basis of comparison between two low-angle antennas in the circuit considered.

Another approach is to employ the equivalent transmitter concept and to compare the performance at each of a series of assumed noise arrival angles. This has the disadvantage of dealing with peak values only and does not yield average grade of service but if the performance curves are read in conjunction with noise maps and known weather conditions for a given locality and season, the relative merits of the antennas, compared on a signal-to-noise basis, can be demonstrated.

---

H 4/4/1



- 4.4.2 -

POWER DENSITY DIAGRAM OF H 4/4/1  
KOOBANS ARRAY. (Reproduced from  
"Antenna Diagrams" by the C.C.I.R. (11))

Figure F 4.4.2.2.

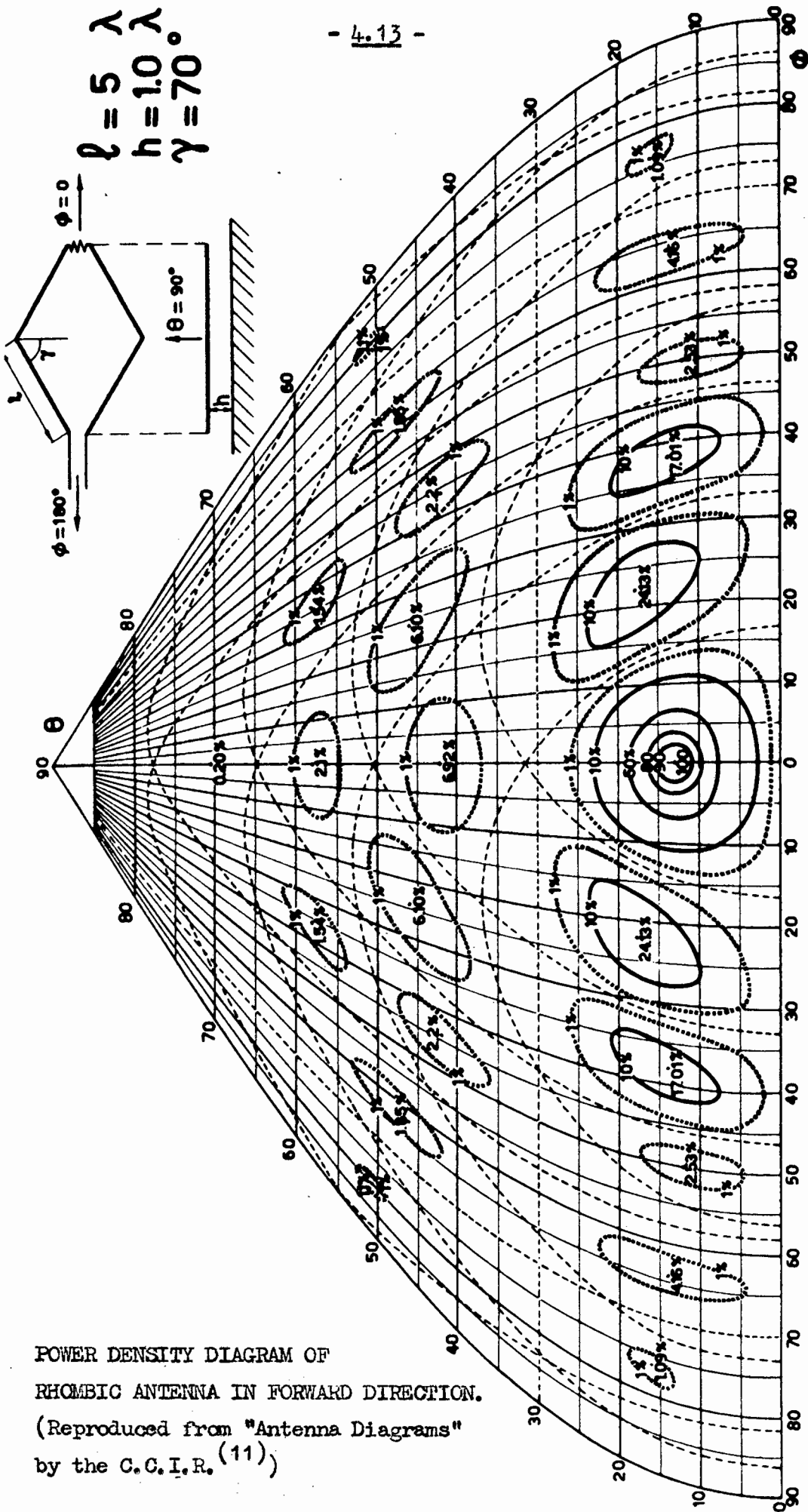


Figure F 4.4.3.1.

of each antenna for noise coming in at various values of  $\Delta$  from a series of hypothetical noise transmitters located on the London-Salisbury great circle.

#### 4.4.3 COMPARISON OF SIGNAL-TO-NOISE RATIO OF ANTENNAS.

The polar diagrams for the two antennas to be compared are reproduced in figures F.4.4.3.1 and F.4.4.3.2. The assumed antenna dimensions have been quoted in assumption (a) of Section 4.4.0.

The signal-to-noise ratio, for any assumed angle of arrival ( $\Delta$ ) of the noise, is calculated by substituting in equation 4.4.0.2 the values:

$E_s = 4 \mu \text{ V/m}$  calculated in Chapter 2, quoted in Section 4.4.0.

$G_s =$  relative gain at signal wave arrival angle ( $8^\circ$ )  
 $= 0.5$  for the Rhombic and  $1.0$  for the Koomans.

$E_\Delta$  is obtained from figure F. 4.4.1.1 (for distant storms) or from equation 4.4.2.2 (for local storms) for any assumed noise arrival angle  $\Delta$ .

$G_\Delta$  is obtained from figures F.4.4.3. 1/2 and is the relative gain at the assumed arrival angle  $\Delta$ , (putting  $\phi = \text{zero}$  except that where  $\phi$  of some other value leads to a greater value of  $G_\Delta$  the more sensitive value of  $G_\Delta$  is assumed).

Calculating the signal-to-noise performance for distant storms, for various values of  $\Delta$ , and plotting this performance against  $\Delta$  leads to figure F. 4.4.3.3. Similar relative results would be obtained from local storms.

It will be observed that in figures F. 4.4.3.1/2 the sensitivity is usually greatest in the  $\phi = 0$  direction. A notable exception is the 6.10% point at  $\phi = 24^\circ$ ,  $\theta (= \Delta) = 46^\circ$  in figure F.4.4.3.1. The signal-to-noise ratio for  $\Delta = 46^\circ$  is at its worst if the noise is assumed to be arriving from the direction  $\phi = 24^\circ$  and this is the value that has been used in drawing up figure F.4.4.3.3. Similarly for other cases. In this respect assumption (c) in Section 4.4.0 has not been rigidly adhered to but it does mean that, for each value of  $\Delta$  considered, the signal-to-noise performance quoted is the worst possible that would be expected.

Both horizontal and vertical polar diagrams of each antenna have therefore been taken into account.

Only the noise due to individual flashes, assumed arriving from discrete directions, has been studied in the foregoing. As shown in Section 4.4.1 the calculated field strengths represent peak values, the average value depending on the frequency of the flashes. The larger the area over which thunderstorms are occurring the greater is the frequency of occurrence expected to be. (a) For a given angle subtended at the receiver, the area is proportional to range. (b) The frequency of flashes increases for climatic reasons as the equator is approached. Both of these aspects are taken into account in the C.C.I.R. noise map (figure F.4.4.1.2) which depicts relative noise power available from a short vertical grounded monopole situated at various points on the map.



throughout the year. Therefore it may be assumed that, for the region 1500 km to 2000 km, thunder activity occurs almost continuously. It is probable that, on a time average basis, the major contribution to the noise measured in Salisbury emanates from Equatorial Africa.

The C.C.I.R. noise predictions<sup>(187)</sup> for the period under consideration, for Salisbury, have been quoted in Section 4.4.0. As the predictions are based on the noise power available from a short, vertical grounded monopole, and as such an antenna is primarily sensitive to noise arriving at low angles (eqn. 4.4.0.1 refers) it follows that there should be agreement between the value predicted as the upper decile (8 db below  $1 \mu \text{ V/m}$ )<sup>(187)</sup> and that calculated for low angles in Table T.4.4.1.1 (7.0 to 7.5 db below  $1 \mu \text{ V/m}$ ). Since the two results are comparable it follows that the results quoted in Table T. 4.4.1.1 are of the correct order of magnitude.

Since it has been shown that the C.C.I.R. predictions do not form a suitable basis for comparing the signal-to-noise performance of the two low-angle antennas, the results contained in Table T. 4.4.1.1 are plotted in figure F. 4.4.1.1 and the resultant smooth curve of  $E_2$  vs  $\Delta$ , for the particular parameters and assumptions laid down in Section 4.4.0, makes it possible to carry out a detailed investigation into the signal-to-noise performance of each antenna for noise coming in at various values of  $\Delta$  from a series of hypothetical noise transmitters located on the London-Salisbury great circle.

#### 4.4.2 RECEIVED NOISE FIELD STRENGTH ( LOCAL STORMS).

When storms are so near that the energy is propagated by direct ray, the noise field strength is obtained from equation 4.3.3.4. Substituting 21.47 for  $f$  in equation 4.3.3.4 the noise field strength obtained is:-

$$E_2 = \frac{2.6 \times 10^3 \sin \theta}{r} \quad (4.4.2.1)$$

where  $E_2 =$  in  $\mu \text{ V/m}$ .

$r =$  the distance in km between storm and receiver.

$\theta =$  the direction of propagation measured from the axis of the doublet.

The " $\sin \theta$ " term may be neglected since the greatest interference will occur when the direction of a stroke is broadside to the direction of the receiving antenna.

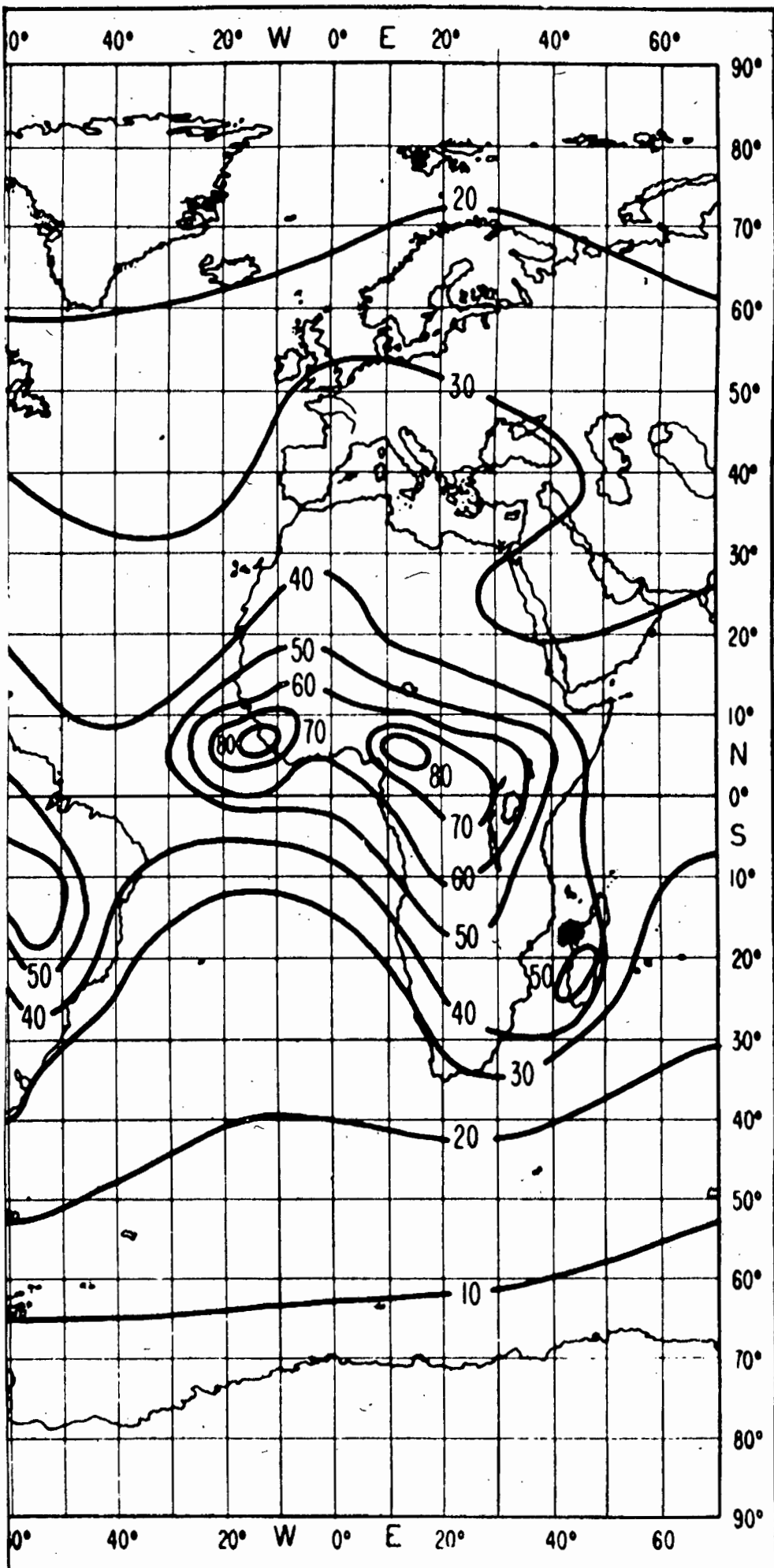
As indicated in Section 4.2.1.0 the "within-cloud" discharges are responsible for the major proportion of short-wave atmospheric noise.<sup>(195)</sup> It was also indicated that these discharges occur at a median height of 6 km. (Also see assumption (c) Section 4.4.0).

Thus  $r = 6/\sin \Delta$

Substituting for  $r$  in equation 4.4.2.1

$$E_2 = 430 \sin \Delta \quad (4.4.2.2).$$

Thus for local storms, as for distant storms, it is possible to carry out a detailed investigation into the signal-to-noise performance



NOISE GRADES ( $F_a$ ) for 1200 - 1600 hrs. September to November.

(Reproduced from C.C.I.R. Report No 65<sup>(187)</sup>)

Figure F 4.4.1.2.

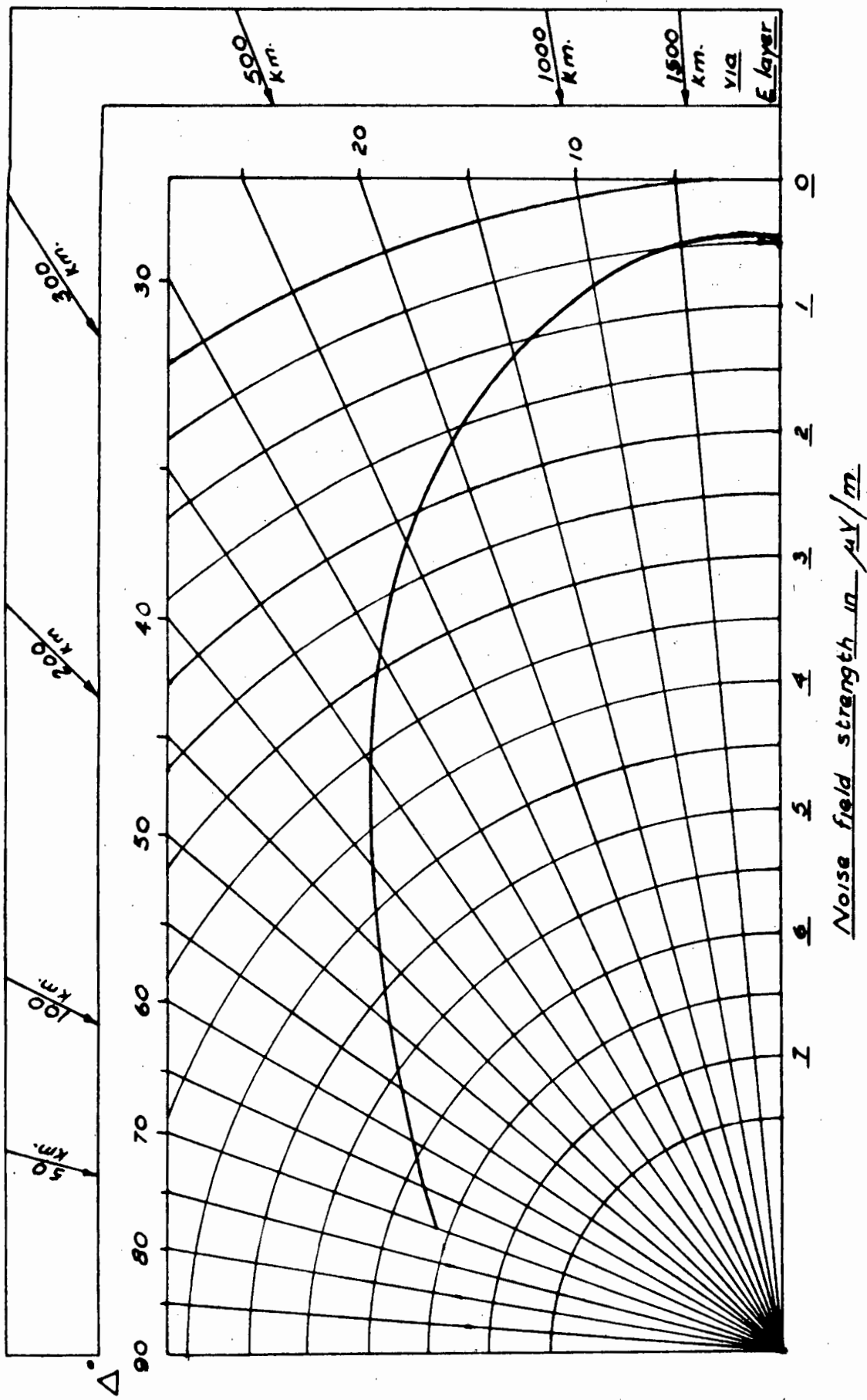


Fig. F 4.4.1.1.

Receiver tuned to 21.47 Mc/s; 10 kc/s I.F. Bandwidth

The latter are therefore disregarded and the results for E mode propagation are given in Table T. 4.4.1.1 below.

Distance from Receiver to Thunderstorm. km.	Unabsorbed field strength db above $1\mu$ V/m.	Absorption db.	Noise field strength $E_2$		Wave arrival angle $\Delta^\circ$
			db above $1\mu$ V/m	$\mu$ V/m	
2000	+ 7.0	14.0	- 7.0	0.45	2
1500	+ 5.5	13.0	- 7.5	0.44	4
1000	+ 7.0	10.0	- 3.0	0.71	10
500	+ 11.0	5.6	+ 5.4	1.86	22
300	+ 15.0	4.2	+ 10.8	3.47	34
200	+ 17.0	3.0	+ 14.0	5.01	46
100	+ 18.5	2.5	+ 16.0	6.31	64
50	+ 19.5	2.4	+ 17.1	7.16	75

TABLE T 4.4.1.1.

It will be noticed that the unabsorbed field strength calculated for a distance of 2000 km is greater than that for 1500 km. This is due to curved-earth focussing effects<sup>(56)</sup> at grazing incidence in which spatial attenuation starts decreasing with increasing distance. 2000 km is the maximum range for one hop in the E mode of propagation.

Thus if at a certain period there is no thunder activity, except at a locality 1500 km from the receiver, each flash may be thought of as producing a noise field strength of 7.5. db below  $1\mu$  V at  $\Delta = 4^\circ$  (Table T.4.4.1.1). The periods between strikes would be silent except for extra-terrestrial and man-made noise. The random flashes will produce e.m.f.'s of approximately equal amplitude in the receiving antenna. Remembering (a) that each leader stroke is made up of a succession of steps each of duration less than one microsecond, separated by about 74 microseconds from each other, (b) that each leader stroke is separated by about 65 milli-seconds from the next, (c) that a complete flash only lasts about 0.2 seconds, and (d) that radiated noise energy emanating from different areas will take differing times to reach the receiver, the statistical probability of overlap between individual steps, in a 10 flashes/minute storm is:

$$\frac{1}{74} \times \frac{1}{65} \times \frac{0.2 \times 10}{60} \quad \text{i.e. 1 chance in } 1.5 \times 10^5.$$

Thus, for practical purposes, the flashes may be considered to be intermeshed in time with one another or following one another in time sequence with one flash concluding before the next commences. The values for  $E_2$  given in Table T.4.4.1.1, will therefore represent peak values. Suppose that in a certain area there is a storm in which the number of flashes per minute is, say, 10. It is probable that this will produce the same peak value for  $E_2$  as another storm, say of 2 flashes per minute, in the same area, but the average value of  $E_2$  for the 10 flashes/minute storm would be higher than that of the other.

It is observed in noise maps,<sup>(187)</sup> e.g. figure F.4.4.1.2, that the noise level in Equatorial Africa is, on average, higher than anywhere else in the world and that the noise level remains high

(via ionosphere) storms, and local (direct ray) storms. In this way the effect of the antenna polar diagram on signal-to-noise ratio can be assessed.

If the median field strength of the received signal is  $E_s$  and the median value of the received noise field strength, calculated for a certain noise wave arrival angle  $\Delta^\circ$ , is  $E_\Delta$  then, if the antenna gain in the direction of arrival of the signal is  $G_s$  (relative to the gain in the most sensitive direction) and relative gain in the direction  $\Delta^\circ$  is  $G_\Delta$ , the signal-to-noise power ratio is equal to:-

$$\frac{(E_s)^2}{(E_\Delta)^2} \times \frac{G_s}{G_\Delta} \quad (4.4.0.2)$$

Suppose that it is required to compare the signal-to-noise performance of the Test Rhombic antenna with that of a Typical Koomans antenna within the framework of the circuit parameters laid down at the beginning of this section. In order to compare the effect of the antenna polar diagrams on their signal-to-noise performance the following assumptions are made regarding the antennas and the noise transmitters:

(a) Assume that the antenna dimensions are:

Rhombic: side length =  $5 \lambda$ ; mean height above ground  $1 \lambda$ ;  
angle of tilt  $70^\circ$ .

Koomans: 4 tiers of 4 co-linear horizontal  $\lambda/2$  dipoles, the bottom row being  $1 \lambda$  above the ground, plus reflector curtain ( $H \lambda/4/1$ )

(b) Assume that the antennas are both located near Salisbury and aligned on London.

(c) Assume that the atmospheric noise is caused solely by a series of thunderstorms 6 km above the ground, on the same bearing as the signal and occurring at discrete distances from Salisbury.

In equation 4.4.0.1,  $E_s$  has been quoted as  $4 \mu \text{ V/m}$ ,  $G_s$  and  $G_\Delta$  are obtainable from the polar diagrams. It is necessary to calculate  $E_\Delta$  for the discrete distances referred to in (c) above, in respect of distant storms and local storms.

#### 4.4.1. RECEIVED NOISE FIELD STRENGTH ( $E_2$ ) (DISTANT STORMS).

As indicated in Section 4.4.0 the operating frequency is 21.47 Mc/s and receiver bandwidth is taken as 10 kc/s. Substituting 21.47 for  $f$  in equation 4.3.3.3.

$P = 0.16$  watts approximately.

For the conditions under consideration, the effective noise field strength,  $E_2$ , arriving in Salisbury from an equivalent transmitter radiating 0.16 watts, located beyond the horizon, can be calculated by Piggott's method<sup>(102)</sup>, for the E, F and double-hop F (i.e. 2F) modes. The calculations indicate that for distances between 50 km and 2000 km the E mode suffers much less absorption than the F and 2 F modes.

In Chapter 4 it was shown that the calculated signal-to-noise ratio is given by:

$$\frac{\text{Signal power}}{\text{Noise power}} = \frac{G_s \times E_s^2}{G_\Delta \times E_\Delta^2}$$

where  $G_s$  = antenna gain in direction of incoming signal.

$E_s$  = field strength of incoming signal.

$G_\Delta$  = gain in direction of incoming noise.

$E_\Delta$  = field strength of noise (same units as  $E_s$ ) arriving at angle  $\Delta^\circ$  to horizontal.

The "worst-condition signal-to-noise ratio" of the H/2/4/1 design will be seen, by inspection of the polar diagrams, to be the same as that of the H/4/4/1 design, but, due to the greater beamwidth in the horizontal plane, it will be more sensitive than the H/4/4/1 design to a greater number of storms occurring on either side of the broadside direction and the probability is high, therefore, that, on time average, the signal-to-noise performance of the H/2/4/1 design will be inferior to that of the H/4/4/1 design.

### 6.6.3 VERTICAL ANTENNA.

Since  $\Delta = 8^\circ$ , any system, which inherently possesses maximum sensitivity along, or almost along, the horizontal, shows fair promise. The polar diagrams for various grounded vertical antennas above a perfectly conducting plane are shown in fig. F.6.3.3.1<sup>(7)(11)</sup>. They may be derived from equation (11.4) in Appendix A. The high-angle lobes which occur when the length (l) exceeds  $\lambda/2$  would make such antennas too sensitive to high-angle noise. All antennas of length exceeding  $\lambda/2$  must therefore be discarded as receiving antennas for the purpose here in mind. Notice in fig. F. 6.3.3.2 that when  $l = 0.625$  the horizontal field strength passes through a maximum but there is also present a large lobe at  $60^\circ$  ( Fig. F. 6.3.3.1).

The  $\lambda/2$  vertical antenna has a promising vertical polar diagram but presents matching problems if it is to be connected at ground level, as an end-fed antenna, to a co-axial line of 70 ohm characteristic impedance ( $Z_0$ ). The  $\lambda/4$  antenna is a natural choice as its input impedance, approximately equal to its radiation resistance ( $R_p$ ) = 37 ohms. (see equation 11.17 of Appendix A). By means of a suitable folded construction the input impedance (or, in the case of a receiving antenna, the impedance of the receiving antenna acting as a generator) can be made equal to the  $Z_0$  of the co-axial feeder.

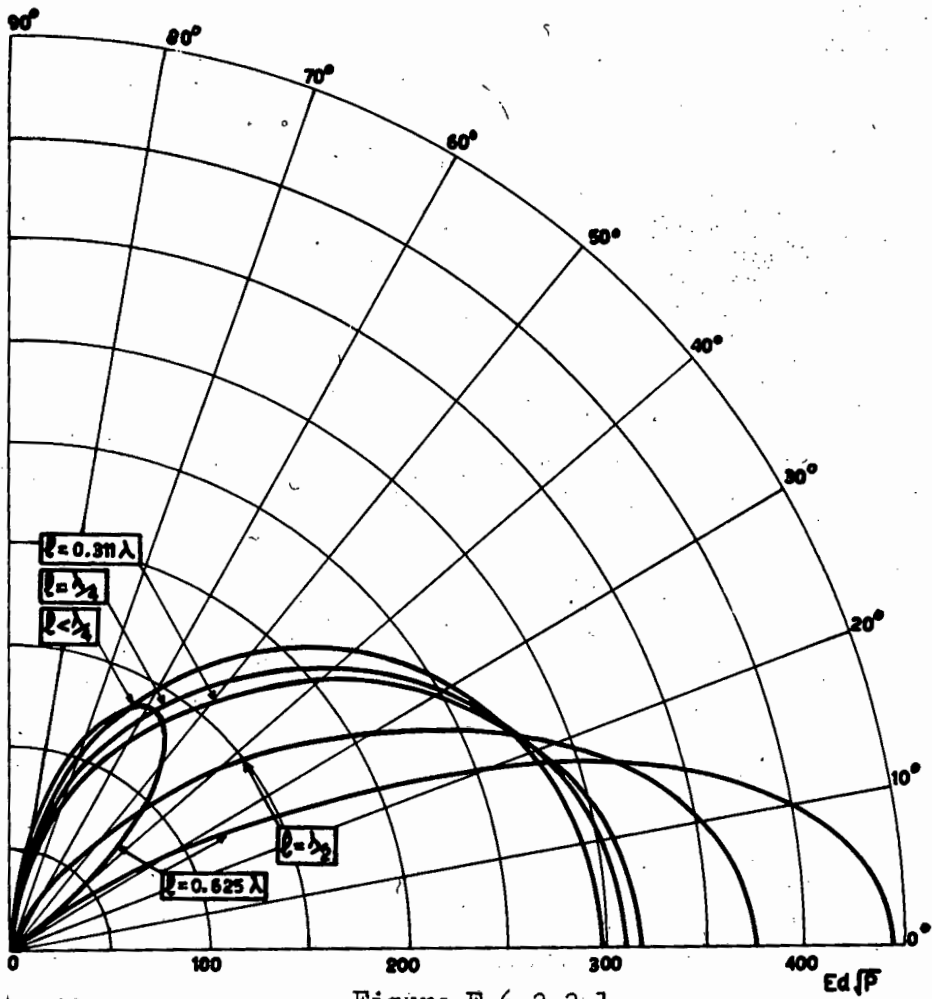


Figure F.6.3.3.1.  
Vertical polar diagrams of vertical monopole  
on ground of infinite conductivity.

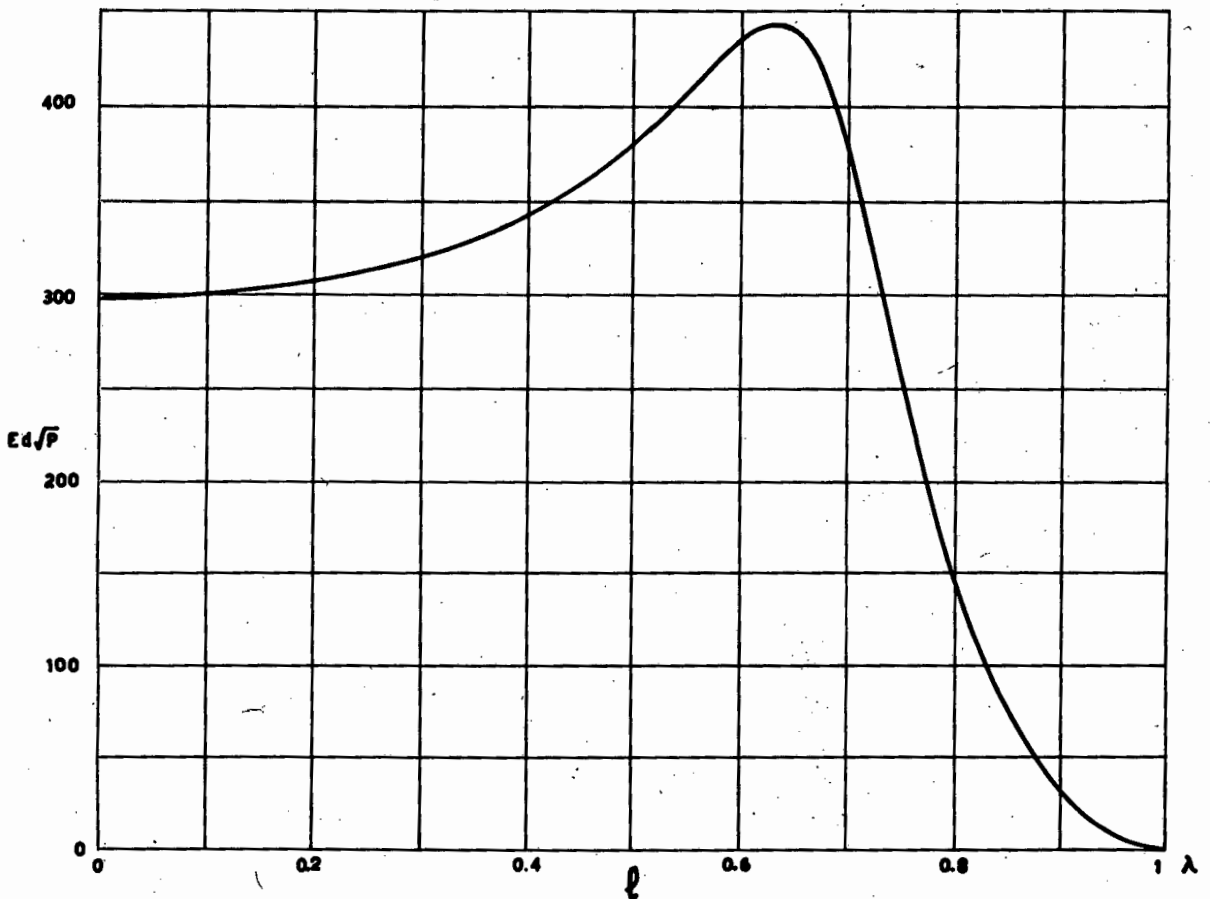


Figure F.6.3.3.2.

Field strength in mV/m at 1 km for 1 kW radiated by  
vertical monopole on a perfectly conducting plane.

(11)

Both figures reproduced from C.C.I.R. "Antenna Diagrams".

The field strength at 1 km. due to a grounded  $\lambda/4$  antenna radiating 1 kw is 314 mV/m<sup>(11)</sup> at  $\Delta = 0$  and 305 mV/m at  $\Delta = 8^\circ$  (fig. F 6.3.3.1/2). From Appendix A, equation 11.19, the corresponding figure for a  $\lambda/2$  dipole in free space is 222 mV/m giving the grounded  $\lambda/4$  monopole a power gain of 3.01 db at  $\Delta = 0$  and 2.77 db at  $\Delta = 8^\circ$ . The gain of a free space dipole over an isotropic antenna<sup>(7)</sup> is 1.64 (2.15 db). Therefore the gain  $G_o$  of the grounded  $\lambda/4$  antenna over an isotropic antenna is 5.16 db at  $\Delta = 0$  and 4.92 db at  $\Delta = 8^\circ$ .

This arrangement has the dual disadvantage of:

- (a) insufficient gain in the direction  $\Delta = 8^\circ$  ( $G_o$  for  $\lambda/4$  is about 5 db at  $\Delta = 8^\circ$  whereas  $G_o$  for the test Rhombic at  $\Delta = 8^\circ$  is 21 db - 3 db = 18 db (see section 4.3.2.6) ) and
- (b) the polar diagram is not sharp enough, giving too much sensitivity at large values of  $\Delta$ .

The "worst condition" signal-to-noise ratio for distant storms is obtained by combining the noise field strength from fig. F 4.3.2.5.1 with  $\lambda/4$  antenna sensitivity from fig F.6.3.3.1. The "worst condition" interference from distant storms occurs at  $\Delta = 45^\circ$  approximately. The signal-to-noise ratio ( assuming, as for the test Rhombic, that signal strength of the wanted signal coming in, at  $\Delta = 8^\circ = 4 \mu\text{V/m}$  and noise field strength, at  $45^\circ = 5 \mu\text{V/m}$ ) is given by:

$$\frac{\text{Signal power fed to receiver}}{\text{Noise power fed to receiver}} = \frac{G_o (4)^2 \lambda^2 \times 10^{12}/4730}{(0.615)^2 G_o (5)^2 \lambda^2 \times 10^{12}/4730}$$

as in section 4.3.2.6.

"Worst condition signal-to-noise ratio" for the distant storms for the  $\lambda/4$  antenna is therefore 1.69/1 (2.28 db). This is 5 db worse than the "worst condition" signal-to-noise ratio calculated for the test Rhombic and 5.8 db better than the "worst condition" signal-to-noise ratio of the  $\lambda/2$  horizontal dipole,  $2 \lambda$  high.

The next step is to improve the sensitivity in the direction of  $\Delta = 3^\circ$  at the expense of the sensitivity in other directions, if possible. Several possible methods of doing this present themselves. For example, a broadside arrangement of vertical  $\lambda/4$  rods, spaced  $\lambda/2$  apart and correctly phased, would sharpen the horizontal polar diagram. Increasing the vertical dimensions would sharpen the vertical polar diagram. However, such an arrangement promises to be an expensive piece of structural engineering. It is proposed instead to sharpen the polar diagram by means of parasitic elements. It is not claimed that a parasitic arrangement provides a unique solution to the problem of providing an antenna to match up to the specification laid down in section 6.1 but it does promise to concentrate the sensitivity in a narrow, low-angle beam. Furthermore it promises to be a fairly inexpensive and compact structure.



#### 6.3.4.0. Reflection.

In the discussion centred on figure F 6.3.3.1./2. the assumption was made that the reflecting surface possesses infinite conductivity. Due to the importance of the ground plane in the design it is necessary to look more deeply into the effect, on vertically polarised waves, of ground planes of various types. In figure F 6.3.4.0.1., reproduced from Williams,<sup>(7)</sup> it is clear that ground conductivity has an important effect on the polar diagram. However figure F 6.3.4.0.1. is in respect of a dipole,  $\lambda/3$  above the earth, and it is necessary now to calculate a number of polar diagrams for a grounded  $\lambda/4$  monopole for various types of reflecting plane. Before doing this it is necessary to examine, in more detail, the mechanism of reflection in various types of ground.

#### 6.3.4.1. The mechanism of reflection.

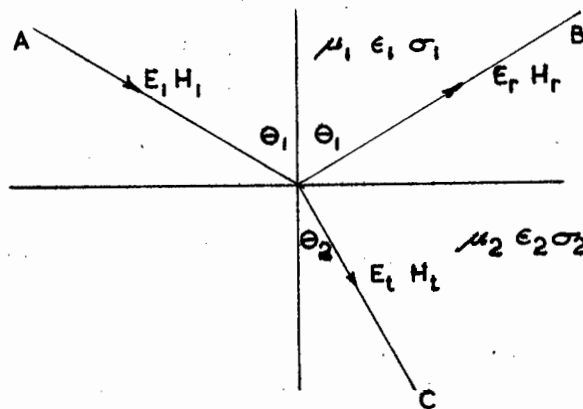


Figure F 6.3.4.1.1.

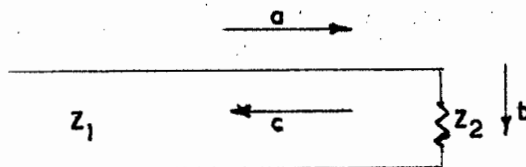
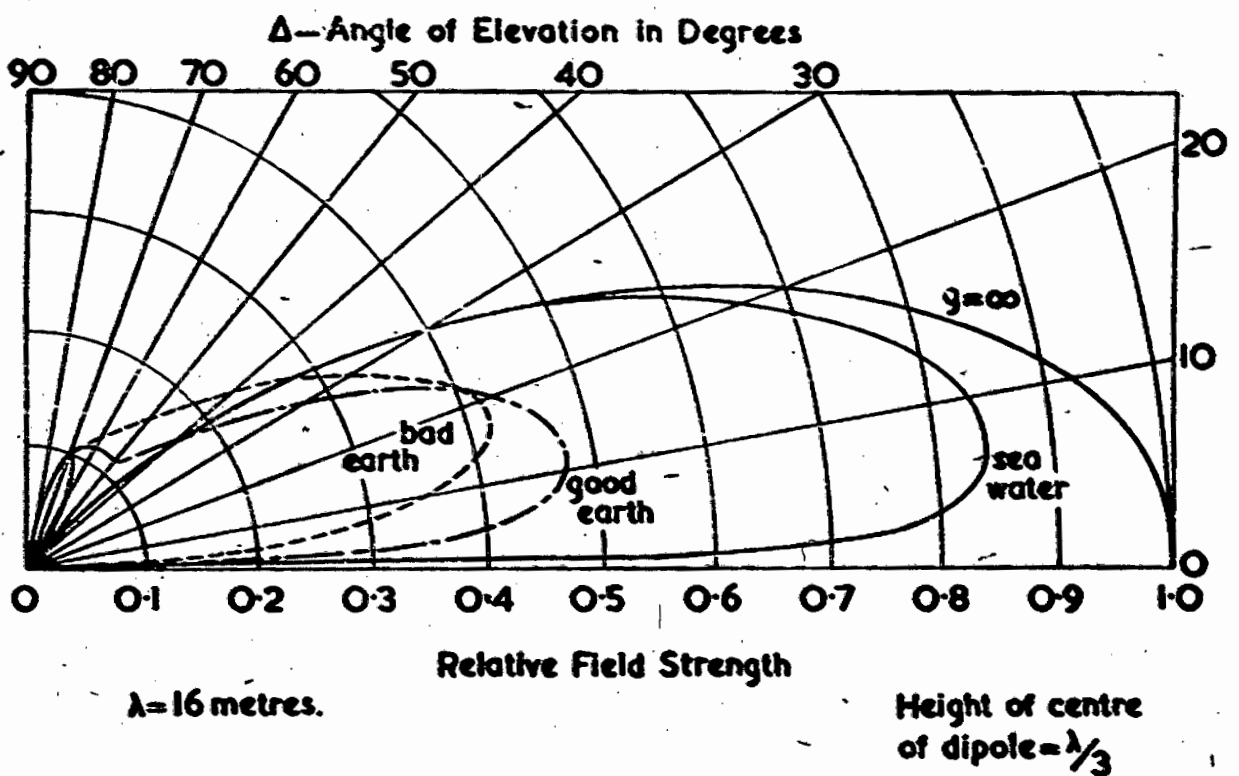


Figure F 6.3.4.1.2.

Booker<sup>(5)</sup> has drawn attention to the similarity that exists between the situation depicted in figure F 6.3.4.1.1. and that depicted in figure F 6.3.4.1.2. When a wave travels down the transmission line, in which the wire spacing is small compared with  $\lambda/2\pi$ , of characteristic impedance  $Z_1$ , there is at the discontinuity,  $Z_2$ , (a) the incident wave, (b) the wave absorbed in  $Z_2$ , and (c) the reflected wave travelling back down the line. The relative magnitudes depend on the degree of matching between  $Z_2$  and  $Z_1$ .

Similarly there is an incident wave (A), a transmitted wave (B), and a reflected wave (C) at the interface between the media (1) and (2). For incidence normal to the interface ( $\theta_1 = 0$ ) the relative amplitudes will depend on the intrinsic impedances  $Z_1$  and  $Z_2$  of the two media and may be found from the relation<sup>(5)</sup>

$$H_i / (Z_1 + Z_2) = H_r / (Z_1 - Z_2) = H_t / (2Z_1) \quad (6.3.4.1.1.)$$



**POLAR DIAGRAMS OF A VERTICAL HALF-WAVE DIPOLE ABOVE  
A GROUND OF FINITE CONDUCTIVITY**

(Feldman, *Proc. I.R.E.*, June, 1933)

(7)

Reproduced from "Antenna Diagrams", by Williams.

Figure F 6.3.4.0.1.

$$\frac{E_i}{Z_1 + Z_2} = \frac{E_r}{Z_2 - Z_1} = \frac{E_t}{2 Z_2} \quad (6.3.4.1.2)$$

where H and E are the magnetic and electric vectors respectively. When  $Z_2 = Z_1$  there is no reflected wave and when  $Z_2 = 0$  or  $\infty$  the reflected wave is equal in magnitude to the incident wave, i.e. reflection is complete.

If  $\theta_1$  is not zero then the field impedances<sup>(5)</sup> of the three waves are given below for vertical polarization. (H parallel to reflecting plane). Then  $Z_{fi}$  and  $Z_{ft}$  should be substituted for  $Z_1$  and  $Z_2$  respectively in 6.3.4.1.1 /2 where  $Z_f$  is the field impedance.

$$Z_{fi} = Z_1 \cos \theta_1 \quad (6.3.4.1.3)$$

$$Z_{fr} = -Z_1 \sec \theta_1 \quad (6.3.4.1.4)$$

$$Z_{ft} = Z_2 \cos \theta_2 \quad (6.3.4.1.5)$$

In eqn. 4.20 of Appendix A it is shown that the intrinsic impedance  $Z$  of a medium of conductivity  $\sigma$  mho/metre, permeability  $\mu$  Henrys/metre, and permittivity (dielectric constant)  $\epsilon$  Farads/metre, is given by:

$$Z = \left( \frac{j \omega \mu}{\sigma + j \omega \epsilon} \right)^{\frac{1}{2}} \quad (6.3.4.1.6)$$

In a dielectric  $\sigma$  is negligible compared with  $j \omega \epsilon$  and the intrinsic impedance of the dielectric becomes:

$$Z = \left( \frac{\mu}{\epsilon} \right)^{\frac{1}{2}} \quad (6.3.4.1.7)$$

and is a resistance.

In free space  $\mu = \mu_0 = 4 \pi \times 10^{-7}$  Henrys/metre and  $\epsilon = \epsilon_0 = \frac{1}{36 \pi \times 10^9}$  Farads/metre and the intrinsic impedance of free space,  $Z_{00}$ , is given by:

$$Z_{00} = \left( \frac{\mu_0}{\epsilon_0} \right)^{\frac{1}{2}} = 120 \pi = 377 \text{ ohms.} \quad (6.3.4.1.8)$$

In a medium of high conductivity, such as a metal,  $\sigma$  is large compared with  $\omega \epsilon$  and

$$\begin{aligned} Z_{\text{metal}} &= \left( \frac{j \omega \mu}{\sigma} \right)^{\frac{1}{2}} = \left( \frac{\omega \mu}{\sigma} \right)^{\frac{1}{2}} \angle 90^\circ \\ &= \left( \frac{\omega \mu}{\sigma} \right)^{\frac{1}{2}} \angle 45^\circ = \left( \frac{\omega \mu}{2 \sigma} \right)^{\frac{1}{2}} (1 + j) \end{aligned} \quad (6.3.4.1.9)$$

$$= R_m + j X_m \quad (6.3.4.1.10)$$

A medium behaves as a dielectric when  $\omega \epsilon$  is much greater than  $\sigma$  and as a conductor when  $\omega \epsilon$  is much less than  $\sigma$ . The change-over occurs when  $\omega = \frac{\sigma}{\epsilon}$  and the transition frequency,  $f_t$ , is given by:

$$f_t = \frac{\sigma}{2 \pi \epsilon} \quad (6.3.4.1.11)$$

where  $\sigma$  is in mho/metre

$\epsilon$  is in Farads/metre.

$f_t$  is in c/s.

In equations 6.7, 6.8, 6.9 of Appendix A it was shown that the "intrinsic propagation constant"  $p$  of the medium is given by:

$$p^2 = j \omega \mu (\sigma + j \omega \epsilon) \quad (6.3.4.1.12)$$

If  $\alpha$  is the attenuation/metre and  $\beta$  the phase change/metre then:

$p = \alpha + j \beta$  and, by separating real and imaginary parts,

$$\alpha^2 = \frac{1}{2} \omega \mu \left( (\sigma^2 + \omega^2 \epsilon^2)^{\frac{1}{2}} - \omega \epsilon \right) \quad (6.3.4.1.13)$$

$$\beta^2 = \frac{1}{2} \omega \mu \left( (\sigma^2 + \omega^2 \epsilon^2)^{\frac{1}{2}} + \omega \epsilon \right) \quad (6.3.4.1.14)$$

Thus for a non-conducting medium  $\sigma = 0$

$$\alpha = 0 \quad (6.3.4.1.15)$$

and  $\beta^2 = \frac{1}{2} \omega \mu (2 \omega \epsilon)$

$$= \omega^2 \mu \epsilon$$

and  $\beta = \omega (\mu \epsilon)^{\frac{1}{2}} \quad (6.3.4.1.16)$

For a conducting medium where  $\sigma$  is much greater than  $\omega \epsilon$ :

$$\alpha = \left( \frac{1}{2} \omega \mu \sigma \right)^{\frac{1}{2}} \text{ nepers/metre.} \quad (6.3.4.1.17)$$

$$= 8.686 \left( \frac{1}{2} \omega \mu \sigma \right)^{\frac{1}{2}} = 6.14 (\omega \mu \sigma)^{\frac{1}{2}} \text{ db/metre.}$$

$$\beta = \left( \frac{1}{2} \omega \mu \sigma \right)^{\frac{1}{2}} \text{ radians/metre.} \quad (6.3.4.1.18)$$

(a) For the case where  $\sigma = 0$ .

Since the medium is non-conducting the intrinsic propagation constant,  $p$ , from eqn. (6.3.4.1.16) is given by:

$$p = j \omega (\mu \epsilon)^{\frac{1}{2}} \quad (6.3.4.1.19)$$

The component of the propagation constant parallel to the interface is proportional to  $\sin \theta$ . Now, to satisfy the boundary conditions at the interface the movement of wave crests on both sides of the interface must be the same.<sup>(5)</sup> Therefore the component of  $p$  parallel to the interface must be the same in medium 1 and 2 giving, from eqn. (6.3.4.1.19),  $(\mu_1 \epsilon_1)^{\frac{1}{2}} \sin \theta_1 = (\mu_2 \epsilon_2)^{\frac{1}{2}} \sin \theta_2$ .

This is Snell's law (also used in Chapter 2) and defines the angle of refraction,  $\theta_2$ . (6.3.4.1.20)

There will be no reflected wave when: <sup>(6)</sup>

$$Z_{fi} = Z_{ft}$$

i.e.  $Z_1 \cos \theta = Z_2 \cos \theta_2$

i.e.  $\left( \frac{\mu_1}{\epsilon_1} \right)^{\frac{1}{2}} \cos \theta_1 = \left( \frac{\mu_2}{\epsilon_2} \right)^{\frac{1}{2}} \cos \theta_2$  from eqn. (6.3.4.1.7)

But  $(\mu_1 \epsilon_1)^{\frac{1}{2}} \sin \theta_1 = (\mu_2 \epsilon_2)^{\frac{1}{2}} \sin \theta_2$  from eqn. (6.3.4.1.20)

$$\text{i.e. } \frac{\tan \theta_1}{(\epsilon_1/\epsilon_2)} = \frac{\tan \theta_2}{(\epsilon_1/\epsilon_2)^{\frac{1}{2}}} = \left( \frac{\mu_2 \epsilon_1 - \mu_1 \epsilon_2}{\mu_1 \epsilon_1 - \mu_2 \epsilon_2} \right)^{\frac{1}{2}} \quad (6.3.4.1.21)$$

This defines the angle  $\theta_1$ , the Brewster angle, at which there is zero reflection.

As  $\theta_1$  changes from  $0^\circ$  to  $90^\circ$  it is seen from equation (6.3.4.1.3) that  $Z_{ft}$  changes from  $Z_1$  (the intrinsic impedance) to zero.  $Z_{ft}$  is obtained in terms of  $\theta_1$  by substituting for  $\theta_2$  from eqn. (6.3.4.1.20) thus:

$$\begin{aligned} Z_{ft} &= Z_2 \cos \theta_2 = \left( \frac{\mu_2}{\epsilon_2} \right)^{\frac{1}{2}} \left( 1 - \frac{\mu_1 \epsilon_1}{\mu_2 \epsilon_2} \sin^2 \theta_1 \right)^{\frac{1}{2}} \\ &= \frac{1}{\epsilon_2} (\mu_2 \epsilon_2 - \mu_1 \epsilon_1 \sin^2 \theta_1)^{\frac{1}{2}} \end{aligned} \quad (6.3.4.1.22)$$

If  $\mu_1 \epsilon_1$  is less than  $\mu_2 \epsilon_1$ ,  $Z_{ft}$  is real i.e. resistive for all angles of  $\theta_1$ .

If  $\mu_1 \epsilon_1$  is greater than  $\mu_2 \epsilon_1$ ,  $Z_{ft}$  changes abruptly from a pure resistance to a pure capacitive reactance at the angle which satisfies the equation  $\mu_2 \epsilon_2 = \mu_1 \epsilon_1 \sin^2 \theta_1$ . (6.3.4.1.23)

At this value of  $\theta_1$  (called the critical angle of incidence)  $\theta_2 = 90^\circ$ .

For values of  $\theta_1$  greater than the critical angle the condition is as though the transmission line in Fig. F 6.3.4.1.2 were terminated with a pure reactance: reflection is therefore total. The phase of the reflected wave relative to the incident wave is governed by the field impedances and varies from  $0^\circ$  at the critical angle to  $180^\circ$  when  $\theta_1 = 90^\circ$ .

Care must be taken not to confuse the critical angle (eqn. 6.3.4.1.23) with the Brewster angle (eqn. 6.3.4.1.21)

(b) For the case where  $\sigma$  is not zero.

(b i) If the reflecting plane is a perfect conductor.

Since  $\sigma$  is infinitely large then, from equations 6.3.4.1.9/11/17/18,

$$R_m = X_m = 0; f_t \text{ is infinite; } \alpha \text{ is infinite; } \beta \text{ is infinite.}$$

Reflection is complete at zero phase angle at all values of  $\theta_1$  from  $0^\circ$  to  $90^\circ$ . This yields polar diagrams such as fig. F.6.3.3.1 and fig. F. 6.3.4.1.3 (curve "a").

(b ii.) If the reflecting plane is sea water.

Here:  $\sigma_2 = 4 \text{ mhos/metre.}$

$$\mu_2 = \mu_0 = 4 \pi \times 10^{-7} \text{ H/metre.}$$

$$\epsilon_2 = 81 \epsilon = 81/36 \pi \times 10^9 \text{ Farads/metre.}$$

From equation (6.3.4.1.11)

$$f_t = \frac{\sigma_2}{2 \pi \epsilon_2} = 890 \text{ Mc/s.}$$

At H.F., therefore, sea water behaves as a good conductor and from eqns. (6.3.4.1.9/10) for  $f = 21.47 \text{ Mc/s}$

$$R = \left( \frac{\omega \mu}{2 \sigma} \right)^{\frac{1}{2}}$$

$$= 4.6 + j 4.6$$

$$(6.3.4.1.24)$$

From eqn. 6.3.4.1.1 the magnitude of the reflection co-efficient is given by:

$$\frac{H_r}{H_i} = \frac{Z_1 - Z_2}{Z_1 + Z_2} \text{ for } \theta_1 = 0 \quad (6.3.4.1.25)$$

$$\text{or } \frac{H_r}{H_i} = \frac{Z_{fi} - Z_{ft}}{Z_{fi} + Z_{ft}} \text{ for } \theta_1 \text{ greater than } 0 \quad (6.3.4.1.26)$$

$$\text{where } Z_{fi} = Z_1 \cos \theta_1 = 377 \cos \theta_1$$

$$\begin{aligned} \text{and } Z_{ft} &= 4.6 + j 4.6 \\ &= 1.42 \times 4.6 \text{ angle } 45^\circ. \end{aligned}$$

Matching between  $Z_{fi}$  and  $Z_{ft}$  is best at that angle  $\theta_1$  where

$$377 \cos \theta_1 = 1.42 \times 4.6$$

$$\text{i.e. } \theta_1 = 89^\circ; \text{ i.e. } \Delta = 1^\circ.$$

At this angle the reflection coefficient passes through a minimum value  $= 1.42 - 1 = .42$  of phase angle  $90^\circ$ . It is not the true Brewster angle defined (when  $\sigma = 0$ ) in equation (6.3.4.1.21) because it does not pass through a value of zero. It is better referred to as the "pseudo Brewster angle".

From the discussion following eqn. (6.3.4.1.22) there is no critical angle in this case because  $\mu_1 \epsilon_1$  is less than  $\mu_2 \epsilon_2$ .

For values of  $\theta_1$  less than the pseudo Brewster angle  $Z_{fi}$  increases due to the  $\cos \theta_1$  term until at  $\theta = 0$ ,  $Z_{fi} = Z_1 = 377$  ohms.

At  $\theta = 0$  the reflection coefficient is

$$\frac{377 - 4.6 - j 4.6}{377 + 4.6 + j 4.6} = 0.98 \text{ (approx).}$$

with reflected and incident waves almost in phase.

For values of  $\theta_1$  greater than the pseudo Brewster angle  $Z_{fi}$  decreases until, at  $\theta_1 = 90^\circ$ ,  $Z_{fi} = 0$  and the reflection coefficient  $= -1$  implying that the phase angle between reflected and incident waves changes from  $90^\circ$  at the pseudo Brewster angle to  $180^\circ$  at  $\theta_1 = 90^\circ$ . Thus there is complete cancellation of the two waves at  $\theta_1 = 90^\circ$  i.e. at  $\Delta = 0^\circ$ .

At  $\theta_1 = 89^\circ$  the combined field will have magnitude  $H_i (1 + 0.42^2)^{\frac{1}{2}} = 1.082 H_i$  where the phase angle between incident and reflected wave is  $90^\circ$ .

$$\text{The polar diagram } E = K \frac{\cos(\frac{\pi}{2} \cos \theta)}{\sin \theta} = f(\theta)$$

given in Appendix A eqn. (11.5 A) is therefore modified, in the case of a vertical dipole (or monopole) situated above an imperfect earth, because of the variation of the magnitude and phase of the reflection co-efficient.

From equation 8.3.3.1.1.26 it is clear that for values of  $\theta$  less than the pseudo Brewster angle the phase angle between the incident and reflected waves falls rapidly and it may be taken that the two waves are nearly in phase from  $\theta = 80^\circ$  to  $\theta = 0^\circ$ . For this range of angles we may say that the combined field strength  $H = H_0 (1 + R_v \exp.(-j\phi))$  when  $R_v$  is the reflection coefficient for vertical polarization and  $\phi$  represents the phase difference in radians between direct and reflected rays due to the difference in the path lengths.  $H_0$ ,  $R_v$ , and  $\phi$  are all functions of  $\theta_1$ . Therefore, the value of  $\theta_1$  at which  $H$  is a maximum could be found from the equation:

$$\frac{dH}{d\theta} = 0.$$

The reflection coefficients for various values of  $\theta$  have been calculated and are given in the table below.

From Snell's Law, substituting in equation 6.3.4.1.20 yields  
 $\sin \theta_1 = 9 \sin \theta_2$

$\theta_1$	$\theta_2$	$Z_{ft} = Z_2 \cos \theta_2$ (field impedance of sea water)	$Z_{fi} = Z_1 \cos \theta_1$ (field impedance of air)	$R_v$ (reflection coefficient)	Polar diagram Factor.
0	0	4.6 + j 4.6	377	0.98	0.99
10	1°6'	4.6 + j 4.6	371	0.98	0.99
20	2°11'	4.6 + j 4.6	354	0.97	0.98
30	3°11'	4.6 + j 4.6	327	0.97	0.98
40	4°6'	4.6 + j 4.6	289	0.97	0.98
50	4°53'	4.6 + j 4.6	242	0.96	0.98
60	5°31'	4.6 + j 4.6	189	0.95	0.97
70	6°1'	4.5 + j 4.5	129	0.93/5°	0.97
80	6°17'	4.5 + j 4.5	65	0.58/1°	0.94
85	6°21'	4.5 + j 4.5	33	0.77/16°	0.88
90	6°23'	4.5 + j 4.5	0	1.0/180°	0.0

TABLE T. 6.3.4.1.1

The phase change  $\phi$  due to the difference in length between direct and reflected waves is negligible at the low angles in which we are interested (being about  $0.4^\circ$  at  $\Delta_1 = 10^\circ$ ) and therefore  $\phi$  has been neglected in the polar diagrams of figure F.6.3.4.1.3

(b iii) If reflecting plane is land of heavy clay soil.

In such land the constants may be taken as: <sup>(8)</sup>

$$\sigma_2 = 4 \times 10^3 \text{ rho/metre}$$

$$\mu_2 = \mu_0 = 4 \pi \times 10^7 \text{ Henrys/metre.}$$

$$\epsilon_2 = 13 \epsilon_0 = 13/36 \pi \times 10^9 \text{ Farads/metre.}$$

From equation (8.3.5.1.16)

$$f_t = \frac{\sigma_2}{2 \pi \epsilon_2} = 5.5 \times 10^6 = 5.5 \text{ Mc/s.}$$

At 21.47 Mc/s, therefore, the reflecting plane acts as a pure dielectric of intrinsic resistance  $Z_2$  given by eqn. 6.3.4.1.7 as

$$Z_2 = \left(\frac{\mu}{\epsilon}\right)^{\frac{1}{2}} = 104.5 \text{ ohms.}$$

From equations 6.3.4.1.5./22 the field impedance of the earth,  $Z_{ft}$ , is given by:

$$\begin{aligned} Z_{ft} &= Z_2 \cos \theta_2 \\ &= \frac{1}{\epsilon_2} (\mu_2 \epsilon_2 - \mu_1 \epsilon_1 \sin^2 \theta_1)^{\frac{1}{2}} \end{aligned}$$

$$\text{Since } \mu_2 \epsilon_2 = 14.4 \times 10^{17} \text{ and } \mu_1 \epsilon_1 = 1.11 \times 10^{17}$$

i.e. since  $\mu_2 \epsilon_2$  is greater than  $\mu_1 \epsilon_1$ ,  $Z_{ft}$  is real, i.e. resistive, for all values of  $\theta_1$ , from  $0^\circ$  to  $90^\circ$ .

$$Z_{ft} = \frac{36 \pi}{13} (144 - 11.1 \sin^2 \theta_1)^{\frac{1}{2}} \quad (6.3.4.1.27)$$

From equation 6.3.4.1.3 :

$$Z_{fi} = Z_1 \cos \theta_1 = 377 \cos \theta_1 \quad (6.3.4.1.28)$$

and the reflection coefficient  $R_v$  is given by:

$$R_v = \frac{Z_{fi} - Z_{ft}}{Z_{fi} + Z_{ft}} \quad (6.3.4.1.29)$$

From equation 6.3.4.1.21 it is seen that the reflection coefficient passes through zero at the angle  $\theta_1$  given by:

$$\frac{\tan^2 \theta_1}{(\epsilon_2 / \epsilon_1)} = \frac{\mu_2 \epsilon_1 - \mu_1 \epsilon_2}{\mu_1 \epsilon_1 - \mu_2 \epsilon_2}$$

Substituting values, R.H. S. = 1

$$\text{Therefore } \tan^2 \theta_1 = \frac{\epsilon_2}{\epsilon_1} = 13.$$

$$\text{and } \tan \theta_1 = 3.61$$

Therefore the brewster angle occurs at  $\theta_1 = 74^\circ 31'$ .

The incident and reflected waves may be assumed to be in phase from  $\theta = 0$  to  $\theta = 70^\circ$  approx., in quadrature at  $\theta = 74^\circ 31'$ , and in antiphase from  $80^\circ$  (approx.) to  $90^\circ$ . The magnitude of the reflection coefficient for various value of  $\theta_1$  is found by combining equations (6.3.4.1.27/28/29) for various values of  $\theta_1$ . Typical results are given in Table T. 6.3.4.1.2 which follows.



$\theta_1$	$Z_{ft}$ (field impedance of earth)	$Z_{fi}$ (field impedance of air)	$R_v$ (reflection coeff.)	Polar diagram Factor.
0	105	377	0.56	0.78
10	104	371	0.56	0.78
20	104	354	0.54	0.77
30	103	327	0.52	0.76
40	103	289	0.47	0.74
50	102	242	0.41	0.71
60	101	189	0.30	0.65
70	101	129	0.12	0.56
74° 31'	100	100	0.00	0.50
80	100	65	-0.21	0.40
90	100	0	-1.00	0.00

TABLE T.6.3.4.1.2

The reflection coefficient ( $R_v$ ) is calculated as though a line of characteristic impedance =  $Z_{fi}$  was terminated by a resistance =  $Z_{ft}$ .

(b iv) If the reflecting plane is a metallic grid of wires.

Suppose that a grid of copper wires is laid on the ground studied in (b iii). Suppose that the wire radius,  $a$ , is much smaller than the spacing,  $d$ , and that  $d$  is less than  $\lambda$ .

Macfarlane<sup>(213)</sup> and Booker<sup>(5)</sup> indicate that wires lying at right angles to the electric vector behave as a capacitive shunt of high reactance and therefore produce negligible effect. The wires lying parallel to the electric vector form an inductive shunt of low reactance,  $X_2$ , given by the equation<sup>(5)</sup>

$$X_2 = 377(d/\lambda) \log_e \frac{d}{2\pi a} \quad (6.3.4.1.30)$$

If  $d = 0.028 \lambda$  and  $a = 9.3 \times 10^{-5} \lambda$  at 21.47 Mc/s ( $12\frac{1}{2}$  S W G copper at 15" centres), then

$$X_2 = 41 \text{ ohms; } R_2 \text{ is negligibly small.}^{(5)}$$

If the plane wave is incident normally on the grating, with the electric vector parallel to the wires, the grating behaves as a reactance of 41 ohms connected across a 377 ohm "transmission line" at the point where the transmission line is terminated in a resistance of 105 ohms assuming the earth to be the same as that investigated in (b iii). The behaviour is as though the transmission line were terminated by an impedance of  $(13.9 + j 35.6)$  ohms. The reflection properties of this grating may be analysed as follows:

Assume in equation 6.3.4.5 that, because<sup>(5)</sup> of the fairly high conductivity of  $Z_2$ ,  $\theta_2 = 0^\circ$ , then

$$Z_{ft} = Z_2 = 13.9 + j 35.6.$$

From eqn. 6.3.4.1.3  $Z_{fi} = Z_1 \cos \theta_1$ .

Optimum matching occurs at the value of  $\theta_1$  which satisfies the equation

$$Z_1 \cos \theta_1 = \text{modulus of } Z_2$$

$$\text{i.e. where } 377 \cos \theta_1 = 38.2$$

$$\theta_1 = 84^\circ 12' \text{ is the pseudo Brewster angle.}$$

At this angle the reflection coefficient,  $R_v$ , is given by:

$$R_v = \frac{377 \cos \theta_1 - 13.9 - j 35.6}{377 \cos \theta_1 + 13.9 + j 35.6}$$

$$= .68, \text{ angle } 90^\circ$$

Similarly  $R_v$  is calculated for other values of  $\theta_1$  and the results are summarised in Table T. 6.3.4.1.3 below.

If the spacing between the  $12\frac{1}{2}$  S W G copper wires of the grating is now made  $7\frac{1}{2}$ " instead of 15", the effective impedance ( $Z_2$ ) terminating the  $(377 \cos \theta_1)$  ohms transmission line will be a reactance of 16.7 ohms in parallel with a resistance of 105 ohms, i.e.  $Z_2 = 2.59 + j 16.3$ . The reflection properties of this grating may be analysed as follows:

Assume, in equation 6.3.4.1.5, that  $\theta = 0$ , then

$$Z_{ft} = Z_2 = 2.59 + j 16.3 \text{ ohms.}$$

$$\text{From eqn. 6.3.4.1.3, } Z_{fi} = Z_1 \cos \theta_1$$

The pseudo Brewster angle is that value of  $\theta_1$  which satisfies the condition for optimum match between  $Z_{ft}$  and  $Z_{fi}$  i.e. when

$$Z_1 \cos \theta = \text{modulus of } Z_2$$

$$377 \cos \theta_1 = 16.5$$

$$\text{i.e. when } \theta_1 = 87^\circ 30'$$

$$\text{At this angle, } R_v = \frac{377 \cos \theta_1 - 2.59 - j 16.3}{377 \cos \theta_1 + 2.59 + j 16.3}$$

$$= 0.854 \text{ angle } 90^\circ$$

Similarly  $R_v$  is calculated for other values of  $\theta_1$  and the results are summarised in Table T. 6.3.4.1.3 below.

For a grating of 12" spacing  $X_2$ , from eqn. 6.3.4.1.30,

is given by

$$X_2 = \frac{377}{42} \times 3.643 = 32.7 \text{ ohms.}$$

In this case the  $(377 \cos \theta_1)$  ohm transmission line is terminated by a reactance of 32.7 ohms in parallel with a resistance of 105 ohms. i.e.  $Z_2 = 9.5 + j 30.2$ . As before the pseudo Brewster angle is that value of  $\theta_1$  which satisfies the equation

$$Z_1 \cos \theta_1 = \text{modulus of } Z_2$$

$$\text{i.e. } 377 \cos \theta_1 = 31.6$$

$$\text{and } \theta_1 = 85^\circ 12'$$

At this angle  $R_v$  is given by the equation:

$$R_v = \frac{377 \cos \theta_1 - 9.5 - j 30.2}{377 \cos \theta_1 + 9.5 + j 30.2}$$

$$= 0.736 \text{ angle } 90^\circ$$

Similarly  $R_v$  is calculated for other values of  $\theta_1$  and the results are summarised in Table T. 6.3.4.1.3 below.

$\theta_1$	Reflection coefficient for grating of $12\frac{1}{2}$ SWG copper laid on ground *		
	0.027 $\lambda$ (15") spacing.	0.022 $\lambda$ (12") spacing	0.014 $\lambda$ ( $7\frac{1}{2}$ ") spacing.
0	0.930 angle $10^\circ 30'$	0.950/ $9^\circ 9'$	0.986/ $5^\circ 6'$
20	0.925 angle $11^\circ 32'$	0.946/ $9^\circ 46'$	0.986/ $5^\circ 9'$
40	0.910 angle $14^\circ 6'$	0.937/ $12^\circ 0'$	0.986/ $6^\circ 28'$
60	0.863 angle $21^\circ 36'$	0.910/ $18^\circ 50'$	0.972/ $9^\circ 34'$
80	0.717 angle $58^\circ 38'$	0.790/ $50^\circ 12'$	0.930/ $28^\circ 1'$
$84^\circ 12'$	0.680 angle $90^\circ$		
35			0.877/ $53^\circ 0'$
$85^\circ 12'$		0.736/ $90^\circ$	
$87^\circ 30'$			0.854/ $90^\circ$
90	1.0 angle $180^\circ$	1.0/ $180^\circ$	1.0/ $180^\circ$

\* The ground constants assumed are as in b(iii) above.

TABLE T. 6.3.4.1.3.

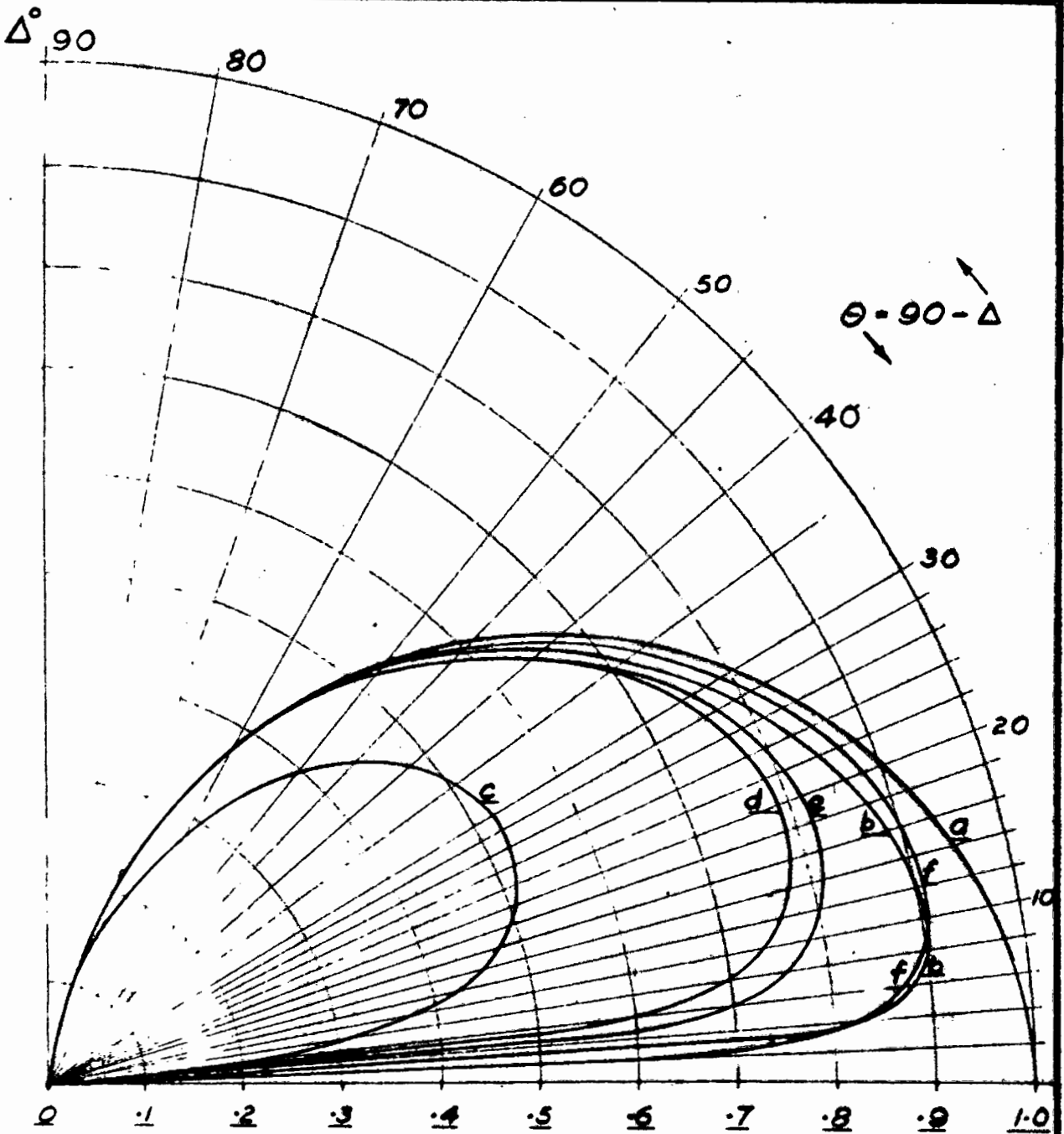
Curves d,e,f in Figure 6.3.4.1.3 represent the calculated vertical polar diagram of a  $\frac{1}{4} \lambda$  vertical grounded monopole above a grid of  $12\frac{1}{2}$  SWG copper wires spaced 15", 12", and  $7\frac{1}{2}$ " respectively at 21.47 Mc/s. These gratings are called type "d", "e" and "f" respectively. If the polar diagram of any grounded, vertically-polarized, antenna is known for a reflecting plane of perfect conductivity then its vertical polar diagram when placed above an imperfectly conducting plane may be plotted by the use of fig. F 6.3.4.1.3.

e.g. Suppose the reflecting plane is land in which  $\epsilon = 13 \epsilon_0$ ,  $\sigma = 4 \times 10^{-3}$  mho/metre, covered by a grating of  $12\frac{1}{2}$  SWG parallel copper wires of 12" spacing pointing in the direction of the distant station and suppose that the vertically polarized antenna is operating on 21.47 Mc/s. Then at  $\Delta = 20^\circ$  i.e.  $\theta = 70^\circ$  the polar diagram of the antenna with perfectly conducting reflecting plane must be multiplied by a factor (see curves "e" and "a" in fig. F.6.3.4.1.3) of  $.81/.90 = .90$ . Similarly for other values of  $\Delta$  the polar diagram is multiplied by the ratio of curve "e" to curve "a".

Other types of reflecting plane may be dealt with in the same way.

It having been decided to sharpen the polar diagram of a  $\lambda/4$  vertical grounded monopole by the use of parasitic elements, the next step is to design such an arrangement which, in conjunction with a ground plane of the type studied in this Chapter, will match up to the specification laid down in section 6.1.

---



DERIVED VERTICAL POLAR DIAGRAMS AT 21.47 Mc/s.

Grounded quarter wave monopole on :

- |   |           |                      |
|---|-----------|----------------------|
| 1. ground of infinite conductivity          | (curve a) | as in fig F 6.3.3.1. |
| 2. sea water                                | (curve b) |                      |
| 3. heavy clay soil                          | (curve c) |                      |
| 4. grid of 15" spacing on "3"               | (curve d) |                      |
| 5. grid of 12" spacing on "3"               | (curve e) |                      |
| 6. grid of 7 $\frac{1}{2}$ " spacing on "3" | (curve f) |                      |

Fig. F 6.3.4.1.3

CHAPTER 7.

THE PARASITIC ANTENNA.

7. 0 SUMMARY OF THIS CHAPTER.

- (a) The theory of parasitic action (E.M.F.method) of a Yagi array is given and the behaviour of one parasitic element plus a radiating element is summarized graphically, following Walkinshaw<sup>(2)</sup>.
- (b) A modern theory (travelling wave method) of the Yagi as proposed by Spector<sup>(209)</sup>, explains that the directors reduce the phase velocity of the wave travelling along the array and it passes through a region of refractive index greater than unity. This index may be adjusted by altering the length and spacing of the directors so that the structure behaves as a convergent lens. It is shown why the self-reactance of a director must be capacitive and that of a reflector inductive. It is also shown that radiation occurs at the discontinuity i.e. at the director farthest from the driven element. Curves are quoted from Spector<sup>(209)</sup> relating beam width, percentage reduction of phase velocity, rod length, and array length. The results are compared with measurements taken by Fishenden and Wiblin.<sup>(27)</sup>
- (c) The optimum phase velocity is derived by Reid's<sup>(3)</sup> method.
- (d) Using this Yagi theory as a guide, a design is proposed which departs from the Yagi arrangement in that (i) the reflector and directors are planted in the earth but insulated electrically from it and (ii) it is proposed, by scale model experiments, to vary both the spacing and the length of the parasitic elements to produce maximum gain. Such an antenna appears to be new to the literature.

### 7.0.1 General.

It is hoped to sharpen the polar diagram of the  $\lambda/4$  vertical antenna, so that maximum sensitivity will occur at  $\Delta = 8^\circ$  (falling away rapidly at angles above  $\Delta = 10^\circ$  and below  $\Delta = 6^\circ$ ) by an end-fire arrangement of parasitic elements. The proposed arrangement will not be a Yagi antenna, but, as parasitic action has been fairly deeply studied in connection with the famous Yagi antenna, it is proposed to approach the theory of the proposed array by first looking into the theory of the Yagi antenna.

### 7.1 The theory of parasitic action. (E M F method).

The literature on this subject is not very extensive but helpful information is to be found in references (1), (2), (3), (7), (8), (24), (25), (26), (27), (28), (29), (30), (31) and (32).

In an infinitely thin conducting wire the current distribution set up by impressed forces is sinusoidal<sup>(1),(2)</sup>. Suppose that in a Yagi arrangement the "reflector" element is number "1", the "driven" element is number "2", the "director" elements are numbers "3", "4", "5", ....etc., the spacings are  $d_{12}$ ,  $d_{23}$ ,  $d_{34}$ ,  $d_{45}$ , etc., the mutual impedances are  $Z_{12}$ ,  $Z_{13}$ ,  $Z_{23}$ ,  $Z_{24}$ , ....etc., and the self impedances are  $Z_{11}$ ,  $Z_{22}$ ,  $Z_{33}$ ,  $Z_{44}$ ,  $Z_{55}$ , .....etc. If each element were approximately  $\lambda/2$  long the mutual impedances could be obtained from Fig. F.7.1.1.<sup>(8)</sup> If the driving voltage, i.e. the voltage applied at the input of element "2" is  $V_2$  the following mesh equations obtain:

$$Z_{11} I_1 + Z_{12} I_2 + Z_{13} I_3 + \dots = 0 \quad (7.1.1).$$

$$Z_{12} I_1 + Z_{22} I_2 + Z_{23} I_3 + \dots = V_2 \quad (7.1.2).$$

$$Z_{13} I_1 + Z_{23} I_2 + Z_{33} I_3 + \dots = 0 \quad (7.1.3).$$

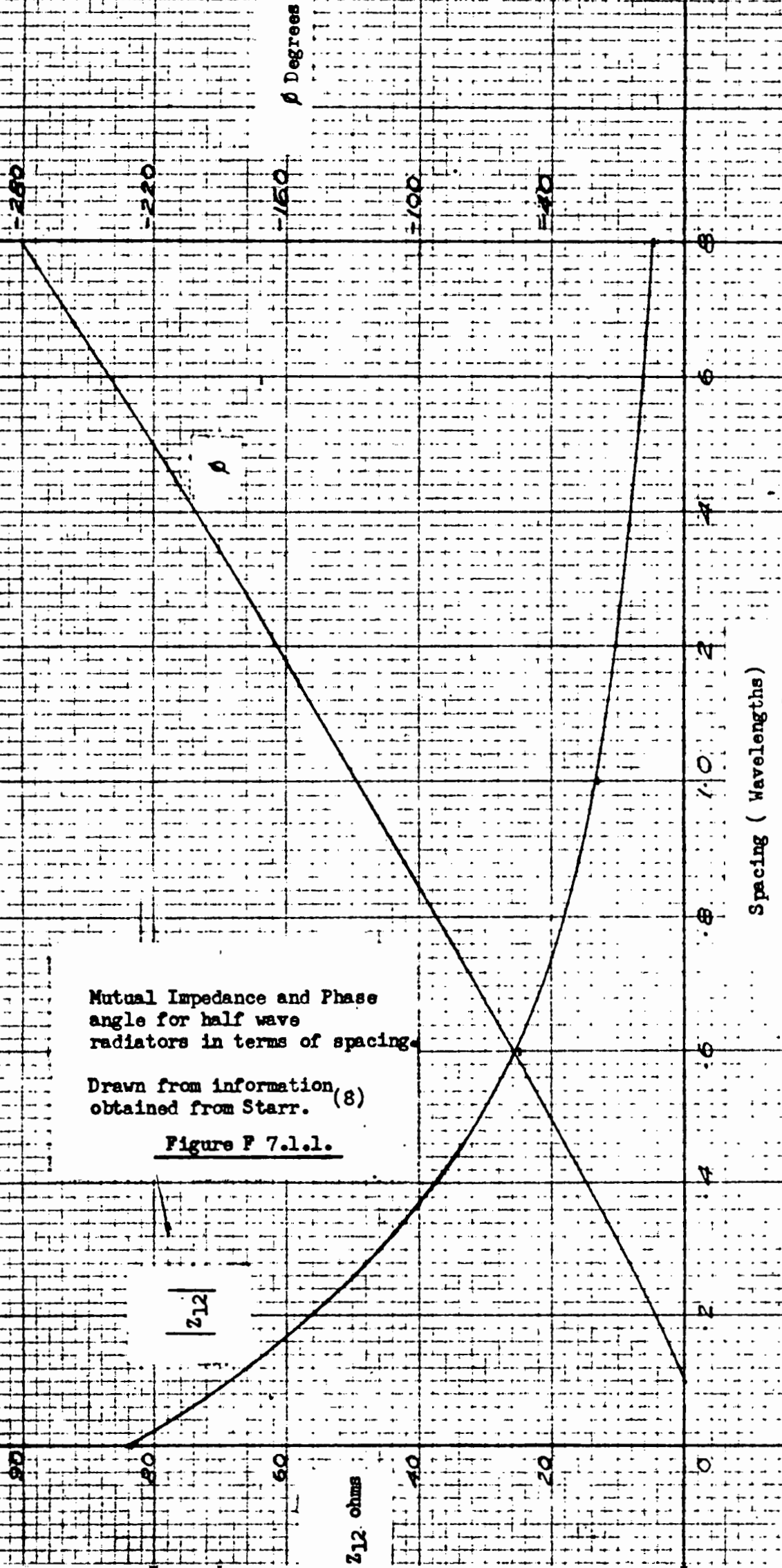
$$Z_{14} I_1 + Z_{24} I_2 + Z_{34} I_3 + \dots = 0 \quad (7.1.4).$$

etc., to equation 7.1.(n - 1) for n elements.

The (n - 1) simultaneous complex equations are best treated by separating real from imaginary parts to form 2(n-1) homogeneous equations.

The input impedance of element "2" is the load presented to the feeder and is  $\frac{V_2}{I_2}$ .

The calculations become very complicated when a large number of elements is involved. Several specific combinations have been worked out by the mathematical group under Dr. H. G. Booker.



Mutual Impedance and Phase angle for half wave radiators in terms of spacing.

Drawn from information obtained from Starr. (8)

Figure P 7.1.1.



Walkinshaw<sup>(2)</sup> has referred to the use for this purpose of a machine designed by Professor Mallock<sup>(34)</sup>. When the  $2(n-1)$  equations have been solved for  $I_s$ , the antenna, if regarded as a linear array of equispaced half wave radiators, will have a polar diagram found from a formula given by Shelkunoff<sup>(1)</sup> (and poorly quoted by Walkinshaw<sup>(2)</sup>) giving the polar function as

$$F(\theta, \phi) = \frac{\cos\left(\frac{\pi}{2} \cos \theta\right)}{\sin \theta} \left| \sum_{s=0}^{n-1} \frac{I_s}{I_2} e^{-j s \beta d \cos \phi} \right| \quad (7.1.5).$$

where  $\phi$  = angle between line of centres of elements, and direction of radiation.

$\theta$  = angle between any element and direction of radiation.

$d$  = spacing between element<sup>s</sup> and the driver.

$\beta = 2 \pi / \lambda$ .

$n$  = number of radiators.

$I_s / I_2$  = ratio of current in the  $s^{\text{th}}$  element to that of the 2<sup>nd</sup> (or driver) element.

Comparing equation (7.1.5) with Appendix A equation (11.5) the first term is clearly the polar diagram of a half wave radiator and the modulus term is the summation at the field point, P, taking account of phase, of all the contributions made by the individual elements, referred to the driven element " $s = 2$ ".  $F(\theta, \phi)$  is the ratio of the field of the Yagi to the field (in the equatorial plane) of a half wave dipole whose feed current is equal to  $I_2$ .

The ratio of the field of the Yagi to that of a half wave dipole of radiation resistance  $R_o$ , radiating the same power

$$= (R_o / R)^{\frac{1}{2}} F(\theta, \phi) \quad (7.1.6).$$

where  $R$  = input resistance to driven element of the Yagi.

The power gain of a Yagi over a half wave dipole is given by:

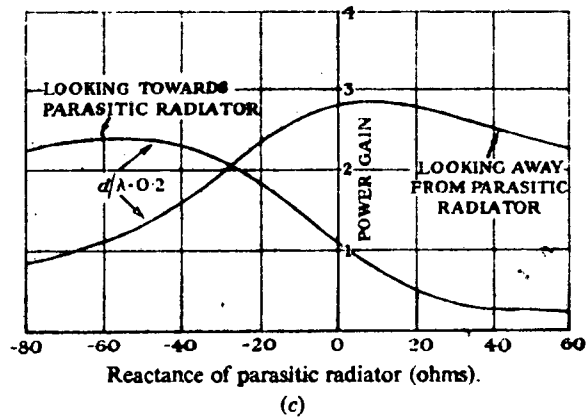
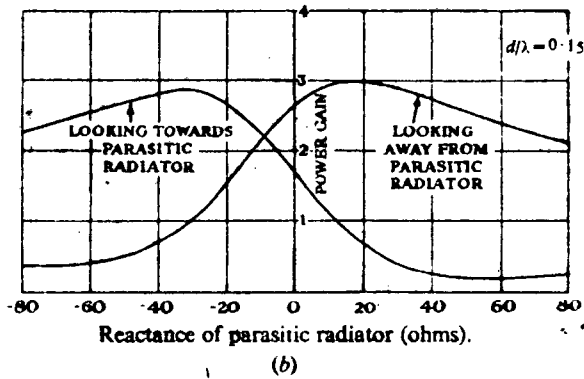
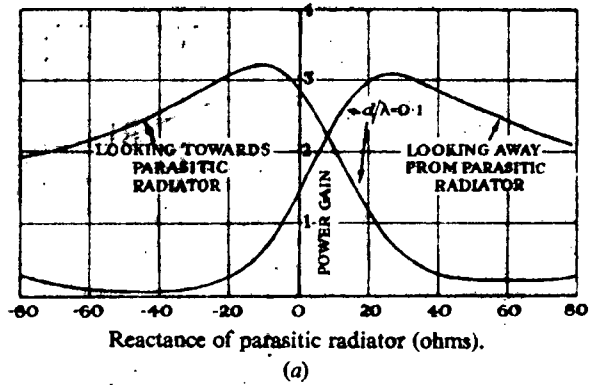
$$G_H = \frac{R_o}{R} \left| \sum_{s=0}^{n-1} \frac{I_s}{I_2} e^{+j s \beta d} \right|^2 \quad (7.1.7).$$

in the forward ( $-j$ ) and backward ( $+j$ ) directions respectively.

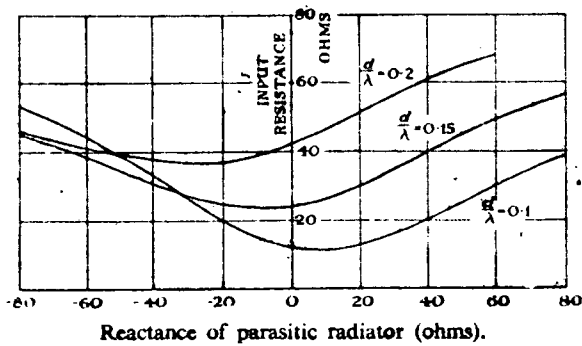
The input resistance, which is the real part of the ratio  $V_2 / I_2$ , is given by

$$R = \text{Real part of } \sum_{s=0}^{n-1} Z_{2s} \frac{I_s}{I_2} \quad (7.1.8).$$

where  $Z_{2s}$  is the mutual impedance between the driver (which is radiator no.2) and each element ( $s = 0, 3, 4, \text{etc.}$ ) and  $I_s / I_2$  is the ratio of current in each of these elements to that in the driver.



Variation of power gain with one parasitic element only.



Variation of input resistance with one parasitic radiator.

Reproduced from a paper by Walkinshaw. (2)

Figure F 7.1.2.

- Using these equations Walkinshaw<sup>(2)</sup> has calculated the behaviour of arrays of 1 to 3 parasitic elements spaced at  $0.1 \lambda$ ,  $0.15 \lambda$ ,  $0.2 \lambda$  and for 3 versions of an array of 4 parasitic elements of spacing  $0.1 \lambda$ ,  $0.2 \lambda$ ,  $0.3 \lambda$  respectively with element reactance varying from 0 to  $\pm 80$  ohms.

As an example some results of his computations, expressed in graphical form, are given in Figure F. 7.1.2. These illustrate the interdependence of parasitic reactance and element spacing.

## 7.2 A more modern theory of parasitic action (travelling wave method).

The theory presented in 7.1 has represented the classical approach for many years but the computation involved makes it of little use to the antenna designer except when only a small number of elements is to be used and Walkinshaw<sup>(2)</sup> has confined himself to this limited application.

Recently Brown and Spector<sup>(207)</sup> have taken up a suggestion made a decade ago by Smith<sup>(208)</sup> and have shown that the physical action of the directors, in a Yagi antenna, is to reduce the phase velocity of the wave travelling along the axis of the Yagi so that the wave travels through a region of refractive index greater than unity. Since the refractive index depends on the dimensions and spacing of the directors these parameters can be adjusted to make the structure behave as a convergent lens. They<sup>(207)</sup> go further and indicate that this is the mechanism by which the other end-fire antennas, such as the helix and the dielectric rod, operate too.

Spector<sup>(209)</sup> has treated an array of equispaced directors of equal lengths as a periodic structure analogous to a loaded transmission line as in Fig. F. 7.2.1.

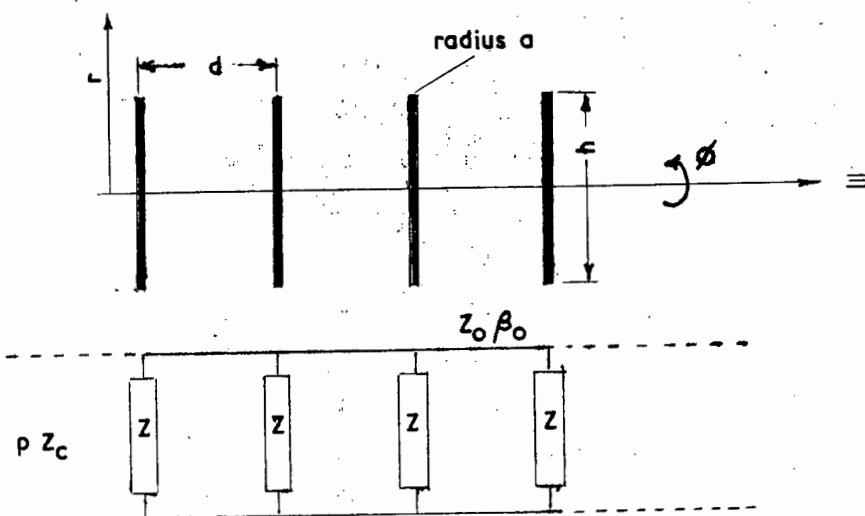


Fig. F. 7.2.1

If the "transmission line" had not been loaded, the characteristic impedance ( $Z_0$ ) and the phase-change coefficient ( $\beta_0 = 2 \pi / \lambda_0$ ) would be those corresponding to free space. The presence of directors has the effect of introducing shunt impedances,  $Z$ , at regular intervals.

The propagation coefficient ( $p = \alpha + j\beta$ ) is given by Stratton<sup>(210)</sup> in terms of the expression:

$$\cosh pd = \cos \frac{2\pi}{\lambda_0} d + j \frac{Z_0}{2Z} \sin \frac{2\pi}{\lambda_0} d. \quad (7.2.1).$$

Assuming (a) that there is no radiation from elements along the structure and (b) that losses in the director rods are negligible then  $Z$  is a pure reactance,  $jX$ , and the propagated wave will not be attenuated, giving  $p = j\beta$ . Since  $\cosh j\theta = \cos \theta$ .

$$\cosh pd = \cos \beta d = \cos \frac{2\pi d}{\lambda_g} \quad (7.2.2).$$

The phase velocity is defined by the wavelength,  $\lambda_g$ , of the guided wave which, in turn, is specified by the equation from 7.2.1/2,

$$\cos \frac{2\pi d}{\lambda_g} = \cos \frac{2\pi d}{\lambda_0} + \frac{Z_0}{2X} \sin \frac{2\pi d}{\lambda_0} \quad (7.2.3).$$

Thus  $\lambda_g$  (and hence the phase velocity) is governed by director reactance  $X$  (which depends on director dimensions) and spacing,  $d$ .

$$\text{Since } \sin \theta = \theta - \frac{\theta^3}{3!} + \frac{\theta^5}{5!} - \dots$$

$$\text{and } \cos \theta = 1 - \frac{\theta^2}{2!} + \frac{\theta^4}{4!} - \dots$$

and since  $\theta^3$  and higher powers may be neglected for small values of  $\theta$ , then, if  $d$  is small compared with  $\lambda$ , equation 7.2.3 can be rewritten:

$$1 - \frac{1}{2} \left( \frac{2\pi d}{\lambda_g} \right)^2 = 1 - \frac{1}{2} \left( \frac{2\pi d}{\lambda_0} \right)^2 + \frac{Z_0}{2X} \frac{2\pi d}{\lambda_0}$$

$$\text{thus; } \frac{Z_0}{X} \left( \frac{2\pi d}{\lambda_0} \right) - \left( \frac{2\pi d}{\lambda_0} \right)^2 + \left( \frac{2\pi d}{\lambda_g} \right)^2 = 0. \quad (7.2.4).$$

Now it must be remembered that when a wave is propagated in a transmission line the phase velocity ( $f\lambda_g$ ) is lower than the velocity of light ( $f\lambda_0$ ). Thus if transmission is to take place,  $\lambda_g$  must be less than  $\lambda_0$ , i.e. the first term in eqn.(7.2.4) must be negative, i.e.  $X$  must be capacitive. If transmission is to be prevented from taking place the first term in eqn.(7.2.4) must be positive i.e.  $X$  must be inductive. The implication is that the self reactance of a director must be capacitive and that of a reflector must be inductive.

Spector<sup>(209)</sup> has conducted an experiment at  $\lambda_0 = 10$  cm. using a surface wave resonator to measure the percentage reduction of phase velocity on periodic rod structures. Fig. 7.2.2 summarises his results for various rod lengths and spacings.

Figure F. 7.2.3 summarises another experiment carried out by Spector.<sup>(209)</sup> When the resonator contained no rods the  $Q$  factor equalled unity. When one director was used the  $Q$  factor dropped and remained low as more directors were added until, when the resonator had been filled with directors, the  $Q$  factor returned to unity. This proves that radiation only occurs from the discontinuity.

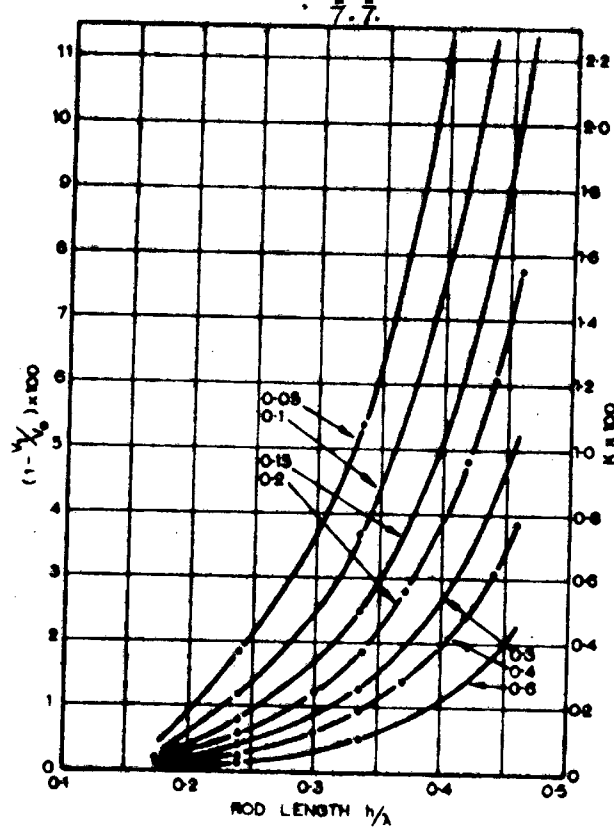


Figure F 7.2.2.

Percentage reduction of phase velocity on periodic rod structures.

The parameter is the spacing  $d/\lambda$ .  
The right-hand scale gives the constant  $K$  of eqn. (13), where  $(1 - \frac{v_1}{v_0}) = K (\lambda/d)$

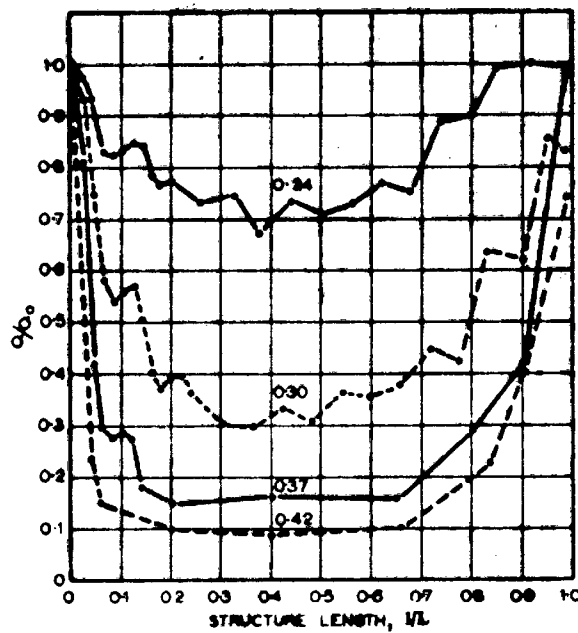


Figure F 7.2.3.

Variation of resonator Q-factor with length of rod structure.

The parameter is the rod length  $h/\lambda$ .  
The spacing is kept constant at  $d/\lambda = 0.1$ .  
 $Q_0$  is the value of the Q-factor when no rods are present.

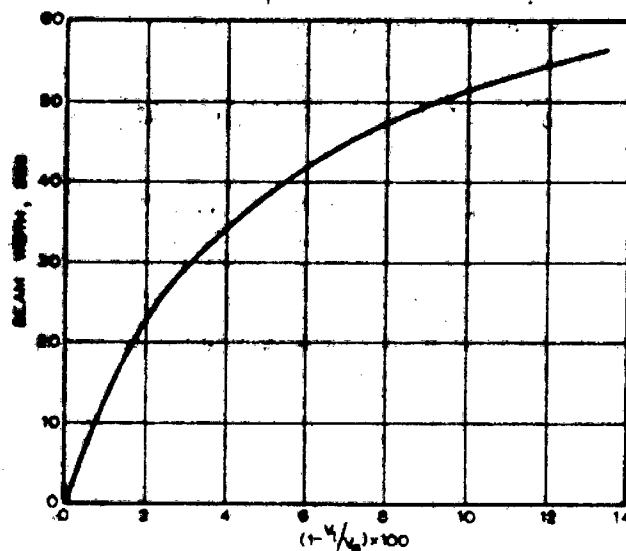


Figure F 7.2.4.

Figures F 7.2.2/3/4 reproduced from a paper by Spector (209)

Theoretical dependence of half-amplitude beam width on the percentage difference between free-space and dipole-wave phase-velocity.

The radiation mechanism of a Yagi is now seen as follows: a dipole-type wave, launched by the radiating element, is propagated along the "transmission line" formed by the directors. In the opposite direction propagation is not supported because of the positive reactance of the reflector element (see eqn. 7.2.4 and discussion immediately following it) and the energy that would have flowed in that direction is added to that which is propagated in the direction of the director elements. The reflector element therefore produces a 3 db gain. At the end of the antenna, i.e. at the last director, there is a radiating aperture which (depending on the size, spacing and number of directors) can be made large so as to give the narrow beam width usually associated with large broadside arrays.

The transverse field distribution,  $F(r, \phi)$ , see Fig. F.7.2.1, in the terminal aperture plane is given by Silver<sup>(211)</sup> as:

$$E(\theta, \alpha) =$$

$$(1 + \cos \theta) \int_0^\infty \int_0^{2\pi} F(r, \phi) \exp(j\beta_0 r \sin \theta \cos(\alpha - \phi)) r dr d\phi. \quad (7.2.5).$$

where  $\theta, \alpha$  are the polar angles and  $\beta_0 = 2\pi / \lambda_0$ .

Spector<sup>(209)</sup> has pointed out that  $\beta$  on the structure is almost the same as  $\beta_0$  and thus, in terms of cartesian co-ordinates, the field components, in a transverse plane outside a cylinder  $r = h/2$  bounding the rod structure, are given by:

$$E_x = A K_0 (k_0 r) \quad (7.2.6),$$

$$E_y = 0 \quad (7.2.7),$$

where  $k_0^2 = \beta^2 - \beta_0^2$  and  $A, K_0$  are constants. (7.2.8).

The field produced for  $r$  less than  $h/2$  is neglected compared with the remainder of the aperture.

Substituting equation 7.2.6 into 7.2.5 gives

$$E(\theta, \alpha) = 2\pi A (1 + \cos \theta) \int_{h/2}^\infty r K_0(k_0 r) J_0(\beta_0 r \sin \theta) dr. \quad (7.2.9),$$

which shows that the pattern is independent of  $\alpha$  indicating that the polar diagram in the plane of polarization will be similar to the polar diagram in the plane perpendicular to it and this is consistent with observed patterns for long arrays remote from ground.<sup>(26)</sup>

Spector<sup>(209)</sup> has integrated eqn. 7.2.9 to give: (7.2.10)

$$E(\theta) = \frac{\pi}{2} A h^2 (1 + \cos \theta) \frac{(k_0 h/2) K_1(k_0 h/2) J_0(u) - u K_0(k_0 h/2) J_1(u)}{(k_0^2 h^2/2) + u^2}$$

where  $u = \beta_0 \frac{h}{2} \sin \theta$  (7.2.11).

and  $J_0, J_1, K_0, K_1$  are constants.

He has shown that eqn. (7.2.10) can be evaluated for any given reduction in phase velocity and the corresponding half-amplitude beam width found. This results in Fig. F.7.2.4.

From figures F.7.2.2 and F.7.2.4 the performance of a long Yagi antenna can be deduced. e.g. Fishenden and Wiblin<sup>(27)</sup> measured a beam width of  $26^\circ$  for a 20-director Yagi in which the spacing was  $0.34\lambda$  and the director length  $0.407\lambda$ . From fig. F. 7.2.2 a long Yagi, using the same director length and spacing is shown to have a 2.5% reduction in phase velocity resulting, from fig. F. 7.2.4, in a  $26^\circ$  beam width. For a 10-director Yagi the measured<sup>(27)</sup> beam width was  $36^\circ$  (director length =  $0.42\lambda$  and spacing =  $0.34\lambda$ ). From figures F.7.2.2. and F 7.2.4 the expected beam width =  $30^\circ$ . Thus correlation between the theoretically derived curves and measured beam width is good for long Yagi antennas but it is not so for short antennas. In the latter case the reason for the discrepancy is that not all the power fed to the antenna is converted into the surface wave: some is radiated directly by the driven element and the combination of the two radiated fields produces a beam which may be broader (as in the above example) or a narrower beam plus side lobes.

It will be noticed in figs. F.7.2.2 and F.7.2.4 that, for a given spacing, the shorter the rod length the narrower the beam. This is because the field is more widespread about the guiding structure when short directors are used, producing a larger radiating aperture. On the other hand from fig. F.7.2.3 it will be noted that the shorter the directors the lower the launching efficiency of the surface wave resulting in greater radiation from the driven element. Clearly a compromise must be sought between these two trends and the work done by Reid<sup>(3)</sup> is a useful guide as to what the optimum director length should be.

### 7.3 Optimum phase velocity.

By postulating a theoretically idealized Yagi array, Reid<sup>(3)</sup> has derived an expression for the power gain of an end-fire array having an infinite number of very closely spaced elements, the currents in successive elements being constant in amplitude but progressively and uniformly retarded in phase.

Referring to fig. F. 7.3.1, the current flow at the origin is  $I_0 e^{j\omega t}$  and at a distance  $x$  from the origin, where  $x$  is less than  $l$ , it is:

$$I_0 e^{j(\omega t - \beta a x)} \quad (7.3.1).$$

where  $\beta = 2\pi/\lambda$

$$a = v_0/v_g$$

$v_0$  = velocity of propagation in free space.

$v_g$  = velocity of propagation along array.

The field at P may be written as:

$$F(P) = \frac{K_1}{R} \sin \Psi \Delta_y \int_{-1}^{+1} dx I_0 \exp j(\omega t - \beta a x - \beta R + \beta x \cos \theta) \quad (7.3.2).$$

where  $K_1$  is a proportionality constant and P is regarded as equidistant to each element as far as amplitude is concerned but not as regards phase.

Reid<sup>(3)</sup> goes on to perform the integration, after substituting

$$(1 - \sin^2 \theta \sin^2 \phi)^{\frac{1}{2}} \text{ for } \sin \Psi, \text{ giving:}$$

$$F(P) = \frac{2 K_1}{\beta R} \frac{\sin \frac{1}{2} \beta l (\cos \theta - a)}{\cos \theta - a} (1 - \sin^2 \theta \sin^2 \phi)^{\frac{1}{2}} I_0 \Delta_y e^{j(\omega t - \beta R)} \quad (7.3.3).$$

The field strength along the array axis, i.e. when  $\theta = 0$ , is given by:-

$$F(R, \theta = 0) = \frac{2 K_1 I_0 \Delta_y \sin \frac{\beta l}{2} (1 - a)}{\beta R (1 - a)} \quad (7.3.4).$$

Expressing equation (8.31) of Appendix A, (the field at P due to a doublet placed at 0) in terms of figure F. 7.3.1 we obtain:

$$F(R, \theta) = \frac{K_1 I_0 \Delta_y}{R} e^{j(\omega t - \beta R)} \sin \Psi$$

$$= \frac{K_1 I_0 \Delta_y}{R} e^{j(\omega t - \beta R)} (1 - \sin^2 \theta \sin^2 \phi)^{\frac{1}{2}} \quad (7.3.5).$$

and the amplitude of the field strength in the equatorial plane for the doublet is given by:

$$F(R, \theta = 0) = \frac{K_1}{R} I_0 \Delta_y \quad (7.3.6).$$

The mean radiated power for a doublet was derived in equation 10.6 of Appendix A. Expressing this in the present units the power is:

$$W_{\text{doublet}} = K_1^2 K_2 (I_0 \Delta_y)^2 \frac{8\pi}{3} \quad (7.3.7).$$

Reid<sup>(3)</sup> has shown that

$$W_{\text{array}} = K_2 \int_0^{2\pi} R d\phi \int_0^\pi R \sin \theta |F(P)|^2 d\theta$$

$$= K_1^2 K_2 \frac{4}{\beta^2} (I_0 \Delta_y)^2 \int_0^\pi \frac{(1 + \cos^2 \theta) \sin \theta \sin^2 \frac{\beta l}{2} (\cos \theta - a)}{(\cos \theta - a)^2} d\theta \quad (7.3.8).$$

$$= K_1^2 K_2 \frac{4}{\beta^2} I_0^2 \Delta_y^2 \left\{ \frac{1+a^2}{2} \left[ \frac{\cos \beta l (1-a)-1}{(1-a)} + \frac{\cos \beta l (1+a)-1}{(1+a)} \right] \right.$$

$$+ \beta l S_2 (1+a) \beta l + \beta l S_2 (1-a) \beta l \Big] + a S_1 (1-a) \beta l$$

$$\left. - a S_1 (1+a) \beta l - \frac{1}{\beta l} \sin \beta l \cos a \beta l + 1 \right\} \quad (7.3.9).$$

$$= K_1^2 K_2 \frac{4}{\beta^2} I_0^2 \Delta_y^2 \left\{ F(a, \beta l, a) \right\} \quad (7.3.10).$$

where use is made of the tabulated functions,<sup>(1)</sup>

$$S_1(x) = \int_0^x \frac{1 - \cos t}{t} dt$$

$$S_2(x) = \int_0^x \frac{\sin t}{t} dt.$$

The power gain of the idealized array over the doublet, from equations (7.3.4/6/7/9),

$$= G_R = \frac{(7.3.4)^2}{(7.3.6)^2} \times \frac{(7.3.7)}{(7.3.9)} \quad (7.3.11).$$





When Reid<sup>(3)</sup> computed this for a number of values of "a", with  $1/\lambda$  as variable, the resulting curve was of oscillatory form. The envelope represents the maximum gain that can be obtained for a given value of  $1/\lambda$ . The equation of the envelope is given by:-

$$G_H = 1.8 + 5.6 \, 1/\lambda.$$

It is not known why Reid<sup>(3)</sup> left the expression in this form. It is more useful to express gain relative to that of a free-space dipole i.e.  $G = 1.65 + 5.13 \, 1/\lambda$  (7.3.12).

and the optimum "a" value for values of  $\frac{1}{\lambda}$  down to 0.4 is given by:-

$$a = 1 + \frac{.55}{1/\lambda} \quad (7.3.13).$$

In fig. F. 7.3.2, a is plotted against  $\lambda/1$

(NOTE. (a) Reid's equation "3 A" is in error and should read:-

$$K_1 \lambda I_o \Delta_y \frac{\sin \frac{\pi}{2} (1-a)}{\pi R (1-a)}$$

and (b) the penultimate term in his eqn. "9" should be:

$$- \frac{\sin n \cos a n}{n} \quad \text{not} + \frac{\sin n \cos a n}{n}$$

These are doubtless printers errors and do not mean that his findings are suspect).

#### 7.4 The inter-dependence of theory and practice.

In the literature it is frequently admitted that in the design of the Yagi antennas the theory is useful only up to a point. Thereafter adjustment of element length and spacing must be by experiment.

e.g. Walkinshaw<sup>(2)</sup> has pointed out that since element self-reactance depends not only on its physical shape but also on the type of support, insulators, and changes of thickness at junctions, an exact determination from the theory of the element length required "is extremely difficult if not altogether impossible". In his view the theory serves "to give a sufficiently good approximation to the general behaviour to be expected.....and in suggesting in which direction adjustments should be made" (2).

Spector<sup>(209)</sup> concludes his modern theory of Yagi antennas, discussed in section 7.2, with the statement that: "The optimum construction of the aerial for best overall performance would have to be found experimentally."

The theory provides the starting point and for that reason it is vital but the final design of element number, size, and spacing, must be achieved by painstaking experiment enlightened by a firm grasp of the theory involved.

#### 7.5 Preliminary design based on the theory.

In section 3.4 it was shown that if the receiver audio output due to the signal were to be <sup>20</sup>20 db above the audio output from the noise generated in an average communication receiver the antenna gain over a free-space dipole must exceed 3.4 (5.3 db) for the particular circuit considered.

From equation 7.3.12 it is clear that a gain of this order is easily achieved even with a small parasitic antenna, but from equation 7.3.13 and figure F 7.2.4. it is clear that short Yagi arrays of optimum phase velocity produce beam widths which are too great. e.g. An array length of  $0.5 \lambda$  will have an optimum "a" value of 2.1 (eqn. 7.3.13) and a beam width of over  $60^\circ$  (figure F 7.2.4.)

Such a beam width would result in too much sensitivity to noise coming in at high wave-arrival angles. Supposing a beam width of  $25^\circ$  is desired; the percentage reduction in phase velocity, from figure F 7.2.4., needs to be 2.5%. This would, for a spacing of, say,  $0.34\lambda$ , require a rod length of  $0.41\lambda$ . (Figure F 7.2.2.) Fishenden and Wiblin's experiments<sup>(27)</sup> indicate that this beam width is obtainable from an array of 20 directors, each of length  $0.407 \lambda$  and spacing  $0.34 \lambda$ .

The array length is therefore  $20 \times 0.34\lambda = 6.8\lambda$ . Clearly a narrow beam width requires an array of great length. From equation 7.3.12 the maximum possible gain is given by

$$G = 1.65 + 5.13 \times 6.8 = 35.5 \text{ i.e. } 15.4 \text{ db.}$$

The gain measured by Fishenden and Wiblin<sup>(27)</sup> is 21, i.e. 13.2 db, and, to use their words<sup>(27)</sup> -

"It is probable that further experimental work with smaller and variable director spacings would enable a larger gain per element to be obtained."

The literature appears to contain no information of experiments in which the spacing of individual elements is varied until optimum is achieved. Likewise it appears to contain no record of experiments in which the length of individual directors is varied until optimum is achieved. Tiresome though such experiments would obviously be, it was resolved that they would be carried out in the parasitic antenna being designed.

## 7.6 Departure from the Yagi arrangement.

In section 7.5 it was seen that, if a Yagi array is to produce a narrow beam, its axial length must be large. This makes the conventional Yagi arrangement a prohibitively large structure at frequencies in the short wave band. If parasitic elements are to be used it is necessary to depart from the Yagi arrangement.

It was shown in chapter 2 that the wanted signal in the London-Salisbury circuit will arrive at an angle of  $8^\circ \pm 2^\circ$  to the horizontal and in chapter 4 that the calculated noise field strength, arriving at various values of  $\Delta$ , increases with higher values of  $\Delta$ . At the conclusion of chapter 6 it was indicated that a vertical array had good possibilities as a receiving antenna for the present purpose if only the polar diagram could be sharpened at low angles. Judging by the effect produced by a reflecting surface of finite conductivity on the polar diagram of a vertical  $\lambda/4$  antenna (see Fig. F 6.3.4.1.3., chapter 6) it is clear that a maximum at  $\Delta = 8^\circ$  may be expected for a vertically polarized antenna if a suitable reflecting plane is used.

A narrow beam, centred on this maximum, should be obtained with the use of parasitic elements.

Instead of attempting to construct a series of centrally supported directors, as in the Yagi arrangement, the earth will be used as the support, planting the directors as a series of vertical rods in line with the  $\lambda/4$  "driven" element. The term "driven" element is used in the transmitting antenna. Bearing in mind the reciprocity between transmitting and receiving antennas the term is used to designate the particular element that is physically connected to the feeder. If these director elements were earthed at the base they would form a vertically polarized Yagi antenna with the earth plane taking the place of the usual supporting rod. This arrangement was, at first, considered but it was noted that each physical director element would be connected to its image by a resistance equal to the earthing resistance of the element. Thus the Q of each director element would be relatively low and the arrangement would be inefficient. Experiment later confirmed this reasoning to be correct.

As it is proposed to depart from the Yagi arrangement, with the vertical reflector and director elements planted in the earth but electrically insulated from it, the insulation resistance must be high enough to preserve a good value of Q for each element but low enough to allow static charges to leak away to earth without a disruptive discharge taking place as this would cause heavy interference.

Use will be made of the theory referred in the foregoing sections of this chapter but, as mentioned by several of the authors quoted, the final dimensions of the antenna system will have to be decided by experiment. The proposed arrangement is a departure from the Yagi pattern of reflector and directors but is sufficiently akin to it for Yagi theory to be useful.

It is proposed, in experimentation, to vary both spacing and length of each element until an optimum for the array has been obtained. This is not usually a practical proposition but, if this experimentation is carried out on a very-high-frequency model of the antenna, then, by reducing the physical dimensions, the many adjustments of length, spacing, and matching can be made relatively easily. It is important to remember, of course, that adjustments made on such a model must be accurate because errors in the model will be magnified when applied to the full-scale version of the antenna.

The construction of the model is dealt with next.

---

CHAPTER 8.

THE V. H. F. SCALE MODEL.

8. 0 SUMMARY OF THIS CHAPTER.

- (a) By the use of an operating frequency of 243 Mc/s for the model a scale factor of about 11 is **employed**.
- (b) From the theory the element lengths are expected to be as follows, assuming  $0.2\lambda$  spacing:
  - driven element :  $0.236 \lambda$
  - reflector element:  $0.476 \lambda$
  - director element:  $0.434 \lambda$ .
- (c) Element lengths are made adjustable so as to give accurately controlled variation above and below the lengths quoted. The inter-element spacing, too, is made adjustable.
- (d) The  $\lambda/4$  grounded vertical monopole on an aluminium ground plane is investigated and the polar diagram is found to differ from the expected shape (Fig. F. 8.3.5.1.1). It is concluded that this is due to the effect, at 243 Mc/s, of the oxide with which the ground plane is coated.
- (e) Several combinations of driven element, reflector, and directors, are set up on the scale model, leading to optimum configurations for arrays having one to six directors. These designs are summarized in fig. F. 8.3.5.2.1.
- (f) From the measured scale-model polar diagrams (curves 1 and 3 of fig. F. 8.3.5.3.1.1) there are derived those that would have been obtained for a ground reflecting plane of infinite conductivity (curves 2 and 4). Hence polar diagrams are derived for the full-scale 4-director and 6-director arrays using a reflecting plane consisting of a grid of copper wires, at 12" centres, laid on a heavy clay soil. (curves 5 and 6 of fig. F. 8.3.5.3.1.1).

- - - - -

### 8.0.1. General

By invoking the Reciprocity Theorem<sup>(4, etc.)</sup> the Array is used as a transmitting antenna in the model as this is the simpler arrangement. The polar diagrams are plotted as a function of the received signal in a loop antenna, which describes an arc in the vertical plane, at a constant distance from the "driven" element. There will be required a V.H.F. transmitter of stable frequency selected to give a suitable scale factor.

### 8.1. Choice of scale factor

The size chosen for the model is influenced by two factors :

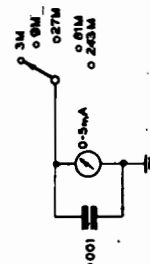
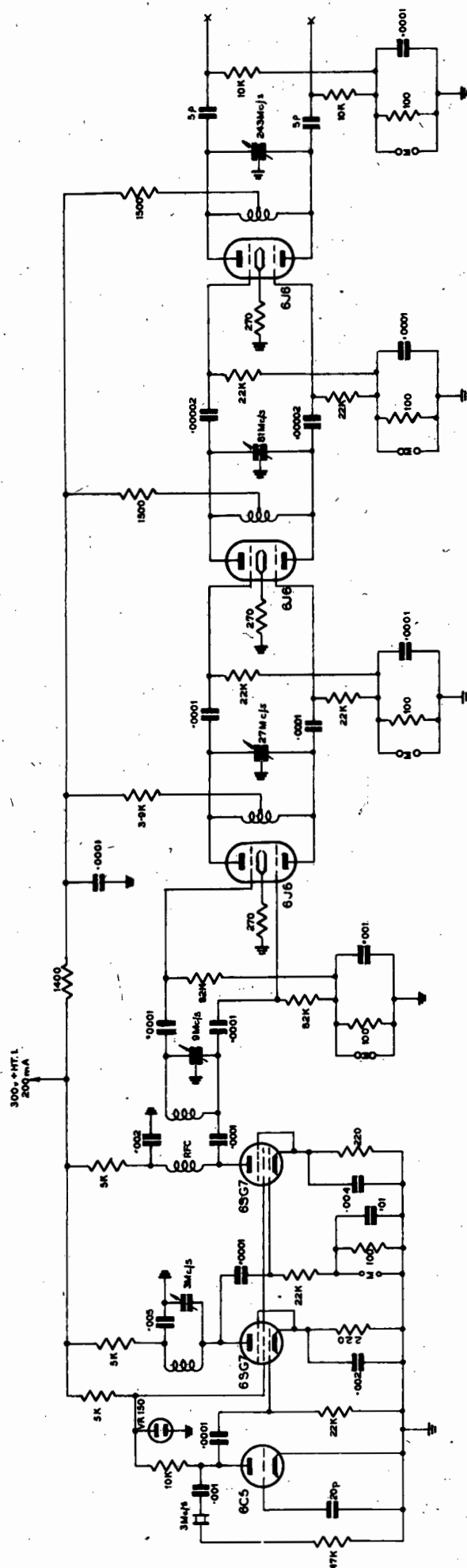
- (a) If too large physically it will be difficult to manipulate.
- (b) If too small it calls for a high degree of precision if the measurements are to be useful for the design of a full-scale antenna. A scale factor of about 10 appears to be suitable.

### 8.2. The transmitter.

This requires to operate on a frequency of the order of  $10 \times 21.47$  Mc/s and feed some 5 to 10 watts into a 70 ohm co-axial feeder. The frequency and output power must be constant. The circuit diagram of a suitable transmitter, designed and constructed by the writer, is shown in figure F 8.2.1. The output frequency from a 3 Mc/s crystal-controlled oscillator is trebled, stage by stage, to multiply it 81 times, giving a stable output at 243 Mc/s. In the main it is of conventional design. As it is desired to select the third harmonic and to suppress the second harmonic, push-pull amplification has been used. At the higher frequencies extremely short leads are necessary. The tuning of the final plate circuit, by means of a shorting bar, presents considerable mechanical difficulty but this is overcome by using a spring-loaded shorting bar, the position of which can be adjusted accurately by a knob which engages a threaded rod. Although capable of 10 watts output the tank circuit is coupled rather loosely to the co-axial feeder to give approximately 4 watts output.

### 8.3. Design of elements.

If, in the model, the permeability, permittivity, and conductivity of the material used are the same as they are in the large antenna, then the model will behave in the same way as the large ~~arrail~~ <sup>arrail</sup> provided the lengths, in each case expressed in wave-lengths, are the same. Care must be taken to ensure that the ratio of element length to diameter is the same in both cases. As the frequency ratio is  $243 / 21.47 = 11.3$ , and since  $2\frac{3}{4}$ " diameter copper pipe is considered suitable and is available in large supply for the 21.47 Mc/s array, the model elements should be of diameter equal approximately to  $2.75/11.3 = 0.243$ ".



400V HT. 2  
300 mA

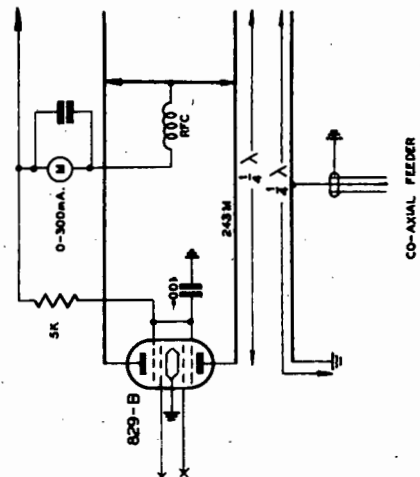


FIGURE 8-2-1  
V.H.F. TRANSMITTER  
243 M./s 10 WATTS NOMINAL O/P

$\frac{1}{4}$ " diameter copper tube has been selected for the model elements. The diameter =  $0.005 \lambda$ .

It is necessary to be able to change the length of the elements accurately and easily. To achieve this the micrometer adjustment, detailed in Fig. F. 8.2.0, is used. In the case of the radiating element the slug can be seen projecting from the tube in Fig. F. 8.3.0.2.

### 8.3.1) The "driven" element.

King and Harrison<sup>(212)</sup> in studies on the cylindrical dipole, have indicated the expected variation of input impedance resulting from changes in antenna thickness but the experiments of Brown and Woodward indicate that Schelkunoff's<sup>(1)</sup> biconical antenna method yields more reliable results. Their experiments indicate that the resonant length of a  $\lambda/2$  dipole is 1% shorter than that calculated by Schelkunoff's method when the length-to-diameter ratio of the conductor is 2000, the difference rising to 2% when the ratio falls to 100. Figure F.8.3.1.1, which is due to Schelkunoff<sup>(1)</sup>, relates self reactance and resistance to rod length. (33)

For cylindrical antennas the characteristic impedance,  $K_a$ , of a monopole above a perfectly conducting plane is given by the expression<sup>(1)</sup>:

$$K_a = 60 \left( \log_e \frac{2h}{a} - 1 \right) \quad (8.3.1.1).$$

where  $h$  = the length of the monopole =  $\lambda/4$ .

$a$  = radius of the conductor =  $0.0025 \lambda$ .

Thus  $h/a = 100$  and  $K_a = 258$  ohms.

When using fig. F. 8.3.1.1, it must be remembered that for a vertical monopole over a perfectly conducting ground the value of the ordinates must be halved.

From fig. F.8.3.1.1 the input impedance  $Z_{in}$  of a  $0.25 \lambda$  vertical rod when  $h/a = 100$  is given by:

$$Z_{in} = 41 + j 21 \quad (8.3.1.2).$$

From fig. F. 8.3.1.1 it is seen that, to make  $Z_{in}$  purely resistive, the length must be reduced to  $0.236 \lambda$  approx. At this length the input resistance  $R_{in} = 33$  ohms.

A slab of  $\frac{1}{4}$ " brass is used as a bedplate. It is drilled and-tapped to receive the threaded end of the  $0.236 \lambda$  adjustable length rod. (Fig. F. 8.3.0.2.) A second hole receives the co-axial adaptor and a third hole allows the polystyrene rod to pass freely through the plate. Adjustment of the knurled nut causes the polystyrene rod (and hence the shorting bar) to move up and down. The short rod is, effectively, an extension of the inner conductor of the co-axial feeder. Thus by tapping the correct impedance point of the resonant " $\lambda/4$ " line, an impedance match is achieved which makes accurate readjustments possible. A range of short rods of varying lengths is made available so that the length extending beyond the shorting bar can be kept reasonably short, so that the reactance, coupled in from this source, is minimised.



-8.4-

SOLID COPPERWELD ROD

2 BA THREADED  
ROD

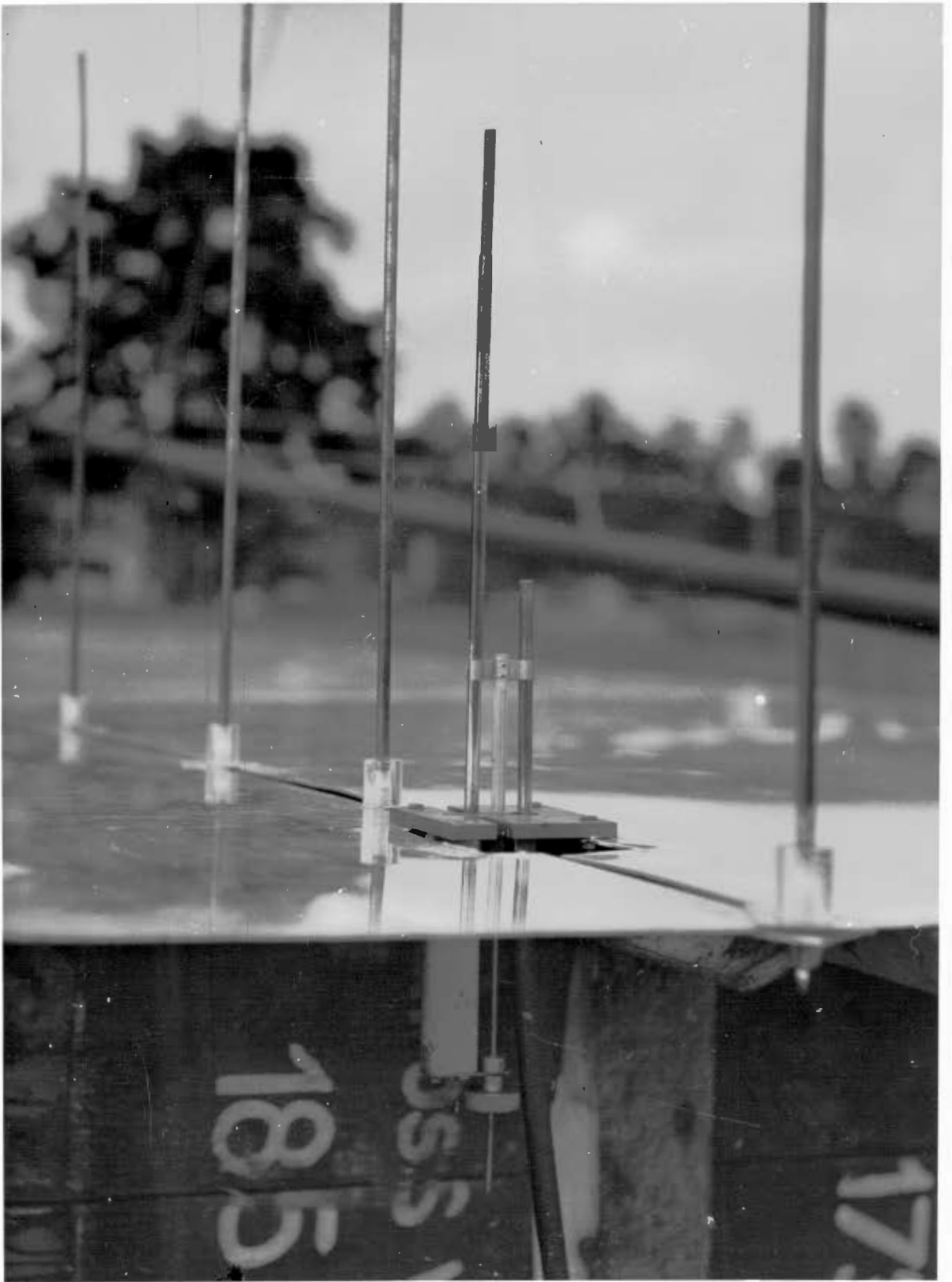
BRASS CYLINDER TAPPED  
2 BA

$\frac{1}{4}$ " DIA COPPER TUBE

CYLINDER GRIPPED BY 4  
CENTRE PUNCH MARKS

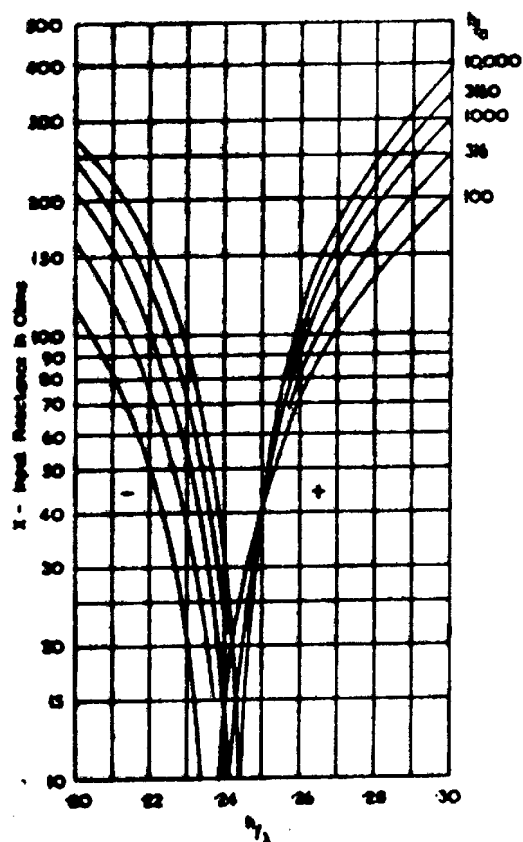
MICROMETER SCREW ADJUSTMENT OF ROD LENGTH AT 243 Mps.

8.1.40



MATCHING ARRANGEMENTS : SCALE MODEL

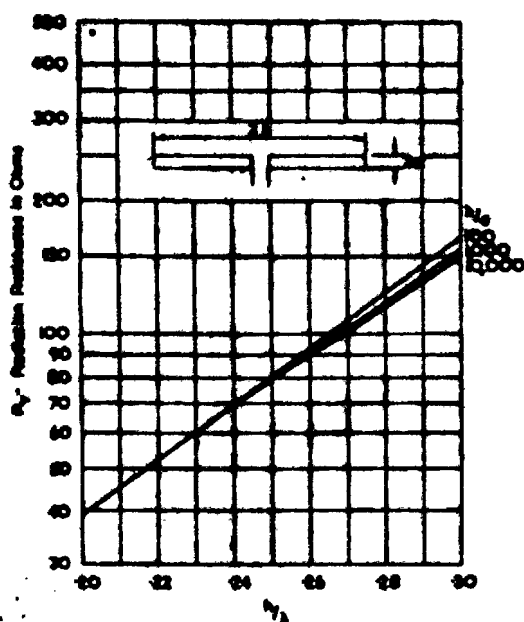
Figure F 8.3.0.2.



INPUT REACTANCE OF A CYLINDRICAL DIPOLE  
(Calculated by Schelkunoff's biconical antenna method)

(From "Electromagnetic Waves", Shelkunoff<sup>(1)</sup>)

Figure F 8.3.1.1.a.



RADIATION RESISTANCE OF A CYLINDRICAL DIPOLE  
(Calculated by Schelkunoff's biconical antenna method)

(From "Electromagnetic Waves", Shelkunoff<sup>(1)</sup>)

Figure F 8.3.1.1.b.

The brass slab is mounted securely on the metal earth plane.

The arrangement provides:

- (a) Rod length variation
- and (b) Adjustable matching of the feeder impedance to the input impedance of the array. (See Fig. F. 8.3.0.2).

### 8.3.2. The parasitic elements.

As these elements are not grounded they must first be treated as short-circuited free-space dipoles of total length  $2l$  equal to approximately  $0.5 \lambda$ . According to Shelkutoff<sup>(1)</sup> the characteristic impedance  $K_a$  for this case is given by the equation:

$$K_a = 120 \left( \log_e \frac{2h}{a} - 1 \right) \quad (8.3.2.1)$$

$$\text{Since } \frac{h}{a} = \frac{0.25 \lambda}{0.0025 \lambda} = 100,$$

$$K_a = 516.$$

For the simple case of one reflector element and one director element Walkinshaw<sup>(2)</sup> showed (see Fig. F. 7.1.2) that at a spacing of, say,  $0.2 \lambda$  the reflector self reactance should be about  $+ 10$  ohms and <sup>(1)</sup> the director self reactance should be about  $- 60$  ohms. From Fig. F. 8.3.1.1 it will be seen that, in the case of the reflector,  $h$  will need to be  $0.238 \lambda$  and, in the case of the director,  $h$  will need to be  $0.217 \lambda$ . Thus the length of the reflector will be of the order of  $0.476 \lambda$  and the length of the director will be about  $0.434 \lambda$ . From the work of Spector<sup>(209)</sup>, Reid<sup>(3)</sup> and Walkinshaw<sup>(2)</sup> reviewed in Chapter 7, it is expected that as the number of directors is increased the optimum spacing will also increase and element lengths will need to decrease accordingly.

The parasitic element lengths can be varied, as in the case of the "driven" element, by a micrometer screw adjustment of the slug. (Fig. F. 8.3.0.1).

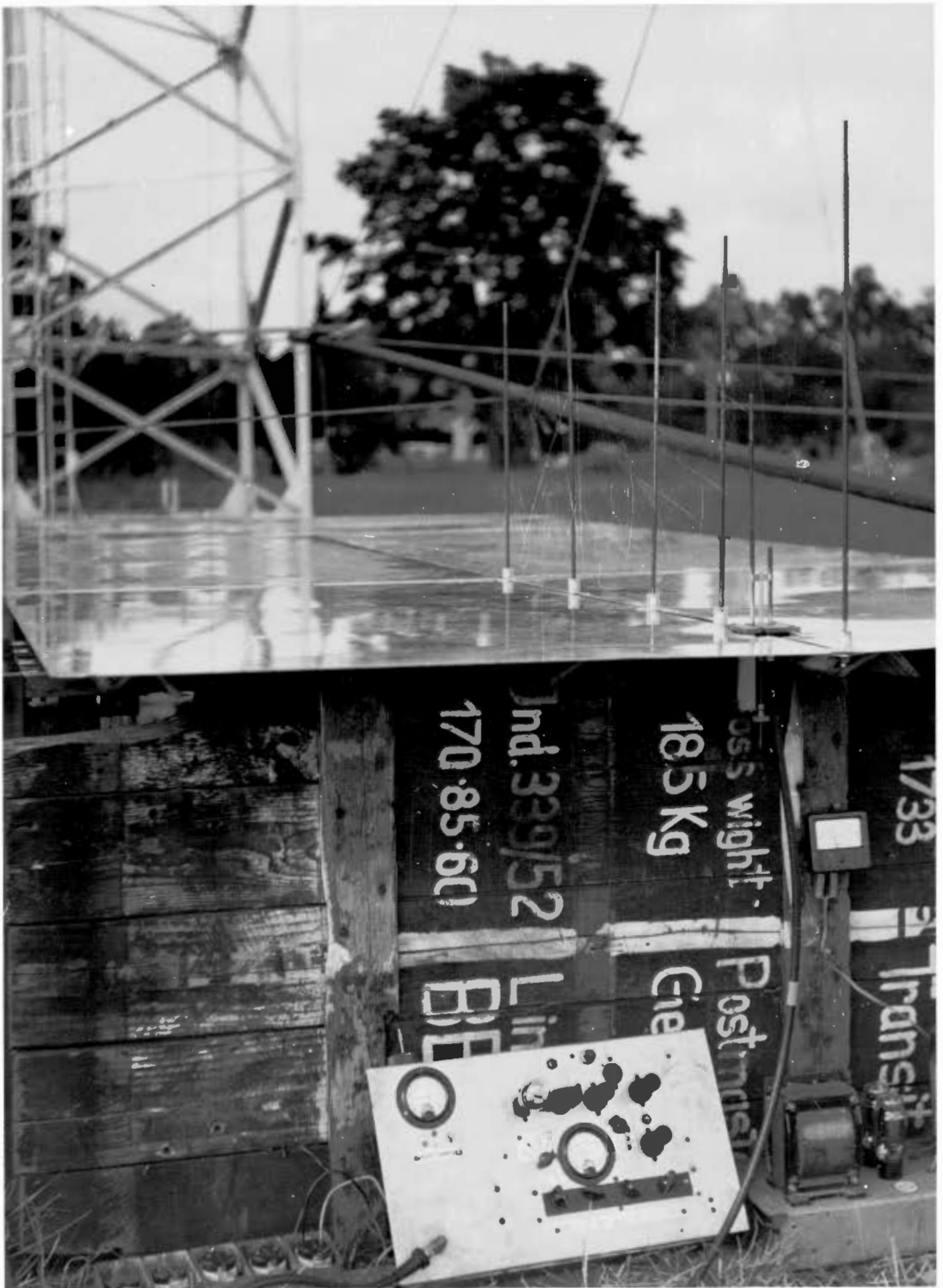
Elements are mounted on polystyrene bases. (Fig. F. 8.3.0.2). The other end of the base is tapped to receive a 2 BA bolt with a butterfly head. With the aid of a large washer on either side of the ground plane the bases are conveniently clamped over the groove that runs down the line of the array in the aluminium ground plane. The spacing is easily adjusted from underneath the ground plane.

The extra capacitance due to the relative permittivity of polystyrene (2.4 to 2.9) will reduce the electrical length of the elements but the effect will not be appreciable.

### 8.3.3 The Receiver.

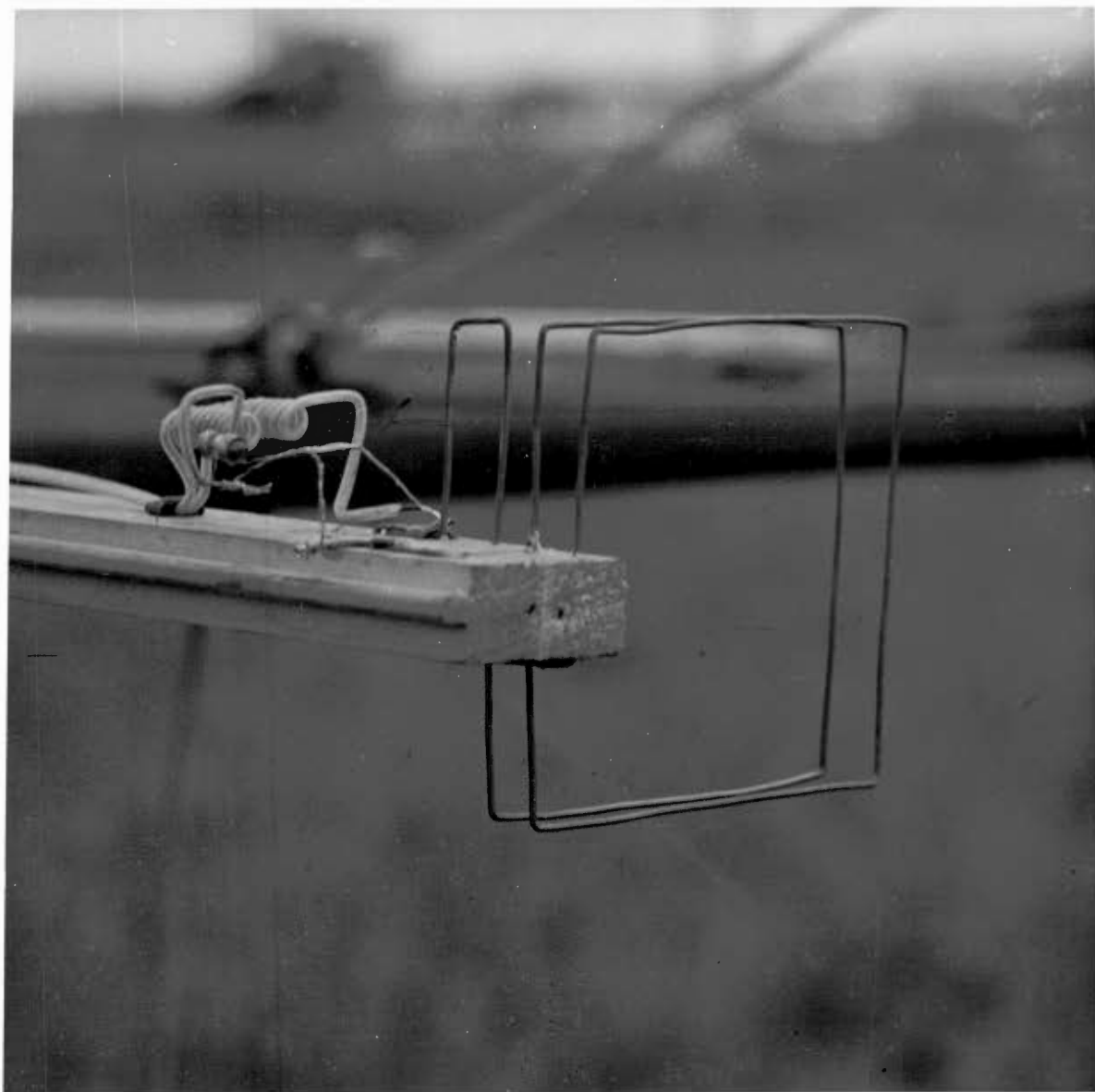
The small receiving loop aerial is mounted as in fig. F. 8.3.3.1 and the radio frequency current is rectified by a CG6G germanium diode. The direct-current output is fed, via a twin lead, to a 0-100 micro-ammeter located near the transmitter for convenience. (Fig. F. 8.3.3.2).

The twin lead is brought down the wooden mast and will produce no noticeable effect on the antenna performance.



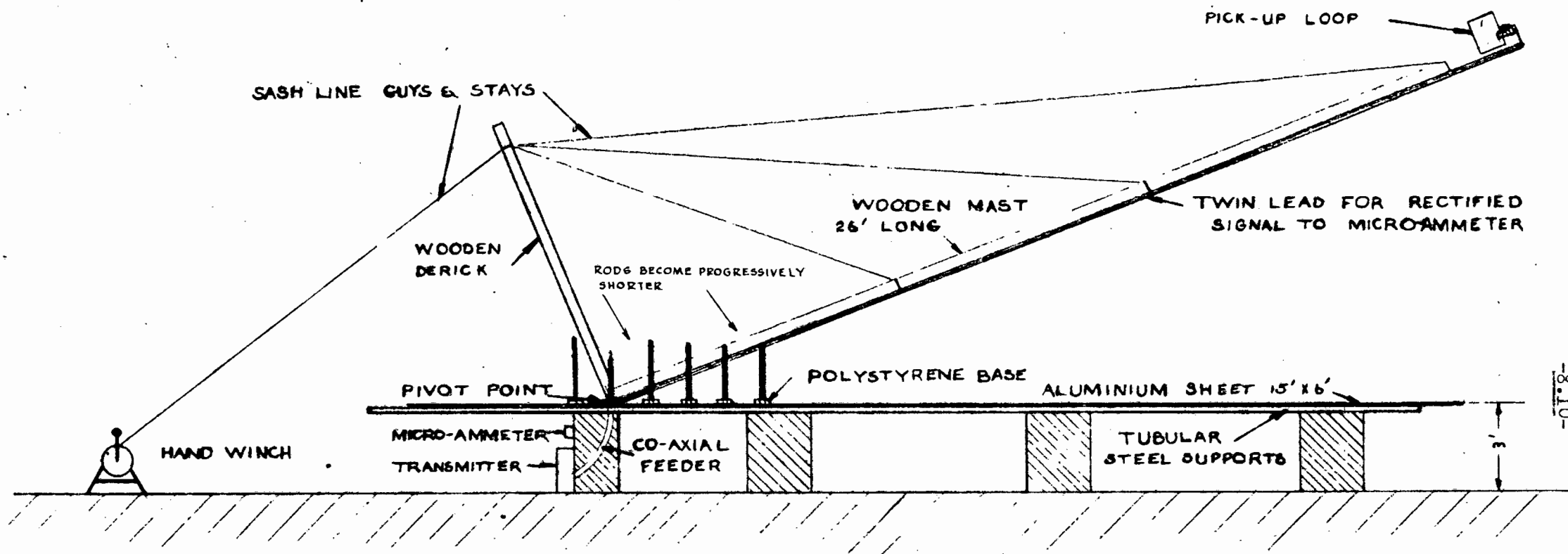
Control cabin : Scale model antenna, showing 4-director design on test.  
Lower left : 243 Mc/s transmitter. Above it, and to the right, is  
received signal strength indicator.

Figure F 8.3.3.2.



THE RECEIVING LOOP : SCALE MODEL ANTENNA

Figure F 8.3.3.1.



MEASUREMENT OF VERTICAL POLAR DIAGRAM AT 243 Mc/s  
(NOT TO SCALE)

The mast (Fig. F.8.3.3.3) carries the receiving loop round the circumference of a circle of radius  $6\frac{1}{2} \lambda$ , centred on the base of the radiating element. Thus the radiation at any angle from  $0^\circ$  to  $90^\circ$  can be measured. (The angle is conveniently measured by means of a transit level with its pivot in line with the pivot of the mast).

The micro-ammeter readings have to be interpreted in terms of e.m.f. generated in the loop. Calibration presents grave problems as it is difficult to inject a measured voltage at 243 Mc/s into the receiver. Calculation of the impressed voltage appears to be virtually impossible because of the many variables in the circuit and so it is necessary to produce a circuit which will behave, at say, 150 Kc/s in a similar manner to the behaviour of the original circuit at 243 Mc/s. The same micro-ammeter and detector as before must be used but the capacitor value is adjusted so that the relationship between time constant and periodic time remains the same for both cases. At a frequency of 150 Kc/s it is a simple matter to feed voltages of the order of  $\frac{1}{2}$  volt from an oscillator and to measure the p.d. accurately. This results in the calibration curve of fig. F.8.3.3.4 which is accurate enough for comparisons between one array and another.

The tension in the main stays that lift the mast is produced by a hand-operated winch in which the gear ratio is so high that the mast moves extremely slowly, making accurate measurements possible.

#### 8.3.4 The ground plane.

A ground plane of aluminium sheet is preferred, on cost considerations, to one of copper even though the resistivity is 1.64 times that of copper.

The "depth of penetration",  $d$ , i.e. the depth at which the electric field strength of the wave, incident upon the sheet, will have fallen to a value  $\frac{1}{e}$  (i.e. 36.8%) of its surface value, is given by equation 6.16 of Appendix A as:

$$d = \frac{1}{(\pi f \mu \sigma)^{\frac{1}{2}}} \quad (8.3.4.1)$$

For aluminium  $\sigma$ , the conductivity, is  $3.54 \times 10^7$  mho/m.

$$\mu = \mu_0 = 4 \pi \times 10^{-7} \text{ Henrys/m.}$$

$$f = 243 \times 10^6 \text{ c/s}$$

$d$  is in metres.

$$\begin{aligned} \text{For this case } d &= 5.43 \times 10^{-6} \text{ metres} \\ &= 0.054 \text{ m.m.} \end{aligned}$$

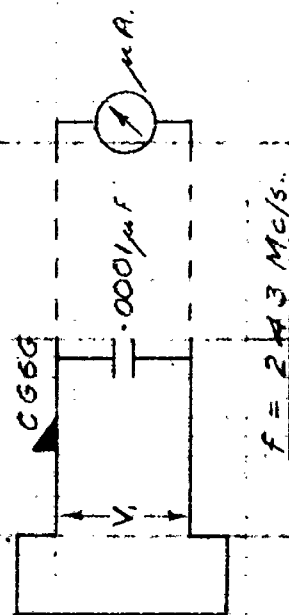
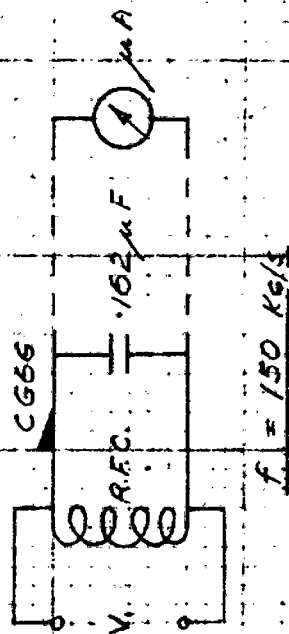
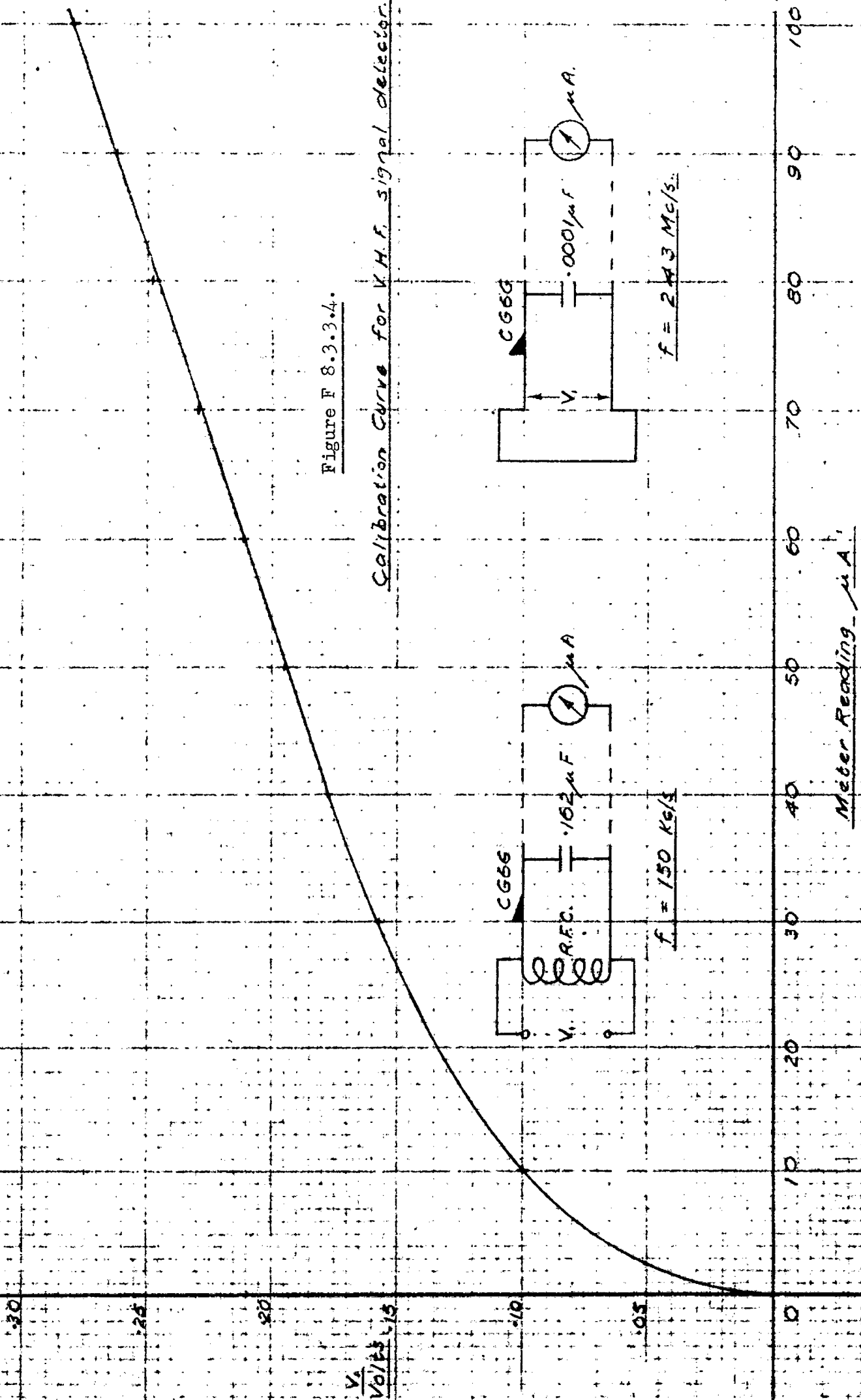
The common 16 SWG aluminium sheeting is suitable for the purpose.

To minimise errors in the receiver, due to capacitance between the ground plane and the receiving loop at low angles, the ground plane extends only to a point  $1\frac{1}{2} \lambda$  from the receiving loop when the latter is at  $0^\circ$  to the horizontal. This also ensures that the surface wave reaching the loop is negligible.



Figure F 8.3.3.4.

Calibration Curve for V.H.F. signal detector.



Meter Reading  $\mu A$

The ground plane must be as flat as possible because undulations are likely to distort the image of the antenna and produce a falsely shaped polar diagram. For this reason poles of good rigidity are used to support the ground plane. (See Fig. F.8.3.3.3).

A sliding groove for adjusting the spacing of directors can be seen in figures F.8.3.0.2 and F.8.3.3.2. It extends for about  $2\lambda$  from the reflector element.

Further to the discussion in section 6.3.4, on the effect ground constants have on the polar diagram, the question now arises: will an aluminium sheet ground plane behave as a perfectly conducting ground at 243 Mc/s? This is answered by performing the same calculations in respect of aluminium as were done for sea water, soil, and a wire grid in section 6.3.4.1 which led to the polar diagrams for a vertical, grounded,  $\lambda/4$  monopole in fig. F.6.3.4.1.3. In this case:

$$\mu_2 = \mu_0 = 4\pi \times 10^{-7} \text{ Henrys/metre.}$$

$$\sigma_2 = 3.54 \times 10^7 \text{ mho/metre.}$$

From eqn. (6.3.4.1.9)

$$Z_2 = \left( \frac{\omega \mu_2}{2 \sigma_2} \right)^{1/2} (1 + j)$$

$$\begin{aligned} Z_2 \text{ at } 243 \text{ Mc/s} \\ = 5.2 \times 10^{-3} (1 + j) \end{aligned} \quad (8.3.4.2)$$

As  $\theta_2$  in metal may be taken as zero<sup>(5)</sup>, the field impedance of the metal,  $Z_{ft} (= Z_2 \cos \theta_2)$  from eqn 6.3.4.1.5, is equal to the intrinsic impedance,  $Z_2$ , the modulus of which is  $1.42 \times 5.2 \times 10^{-3}$  ohms.

From eqn. (6.3.4.1.3);

$$Z_{fi} = Z_1 \cos \theta_1 = 377 \cos \theta \quad (8.3.4.3)$$

Thus a wave incident at an angle  $\theta_1$  on the metal sheet may be considered as travelling down a transmission line of characteristic impedance  $(377 \cos \theta_1)$  ohms. This encounters a termination of impedance  $(7.4 \times 10^{-3} \text{ angle } 45^\circ)$  ohms. The reflected wave is a minimum when

$$377 \cos \theta_1 = 7.4 \times 10^{-3}$$

i.e. when  $\cos \theta_1 = 1.96 \times 10^{-5}$

Thus the pseudo Brewster angle has a value between  $89^\circ 59'$  and  $90^\circ$ . At this value of  $\theta_1$  the phase angle of the reflection coefficient ( $R_v$ ) is, as is always the case<sup>(5)</sup>, equal to  $90^\circ$ . For values of  $\theta_1$  less than the pseudo Brewster angle the phase angle of  $R_v$  may be taken as zero and for values of  $\theta_1$  lying between the pseudo Brewster angle and  $90^\circ$  the phase angle changes rapidly from  $90^\circ$  to  $180^\circ$ .

The magnitude of  $R_v$  is given, from equations 6.3.4.1.1./3/5, as:

$$R_v = \frac{377 \cos \theta_1 - 5.2 \times 10^{-3} - j 5.2 \times 10^{-3}}{377 \cos \theta_1 + 5.2 \times 10^{-3} + j 5.2 \times 10^{-3}}$$

Thus :  $R_v = 1 \angle 0^\circ$  for all values of  $\theta_1$  from  $0^\circ$  to a value almost equal to the pseudo Brewster angle, at which angle, say  $89^\circ 59'$ , it equals  $0.42 \angle 90^\circ$  and then it changes rapidly, becoming  $1 \angle 180^\circ$  i.e. -1, at  $\theta_1 = 90^\circ$ .

The polar diagram for an antenna situated above such a reflecting plane is therefore expected to be the same as for an antenna above a plane of infinite conductivity except for angles of elevation less than one minute.

#### 8.3.5.0 Tests with the scale model.

In conducting these tests the following precautions are necessary:-

- a) The available power from the transmitter must remain constant throughout the tests. Frequent checks must, therefore, be made on tank circuit tuning, P.A. drive, and the mains supply voltage.
- b) The antenna matching must always be optimum and the load presented to the transmitter must always be resistive. Adjustments, to achieve this objective, are therefore legion and must be made with great accuracy.
- c) The model must be sited in open country at least  $10\lambda$  from reflecting objects. Objects moving near the model can cause significant changes in the received field. Therefore, as will be seen in Fig. F.8.3.3.2, the scale model is operated from a cabin below the metal reflecting plane. The adjustment of the match between co-axial feeder and the  $\lambda/4$  radiating element is effected by turning the knurled knob (seen more clearly in the close-up view, fig. F.8.3.0.2). The received signal is indicated in the large micro-ammeter seen directly below the reflector element in fig. F.8.3.3.2.

#### 8.3.5.1 Test with $\lambda/4$ rod alone.

When the rod length is varied by small amounts using the micro-meter type adjustment on the slug, being careful to check for optimum matching conditions each time the length is varied, the resonant length is found. It was forecast, in section 8.3.1, that the length of a  $\lambda/4$  monopole above a conducting plane is expected to be  $0.236 \lambda$ . In the experiment the length was found to be  $0.241 \lambda$ . The small difference in length is doubtless due to the fact that it is necessary to neutralize the small reactance coupled in by the matching device. (See Fig. F. 8.3.0.2). Various sizes of stub rod are provided to keep the length protruding beyond the shorting slider to a minimum. The resonant length of the  $\lambda/4$  rod will vary slightly according to the length of this protrusion.

The measurements taken when the receiving loop is moved through angles of  $\Delta$  from  $0^\circ$  to  $90^\circ$  are given in Appendix C. If these points are plotted and a smooth curve drawn through their mean values, curve "x", Figure F. 8.3.5.1.1, is obtained.

In section 8.3.4 it was concluded that even at 243 Mc/s the aluminium ground plane would behave as if it were a reflector of perfect conductivity for all values of  $\Delta$  greater than about  $1^\circ$ . However, in fig. F.8.3.5.1.1, this is clearly not the case and there is a serious disparity between curve "a" of fig. F.6.3.4.1.3 and curve "x" of fig. F. 8.3.5.1.1. Curve "y" is the shape of curve expected. It appears that the aluminium sheet at 243 Mc/s is, after all, not behaving as a plane of almost perfect conductivity but rather is behaving much as sea water does in the H.F. band. (See Fig. F.6.3.4.1.3). The explanation probably lies in the fact that the conductivity assumed for aluminium is the conductivity between opposite faces of a metre cube of material. It was shown in section 8.3.4 that at 243 Mc/s a skin only 0.0054 m.m. thick carries 63.2% of the current induced by the incident wave. Of the same order of magnitude as that skin is the thin oxide coating with which aluminium always is protected against further oxidation. Thus, at very high frequencies sheet aluminium and copper behave as though they possess much less conductivity than at low frequencies because of the oxide coating.

In the scale model tests, therefore, from about  $\Delta = 15^\circ$  to about  $\Delta = 1^\circ$  the field strength will be much less than if the same test had occurred at, say, 21 Mc/s. The scale model polar diagrams, unless corrected, will not depict accurately what will occur at 21 Mc/s for values of  $\Delta$  below about  $20^\circ$ . Corrected they will give a fairly accurate representation of the polar diagram for values of  $\Delta$  from  $0^\circ$  to  $90^\circ$  in addition to the primary function of the scale model, which is to provide a manageable means of optimising the element lengths and spacings of a series of multiple-director parasitic arrays.

#### 8.3.5.2 Test with $\lambda/4$ rod plus parasitic elements.

- a) The parasitic reflector is now set up and the length is made equal to the value calculated in section 8.3.2, i.e.  $0.476 \lambda$  spaced  $0.2 \lambda$  behind the radiator. When the driven element length and matching, as well as reflector length and spacing, are adjusted and re-adjusted many times to give maximum received signal at a small value of  $\Delta$ , it is found that the optimum length of the reflector is  $0.476 \lambda$  (identical to the calculated value) but the optimum spacing is  $0.233 \lambda$ .

At  $\Delta = 8\frac{1}{2}^\circ$  the gain over the single  $\lambda/4$  rod =

$$\left(\frac{103}{76}\right)^2 = 1.84 = 2.64 \text{ db.}$$

If the reflector reduces the backward radiation to zero it must produce a 2:1, i.e. 3 db, change in the forward radiation. This reflector has achieved this objective to the extent that may reasonably be expected of a single element in practice. It is probably not worth making a more complicated reflector for the purpose of obtaining some of the remaining 0.36 db gain.

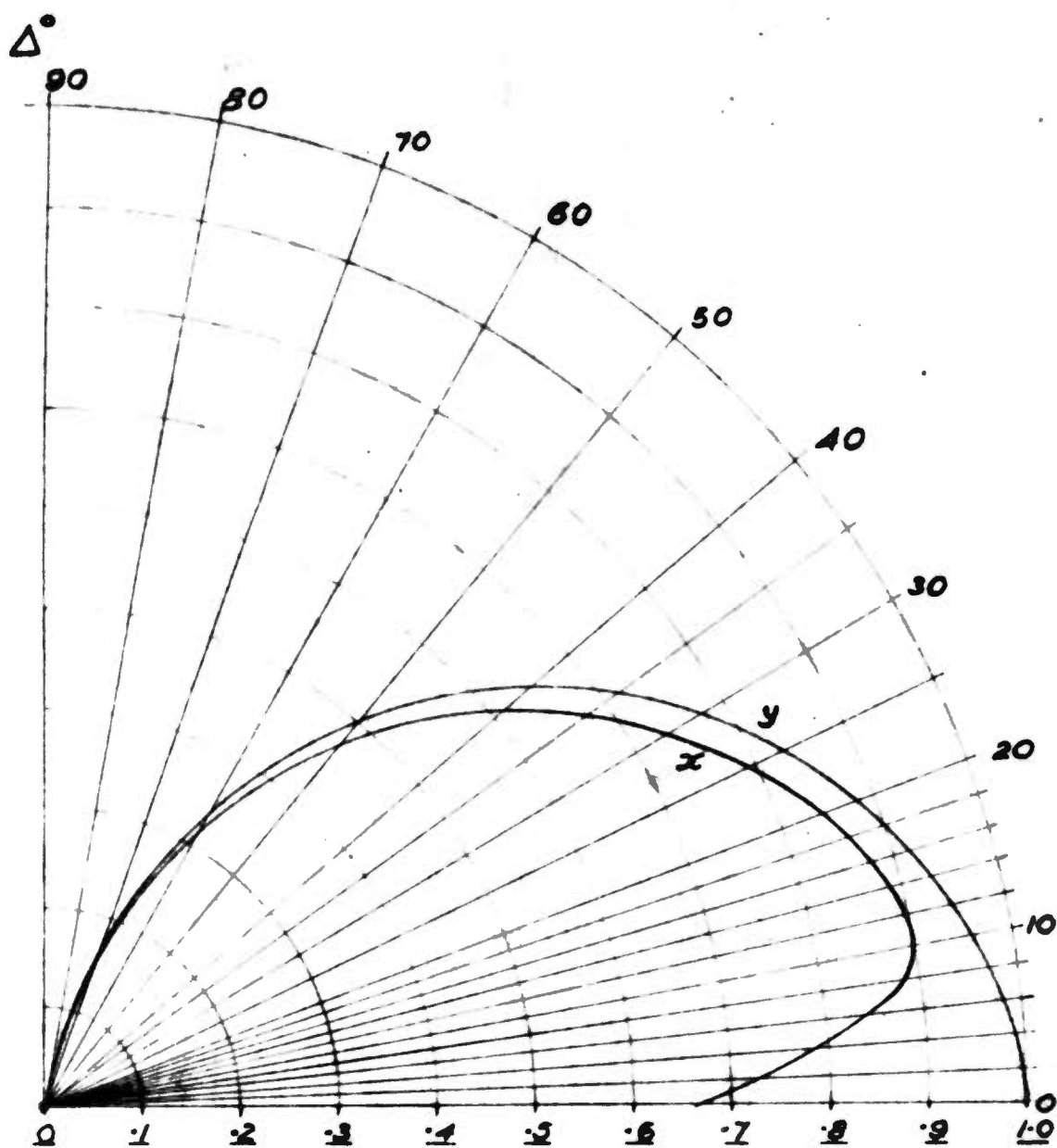


*Fig. F 8.3.5.1.1*

POLAR DIAGRAMS,  $\lambda/4$  VERTICAL MONOPOLE.

Curve "x" : Measured polar diagram at 24.3 Mc/s over an aluminium reflecting plane.

Curve "y" : Polar diagram expected for a perfectly conducting ground plane.

- b) A director is now added to the reflector and driven element combination. Where must it be placed and how long should it be? Walkinshaw's <sup>(2)</sup> calculation, summarised in figure F 7.1.2., indicates maximum gain for  $0.1 \lambda$  spacing when  $X = -10$  ohms, i.e. element length (fig. 8.3.1.1.) equal to  $0.46 \lambda$ ; or at  $0.15 \lambda$  spacing when  $X = -30$  ohms, i.e. element length equal to  $0.452 \lambda$ ; or at  $0.2 \lambda$  spacing when  $X = 60$  ohms, i.e. element length equal to  $0.434 \lambda$ . In section 7.2 it was pointed out that Spector <sup>(209)</sup> has shown that the shorter the director length the narrower the beam but the shorter the director length the worse the launching efficiency of the antenna. The optimum exists as a compromise between these two opposing trends and is found experimentally.

Commencing with a director-to-driven element spacing of  $0.2 \lambda$  and director length equal to  $0.434 \lambda$  the director length and spacing, the driven element length and matching, and the reflector length and spacing, are adjusted, and re-adjusted many times, until maximum signal is induced in the receiving loop for a low value of  $\Delta$ . This yields design B in figure F 8.3.5.2.1.

By repeating the same process each time another director is added, designs B, C, D, E, F, and G have been produced employing 1, 2, 3, 4, 5, and 6 directors respectively. These are summarised in figure F 8.3.5.2.1. which is a valuable document, (a) because of the amount of work necessary for its compilation and (b) because of the amount of information summarised therein. The test results are summarised in Appendix C.

It will be noted that:-

- a) The greater the length of the array the shorter is the last director. This is experimental confirmation of Spector's <sup>(209)</sup> theory that good launching efficiency is achieved in a long array and that in this case a short final director will achieve a bigger aperture, and hence a narrower beam (higher gain), than a long final director. (Sect. 7.2.)
- b) Each additional director is not only shorter than its predecessor but is at a greater spacing. This is experimental confirmation of Reid's <sup>(3)</sup> contention (Sect. 7.3.) that the longer the array the more nearly equal will be the optimum phase velocity of the guided wave to the free space phase velocity. (Equation 7.3.13. refers).

Figure F 7.2.2. shows, as would be expected, that, for a given element length, the greater the spacing the more nearly equal will be the phase velocities of the guided and free-space waves. Conversely it shows that, for a given spacing, the shorter the element length the more nearly equal will be the phase velocities of the guided and free-space waves.

#### 8.3.5.3.0. Interpretation of the scale model results.

As discussed in section 8.5.5.1. the depth of penetration in aluminium at 24.3 Mc/s is so very small that the oxide coating is forced

	<p><u>G.</u> 6-Dir. Array Lobe 8° Gain 9.6 db</p>
	<p><u>F.</u> 5-Dir. Array Lobe 8.5° Gain 9.2 db</p>
	<p><u>E.</u> 4-Dir. Array Lobe 9.5° Gain 8.8 db</p>
	<p><u>D.</u> 3-Dir. Array Lobe 10° Gain 7.5 db</p>
	<p><u>C.</u> 2-Dir. Array Lobe 10° Gain 6.5 db</p>
	<p><u>B.</u> 1 Dir. Array Lobe 10° Gain 5.8 db</p>
	<p><u>A.</u> <math>\frac{\lambda}{4}</math> Rod + Refl. Lobe 11° Gain 2.6 db</p>

## Array Designs

Gain figures relative to  $\frac{\lambda}{4}$  rod

Fig F 8-3-5-2-1

to carry an appreciable proportion of the current and at very high frequencies it appears that the reflection properties of aluminium are similar to those of sea water at high frequencies.

#### 8.3.5.3.1 Scale model polar diagrams.

As shown in fig. F. 8.3.3.3, the receiving loop is made to rotate at a radius of  $6.5 \lambda$  from the base of the driven element in order to indicate the field strength at various angles of elevation from  $0^\circ$  to  $90^\circ$ . Strictly speaking, as the radiating aperture is at the last director of the array the rotation should take place about the mid-point of the aperture (see section 7.2) but this is experimentally inconvenient. If the distance to the receiver is long compared with the length of the array, negligible error is introduced by rotating about the base of the driven element. A radius such as is used in the model ( $6.5 \lambda$ ) is acceptable because, although a certain amount of error will be introduced, the error is seen to be of no consequence since the prime purpose of the model is to produce optimum values for element length and spacing. The polar diagrams obtained will be fairly accurate, notwithstanding the errors indicated above, and will serve the useful purpose of indicating roughly what sort of pattern to expect from a given arrangement.

The measured vertical polar diagrams for the 4-element and 6-element arrays are drawn as curves (1) and (2) respectively in fig. F. 8.3.5.3.1.1. Multiplication of curves (1) or (2) by the ratio  $y/x$ , for each corresponding value of  $\Delta$  in fig. F. 8.3.5.1.1, yields curves (3) or (4) of fig. F. 8.3.5.3.1.1. Curves (3) and (4) represent the derived polar diagrams, for a perfectly conducting reflection plane, of a 4-director array and 6-director array as per Table T.8.3.5.3.1.1 below:

$\Delta^\circ$	Measured ( m V ) 4-director Array.	Measured ( m V ) 6-director Array.	$y/x$ from Fig. F.8.3.5.1.1	Derived ( m V ) 4-director infinite $\sigma$	Derived ( m V ) 6-director infinite $\sigma$
0	173	195	1.51	261	295
2	186	212	1.37	255	291
4	194	218	1.27	246	278
6	205	227	1.17	240	266
8	208	230	1.10	229	253
10	210	226	1.07	225	242
12	205	212	1.05	215	223
14	197	198	1.05	207	208
16	186	182	1.04	194	189
20	166	142	1.03	171	146
25	115	65	1.03	118	67
30	95	0	1.03	98	0
40	43	0	1.06	48	0
45-90	0	0	1.06	0	0

T A B L E T.8.3.5.3.1.1



By multiplying each of the curves "2" and "4" for infinite conductivity by the ratio  $b/a$ ,  $c/a$ ,  $d/a$ ,  $e/a$ ,  $f/a$  for various values of  $\Delta$  in fig F. 6.3.4.1.3 the polar diagrams for the 4-director or 6-director arrays over sea water, heavy clay soil, and gratings of  $12\frac{1}{2}$  SWG copper wire at 15", 12" and  $7\frac{1}{2}$ " centres, called type "d", "e", and "f" respectively, can be found for a frequency of 21.47 Mc/s. (N.B. the wires in the grating are pointing in the direction of the distant station).

In Table T. 8.3.5.3.1.2 the expected polar diagrams of a 4-director and a 6-director array, over a 12" grating, are derived for 21.47 Mc/s from Table T. 8.3.5.3.1.1 and curves (a) and (e) of fig. F. 6.3.4.1. 3. The derived polar diagrams appear in fig. F 8.3.5. 3.1.1 as curves (5) and (6) respectively.

$\Delta^\circ$	Derived (mV) for infinite $\sigma$ from Table T.8.3.5.3.1.1		e/a from figure F.6.3.4.1.3	Derived (mV) 12 $\frac{1}{2}$ SWG copper wire grating at 12" centres at 21.47 Mc/s.	
	4-director	6-director		4-director	6-director
0	261	295	0	0	0
2	255	291	0	0	0
4	246	278	.10	25	28
6	240	266	.72	173	192
8	229	253	.78	179	197
10	225	242	.81	185	196
12	215	223	.83	179	185
14	207	208	.86	178	179
16	194	189	.87	169	164
20	171	146	.90	154	131
25	118	67	.92	105	62
30	98	0	.94	92	0
40	48	0	.97	47	0
45-90	0	0	1.00	0	0

TABLE T. 8.3.5.3.1.2

It should be noted that although the scale tests indicate that the 6-director design will possess maximum sensitivity in the desired direction ( $8^\circ$ ) when used above a grating of  $12\frac{1}{2}$  SWG copper wires spaced at 12" centres, a ground of infinite conductivity would produce (from table T.8.3.5.3.1.2) an improvement of  $20 \log \frac{253}{197} = 4.2$  db at this angle. Similarly, the use of a spacing of  $7\frac{1}{2}$ " would (from fig. F.6.3.4.1.3) produce an improvement at  $8^\circ$  of 1.5 db compared with the 12" spacing. There is, of course, an economical limit to the smallness of the spacing but this limit cannot easily be defined because it will depend, among other things, on the availability of scrap copper wire.

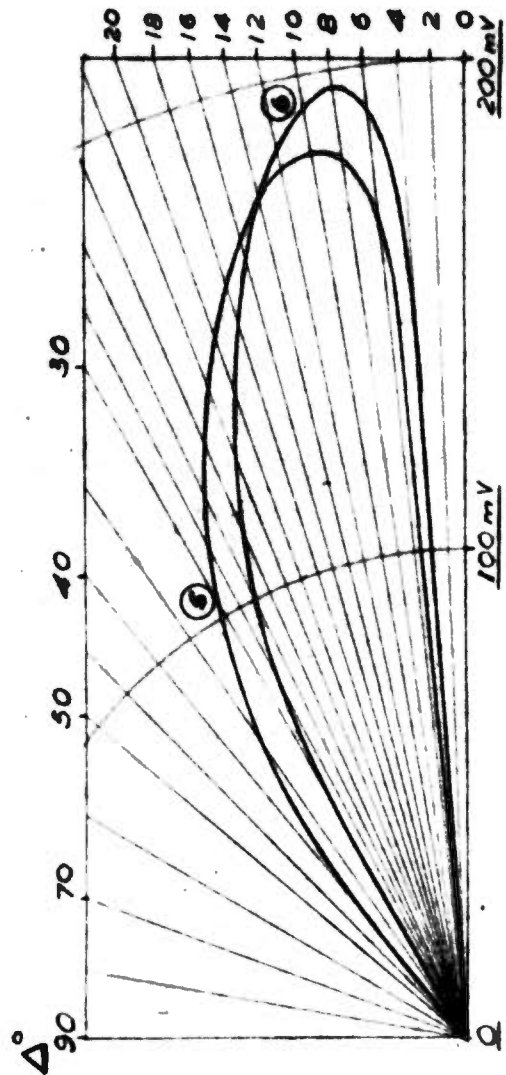
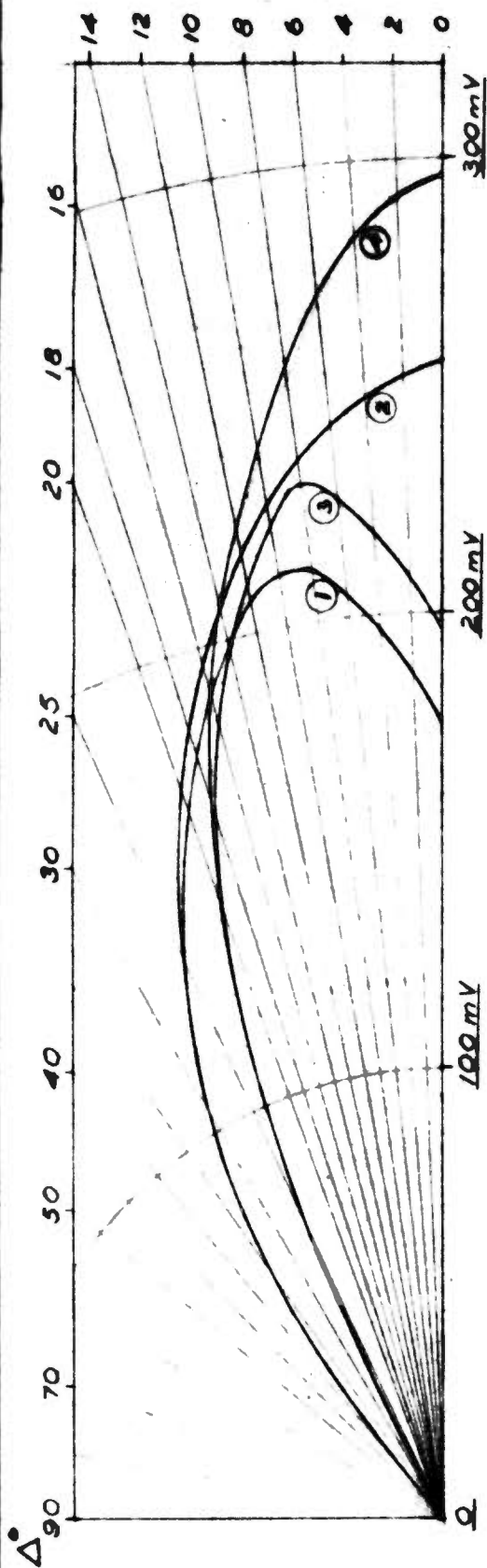


Fig.

Curve 1 : Measured polar diagram (24.3 Mc/s),  
4-director array, over aluminum sheeting.

Curve 2 : Derived polar diagram, 4-director array,  
over perfectly conducting ground.

Curve 3 : Measured polar diagram (24.3 Mc/s),  
6-director array, over aluminum sheeting.

Curve 4 : Derived polar diagram, 6-director array,  
over perfectly conducting ground.

Curve 5 : Derived polar diagram ( 21.47 Mc/s),  
over grating.

Curve 6 : Derived polar diagram ( 21.47 Mc/s),  
over grating.

\*The grating consists of 12½ SW copper wires, 144  
in the direction of the distant station, at 12°  
centres ( see chapter 6 ).

Figure F 6.3.5.3.1.1

In a receiving antenna the main requirement is high signal-to-noise ratio and it is therefore advantageous to have a maximum at  $8^\circ$  (the expected wave arrival angle) with a rapid decrease in sensitivity for values of  $\Delta$  below  $8^\circ$  as well as for values above  $8^\circ$  so that there is discrimination, not only against noise and other unwanted energy coming in at high angles (see Chapter 4), but also against interference coming in at angles below  $8^\circ$ . A 6-director design, with a grating of spacing 12" or less would appear to be suitable, for use on the London-Salisbury circuit.

The horizontal polar diagram of the 4-director design has been measured but it is of minor importance. Because the received signal at 24.3 Mc/s is so greatly affected by the height above ground of the receiving loop, the results are not reliable as the experimental errors are great.

#### 8.3.5.3.2 Scale model relative gains.

In fig. F. 8.3.5.2.1 the gain of each of the designs A to G has been inserted. As these are taken from the unadjusted, scale-model polar diagrams the figures should not be taken too seriously. It will be observed, for instance, that the 6-director design is quoted as being 0.8 db more sensitive at  $8^\circ$  than the 4-director design is at  $9.5^\circ$ . In Table T.8.3.5.3.1.2 it will be observed that when these designs are used over a perfectly conducting ground the difference in maximum sensitivity (i.e. at  $0^\circ$ ) is 1.06 db and when used above a grating of  $12\frac{1}{2}$  SWG copper wires pointing in the direction of the distant station and spaced at 12" centres (type "e") the sensitivity of the 6-director design at  $8^\circ$  (max) is only 0.54 db better than that of the 4-director design at  $10^\circ$  (max). The gain figures in fig. F. 8.3.5.2.1 have been inserted mainly to show how each additional element affects the gain, and hence, the relative sharpening of the beam.

#### 8.3.5.3.3 Review of Chapter 8.

By means of the scale model and using the theory of parasitic action developed in Chapter 7, coupled with the theory of reflecting surfaces developed in Chapter 6, various optimised designs have been produced. Two of the designs have been taken (the 4-director design and the 6-director design) and the probable polar diagrams at 21.47 Mc/s have been plotted assuming that they are to be used over a certain reflecting plane made of a grating of copper wires laid on top of a heavy clay soil. The accuracy of the predictions must now be tested by measuring the polar diagram of one of the designs at 21.47 Mc/s.

Within rather narrow limits any desired value of  $\Delta$  can be achieved by a suitable combination of ground plane and number of directors.

- - - - -

#### 9.0.1 Reason for construction of the test array.

Before use can be made of the designs derived from the V.H.F. scale model, and summarised in figure F.8.3.5.2.1, at communication frequencies, it is necessary to build a full-scale array and test it (a) to see if the dimensions given in figure F.8.3.5.2.1 are, in fact, optimum and (b) to see if the measured polar diagram bears any resemblance to the derived polar diagram of figure F.8.3.5.3.1.1. The test array will be pointed at a 260 ft. mast in Salisbury which affords a convenient means of elevating a "transmitter" (a battery-driven signal generator will provide adequate radiated power) so that the polar diagram can be measured. Bearing in mind the limitations placed on area, the economics of the matter, and the greater ease with which a fairly small array can be checked, the four-director design is chosen as the test array.

#### 9.1 Design of element dimensions for 21.47 Mc/s.

The lengths of the elements and their respective spacings are made in accordance with the dimensions laid down in Fig. F.8.3.5.2.1 (E).

The wavelength,  $\lambda$ , is given by the well-known relationship:

$$\lambda = \frac{984}{f} \quad (9.1.1).$$

where  $f$  is in Mc/s.

When  $f = 21.47$  then  $\lambda = 45.83$  ft.

In the scale model at 243 Mc/s,  $\frac{1}{4}$ " (0.005  $\lambda$ ) diameter rod was chosen because it was known that  $2\frac{3}{4}$ " (0.005  $\lambda$ ) diameter tubing was available in large quantities for the 21.47 Mc/s antenna.

A dry wooden block, turned to fit snugly into the copper tube, and mounted on an 18" angle iron picket, forms a convenient method of insulating and supporting each element for the test.

#### 9.2 Matching arrangements.

It is necessary to match the impedance of the "driven" element to that of the co-axial feeder line. The term "driven" element should only be applied to a transmitting antenna but it is so widely used to designate the element which is coupled to the feeder that, although this is a receiving antenna, this element will be referred to as the "driven element". It is impractical to use the same matching method which gave such good results in the scale model. Instead it is necessary to use the arrangement shown in figures F.9.2.1 and F.9.2.2 in which the antenna and co-axial feeder are each matched to the tuned circuit.

THE 4-DIRECTOR TEST ARRAY AT 21.47 Mc/s.

9.0 SUMMARY OF THIS CHAPTER.

The validity of the scale model design figures and the derived polar diagrams are tested by measuring the performance, at 21.47 Mc/s, of a 4-director array constructed in accordance with the dimensions obtained from the scale model experiments. As a ground plane a grid of copper wires at 12" spacing is laid on a heavy clay soil.

The predicted polar diagram (curve 5 of fig. F.8.3.5.3.1.1) and the measured polar diagram (fig. F.9.6.2) are in good agreement, the maxima occurring at  $\Delta = 10^\circ$  and  $\Delta = 9\frac{1}{2}^\circ$  respectively. Aspects in which they differ are discussed in the text. The horizontal polar diagram has been plotted.

A frequency run on the antenna shows a maximum response at the design frequency.

The spacing between elements is varied in an attempt to increase the gain of the array but it is not found possible to improve on the diagram obtained from the scale model experiment.

The gain of the array, relative to a  $\lambda/4$  vertical grounded monopole, is measured.

It is concluded that the design dimensions can be accepted as optimum.

- - - - -

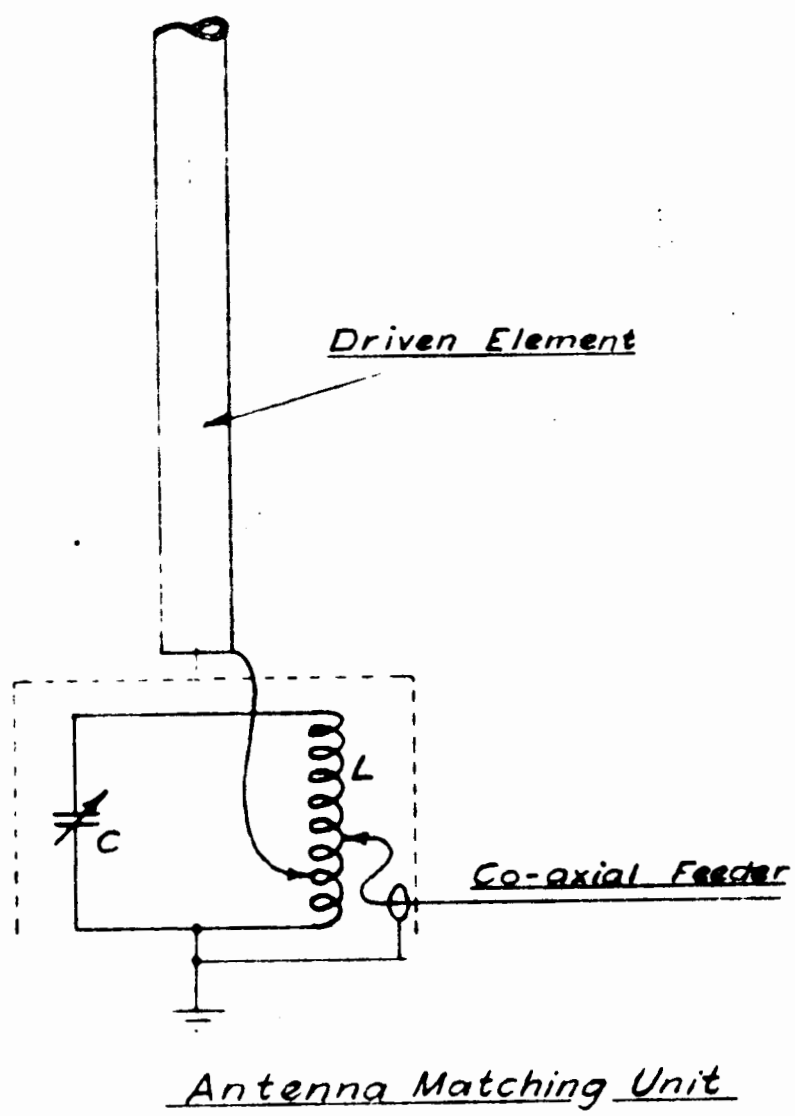


Figure 2.2.1.



ANTENNA MATCHING UNIT.

Figure F 9.2.2.

### 9.3 The earth mat.

In figure F.8.3.5.3.1.1 the derived polar diagram for a 4-director array is in respect of a reflecting plane which consists of a grating of  $12\frac{1}{2}$  SWG copper wires, laid, under tension, in the direction of the distant station, at 12" centres, over a heavy clay soil assuming an operating frequency of 21.47 Mc/s. The grating to be used for the test array must be the same. In order to maintain the wires at the correct distance apart, **cross-connecting wires are soldered** to the main grating at 24" centres.

These will have negligible effect on the reflection properties of the grating but will make for good mechanical stability. The earth mat is efficiently earthed at the base of the radiating element. The grating is  $4\lambda$  long by  $\lambda/2$  across.

### 9.4 The Transmitter.

A battery-driven Marconi signal generator fig.F. 9.4.1, is coupled to a short vertical antenna acting, virtually, as a point source. The ensemble is suspended from a halyard which passes over a pulley on the boom so that the transmitter may be moved up and down, nearly a wavelength from the vertical position of the mast, as in fig. F. 9.4.2. The generator frequency and power output will remain substantially constant throughout the test.

### 9.5 The Receiver.

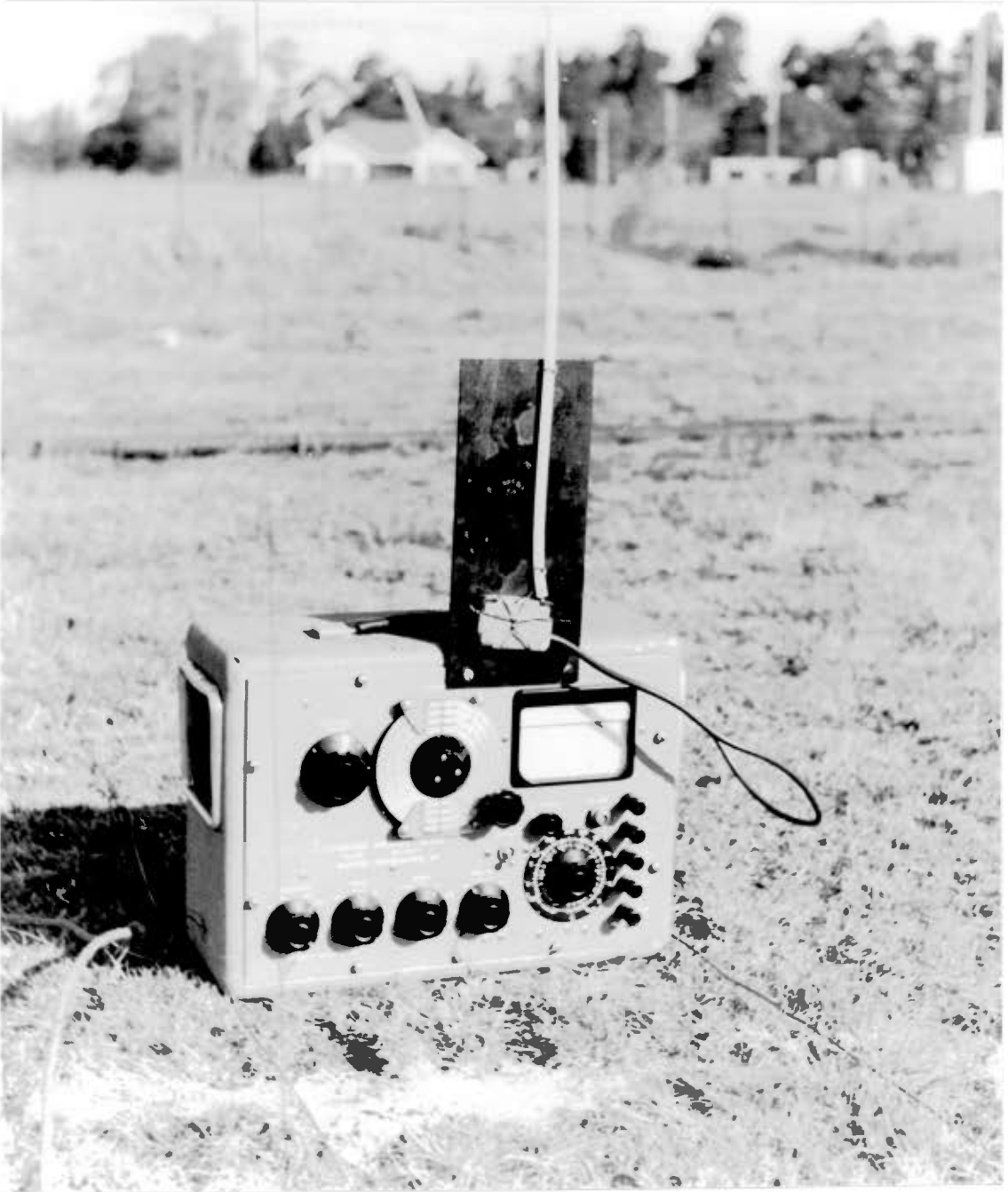
This is an Eddystone Communications Receiver with a signal strength meter in the A.V.C. circuit. By injecting a known signal, from a signal generator, into the aerial input of the receiver and, at the same time, noting the readings of the signal strength meter, the receiver is calibrated. The calibration curve is given in figure F. 9.5.1 and is used to translate set readings to signal input in  $\mu V$ .

### 9.6 The tests on the 4-director array.

The following tests are now made and the numerical results appear in Appendix C:

- (a) With the antenna located  $5\lambda$  away from the 260 ft.mast(see fig. F.9.4.2) the received signal is noted when the transmitter is elevated to various angles between  $0^\circ$  and  $40^\circ$ . The angles are measured with a transit level,fig. F. 9.6.1.
- (b) The tests are repeated with the antenna removed to a distance of approximately  $10\lambda$  from the 260 ft.mast so that now, for the same angle, the transmitter is higher up the mast than in (a). **Angles** are limited to the range  $0^\circ$  to  $20^\circ$  approximately, but, over this range, the results bear the same relationship to each other as those in (a) thus proving that in (a) the ground reflections near the signal generator did not materially influence the results. Also the fact that the transmitter moves vertically, and not on a  $10\lambda$  radius centred on the array, will have negligible effect.



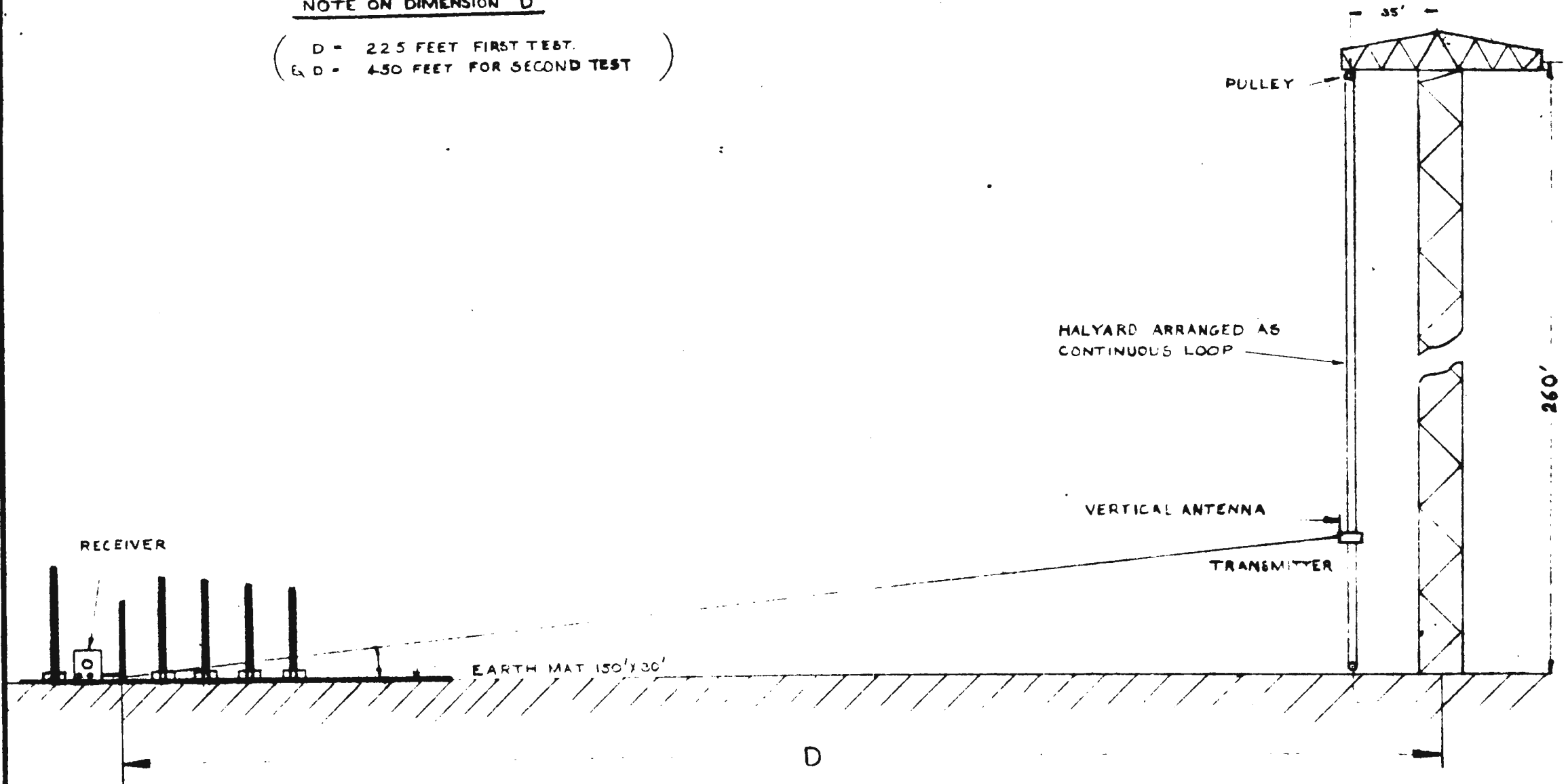


The 21.47 Mc/s Test Transmitter.

Figure F 9.4.1.

NOTE ON DIMENSION "D"

( D = 225 FEET FIRST TEST.  
& D = 450 FEET FOR SECOND TEST )



MEASUREMENT OF VERTICAL POLAR DIAGRAM OF ARRAY AT 21.47 Mc/s  
(NOT TO SCALE)

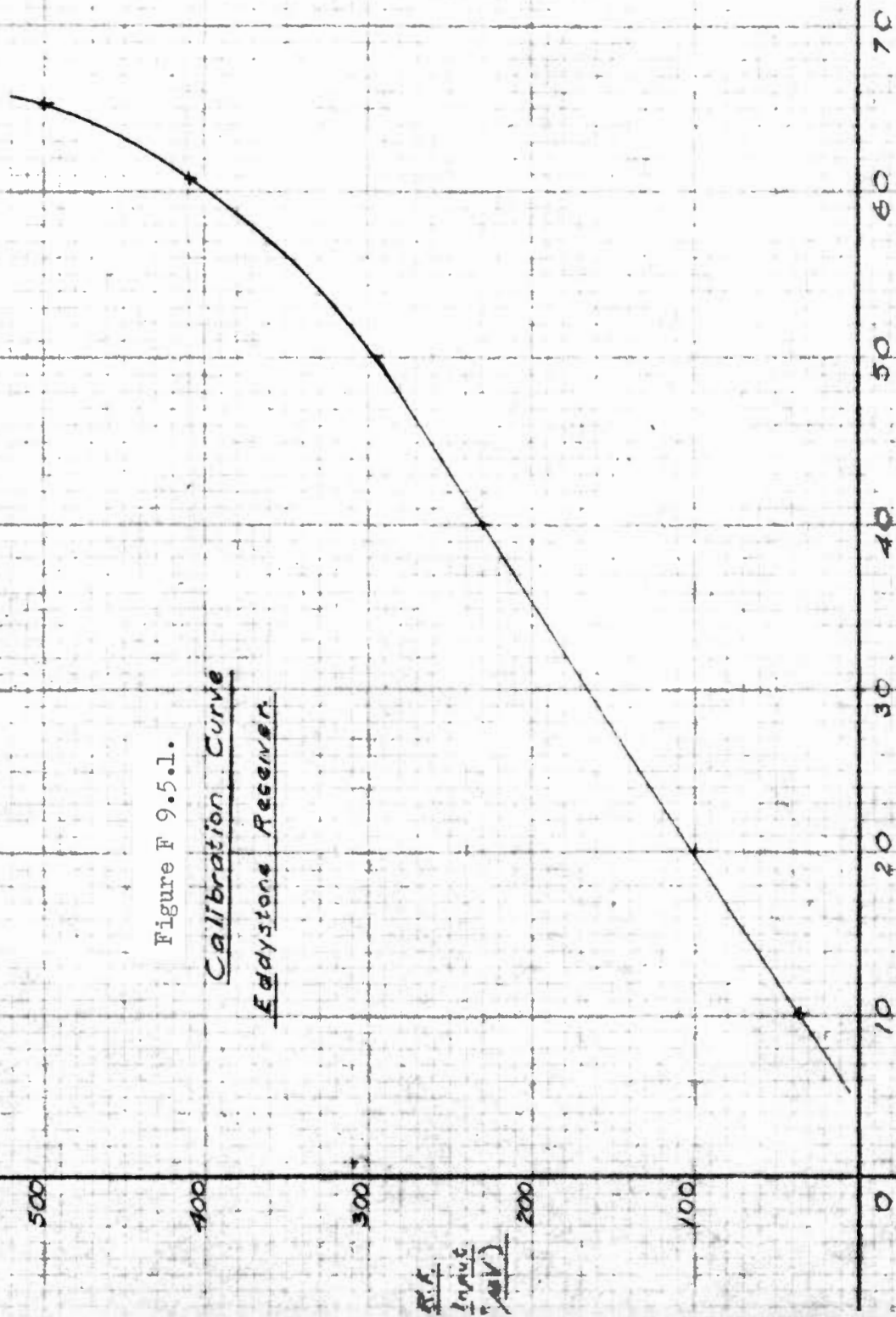
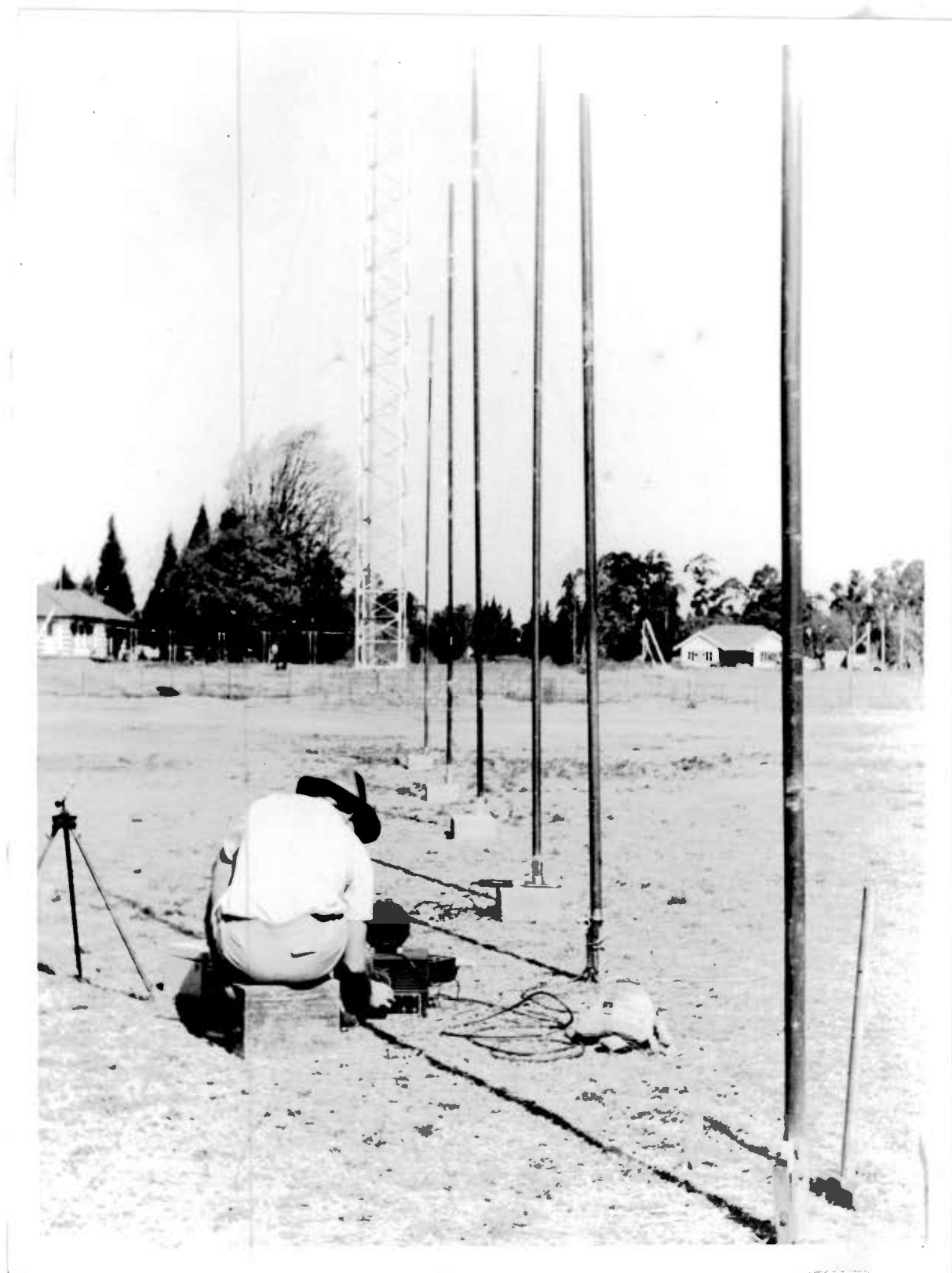


Figure F 9.5.1.

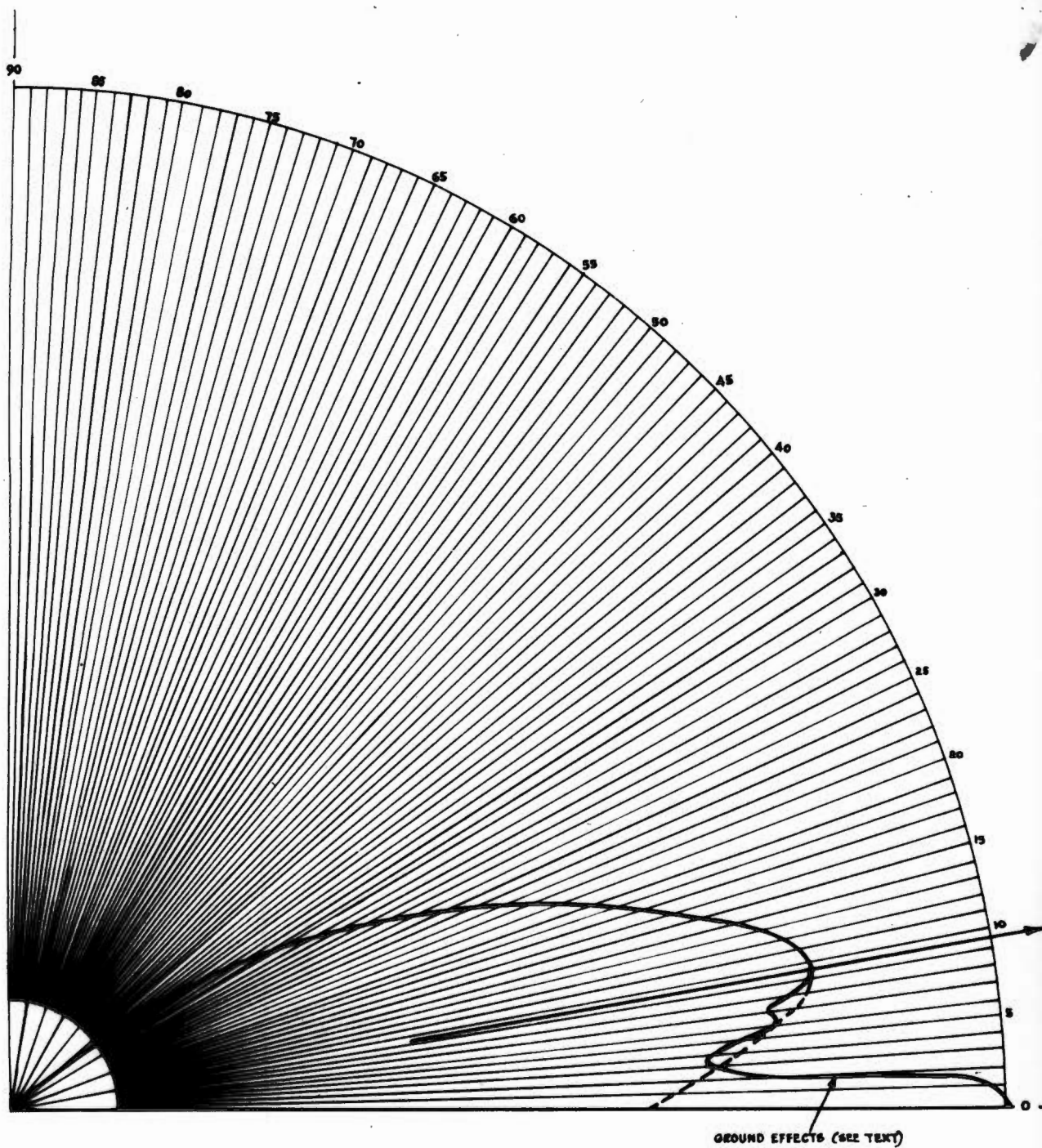
Calibration Curve  
Eddystone Receiver

See Reading MA



The 21.47 Mc/s, 4-Director Test Array

Figure F 9.6.1.



VERTICAL POLAR DIAGRAM  
4-DIRECTOR ARRAY AT 21.47 Mc/s.



9.10

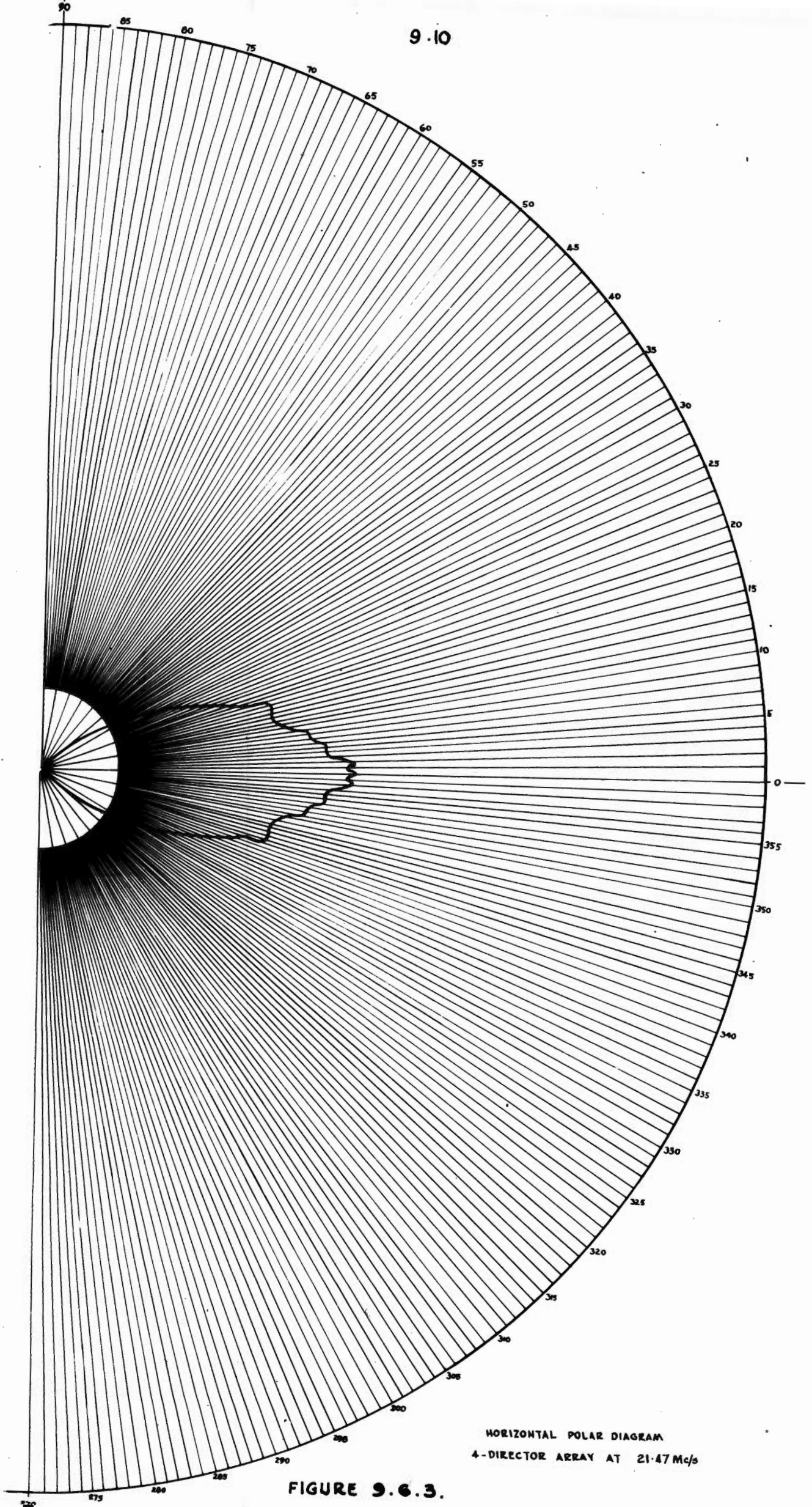


FIGURE 9.6.3.

The measured polar diagram for  $\Delta = 0^\circ - 40^\circ$  is shown in fig. F. 9.6.2. The sensitivity at  $40^\circ$  is so small that it is not difficult to project the curve for values of  $\Delta$  from  $40^\circ$  to  $90^\circ$ . There is a remarkable similarity between the measured polar diagram of figure F. 9.6.2 and that which was predicted (curve 5 of figure F.8.3.5.3.1.1). The maxima occur at  $\Delta = 9\frac{1}{2}^\circ$  and  $\Delta = 10^\circ$  respectively in the two polar diagrams.

At higher values of  $\Delta$  the measured polar diagram falls away to zero slightly more rapidly than predicted. At low values of  $\Delta$  the surface wave masks the space wave, producing a large signal at  $\Delta = 0^\circ$ . The surface wave field strength decreases exponentially in the upward direction and is negligible for values of  $\Delta$  greater than a couple of degrees according to Williams (7, pages 16 and 367-369). At high frequencies the surface wave is attenuated to negligible strength in a relatively short distance; that portion of the measured polar diagram in figure F. 9.6.2 below  $\Delta = 3^\circ$  should therefore be disregarded. The beam width (to the half power points) is  $20\frac{1}{2}$  degrees measured and 21 degrees predicted.

- (c) The frequency of the transmitter is now varied above and below the design frequency with receiver tuning following it and the received signal is noted. It is observed that the half power points occur at 18.47 Mc/s and 23.97 Mc/s (a little lower than expected) and it is noted with pleasure that maximum received signal occurs at 21.47 Mc/s. Clearly this is not a wide band antenna. Its tuning range is only about  $\pm 2.5$  Mc/s. In a point-to-point installation each working frequency will require its own antenna but this is not as great a disadvantage as one might at first imagine.
- (d) The horizontal polar diagram is obtained by moving the transmitter around on an accurately controlled radius of  $1.09 \lambda$ . This distance should be larger for accurate results but practical limitations make it undesirable to use a greater radius. The measured horizontal polar diagram is given in figure F. 9.6.3. The fluctuations are doubtless due to the experimental errors and a fairly accurate representation would probably be given by a smooth curve drawn through the fluctuations. The beam width (to the half power points) is  $34^\circ$ .
- (e) A comparison is now made between the field strength received by the array and that received by a single  $\lambda/4$  rod when the transmitter is elevated to  $\Delta = 9^\circ$ . The difference in signal strength (11.7 db) is 3 db higher than was obtained in a similar comparison in the V.H.F. scale model probably due to mismatch in the full scale test between the single  $\frac{\lambda}{4}$  rod and the feeder.

CHAPTER 10.

THE 6-DIRECTOR DESIGN.

10. 0 SUMMARY OF THIS CHAPTER.

It having been decided that a 6-director design promises to produce satisfactory sensitivity at  $\Delta = 8^\circ$ , the polar diagrams are derived for this array on gratings of copper wire spaced at 15", 12" and  $7\frac{1}{2}$ " centres laid on a heavy clay soil (Fig. F 10.2.1.1). The signal gain is estimated and the "worst-condition signal-to-noise ratio" is calculated for each of the three types of reflecting ground plane (Table T 10.2.3.1/2).

As a check on these calculations tests have been conducted in which (a) the performance of the 6-director design, using a ground plane of copper wire, spaced at 12" centres, is tested against that of a  $\lambda/2$  dipole at various heights and (b) the performance of the 6-director design, using a ground plane of copper wires spaced at 15" centres, is tested against that of the Test Rhombic antenna.

The tests having confirmed the reliability of the calculations, the practical design is given for a double 6-director array as

" a short-wave receiving antenna for use in high-noise areas on long-distance circuits"

with particular reference to the London-Salisbury circuit at noon in September, 1956. The optimum reflecting plane is specified, the vertical polar diagram is given, and the signal-to-noise ratios, at various wave arrival angles for the incoming noise, are calculated in respect of the six-director array and the Test Rhombic antenna. (Table T.10.3.2. 1/2). The "worst-condition signal-to-noise ratio" of the 6-director array is calculated to be better than that of the Test Rhombic by 2.3 db (for distant storms) and 3.0 db (for local storms), the improvement being great (11 db or more) when the noise wave arrival angle exceeds  $40^\circ$ .

It is concluded that, during periods when heavy electrical storms are numerous, the signal-to-noise ratio of the suggested design is likely to be better than that of the Test Rhombic.

- - - - -



### 10.0.1 General.

In Chapter 2 the expected median wave arrival angle, in the London/Salisbury circuit at 21.47 Mc/s, was derived as  $8^\circ$ . It having been decided that a 6-director design with a suitable reflecting plane should be a satisfactory antenna for receiving at this angle, it is now necessary to test it against other antennae of known characteristics and to make such other tests as are necessary before finalizing the design.

### 10. 1.0 Preliminary tests.

These are conducted, for convenience, over the same type "e" grating used for the tests conducted on the 4-director design described in Chapter 9.

### 10. 1.1 Comparison with $\lambda/2$ dipole.

The 6-director array is set up temporarily to receive the B.B.C. 21.47 Mc/s transmission and its output is fed to a communications receiver C.R.88. In addition a  $\lambda/2$  horizontal dipole is constructed at a height of  $1\lambda$ , then  $0.5\lambda$ , and  $0.25\lambda$ . By the operation of a change-over switch either the array or the dipole can be connected to the receiver thus facilitating a comparison between the two.

It is necessary to conduct listening tests in order to look into some aspects that are not reflected in simple level measurements. A group of listeners noted that (a) when the received level from the array was of the same order as the dipole at the height of  $1\lambda$  there was a noticeable improvement in the quality of the speech or music when the array was in use. The reason for this is that when  $H = \lambda$  (see section 6.3.1) the lobe maxima occur at  $\Delta = 15^\circ$  and  $\Delta = 50^\circ$ . It will respond more or less equally to energy arriving at  $\Delta = 8^\circ$  (having taken 3 hops to reach Salisbury), that arriving at  $\Delta = 60^\circ$  (having taken 20 hops to cover the same distance),  $\Delta = 45^\circ$  (having taken 13 hops),  $\Delta = 22^\circ$  (having taken 6 hops). It will respond with greater sensitivity to energy coming in at  $\Delta = 13^\circ$  (having taken 4 hops),  $\Delta = 18^\circ$  (having taken 5 hops) and  $\Delta = 50^\circ$  (having taken 15 hops). As all these components differ in time phase, their combined effect is bound to result in serious distortion. The absence of high angle lobes in the case of the array reduces the amount of interference and distortion. (b) Strong adjacent channel interference received on the dipole from an unidentified station was hardly audible on the array. Presumably the transmission from this station was coming in on a fairly high angle.

### 10.1.2 Effect of nearby arrays.

The 6-director test array was found to be virtually unaffected by the presence of another similar array provided the distance between the two arrays is greater than half a wavelength.

and then deriving the diagram appropriate to the behaviour of a particular ground plane at the operating frequency. Chapter 9 showed that the measured polar diagram of a 4-director design has confirmed that the derived diagram for a type "e" grating is reliable. It is proposed now ~~to~~ proceed to derive the polar diagrams for the 6-director design for a reflecting plane of heavy clay soil covered by a grating type "d" and "f". The gain at  $\Delta = 8^\circ$  will also be derived for these gratings.

It will then be possible, with the information obtained in Chapter 4 on noise field strengths arriving at various values of  $\Delta$  resulting from distant and local storms, to calculate the signal-to-noise ratio for a 6-director design used with gratings "d", "e" and "f".

#### 10. 2.1 Six-director design: Derivation of Polar Diagram.

The polar diagram for the array over a type "e" grating on heavy clay soil has been derived in section 8.3.5.3.1 and appears as curve "6" in fig. F. 8.3.5.3.1.1.

Make the same assumptions, that is, that the soil is a heavy clay in which the earth constants may be taken<sup>(4)</sup> as :-

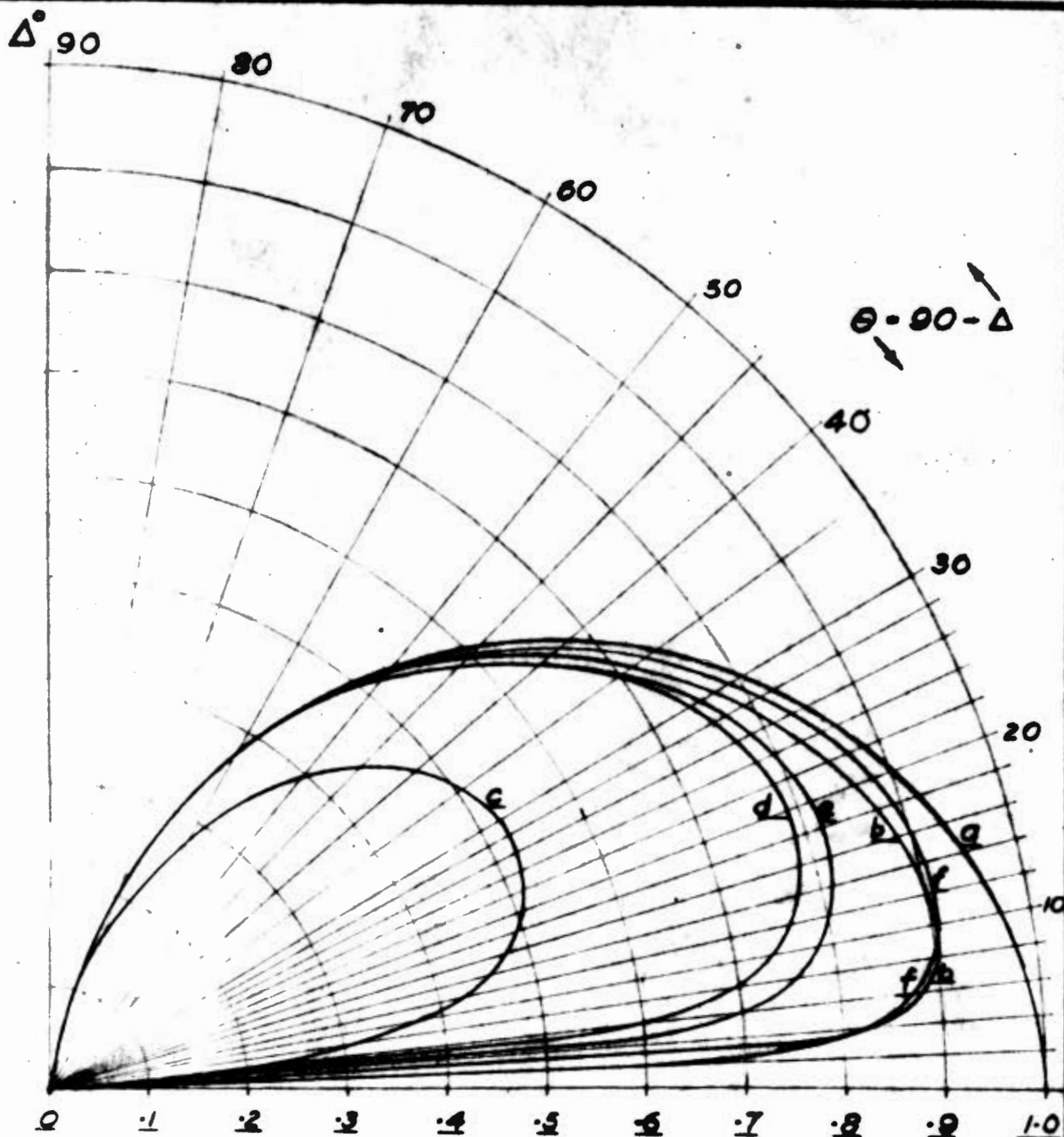
$$\epsilon = 13 \epsilon_0$$

$$\sigma = 4 \times 10^3 \text{ mho/metre.}$$

and that on this soil is laid a grating of the type investigated theoretically in section 6.3.4.1 in which the  $12\frac{1}{2}$  SWG wires, lying parallel to one another and in the direction of the distant station, spaced at 15" ( $0.273 \lambda$ ), 12" ( $0.218 \lambda$ ), and  $7\frac{1}{2}$ " ( $0.136 \lambda$ ) centres are referred to as gratings "d", "e" and "f" respectively, yielding curves "d", "e" and "f" in fig. F. 6.3.4.1.3.

In Table T. 10.2.1.1 below, the values for "a", "d", "e" "f" are obtained from fig. F. 6.3.4.1.3 and those of curve "4" from fig. F. 8.3.5.3.1.1. The values of "x", "y", and "z" represent the derived vertical polar diagrams of the 6-director design over gratings type "d", "e" and "f" respectively and are plotted in fig. F. 10.2.1.1.

For convenience figures F. 6.3.4.1.3 and F. 8.3.5.3.1.1 are repeated as pages 10.4 (a) and 10.4 (b) as they are required for the compilation of Table T. 10.2.1.1 on page 10.4 .



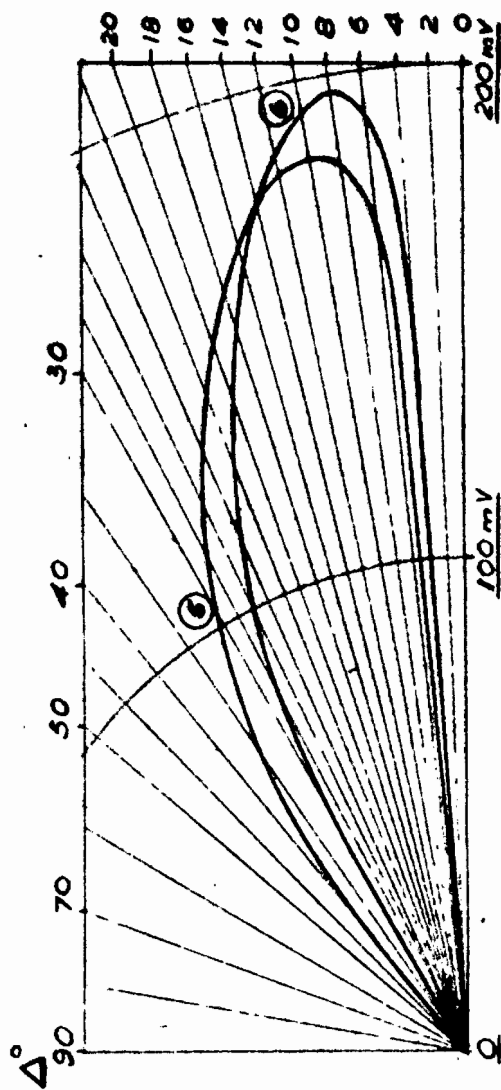
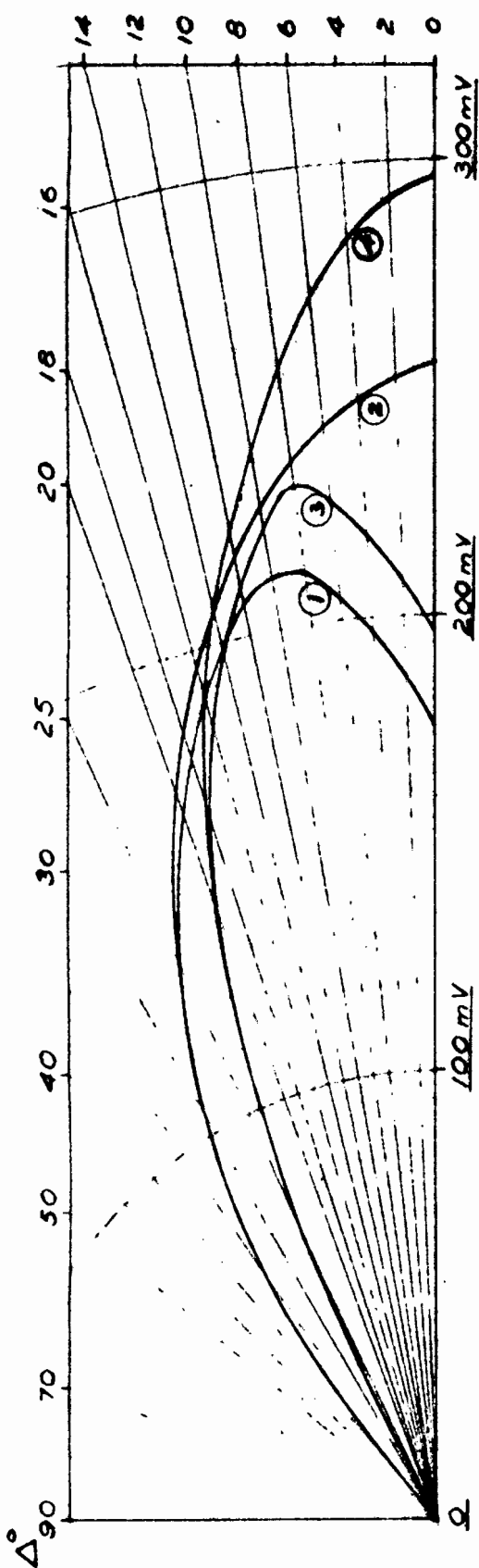
DERIVED VERTICAL POLAR DIAGRAMS AT 21.47 Mc/s.

Grounded vertical  $\lambda/4$  monopole on :

- |                                    |           |                  |
|------------------------------------|-----------|------------------|
| 1. Ground of infinite conductivity | (curve a) | as in F 6.3.3.1. |
| 2. Sea water                       | (curve b) |                  |
| 3. Heavy clay soil                 | (curve c) |                  |
| 4. Grid of 15" spacing on "3"      | (curve d) |                  |
| 5. Grid of 12" spacing on "3"      | (curve e) |                  |
| 6. Grid of 7½" spacing on "3"      | (curve f) |                  |

**Fig. F 6.3.4.1.3**

(Repeated here for convenience)



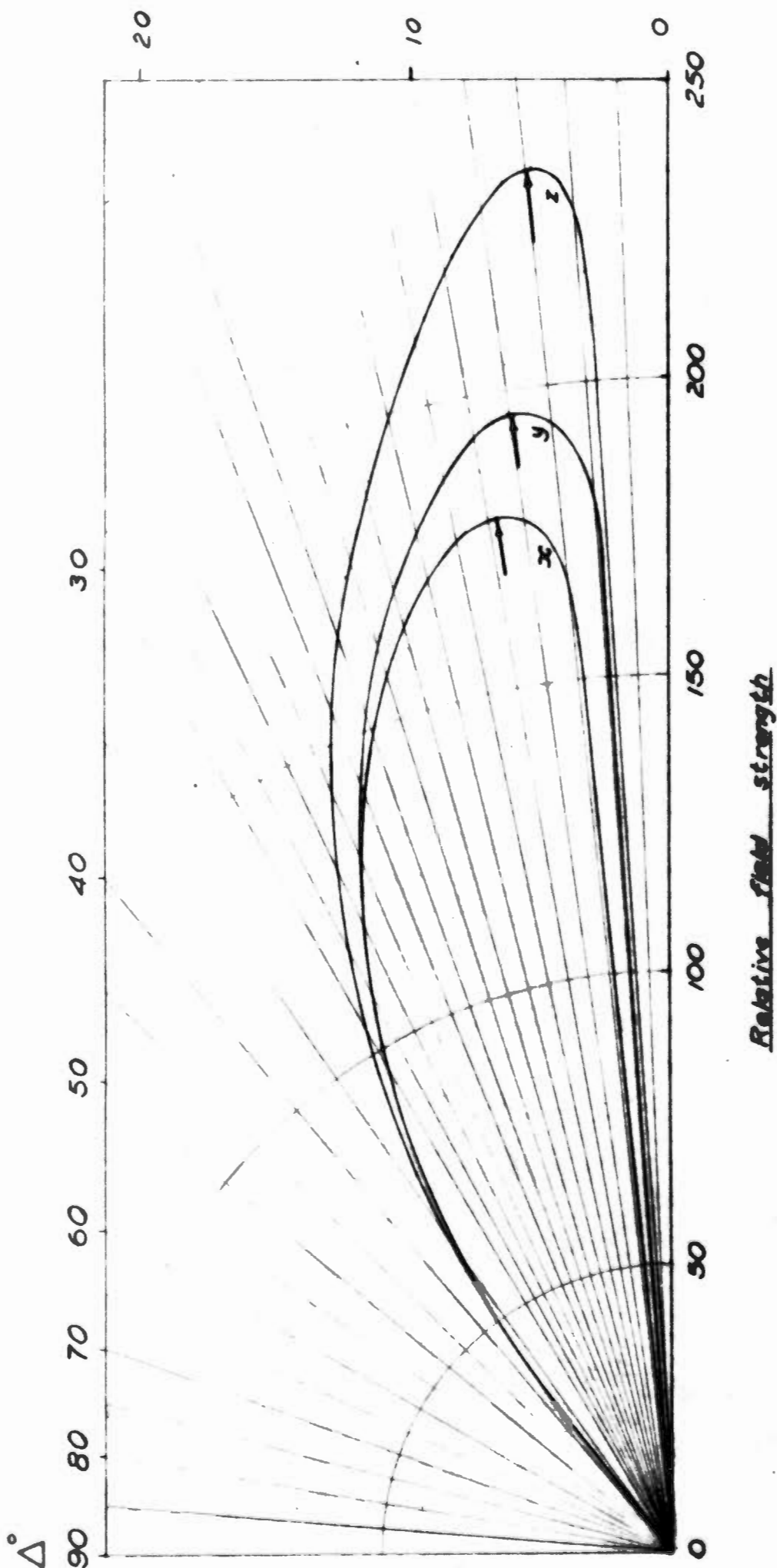
**Key.**

- Curve 1 : Measured polar diagram (24.3 Mc/s), 4-director array, over aluminum sheeting.
- Curve 2 : Derived polar diagram, 4-director array, over perfectly conducting ground.
- Curve 3 : Measured polar diagram (24.3 Mc/s), 6-director array, over aluminum sheeting.
- Curve 4 : Derived polar diagram, 6-director array, over perfectly conducting ground.
- Curve 5 : Derived polar<sup>+</sup> diagram ( 21.47 Mc/s), over grating.
- Curve 6 : Derived polar<sup>+</sup> diagram ( 21.47 Mc/s), over grating.

<sup>+</sup>The grating consists of 12½ SWG copper wires, laid in the direction of the distant station, at 12° centres ( see chapter 6 ).

**Figure P 8.3.5.3.1.1**

( Repeated here for convenience )



*Relative field strength*

*Fig. F 10.2.1.1*

Derived vertical polar diagrams of 6-director array using, as ground plane, grid of copper wires spaced at 15" centres (curve x), 12" (curve y), 7 $\frac{1}{2}$ " (curve z).

### 10. 2.3 Six-director design: derivation of signal-to-noise ratios.

#### (a) Distant Storms.

The same calculations will be made in respect of the 6-director array as those applied to the test Rhombic antenna in section 4.3.2.6, the H 4/4/1 Koonans array, and the other types dealt with in sections 6.3.1/2/3. As indicated in Chapter 2 the wanted signal is assumed to be coming in at  $\Delta = 8^\circ$  at the median field strength of  $4\mu\text{V/m}$ . Figure F. 4.4.1.1 summarised the calculations performed in Chapter 4 to produce the noise field strength coming in at various values of  $\Delta$  as a result of distant storms.

By comparing the noise field strength distribution (fig. F. 4.4.1.1) with the antenna vertical polar diagrams (fig. F. 10.2.1.1) there can be calculated, as described in Chapters 3 and 4, the signal-to-noise ratio, for various values of  $\Delta$  for the 6-director design with the three types of reflecting plane. As derived in Chapter 3 the power fed to the receiver by an antenna of  $G_\Delta$  in the direction  $\Delta^\circ$  to the horizontal due to a wave of wavelength  $\lambda$ , of strength  $E_\Delta \mu\text{V/m}$ , arriving at an angle  $\Delta^\circ$  to the horizontal, (assuming correct matching) is equal to

$$G_\Delta \times \lambda^2 \times E_\Delta^2 \times 10^{-12} / 4730 \text{ watts.}$$

If the noise energy were to be arriving at a particular angle,  $\Delta$ , then if the antenna gain at that angle is  $G_\Delta$  and the noise field strength =  $E_\Delta \mu\text{V/m}$ , the noise power fed to the receiver is equal to:-

$$G_\Delta \times \lambda^2 \times E_\Delta^2 \times 10^{-12} / 4730 \text{ watts}$$

and the signal power fed to the receiver is equal to

$$G_8 \times \lambda^2 \times 4^2 \times 10^{-12} / 4730 \text{ watts.}$$

The signal-to-noise ratio for noise coming in at the one value of  $\Delta$  only.

$$= \frac{\text{Signal power}}{\text{Noise power.}}$$

$$= \frac{G_8 \times 4^2}{G_\Delta \times E_\Delta^2} = \left( \frac{x_8 \times 4}{x_\Delta \times E_\Delta} \right)^2 \text{ or } \left( \frac{y_8 \times 4}{y_\Delta \times E_\Delta} \right)^2 \text{ or } \left( \frac{z_8 \times 4}{z_\Delta \times E_\Delta} \right)^2$$

as the case may be for the three curves, x, y and z of fig. F. 10.2.1.1.

The results of this series of calculations appear in Table T 10.2.3.1 below.

P.T.O. for Table T. 10.2.3.1.

$\Delta$	$E_{\Delta}$ noise $\mu$ V/m	Type "d" grating		Type "e" grating		Type "f" grating	
		$x_8/x_{\Delta}$	S-t-n ratio.	$y_8/y_{\Delta}$	S-t-n ratio.	$z_8/z_{\Delta}$	S-t-n ratio.
8	.60	1.00	44.4	1.00	44.4	1.00	44.4
10	.75	.99	27.9	1.01	29.0	1.04	30.8
12	.80	1.00	25.0	1.05	27.5	1.10	30.2
14	1.05	1.03	15.4	1.10	17.6	1.16	19.5
16	1.25	1.07	11.7	1.14	13.3	1.21	15.0
18	1.40	1.12	10.2	1.20	11.8	1.29	13.6
20	1.65	1.18	8.2	1.27	9.5	1.38	11.2
22	1.80	1.25	7.7	1.36	9.1	1.46	10.5
24	2.10	1.33	6.6	1.50	8.2	1.60	9.3
26	2.30	1.47	6.5	1.64	8.1	1.77	9.5
28	2.60	1.61	6.1	1.78	7.5	1.95	9.0
30	2.85	1.77	6.2	1.96	7.6	2.15	9.1
32	3.20	2.06	6.6	2.27	8.0	2.45	9.4
34	3.50	2.50	8.2	2.74	9.8	2.88	10.8
36	3.75	3.14	11.2	3.44	13.4	4.15	15.6
38	4.10	4.30	17.6	4.80	21.9	5.90	33.1
40	4.35	6.65	37.5	7.26	44.5	8.80	65.3
42	4.60	$\infty$	$\infty$	$\infty$	$\infty$	$\infty$	$\infty$

TABLE T. 10.2.3.1

It should be noted that the values of  $E_{\Delta}$ , the noise field strength for various values of  $\Delta$ , relate to particular storms. If, for example, a storm is occurring beyond the horizon such that the noise energy is arriving from the ionosphere at an angle of elevation  $\Delta = 16^{\circ}$  then the effective noise field strength for a receiver of 10 kc/s bandwidth tuned to 21.47 Mc/s (see Chapter 4) will have a median value of 1.25  $\mu$  V/m and, for a wanted signal of strength 4  $\mu$  V/m arriving at  $\Delta = 8^{\circ}$ , will produce a signal-to-noise ratio of 11.7, 13.3, and 15.0 in a 6-director design on types "d", "e" and "f" grating respectively for the duration of the lightning flash. If the next flash occurs at such a distance as, for example, to make  $\Delta = 12^{\circ}$  the signal-to-noise ratio for the duration of this flash will be 25.0, 27.5 and 30.2 respectively for the array on the three different reflecting planes.

The "worst condition" signal-to-noise ratio occurs in each case when  $\Delta = 28^{\circ}$  and the values are:-

- (i) for the 6-director design on type "d" grating:  
6.1 i.e. 7.8 db.
- (ii) for the 6-director design on type "e" grating:  
7.5 i.e. 8.8 db.
- (iii) for the 6-director design on type "f" grating:-  
9.0 i.e. 9.5 db.



(b) Local storms.

A method for the calculation of the effective noise field strength  $E_{\Delta}$   $\mu$  V/m arriving at angle of elevation  $\Delta$  in respect of local storms, was derived in section 4.4.2. An expression for the special case of the effective noise field strength for a receiver of 10 Kc/s bandwidth, tuned to 21.47 Mc/s is given in eqn. 4.4.2.2 as:

$$E_{\Delta} = 430 \sin \Delta.$$

The signal-to-noise ratio, for a wanted signal, of strength  $4\mu$  V/m, arriving at  $\Delta = 8^{\circ}$ , is given, as before, by the expression:

$$S. to n. ratio = \frac{G_8 \times 4^2}{G_{\Delta} \times E_{\Delta}^2}$$

For the 6-director design over the type "d", "e" and "f" reflecting plane the S. to n. ratio is given by:

$$S. to n. ratio = \left( \frac{x_8 \times 4}{x_{\Delta} \times E_{\Delta}} \right)^2 \text{ or } \left( \frac{y_8 \times 4}{y_{\Delta} \times E_{\Delta}} \right)^2 \text{ or } \left( \frac{z_8 \times 4}{z_{\Delta} \times E_{\Delta}} \right)^2$$

from the curves "x", "y", "z" from fig. F.10.2.1,1 corresponding to types "d", "e" and "f" grating respectively.

The result of this series of calculations appear in Table 10.2.3.2 below.

$\Delta^{\circ}$	$E_{\Delta}$ noise.	Type "d" grating.		Type "e" grating.		Type "f" grating.	
		$x_8/x_{\Delta}$	S. to n. ratio.	$y_8/y_{\Delta}$	S. to n. ratio.	$z_8/z_{\Delta}$	S. to n. ratio.
			$10^3$		$10^3$		$10^3$
8	60	1.00	4.45	1.00	4.45	1.00	4.45
10	74	.99	2.85	1.01	2.98	1.04	3.15
12	89	1.00	2.01	1.05	2.22	1.10	2.45
14	104	1.03	1.56	1.10	1.79	1.16	1.99
16	118	1.07	1.32	1.14	1.50	1.21	1.68
18	133	1.12	1.13	1.20	1.30	1.29	1.50
19	140	1.15	1.08	1.23	1.23	1.34	1.47
20	147	1.18	1.03	1.27	1.19	1.38	1.41
21	154	1.21	.99	1.32	1.18	1.42	1.36
22	161	1.25	.97	1.36	1.14	1.48	1.35
23	168	1.30	.96	1.42	1.14	1.55	1.36
24	175	1.35	.95	1.50	1.18	1.62	1.37
26	189	1.47	.97	1.64	1.20	1.77	1.40
28	202	1.61	1.02	1.78	1.24	1.95	1.49
30	215	1.77	1.08	1.96	1.33	2.15	1.60

TABLE T. 10. 2.3.2.

The "worst-condition" signal-to-noise ratio occurs in each case as follows:

- (iv) 6-director design on type "d" grating:  
 $0.95 \times 10^3$  at  $\Delta = 24^{\circ}$ .
- (v) 6-director design on type "e" grating:  
 $1.14 \times 10^3$  at  $\Delta = 22\frac{1}{2}^{\circ}$ .
- (vi) 6-director design on type "f" grating:  
 $1.35 \times 10^3$  at  $\Delta = 22^{\circ}$ .



### 10. 3.0 Comparisons: Test Rhombic vs. 6-director design.

The Test Rhombic investigated theoretically in Chapters 3 and 4 as regards signal and noise pick-up respectively, represents a large version of the design. As stated earlier, the dimensions are as follows:

Side length =  $5 \lambda$

Height =  $1 \lambda$

$\psi = 70^\circ$

For example, this is the largest design considered in the C.C.I.R. publication "Antenna Diagrams"<sup>(11)</sup>.

First will be made a comparison of the calculated gain of the two antennas, then a comparison of their calculated signal-to-noise ratios, and finally a comparison resulting from practical measurements.

After this it will be seen if the proposed 6-director design offers any advantage over the Test Rhombic.

### 10. 3.1 Comparison of calculated signal gain of Test Rhombic and 6-director design.

#### Calculated gain of Test Rhombic.

Using equation 12.18 derived in Appendix A, it was calculated in section 3.3 that the gain of a Rhombic, of the dimensions quoted for the Test Rhombic, in the direction  $\Delta = 0^\circ$ , will be 18.4 db above that obtained in the equatorial plane of a  $\lambda/2$  dipole in free space.

In section 6.3.2 the C.C.I.R. "Antenna Diagrams"<sup>(11)</sup> was quoted as indicating that in the maximum radiation direction ( $\Delta = 12.5^\circ$ ) an antenna of dimensions equal to that of the Test Rhombic produced a measured field strength of 2000 mV/m at 1 km, when the radiated power was 1 kw. The field strength produced in the equatorial plane at a distance of 1 km, in the case of a free-space  $\lambda/2$  dipole radiating 1 kW, is 222 mV/m as derived in Appendix A, eqn. 11.19. The gain at  $\Delta = 12.5^\circ$ , therefore is:

$$\left(\frac{2000}{222}\right)^2 = 19.09 \text{ db.}$$

At  $\Delta = 0^\circ$  the gain will be  $19.09 - 3.01 = 16.08 \text{ db. (Fig. F.4.4.3.1).}$

This result is preferred to the one 2.3 db greater, quoted above, because the C.C.I.R. result has taken into account such modifying factors as sag of wire, imperfections in the reflection coefficient of the soil, which inevitably occur in a practical antenna.

The Test Rhombic is a horizontally polarized antenna. At  $\Delta = 0^\circ$  the Reflection Coefficient ( $R_H$ ) for heavy clay soil, from Appendix A, equation 7.15, or from the curves reproduced by Williams<sup>(7)</sup>, may be taken as 0.92 angle  $15^\circ$  with the result that the Test Rhombic sensitivity, over heavy clay soil, is about  $(1+0.92)/2 = 0.96$  of what it would be over perfectly conducting ground. The difference is negligible.

Calculated gain of the 6-director design.

As derived in section 10. 2.2 the gain in the direction  $\Delta = 8^\circ$ , of the 6-director design over a free-space dipole, is:

Using type "d" grating : 8.9 db.

Using type "e" grating : 9.7 db.

Using type "f" grating : 11.2 db.

Summary of comparison.

At  $\Delta = 8^\circ$  the comparison between the calculated results is summarised in Table T. 10. 3.1 below:-

Type:	Gain over dipole	Gain over Test Rhombic
6-director design, type "d" grating.	8.9 db.	-7.2 db.
6-director design, type "e" grating.	9.7 db.	-6.4 db.
6-director design, type "f" grating.	11.2 db.	-4.9 db.

T A B L E T 10.3. 1.

10.3.2 Comparison of calculated signal-to-noise ratio:

(a) Distant Storms.

$\Delta/\phi$	Signal-to-noise ratio 6-director design on grating			S.to N.ratio Test Rhombic.	S.to N. of 6-director S.to N. of Test Rhombic expressed in db.
	type "d"	type "e"	type "f"		
8/0	44.4	44.4	44.4	44.4	0.
10/0	27.9	29.0	30.8	17.8	+2.4
12/0	25.0	27.5	30.2	12.5	+3.8
14/0	15.4	17.6	19.5	7.7	+4.1
16/0	11.7	13.3	15.0	6.1	+4.0
18/0	10.2	11.8	13.6	8.2	+2.2
20/0	8.2	9.5	11.2	7.4	+1.8
22/0	7.7	9.1	10.5	12.1	-0.2
24/0	6.6	8.2	9.3	36.3	-5.9
26/0	6.5	8.1	9.5	151.0	-42.0
28/0	6.1	7.5	9.0	237.0	-14.0
30/0	6.2	7.6	9.1	476.0	-17.2
32/0	6.6	8.0	9.4	155.0	-12.07
34/0	8.2	9.8	10.8	131.0	-10.8
36/0	11.2	13.4	19.6	61.7	-5.0
38/0	17.6	21.9	33.1	23.8	+1.4
40/0	37.5	44.5	65.3	10.6	+7.9
42/0	$\infty$	$\infty$	$\infty$	5.5	+ $\infty$
46/24	$\infty$	$\infty$	$\infty$	5.2	+ $\infty$
57/0	$\infty$	$\infty$	$\infty$	10.8	+ $\infty$
57/36	$\infty$	$\infty$	$\infty$	14.9	+ $\infty$

T A B L E T. 10. 3.2.1 (see T. 10.2.3.1).

Table T.10. 3.2.1 sets out the signal-to-noise ratio of the 6-director array, using type "d" grating (15" centres), type "e" grating, (12" centres), and type "f" grating (7½" centres) respectively, laid on a heavy clay soil, in respect of distant storms. Table T. 10.3.2.2 does the same for local storms.

(b) Local storms.

$\Delta^\circ$	$E_{\Delta}$ noise	Signal-to-noise ratio $\times 10^{-3}$ 6-director design on grating:			S.to n.ratio Test Rhombic $\times 10^{-3}$	S.to n.ratio of 6-director type "f" Test Rhombic expressed in db.
		type "d"	type "e"	type "f"		
8	10	4.45	4.45	4.45	4.45	0
10	74	2.85	2.98	3.15	1.80	+2.4
12	89	2.01	2.22	2.45	1.03	+3.8
14	104	1.56	1.79	1.99	0.78	+4.1
16	118	1.32	1.50	1.68	0.67	+4.0
18	133	1.13	1.30	1.50	0.91	+2.2
20	147	1.03	1.19	1.41	0.93	+1.8
22	161	0.97	1.14	1.35	1.54	-0.6
24	175	0.95	1.18	1.37	5.3	-5.9
42	288	very high	very high	very high	1.4	$+\infty$
46	309	,,	,,	,,	1.37	$+\infty$
57	361	,,	,,	,,	2.93	$+\infty$

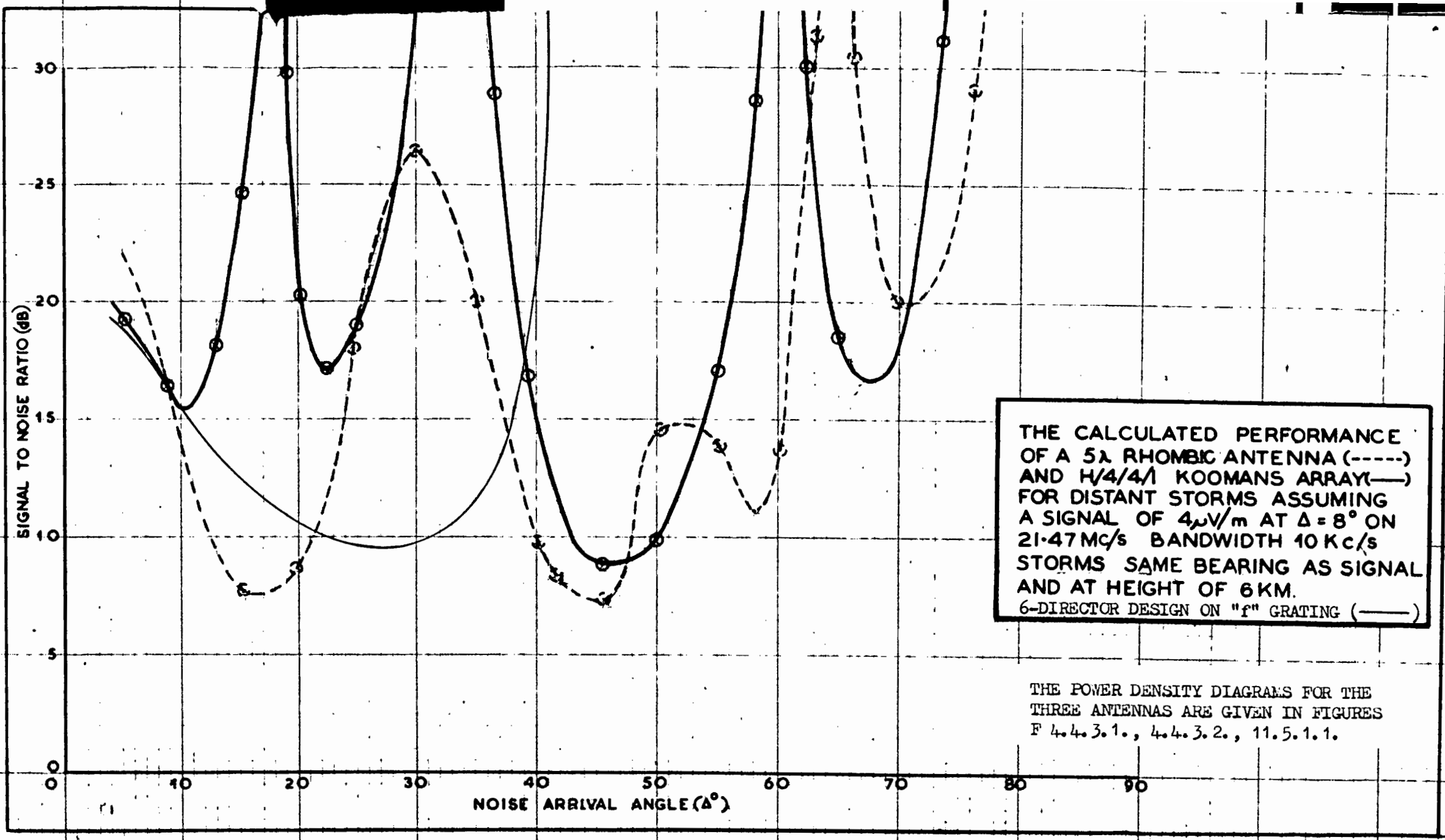
T A B L E T. 10.3.2.2. (See T. 10.2.3.2).

Clearly the signal-to-noise ratio will depend, in the case of each of the antennas, upon the position of the storm at any given time. e.g. If the grating is of the "f" type and the storm is at that distance which will cause  $\Delta$  to be  $16^\circ$ , then from the Tables T. 10.3.2.1/2 the signal-to-noise ratio of the 6-director design is expected to be about 4 db better than the Test Rhombic. On the other hand if the noise is coming in at  $\Delta = 24^\circ$  the signal-to-noise ratio of the 6-director design is expected to be about on a par with that of the Test Rhombic. For a given value of  $\Delta$  the ratio of the two signal to noise ratios is the same whether distant or local storms are being considered and this aspect forms a useful means of checking the results.

It should be clear from the foregoing that the term "measured signal-to-noise" ratio is virtually meaningless unless related to closely defined parameters such as the wave arrival angle of the noise energy. In Chapter 4 it was stated that, when judging between two antennas, it is of value to compare the signal-to-noise ratios at those values of  $\Delta$  when the ratio is worst for each of them, i.e. to compare their "worst condition signal-to-noise ratios". Calculation is more profitable than any attempt to measure the ratios at these particular values of  $\Delta$ .

The "worst signal-to-noise ratio" occurs, in the case of distant storms, when  $\Delta / \phi = 46^\circ/24^\circ$  for the Test Rhombic (7.2 db) and when  $\Delta / \phi = 28^\circ/0^\circ$  for the 6-director design type "f" (9.5 db). In the case of local storms it occurs when  $\Delta / \phi = 16^\circ/0^\circ$  for the Test Rhombic (-31.3 db) and when  $\Delta / \phi = 22^\circ/0^\circ$  for the 6-director design type "f" (-28.4 db). In both cases an improvement is effected by the 6-director design with type "f" grating, the improvement being 2.3 db and 2.9 db respectively.

The results are summarised in Fig. F. 10.3.2.1 where the variation of signal-to-noise ratio is plotted against  $\Delta$  for the Test Rhombic, a H/4/4/1 Koonmans Array, and the 6-director type "f" design. The relation between the curves will be the same for local storms.



THE CALCULATED PERFORMANCE OF A  $5\lambda$  RHOMBIC ANTENNA (----) AND H/4/4/1 KOOMANS ARRAY (—) FOR DISTANT STORMS ASSUMING A SIGNAL OF  $4\mu\text{V/m}$  AT  $\Delta = 8^\circ$  ON 21.47 MC/s BANDWIDTH 10 KC/s STORMS SAME BEARING AS SIGNAL AND AT HEIGHT OF 6 KM.  
6-DIRECTOR DESIGN ON "f" GRATING (—)

THE POWER DENSITY DIAGRAMS FOR THE THREE ANTENNAS ARE GIVEN IN FIGURES F 4.4.3.1., 4.4.3.2., 11.5.1.1.

Figure F 10.3.2.1.

It is observed:

- (a) that the 6-director design with type "f" grating is expected to have a better s.-to-n. performance than the Test Rhombic for all values of  $\Delta$  above  $8^\circ$  except for the range  $\Delta = 21^\circ$  to  $38^\circ$ ; (b) that for values of  $\Delta$  greater than  $40^\circ$  the s.-to-n. performance of the 6-director design is expected to be considerably better than that of the Test Rhombic and the H/4/4/1 Koomans Array; (c) that the s.-to-n. performance of the Koomans Array is superior to that of the 6-director design for all values of  $\Delta$  below  $40^\circ$ .

It would thus be expected that on occasions when thunder activity is limited to areas more than 1000 km. away, the s.-to-n. performance of all three antennas will be good. When the thunder activity is occurring 550 to 1000 km. away the performance of the 6-director design is expected to surpass that of the Test Rhombic but be inferior to that of the Koomans Array. When the thunder activity is occurring 250-550 km. away the performance of both the Test Rhombic and the Koomans Array is expected to surpass that of the 6-director design but for storms nearer than 250 km. the performance of the 6-director design is expected to be considerably better than that of the other two.

As indicated in Chapter 4, the concept of the equivalent noise transmitter provides a useful means of comparing the probable performance of receiving antennas because the thunder storm can be arranged to "occur" in any desired locality thus making possible a more comprehensive comparison than is usually possible from practical measurements.

As a practical check on the validity of the calculated performance, tests were conducted (a) to measure the difference in gain, as evidenced on the incoming signal from London, between the Test Rhombic and the 6-director design and (b) to measure the difference in power fed to the receiver, in the absence of the signal, due to distant storms and local storms.

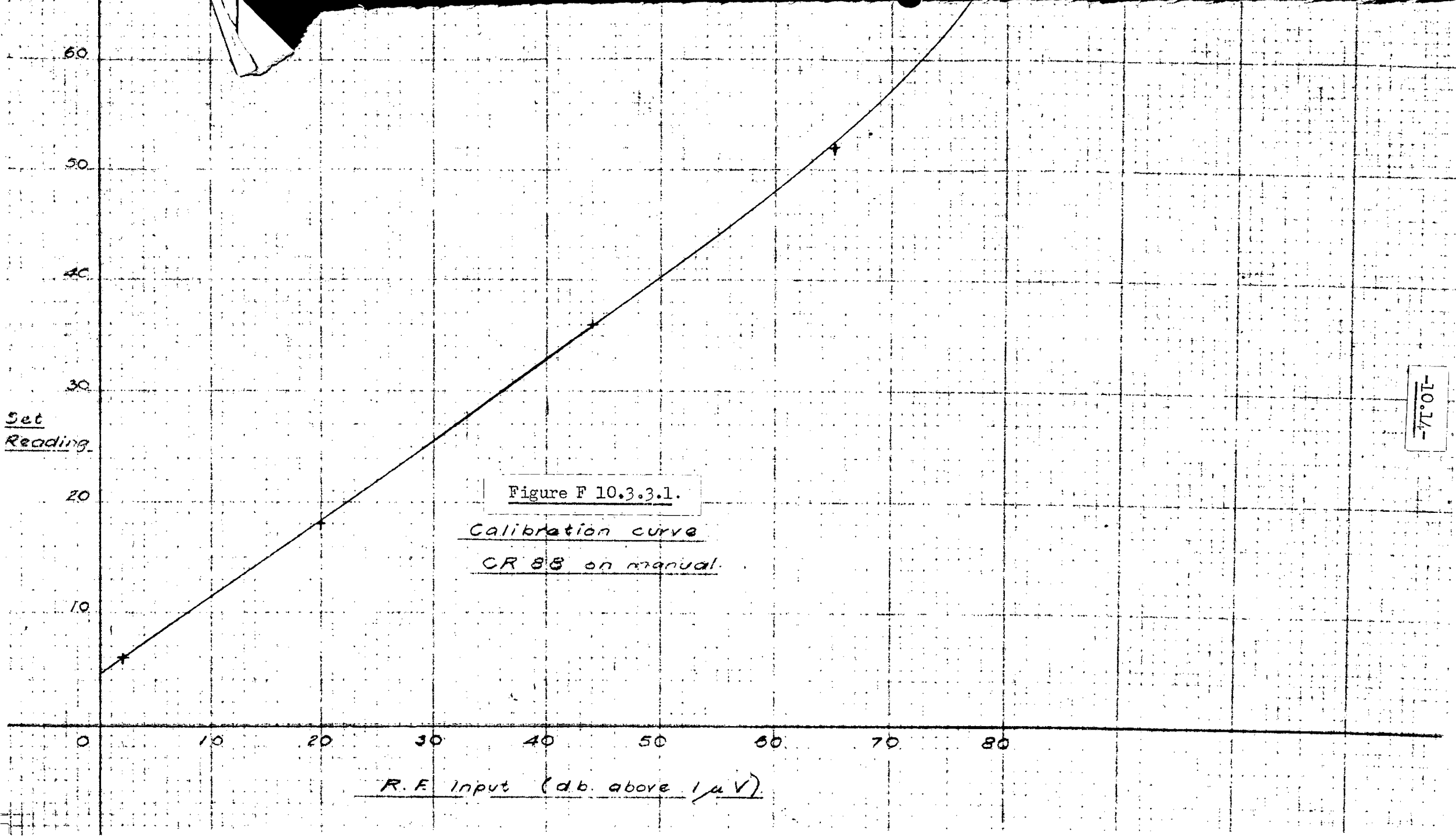
### 10.3.3 Comparison of measured gain of Test Rhombic and 6-director design.

The centre tap of the terminating resistor of the Test Rhombic is earthed to minimise noise from static build-up. The Rhombic is aligned on London.

The 6-director design is as specified in Fig. F.8.3.5.2.1 and is aligned on London. As the tests are merely for the sake of checking the reliability of the calculations, the type "d" grating, which is the cheapest of the three considered, was chosen.

The output from each antenna was connected, in turn, at frequent intervals, via matched co-axial feeder, to a CR 88 receiver. The "set-readings" of the signal strength meter were converted to "R.F. input in db above  $1\mu V$ " using the calibration curve of Fig. F.10.3.3.1. Tests were made over a long period during the latter half of 1956 when the signal was strong and steady.

It was found that the average difference in signal strength was about 8 db in favour of the Test Rhombic.



The expected difference in sensitivity, calculated in section 10.3.1., is 7.2 db for the type "d" grating ( see Table T.10.3.1.).

The two results are so alike that the measured results are taken to confirm that the theoretically-derived performance is reliable. However, a reduction will be accepted in the calculated gain of the 6-director design as follows :-

With type "d" grating : 8.1 db at  $\Delta = 8^\circ$

With type "e" grating : 8.9 db at  $\Delta = 8^\circ$

With type "f" grating : 10.4 db at  $\Delta = 8^\circ$ .

All are relative to the gain in the equatorial plane of a free-space  $\lambda/2$  dipole.

#### 10.3.4. Comparison of measured noise of Test Rhombic and 6-director design.

The noise output was due to :

- (a) Noise generated in the receiver.
- (b) Noise induced in the antenna.

The signal strength meter in the receiver was found to be not sufficiently sensitive to measure noise. Therefore a G.P.O. Transmission Measuring Set was connected to the 600 ohm output of the receiver and the audio frequency noise output was measured. First the receiver noise was measured by taking the noise output when the antenna was disconnected and the aerial terminals were joined by a resistance equal to the characteristic impedance of the feeder. Next the noise output was taken when the same receiver was connected in turn to the Rhombic antenna and to the array. These measurements were made on a number of occasions over a long period at the same time as the signal strength tests were made.

Two sets of typical results are given which are representative of

- (a) widespread thunder activity beyond the horizon, and
- (b) local thunder activity ( maximum surge readings given).

On both occasions the difference in signal strength was about 8 db.

#### (a) Distant Storms

	6-director design		Test Rhombic	
	A.F. level db <sub>o</sub>	Power mW.	A.F. level db <sub>o</sub>	Power mW
Noise generated in receiver (X)	-23	.005	-23	.005
(X) plus atmospheric noise	-15.5	.028	-7.5	.178
Therefore Atmospheric noise		.023		.173

$$\frac{\text{Noise received by Rhombic}}{\text{Noise received by 6-director array}} = \frac{.173}{.023} = 7.5 \text{ (power ratio)} = 8.7 \text{ db.}$$

(b) Local Storms.  
Peak readings only.

Noise generated  
in receiver (I)  
(I) atmospheric noise.  
.. atmospheric noise

6-director design		Test Rhombic	
A.F. level db <sub>o</sub>	Power mW	A.F. level db <sub>o</sub>	Power mW
-23	.005	-23	.005
-13	.050	+ 6	3.98
	.045		3.97

$$\frac{\text{Noise received by Rhombic}}{\text{Noise received by 6-director design}} = \frac{3.97}{.045} = 88 \text{ (i.e. 19.45 db.)}$$

From fig. F. 10. 3.4.1 it will be seen that the gain of the receiver is reasonably constant up to a R.F. input of about 20 db above  $-1\mu\text{V}$  and therefore the A.F. output can be taken as a measure of the R.F. noise input. But also from fig. F. 10.3.4.1 it will be seen that for an R.F. input of 20 db or more above  $1\mu\text{V}$  the receiver A.F. output, even when switched to "Manual", is not proportional to the R.F. input and therefore A.F. measurements would be misleading if used as a measure of signal strength. Hence the use of the signal strength meter plus calibration curve, Figure F. 10.3.3.1, for comparing signal strength received by the two antennas and T.M.S. measuring audio output when comparing noise received by the two antennas.

10. 3.5 "Measured" signal-to-noise ratio.

In section 10. 3.2 it was stated that measured results would be used as a check on the validity of the theoretical deductions.

These measured results are now interpreted.

Since, in the case of antennas, the term "signal-to-noise ratio" can only be used to describe the situation at a particular time because the signal and the noise may vary independently, an antenna cannot be quoted as having a particular "signal-to-noise ratio". However, it is permissible to discuss the improvement or otherwise, for a particular set of parameters, of one "signal-to-noise ratio" relative to the other. It can be said, for example, that on a certain occasion the signal power output from the Rhombic antenna was 10 db stronger than that from the 6-director design. It could also be said that on the same occasion the Rhombic was noisier than the 6-director design by 16 db. Then, while those conditions last, the signal-to-noise ratio of the 6-director design is 6 db better than that of the Rhombic.

It will be seen from sections 10. 3.3 and 10. 3.4 that:-

- during distant thunderstorms the signal-to-noise ratio of the "d" type 6-director design was of the order of  $8.7-8 = 0.7$  db better than that of the Rhombic antenna; and
- during local thunderstorms, the signal-to-noise ratio of the 6-director array was approximately  $19-8 = 11$  db. better than that of Test Rhombic; and

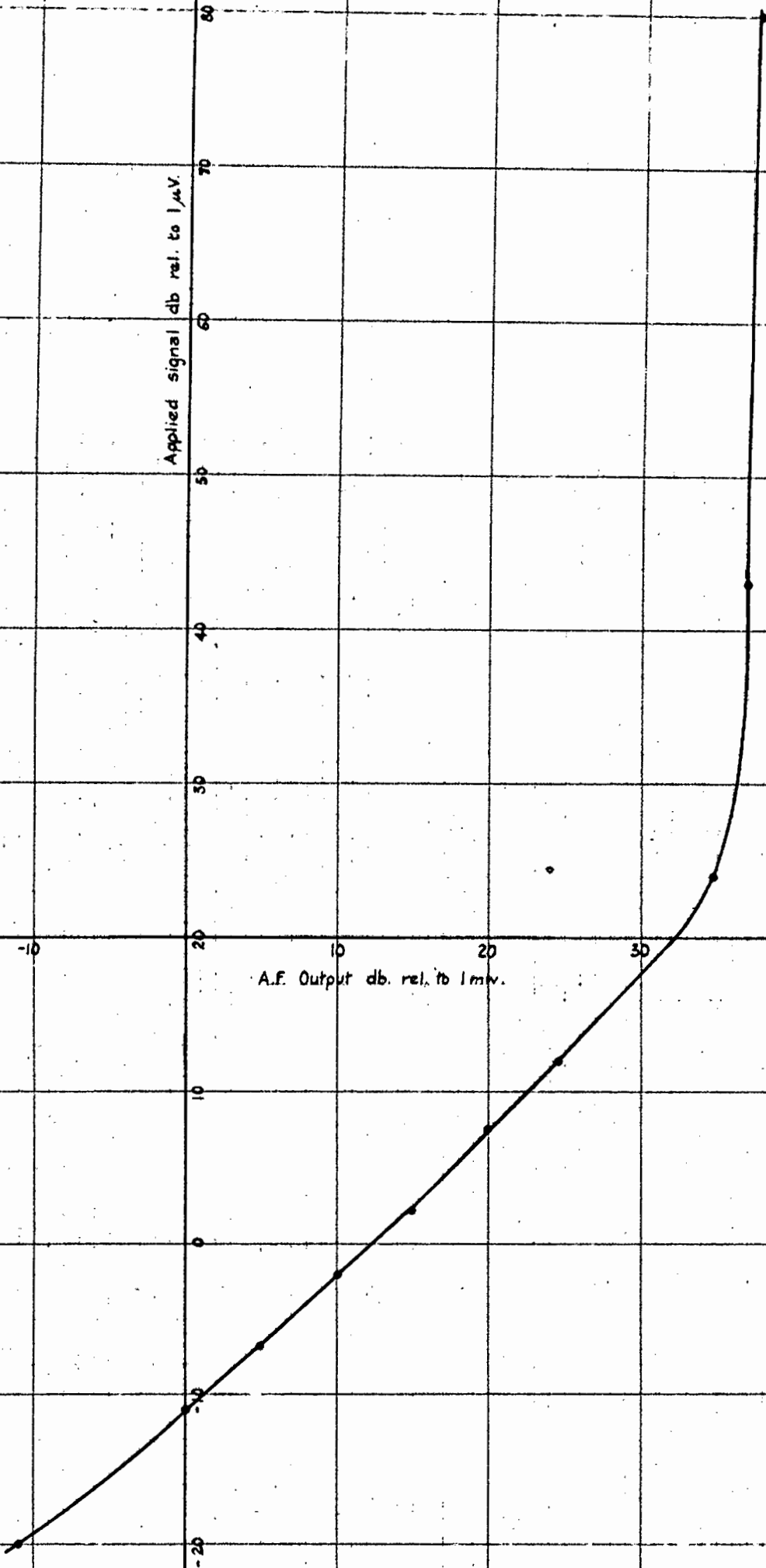


Applied signal db rel. to  $1\mu V$ .

A.F. Output db. rel. to 1mv.

Figure F 10.3.4.1.

LARGE RANGE OF MODULATED  
R.F. SIGNAL  
vs  
A.F. OUTPUT.



- (c) during very quiet periods, when the apparatus noise becomes the limiting factor, the greater sensitivity of the Rhombic antenna may be expected to give the system a better signal-to-noise ratio than does the 6-director design. It should be noted, however, that in these circumstances the signal-to-noise ratio of both antennas is very high.

The result (b) above reflects maximum peak readings recorded during a thunderstorm which was very close.  $\Delta$  may be considered as being over 40 degrees. The same receiver and measuring equipment were used throughout. The two antennas were connected, for short intervals, in turn to the receiver. A third independent receiver was used as a monitor to ensure that the peak readings in each case were produced by noise field strengths of the same order of magnitude.

The result in (a) appears to confirm the result derived theoretically that the average signal-to-noise ratio of the two antennas will be roughly the same for distant storms (6-director design better for storms between 550 and 1000 km. away and Test Rhombic better when storms are 250 - 550 km. away). The result in (b) appears to confirm the theoretical derivations for  $\Delta$  equal to about  $40^\circ$ . The "worst condition signal-to-noise ratio" of the 6-director design is calculated as being superior to that of the Test Rhombic for both distant and local storms but it is only when  $\Delta$  is about  $40^\circ$  or more that the 6-director design is expected to possess an appreciable advantage.

#### 10.3.6 Noise voltages induced in feeders.

Mention is made in Chapter 1 of the open wire feeders used on the Rhombic antennas. There are a considerable number of receiving Rhombic antennas located at Hatcliffe receiving station. Each occupies a large area. Of necessity, therefore, they are situated far from the receiver building. Feeders of length approx. 1 mile are used. For economic reasons these feeders are of the open-wire type. On the other hand, the 6-director design is so compact that it can be situated near the receiver building and air-spaced co-axial feeder line is an economical proposition. The noise picked up by the open-wire line, particularly during near-zone thunder activity, will produce a worse signal-to-noise ratio than that calculated for the Test Rhombic thus further increasing the improvement effected by the 6-director design.

#### 10.4.0 Overall signal-to-noise ratio: double 6-director array.

It was pointed out in Chapter 3, section 3.4, that even if the noise from external sources is zero, the internal noise output from an average good-quality communications receiver is such that, if a 30% modulated signal is to override that noise by more than 20 db, it is necessary for the signal input to the receiver to be at least 16  $\mu$ V across the 70 ohm receiver input terminals. (See Table T. 3.5.1). This is 24 db above 1  $\mu$ V. It follows that, although the 6-director design is superior to the Test Rhombic in signal-to-noise ratio its comparative lack of sensitivity could produce an inferior signal-to-noise ratio, during signal fades, due to the ever-present apparatus noise.



THE DOUBLE 6-DIRECTOR ARRAY

Figure F 10.4.0.1.



It is profitable, therefore, to increase the sensitivity by producing a broadside in-phase arrangement of two 6-director arrays separated by  $\lambda/2$  as in fig F. 10.4.0.1. If the reflecting plane is of type "d", "e", or "f" grating laid on the ground then each 6-director array plus ground image will have a polar diagram represented by curves "x", "y" or "z" respectively of fig. F. 10. 2. 1.1. The vertical polar diagram, according to Aldred,<sup>(26)</sup> will be virtually the same whether one or two arrays are used. The horizontal polar diagram of the double 6-director array will be obtained by multiplying the horizontal polar diagram of one 6-director array by a factor calculated on the assumption of point sources of uniform phase at the centre of the radiating aperture of each of the arrays. This factor is derived below and is similar to the ground reflection factor derived for positive images in Appendix A, section A.11.4.0.

#### 10.4.1. Gain of a double 6-director design.

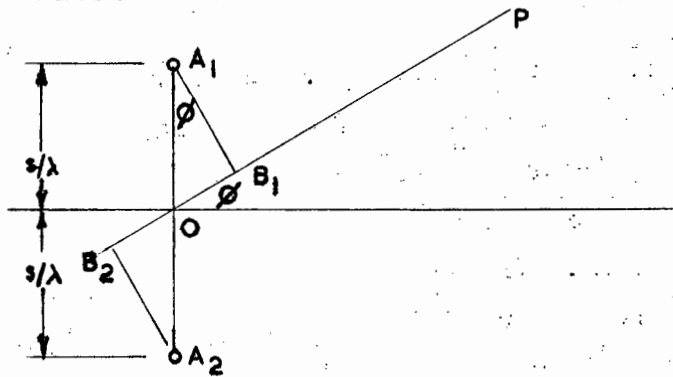


Fig. F. 10. 4.1.1

In fig. F. 10.4.1.1, P is assumed to be so far away that  $A_1 P$ ,  $O P$ , and  $A_2 P$ , may be considered as equal.  $\phi$  is the angle in the horizontal plane between  $OP$  and the centre line of the array. The currents in antennas  $A_1$  and  $A_2$  are in phase.

In fig. F. 10. 4.1.1,  $O B_1 = S/\lambda \sin \phi = \beta S \sin \phi$  radians putting  $\beta = 2\pi/\lambda$ .

Similarly  $O B_2 = -\beta S \sin \phi$ .

Relative to reference point O the field strength  $E_1$  at pt. P due to antenna  $A_1$  will be advanced by  $\beta S \sin \phi$  radians and the field strength at pt. P due to antenna  $A_2$  will be retarded by  $\beta S \sin \phi$  radians.

If  $E_0$  is the field strength that either antenna would produce on its own at P then the total field at P due to antenna  $A_1$  and  $A_2$  is given by:

$$\vec{E} = E_0 \text{ angle } (\beta S \sin \phi) + E_0 \text{ angle } (-\beta S \sin \phi)$$

Combining the two vectors gives:

$$E = 2 E_0 \cos (\beta S \sin \phi).$$

The original horizontal polar diagram must be multiplied by the factor  $2 \cos (\beta S \sin \phi)$ . If the two arrays are separated by  $\lambda/2$ ,  $S = \lambda/4$  and the factor becomes, putting  $\beta = 2\pi/\lambda$ :

$$2 \cos\left(\frac{\pi}{2} \sin \phi\right)$$

In the direction of the centre line of the array  $\phi$  is zero and the factor = 2, i.e. 6 db.

If  $A_1$  and  $A_2$  each radiate half the radiated power they will together produce a field strength at P (for  $\phi = 0$ ) which is 6 db = 3 db = 3 db greater than would be produced by  $A_1$  provided  $A_1$  on its own radiates the same power as do  $A_1$  and  $A_2$  combined.

Matching has to be designed carefully.  $A_1$  and  $A_2$  must each be matched to their respective feeders. If these feeders branch from a common feeder the  $Z_0$  of the common feeder should be half the  $Z_0$  of the two branching feeders otherwise reflection will take place at the junction and the full 3 db gain will not be realised.

This point must be watched also in the reception case. As shown in Chapter 3 a receiving antenna behaves as a generator of emf  $e$  (proportional to effective length  $\times$  field strength) and internal resistance  $R$  (approximately equal to the radiation resistance). For optimum power transfer to the feeder line  $Z_0$  of the feeder should equal  $R$ . If the  $Z_0$  of the ~~common~~ feeder is made equal to half the  $Z_0$  of the two branch feeders and this in turn is made equal to  $R$ , the internal resistance of the "generator", then two in-phase receiving antennas will feed 3 db more power to the load than could have been achieved by one of them alone provided they were sufficiently well separated as to suffer no mutual interference. In effect the two in-phase generators behave as one having emf  $e$  volts and internal resistance  $R/2$  ohms feeding into a load of  $R/2$  ohms. This delivers twice the power (3 db) that would have been fed by a generator having emf  $e$  volts and internal resistance  $R$  ohms working into a load of  $R$  ohms.

Supposing, however, that the two antennas are each matched to their respective 70 ohm co-axial branch feeders and that the branch feeders are connected, in parallel, by a T coupling to a 70-ohm common feeder then, if the two antennas are identical, the induced emfs in phase, and the branch feeders of equal length, the voltages developed across the common feeder input will be in phase. The two generators of emf  $e$  volts and internal resistance  $R$  ohms behave as one of emf  $e$  volts and internal resistance  $R/2$  ohms and develop a voltage equal to  $2e/3$  volts across the load  $R$ . The power delivered to the load is  $16/9 = 1.7^*$  i.e. 2.5 db more than would have been delivered had one of the antennas been disconnected. This is a likely situation in practice because it is usually not possible to have the choice of various co-axial feeders with a 2 to 1 range of characteristic impedance and there will, therefore, be a tendency to use lines of the same  $Z_0$  for common and branch feeders.

These considerations were put to the test as follows: The branch feeders were made from 70-ohm co-axial line and branching was conveniently achieved by a T co-axial coupling. A signal generator was set up at a point about 10λ in front of the double 6-director array and on its centre line. The output from the T coupling was fed directly into the 70-ohm input terminals of a receiver. The measured gain of the double 6-director array was found to be 2.8 db greater than the single 6-director array. The difference in gain should have been 2.5 db. as explained above. The effective internal impedance of each of the arrays may have been about 20% greater than the  $Z_0$  of the feeder or the receiver may have presented a load about 20% lower than 70 ohms. Either of these possibilities would have produced 2.8 db difference between the measured gains of the two arrays (c.f. Figs. B/ 5.4.1/2 where, due to close spacing, gain is 2.8 db too).

The "worst condition signal-to-noise ratio" for distant storms and local storms will be the same in the case of the double 6-director design and the single 6-director design. In any direction displaced  $\theta^\circ$  from the centre line of the array in the horizontal plane the gain of the double array will be  $1.8 \cos(\frac{\pi}{2} \sin \theta)$  times the gain of the single array. This narrowing of the horizontal polar diagram makes the double array more selective than the single array against storms which take place in directions other than along the centre line of the antenna. More important, however, is the fact that an increase of sensitivity of 3 db (if perfect matching is achieved throughout), or 2.5 db (if the branch feeders and the common feeder are all of the same  $Z_0$ ), is obtained by the use of the double array, resulting in a greater difference between signal level and the apparatus noise level. Having regard to the expected median field strength and the level of the apparatus noise this gain makes the double array a worthwhile proposition in the circuit under consideration, yielding an estimated median terminal voltage of 32 db above 1μV.

10. 5.0 Design of the permanent installation.

By the employment of a single 6-director design with an "f" type grating, the expected "worst condition signal-to-noise ratio" will be 2.3 db better than the Test Rhombic for distant storms and 2.9 db better for local storms, the latter figure rising sharply when the storm is almost overhead, i.e. when  $\Delta$  exceeds  $40^\circ$ . (sections 10.3.2 to 10.3.4 refer). By using a double 6-director array the sensitivity will be increased by 2.5 db or 3.0 db, depending upon the efficiency of the feeder matching arrangements, thereby increasing the difference between the signal level and the apparatus noise level.

There remains the need to specify the practical details necessary for a permanent installation.

As calculated in section 2.5.3 the centre line of the array should point in the direction  $19^\circ$  West of true North.

#### 10.5.1.0 Weatherproofing and design of elements.

It is required to provide all-weather insulation of all elements, this insulation to be shunted by a 100 K ohm discharge resistor on each parasitic element to ensure against static build-up (See section 10.1.3).

#### 10.5.1.1 Base arrangements for parasitic elements.

The diameter of the copper tubing from which the elements are made is  $2\frac{3}{4}$ " . This matter has been dealt with fully in section 9.1.

The mechanical arrangements for mounting the elements and the provision of all-weather insulation and static dischargers are shown in figure F. 10.5.1.1.1.

Fig. F. 10.5.1.1.2 is a photograph of the base with the element in its normal position. This also shows a type "d" grating but a type "f" is recommended (details in section 10.2.0). It also shows the earth lead. Fig. F. 10.5.1.1.3 is a photograph of the base when the element has been lifted to reveal the two lower insulators and one of the two 200 K ohms resistors, connected in parallel, which allow static charge to leak away. Wound on each resistor is a  $\frac{1}{16}$ " spark gap to protect the resistor in particularly heavy weather. The copper apron keeps the insulators dry. The top of the copper pipe is sealed. The width of the copper apron plus the height of the copper pipe is made equal to the design length of each parasitic element given in fig. F. 8.3.5.2.1 (G).

#### 10.5.1.2 Base arrangements for the driven elements.

##### (a) Driven element type 1.

One method is to use the antenna matching unit as in figs. F. 9.2.1/2. It is housed in a copper container at the base of the driven element. This makes it necessary for the copper can to be larger in this case than was necessary on the parasitic elements. The arrangements for insulation are the same as those used for the parasitic elements but no discharger resistor is necessary. The top of the copper pipe is sealed.

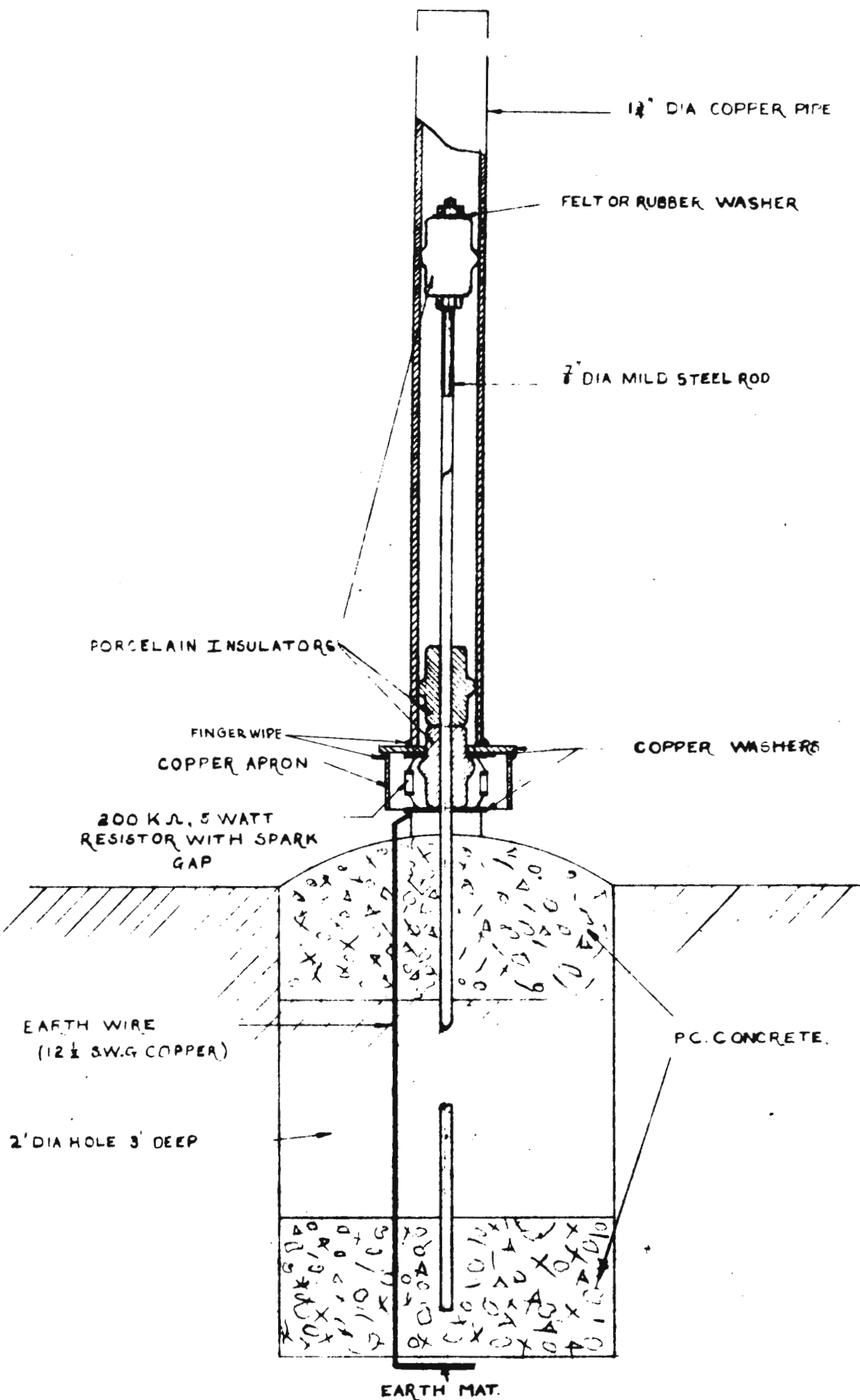
The design is shown in fig. F. 10.5.1.2.1 and a photograph of the base is reproduced in fig. F. 10.5.1.2.2.

The length from the lower edge of the apron to the lower edge of the copper pipe plus the height of the copper pipe is made equal to the design length of the driven element given in fig. F. 8.3.5.2.1.(G)

##### (b) Driven element type 2.

A better method of matching the driven element to the co-axial feeder is to use a folded construction for the driven element. Then the matching problems discussed in section 10.4.1 may be overcome by making the length of the branch feeders  $\lambda/2$  and the impedance of each of the two antennas equal to twice the  $Z_0$  of the feeder.

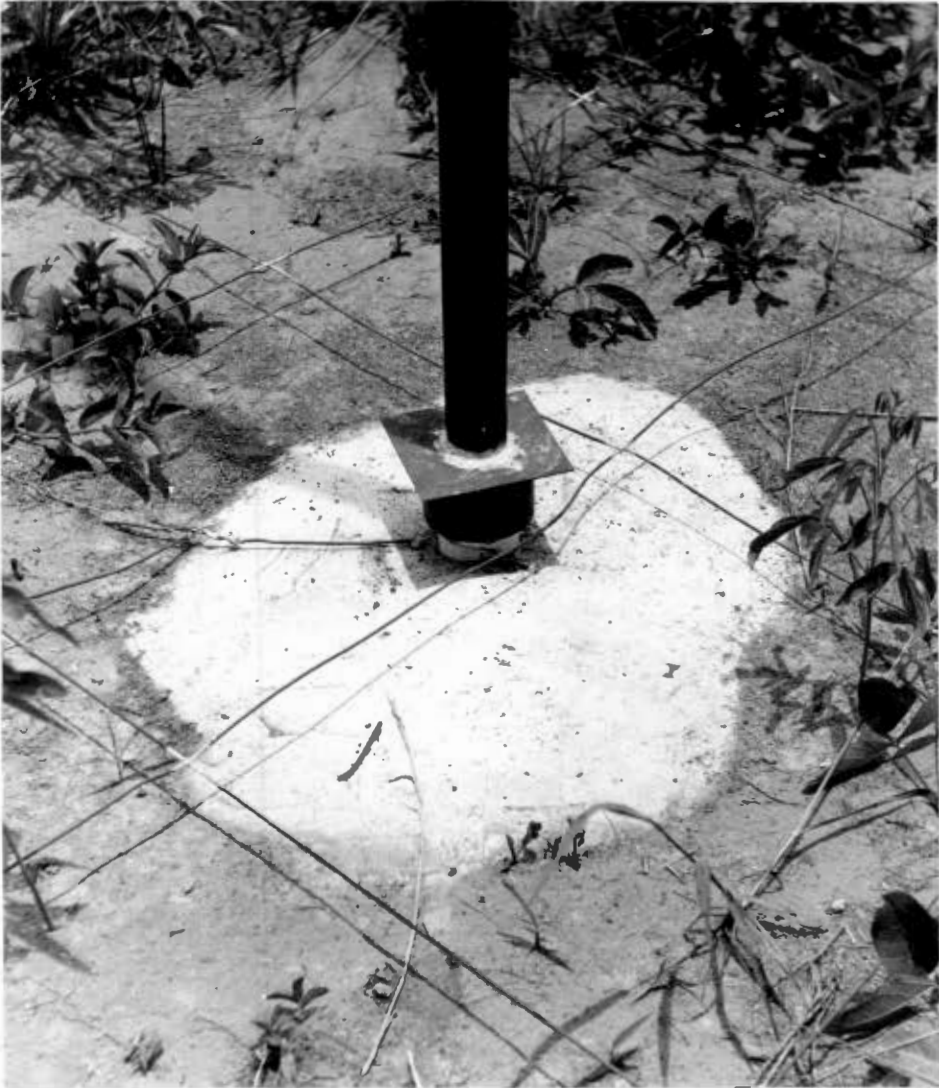




DESIGN FOR INSULATED PARASITIC ELEMENTS

20.24

Figure 10.5.5.1.1.



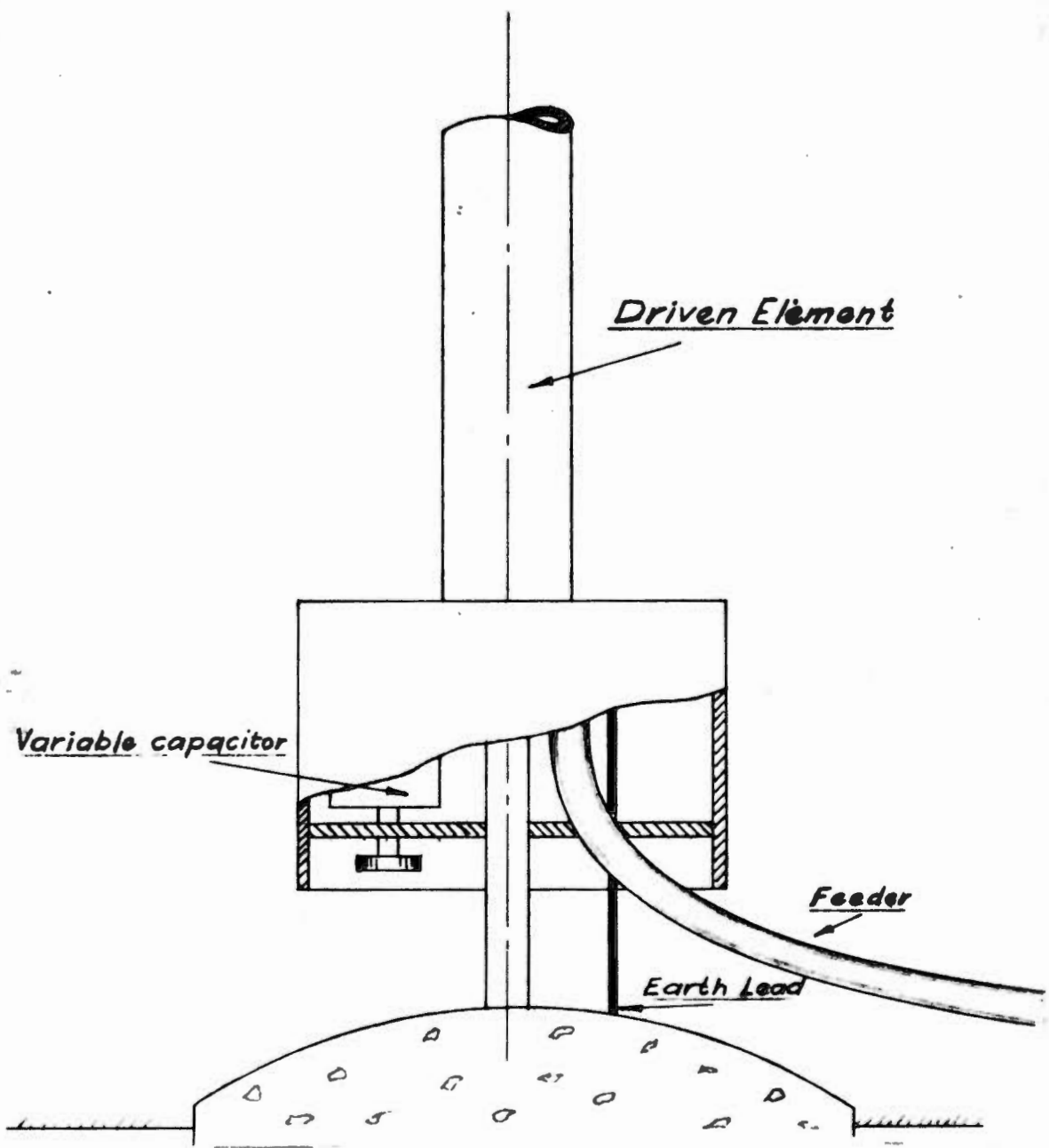
INSULATED PARASITIC ELEMENT : BASE

Figure F 10.5.1.1.2.



INSULATED PARASITIC ELEMENT : DISMANTLED VIEW.

Figure F 10.5.1.1.3.



Base Design of Driven Element

Figure F 1C.5.1.2.1.



THE DRIVEN ELEMENT.

Figure F 10.5.1.2.2.

If the input impedance of the array is  $(2)$  x ohms then a folded monopole of y elements, all of the same diameter, following the usual practice described in several textbooks (e.g. Jordan<sup>(10)</sup> p.535) will present an impedance of  $y^2$  x ohms. This is transferred without change to the feeder junction by the half wave one-to-one transformer. Alternatively, if a two-element folded monopole is required it can be arranged for the fed and unfed elements to have different radii to produce the required impedance  $Z_f$  at the terminals.

$$Z_f = Z_a \left( 1 + \frac{\log a/r_1}{\log a/r_2} \right)^2 \quad 10.5.1.2.1.$$

where a is the axial separation in the same units as  $r_1$  and  $r_2$

$r_1$  is the radius of the fed element

$r_2$  is the radius of the unfed element

$Z_a$  is the impedance when monopole is unfolded, = 25 ohms (measured)

If the branch feeders are  $\lambda/2$  long and  $Z_f$  of each antenna equals twice the  $Z_0$  of the feeder, the two generators will be matched to the load.

Equation 10.5.1.2.1. is reproduced from the recently published Services Textbook of Radio.<sup>(35)</sup>

#### 10.5.2 The reflecting ground plane.

As stated in the earlier chapters the soil on which this installation is to be operated is heavy clay in which it may be assumed<sup>(4)</sup> that for most of the year

$$\epsilon = 13\epsilon_0$$

$$\sigma = 4 \times 10^{-3} \text{ mho/metre.}$$

The reflecting properties of types "d" "e" and "f" gratings would be different from those calculated in Chapters 6 and 8, and sections 10.2.2., 10.2.3., 10.3.2. of the present chapter, if they were laid on soil of permittivity and conductivity considerably different from those quoted above. They would also be different if the gratings were buried in the soil instead of being laid on the soil.

Assuming that the radiating aperture is  $\lambda/2$  high, the whole image of the aperture will be visible at  $\Delta = 8^\circ$  if the reflecting plane extends for  $(\lambda/2) \cot 8 = 3.6 \lambda$ . Therefore if the grating extends for  $4 \lambda$  from the reflector element this should be adequate. In width it should extend  $\lambda/4$  beyond the centre lines of each 6-director array and should therefore be  $1\lambda$  wide.

It would be wasteful to use a grating more closely spaced than  $0.136 \lambda$  (type "f") with the 6-director design but the spacing should not exceed  $0.218 \lambda$  (type "e"). Although when type "e" is used the array produces a maximum at  $\Delta = 8^\circ$ , (the expected arrival angle of the signal) and when type "f" is used the array produces a maximum at  $\Delta = 6^\circ$ , the use of type "f" will result in a gain of 1.5 db at  $\Delta = 8^\circ$  over the gain of the array when type "e" is used (See fig. F. 10.2.1.1) and the noise field arriving at  $\Delta$  less than  $8^\circ$  is small. (Fig. F.4.3.2.5.1).

CHAPTER 11.

INDICATION OF APPLICABILITY.

11.0 GENERAL.

From the calculations and measurements it appears that the proposed antenna could, with advantage, be used in tropical countries, especially during those months when thunderstorms in the vicinity of the receiving station are prevalent. Assuming for example that Rhombic antennas are expected to be too noisy for the period September-December 1960 on the London-Salisbury circuit, and that reception is required daily from 0600 hrs. to 2400 hrs., Local Mean Time, the approach could be as follows:

11.1 CHANNEL FREQUENCIES.

By consulting Radio Propagation Predictions<sup>(99)</sup>, the B.B.C. transmission channels indicated for the period under consideration are given in Table T. 11. 1.1:-

Period (L.M.T.)	Frequency (Mc/s)	Channel Code name:
0600 - 0800	11.77	GVU
0800 - 1000	21.47	GSH
1000 - 2000	25.72	GSR
2000 - 2200	21.47	GSH
2200 - 2400	17.81	GSV

T A B L E T. 11.1.1.

The frequencies quoted are all slightly below the predicted optimum values for the period considered but, bearing in mind the variability of a triple-hop path, it may be found on occasions that these will be too high. On these occasions an adjacent channel will usually be suitable.

11.2 MEDIAN SIGNAL STRENGTH.

It may be assumed that the only part of the path attenuation affected by an alternation in frequency, season, and time of day, is the ionospheric absorption. Using Piggott's method<sup>(102)</sup>, curves B. 6.2.9. 1/5, the absorption on the selected transmission channels has been calculated and is summarised in TABLE T.11.2.1. By comparing this with the 42 db calculated in Appendix B for 21.47 Mc/s at September noon 1956, (when E was calculated as 12 db above  $1\mu V/m$ ) the estimated median field strength is readily obtained. It is quoted in Table T. 11.2.1.

One of the few effective methods of combating selective fading in long distance circuits is to use a highly directive antenna which will select only one of the possible propagation modes.<sup>(182)</sup> The 6-director design on an "f" type grating, with a vertical beam width of about  $17^\circ$  to the half power points (as in fig. F. 11.5.1.1) will give a fair amount of discrimination in this respect but if severe selective fading is experienced it may be necessary to employ a design with more directors so that a shorter end-director can be used without affecting the launching efficiency. As indicated in Chapter 7, the shorter the end-director the narrower the beam. As with the designs already dealt with, such a design can best be obtained from a suitable scale model. Further improvement may be obtained by the use of two or three such antennas in a diversity arrangement in which the strongest signal is automatically selected. The antennas should be arranged to be roughly in line with the distant station and separated one from the other by about  $10 \lambda$ .

Non-selective fading occurs where the amplitude of the signal as a whole varies. This variation is usually slow and is easily taken care of by the automatic gain control of the receiver.

Observations made at Hatcliffe indicate day-to-day fluctuations of about 40 db in the intensities of both signal and atmospheric noise. The C.C.I.R.<sup>(206)</sup> indicate the same value for these fluctuations and their present conclusions, for frequencies between 3 and 30 Mc/s, point to a Rayleigh distribution<sup>(182)</sup> of amplitudes for a fading signal observed over periods of a few minutes, and to a log-normal distribution over periods of 15 minutes to one hour as in fig. F. 11.4.1.

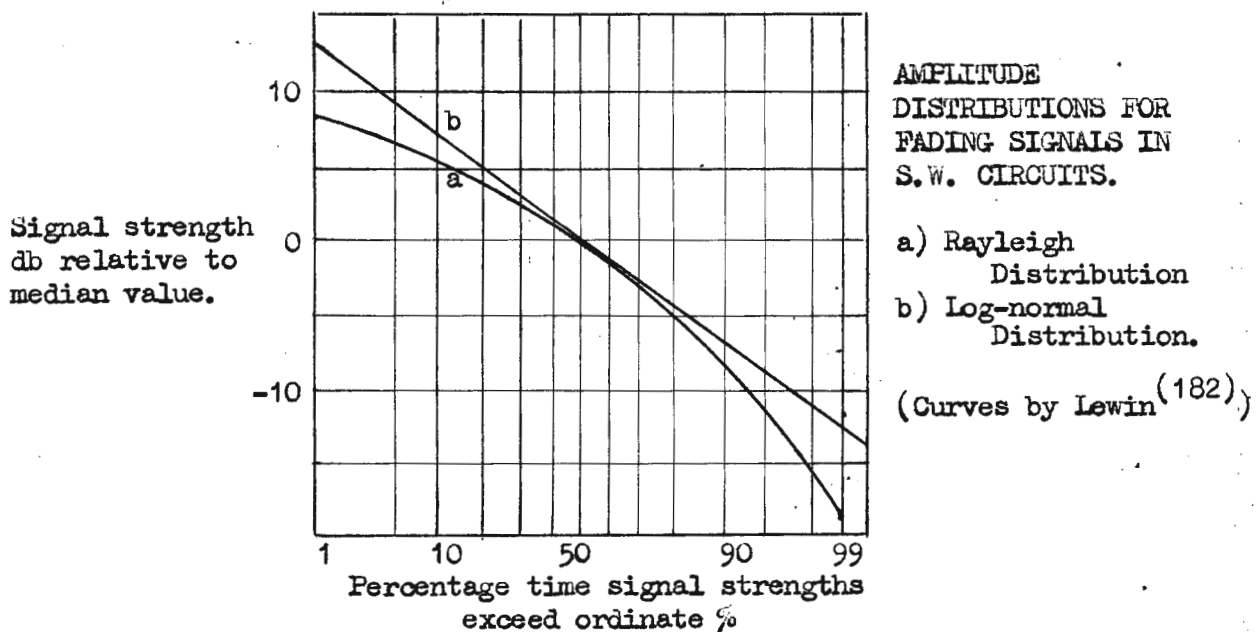


Fig. F. 11.4.1

#### 11.5.0 THE MULTIPLE ANTENNA ; GENERAL CONSIDERATIONS.

To cater for the channels indicated in Table T.11.2.1 a double six-director design on a type "f" grating should be set up for each of the required frequencies. The four arrays should be connected to the

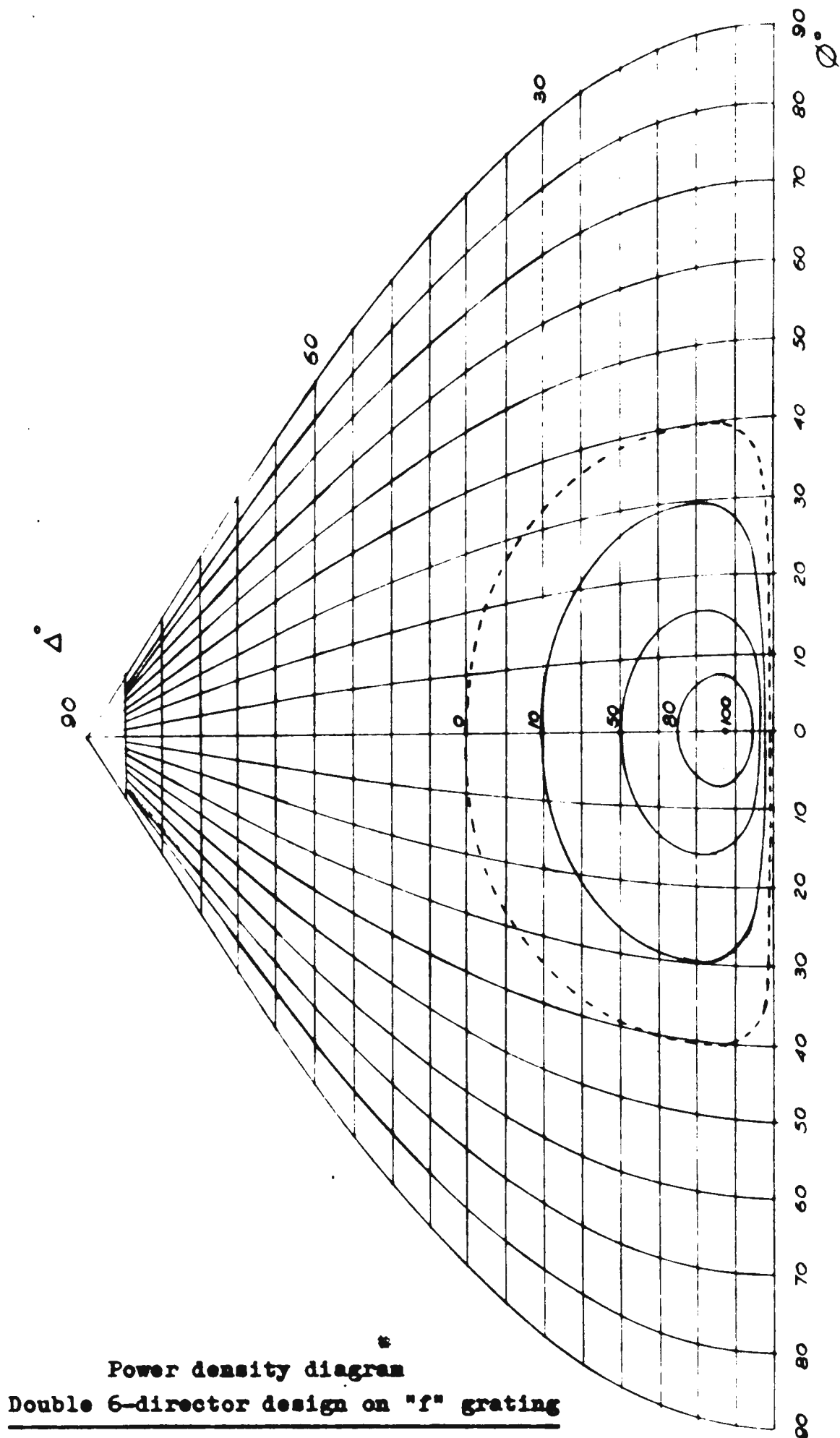


(c) POLAR DIAGRAM.

The vertical polar diagram is expected to be similar to that derived as curve "z" in fig. F.10.2.1.1. The horizontal polar diagram is expected to be similar to the curve of fig. F. 9.6.3 (single array) multiplied by the factor  $1.8 \cos \left( \frac{\pi}{2} \sin \theta \right)$  derived in section 10.4.1 for two arrays. Combining the vertical and horizontal polar diagrams, and plotting as a power density diagram, results in fig. F.11.5.1.1. When this is compared with the power density diagrams of the Test Rhombic (fig. F.4.4.3.1) and the Koomans array H/4/4/1 (fig. F.4.4.3.2) the reduction in high-angle sensitivity is demonstrated.

11.5.0 CONCLUDING NOTE.

The proposed antenna is indicated for use in high-noise areas where an appreciable proportion of the noise energy is arriving at high angles but during these periods when local thunder activity is negligible the performance of the proposed antenna is expected to be about the same as that of a typical Rhombic antenna.



Power density diagram  
Double 6-director design on "f" grating

ACKNOWLEDGEMENTS

I am indebted to the Chief Engineer, Federal Ministry of Posts, Salisbury, for permission to use the results of experiments conducted on behalf of the Ministry.

I am grateful, too, for the assistance and advice given me by Professor R. Guelke and Dr. L. Besseling of the University of Cape Town.

My colleagues in the Ministry of Posts have assisted me in many ways and to Mr D. J. Sibbelee I wish to offer special thanks for his assistance with much of the typing.

---



# B I B L I O G R A P H Y .

- (1) Shelkunoff, S.A. "Electromagnetic waves"(Van Nostrand)(1943).
- (2) Walkinshaw, W. J.I.E.E. Vol. 93, Pt IIIA No. 3 (1946).
- (3) Reid, D.G. J.I.E.E. , , , , , , , (1946).
- (4) Terman, F.E. "Radio Engineers Handbook"(McGraw-Hill)  
(1943)
- (5) Booker, H.G. J.I.E.E. Vol. 94, Pt III, No 29 (1947).
- (6) Feldman, C.B. Proc. I.R.E. June (1933).
- (7) Williams, P. "Antenna Theory and Design, Vol. I and II  
(Pitman) (1950).
- (8) Starr, A.T. "Radio and Radar Technique"(Pitman)(1952)
- (9) Harper, A.E. "Rhombic Antenna Design". (McGraw-Hill)(1941)
- (10) Jordan, E.C. "Electro magnetic waves and radiating  
systems". (Constable) (1953).
- (11) C.C.I.R. "International Radio Consultative Committee,  
(Geneva) Antenna Diagrams (1953)."
- (12) Reference data for Radio Engineers (I.T.T.) (New York) (1957).
- (13) Terman, F.E. "Radio Engineering" (McGraw-Hill)(1937).
- (14) H. Fries, C.C. Feldman and W.M. Sharpless Proc. I.R.E. Vol. 22, January (1934).
- (15) Sandeman, E.K. "Radio Engineering" (Chapman and Hall)(1947).
- (16) Lowry and Hayden. "Advanced Mathematics for technical students"  
Pt. II.
- (17) Jahnke, E, and Emde, F. "Tables of Functions", (Teubner, Leipzig)
- (18) Pierce, G.W. "Electric Oscillations and Electric waves"  
(McGraw-Hill) (1920).
- (19) Bruce, Beck and Lowry. Proc. I.R.E. January (1935).
- (20) Cafferata, H. "A generalized radiation formula for hori-  
zontal Rhombic aeriols" , Marconi Review,  
January-March (1946).
- (21) Foster, D. "Radiation from Rhombic antennas" .Proc.  
I.R.E. October, (1937).
- (22) Bruce, E. "Developments in Short wave directive an-  
tennas". Bell System Technical Journal,  
October (1931).
- (23) Lewin, L. "Rhombic transmitting aerial efficiency".  
Wireless Engineer, May (1941).
- (24) Yagi, H. "Beam Transmission of Ultra Short Waves",  
Proc. I.R.E. Vol. 16. (1928).
- (25) Brown, G.H. "Directional Antennas". Proc. I.R.E. Vol. 25  
(1937).
- (26) Aldred, R.V. "Experiments with Yagi Aerials at 600 Mc/s"  
J.I.E.E. Vol. 93, Pt. IIIA, No. 3, (1946).
- (27) Fishenden and Wiblin. "Design of Yagi Aerials". J.I.E.E. Vol. 96,  
Part. III, January (1949).
- (28) Starkey, B.J. and Fitch, E. "Mutual impedance and self-impedance of  
coupled parallel aeriols". J.I.E.E. Vol. 97,  
Pt. III, May (1950).
- (29) King, R. "A dipole with a tuned parasitic radiator"  
J.I.E.E. Vol. 99, Pt. III, January (1952).

- (30) Cox, C.R. "Mutual impedance between Vertical Antennas of Unequal heights". Proc.I.R.E. Vol.35, (1947).
- (31) Tai, C.T. "Coupled Antennas" Proc. I.R.E. Vol 36, p.487, April,(1948).
- (32) McPetrie,J.S. and Santon,J.A. "Some experiments with Linear Aerials", Wireless Engineer, Vol.23 (1946).
- (33) Brown, G.H. and Woodward,O.M. "Experimentally determined impedance characteristics of cylindrical antennas". Proc.I.R.E. Vol.33, April (1945).
- (34) Mallock, R.R.M. "An electrical calculating machine." Proc. of the Royal Society, Vol.140,p.457,
- (35) Services Handbook of Radio. Vol.5(H.M.S.O.)(1958).
- (36) Appleton,E.V. and Ratcliffe,J.A. "Some simultaneous Observations on Downcoming Wireless Waves" Proc. Royal Soc. (A), Vol.128, (1930).
- (37) Baker, W.G. and Rice, C.W. "Refraction of short waves in the upper-atmosphere". Trans A.I.E.E. Vol.45, page 302, (1926).
- (38) Allcock,G. "The Prediction of maximum usable frequencies for radiocommunication over a trans-equatorial path" Proc. I.E.E.,Part B, July (1956).
- (39) Shearman, E.D.R. "A study of ionospheric propagation by means of ground back scatter". Proc.I.E.E. Part.B.,October (1955).
- (40) Allan, A.H. "Variations of received frequency WWVH" J.I.E.E. Vol I,(new series)No.10.October(1955).
- (41) Humby,A.M. and Minnes, C.M. "Asymmetry in the performance of High-frequency radiotelegraph circuits". Proc. I.E.E. Part B, page 553,July(1956).
- (42) Whale,H.A. "A rotating interferometer for measurement of the directions of arrival of short radio waves". Proc. of Physical Society B, Vol.67, page 553.(1954).
- (43) Burrows, J. "Radio propagation over a plane earth-field strength curves". B.S.T.J. Vol.16. January.(1937).
- (44) McPetrie,J.S. "The reflection coefficient of the earth's surface for Radio waves". J.I.E.E. Vol.82, page 82,(1938) and J.I.E.E. Vol.87,page 135,(1940).
- (45) Day,J.P. and Trolese,L.G. "Propagation of short radio waves over desert terrain". Proc. I.R.E. February, 1950.
- (46) Ford,H. and Oliver,R. "An experimental investigation of the reflection and absorption of radiation of 9 cm wavelength". Proc. Phys.Soc.(London), Vol. 58, May. (1946).
- (47) Appleton,E.V. "Wireless studies of the Ionosphere".J.I.E.E. Vol.71, page 642,(1932).
- (48) Hartree, D.R. "The propagation of E.M.waves in a stratified medium". Proc.of Cambridge Philosophical Soc. Vol.25, page 97,(1929).
- (49) Booker, H.G. "The application of the Magneto-Ionic theory to the Ionosphere". Proc. Royal Soc. (A),page 267,(1935).

Bibliography. (continued).

- (50) Nicholls, H.W. and Shelling, J.C. "Propagation of Electric Waves over the earth". B.S.T.J. Vol. 4, April. (1925).
- (51) Chapman, S. "The absorption and dissociative or ionizing effect of monochromatic radiation in an atmosphere on a rotating earth". Proc. Phys. Soc. Vol. 43, pages 26 and 433, January (1931).
- (52) Hacke, J.E. and Kelso, J.M. "An approximate solution of the problem of Path and Absorption of a Radio Wave in a deviating Ionosphere Layer". Proc. I.R.E. December (1948).
- (53) Hacke, J.E. "An approach to the approximate solution of the ionosphere absorption problem". Proc. I.R.E. June. (1948).
- (54) Pierce, J.A. "The true height of the ionosphere layer". Phys. Review, Vol. 71, May. (1947).
- (55) Jaeger, J.C. "Equivalent path and absorption in an ionosphere region". Proc. Phys. Soc. Vol. 59, January. (1947).
- (56) Piggott, W.R. "The reflection and absorption of radio waves in the ionosphere". Proc. I.E.E. Part III, March 1953.
- (57) Appleton, E.V. "Regularities and irregularities in the ionosphere". Proc. Royal Soc. (A), Vol. 162, page 451 (1937).
- (58) Appleton, E.V. "A method of measuring the collisional frequency of electrons in the Ionosphere". Nature, Vol. 135, page 618. (1935).
- (59) Allcock, G. "Ionospheric absorption at vertical and oblique incidence". Proc. I.E.E. Part III, November. (1954).
- (60) Beynon, W.J.G. "Some notes on the absorption of radio waves reflected from the ionosphere at oblique incidence". Proc. I.E.E. Part III, January. (1954).
- (61) Haves, R.J., Koll, R.T. and La Gow, H.E. "The pressure, density and temperature of the earth's atmosphere to 160 km." Journal of Geophysical Research. Vol. 57, page 59. (1952).
- (62) Whipple, F.L. "Meteors and the earth's upper atmosphere". Review of Modern Physics. Vol. 15, page 264, (1943).
- (63) Paton, J. "Aurora and Luminous Night clouds". Proc. Physical Society, (B), Vol. 63, page 1039, (1950).
- (64) Nicolet, M. "Effects of the atmospheric scale height gradient on the variation of ionization and short wave absorption". Journal of atmospheric and terrestrial Physics, Vol. I, page 141. (1951).
- (65) Martyn, D.F. "The propagation of medium radio waves in the ionosphere". Proc. Phys. Soc. Vol 47, page 32, (1935).
- (66) Pannekoek, A. "Proc. Amsterdam Acad." Vol. 29, page 1165, (1926).
- (67) Saha, M.N. Phil. Mag. Vol. I, page 1025. (1920).
- (68) Woltjer, J. "Physica", Vol. 5, page 406. (1925).

Bibliography. (continued).

- (132) Chapman, S. and Ferraro, V.C.A. Terr. Mag. and Atmos. Elec. Vol. 36, p. 77 and 171 (1931).
- (133) Chapman, S. and Ferraro, V.C.A. ditto. Vol. 37, p. 147, (1932).
- (134) Ferraro, V.C.A. Jour. Geophys. Res. Vol. 57, p. 15, (1932).
- (135) Martyn, D.F. "Nature", Vol. 167, p. 92 (1951).
- (136) Maris, H.B. and Hulburt, E.O. Phys. Rev. Vol. 33, p. 412, 4046, (1929)
- (137) Hulburt, E.O. Phys. Rev. Vol. 34, p. 344, 1169. (1929)
- (138) Hulburt, E.O. Phys. Rev. Vol. 36, p. 1560, (1930).
- (139) Chapman, S. Phys. Rev. Vol. 32, p. 993 (1928).
- (140) Chamberlain, J.W. Journal Astrophys. Vol. 126, p. 245. (1957).
- (141) Bierman, L. "Observatory" Vol. 77, p. 109, (1957).
- (142) Parker, E.N. Phys. Rev. Vol. 107, p. 924 (1957).
- (143) Storey, L.R.O. Phil. Trans. Roy. Soc. Vol. 246, p. 113. (1954).
- (144) Parker, E.N. Phys. Rev. Vol. 112, Dec. (1958).
- (145) Pierce, J.R. J. Appl. Phys. Vol. 49, p. 231, (1948).
- (146) Tremellen, K.W. and Cox, J.W. J. I. E. E., Vol. 94, Pt. IIIA p. 200 (1947).
- (147) Appleton, E.V. and Naismith, R. Proc. Phys. Soc., Vol. 52, p. 402, (1940).
- (148) Skellett, A.M. Proc. I. R. E. Vol. 20, p. 1933, (1932).
- (149) Schafer, J.P. and Goodall, W.M. Proc. I. R. E. Vol. 20. p. 1941, (1932).
- (150) Mitra, S.K. and Ghosh, B.N. "Nature", Vol. 133, p. 523, (1933).
- (151) Bhar, J.N. Ind. Jour. Phys. Vol. 42, p. 109, (1937).
- (152) Pineo, V.C. "Science", Vol. 110, p. 280 (1949).
- (153) Pineo, V.C. ditto, Vol. 112, p. 50, (1950).
- (154) Appleton, E.V. and Ratcliffe, J.A. Proc. Roy. Soc. Vol. 128, p. 133, (1930).
- (155) Bhar, J.N. and Syam, P. Phil. Mag. Vol. 23, p. 513, (1937).
- (156) Appleton, E.V. and Naismith, R. Proc. Phys. Soc. (London) Vol. 45, p. 389, (1933).
- (157) Martyn, D.F. and Fulley, O.O. Proc. Roy. Soc. A, Vol. 154, p. 455, (1936).
- (158) Rangi, I. "Nature" Vol. 130, p. 368, (1932).
- (159) Appleton, E.W., Watson-Watt, R.A. and Herd, J.F. Proc. Roy. Soc. A, Vol. 111, p. 615, (1926).
- (160) Healey, R.H. "Tech. Review", Vol. III, p. 245, (1938).
- (161) Paton, J. Proc. Phys. Soc. B. Vol. 63, p. 1039, (1950)
- (162) Manning, L.A. and Co. Technical Report No. 22 of Electronics Research Laboratory, Stanford University, (1950).
- (163) Hey, J.S. "Nature", Vol. 159, p. 119, (1947).



Bibliography. (continued).

- (164) Minno, H.R. Rev. Mod. Phys. Vol.9, p.1 (1937).  
(165) Meek, J.H. Jour. Geophys. Res. Vol. 54, p. 284, (1949).  
(166) Munro, G.H. "Nature", Vol. 162, p. 886, (1948).  
(167) Beynon, W.J. "Nature", Vol. 162, p. 887, (1948).  
(168) Martyn, D.F. Proc. Roy. Soc. A, Vol. 189, p. 241, Vol. 190, p. 273, (1947).  
(169) Martyn, D.F. ditto. Vol. 194, p. 429, 445, (1948).  
(170) Martyn, D.F. "Nature", Vol. 163, p. 34, (1949).  
(171) Martyn, D.F. Aust. J. Phys. Vol. 9, p. 161, (1956).  
(172) North, D.O. R. C. A. Rev. Vol. 6, p. 3 (1942).  
(173) Bates, D.R. Proc. Phys. Soc. London, Vol. 64, p. 805 (1951).  
(174) Letter from Muggleton to Appleton dated 1-8-59.  
(175) Letter from Appleton to Muggleton dated 18-8-59.  
(176) Letter from Figgott to Muggleton dated 20-8-59.  
(177) Letter from Muggleton to Figgott dated 27-8-59.  
(178) Letter from Figgott to Muggleton dated 8.10.59.  
(179) Nyquist, H. Phys. Rev. Vol 32, No. 1, p. 110, (1928).  
(180) Johnson, J.B. Phys. Rev. Vol. 32, No. 1, p. 97, (1928).  
(181) Goldman, S. "Frequency Analysis, Modulation and Noise" (McGraw Hill) (1948).  
(182) Laver, J.F.M. Proc. I.E.E., Part B, Vol. 102, p. 733, (1955).  
(183) C.C.I.R. Recommendation No. 94 "Noise and sensitivity of receivers". (1953)  
(184) Ryle, M. Phys. Soc. Reports, Vol. 13, p. 184, (1950).  
(185) Tremellen K. W. and Cox, J.W. J. I. E. E. Vol. 94, Part A. P. 200, (1947).  
(186) Thomas, H.A. Proc. I.E.E. Vol. 97, Part III, p. 335, (1950).  
(187) C.C.I.R. Report No. 55 (1956).  
(188) Srivastava, S.M. Proc. I.E.E. Vol. 103, Part B. p. 542, (1956).  
(189) Schonland, B.F.J. and Allibone, T.E. "Nature" Vol. 128, p. 794, (1931).  
(190) Schonland, B.F.J. and Collins, H. Proc. Roy. Soc. Vol. 143, p. 654, (1936).  
(191) Schonland, B.F.J. and Craib, J. Proc. Roy. Soc. Vol. 114, p. 229, (1927).  
(192) Schonland, B.F.J. Malan, D.J. Proc. Roy. Soc. Vol. 152, p. 595, (1935). and Collens, H.  
(193) Schonland, B.F.J. Hodges, D.B. Proc. Roy. Soc. Vol. 166, p. 56, (1938). and Collens, H.  
(194) Schonland, B.F.J. and Malan, D.J. Proc. Roy. Soc. A. Vol. 209, p. 158, (1951).  
(195) Aiyar, S.V.C. Proc. I.R.E. Vol. 43, p. 966, (1955).  
(196) Appleton, E.V. and Chapman, F.W. Proc. Roy. Soc. Vol. 158, p. 1 (1937).  
(197) Watson-Watt, R.A., Herd, J.F. Proc. Roy. Soc. Vol. 162, p. 267, (1937). and Lutkin, F.E.  
(198) Berger, K. Assoc. Swiss Electr. Bull. Vol. 25, p. 213, (1934).

- (199) Thomas, H.A. and Burgess, R.E. Radio Research Special Report No.15, H.M.S.O. London. (1947).
- (200) Aiyar, S.V.C. Jour. Atmos. Terr. Phys. Vol.5, p.230, (1954).
- (201) Aiyar, S.V.C. Proc. I.R.E. Vol.46, p.580. (1958).
- (202) Davis, A.M. I.I.E.E. Vol.83, p.249, (1938).
- (203) Aiyar, S.V.C., Khot, C.G. J. Sci. Ind. Research (India) Vol.14, Phadke, K.R. and Sane, C.K. B, p.361, (1955).
- (204) Bostick, W.H. and Lebacqz, J.V. "Pulse duration and amplitude". Mass. Inst. Tech. Rad. Lab. Series. No.5, McGraw-Hill. (1948).
- (205) Osborne, B.W. Jour. Atmos. and Terr. Phys. Vol.2, p. 66, (1951).
- (206) C.C.I.R. Report No.27. "Fading of H.F. and M.F. signals propagated by the Ionosphere". (VIIIth Plenary Assembly, London). (1953).
- (207) Brown, J. and Spector, J.O. Proc. I.E.E. Part B, Vol.104, p. 27 (1957).
- (208) Smith, R.A. "Aerials for metre and decimetre wavelengths". (Cambridge University Press. (1949).
- (209) Spector, J.O. Proc. I.E.E. Part B, Vol.105, p.38, (1958).
- (210) Stratton, J.A. "Electro-magnetic Theory", McGraw-Hill (1941).
- (211) Silver, S. "Microwave Antenna Theory and Design". (Mc Graw-Hill), (1949).
- (212) King, R. and Harrison, C.W. Proc. I.R.E. Vol. 31, p.548, (1943).
- (213) MacFarlane, G.G. J.I.E.E. Part III, A, Vol.93, p.1523, (1946).
- (214) La Port, E.A. "Radio Antenna Engineering" (McGraw-Hill) (1952).
- (215) Marconi Equipment Catalogue (1959).
-

ANTENNA THEORY.

SUMMARY OF APPENDIX A.

Commencing at Maxwell's Equations the theory is developed for:

- Uniform plane waves in free space;
- intrinsic impedance of a medium;
- plane waves in a dielectric;
- plane waves in a conductor;
- reflection at a conducting surface of vertically and horizontally polarized waves;
- radiation;
- energy flow in a medium;
- radiated power and radiation resistance of a doublet antenna;
- radiation from a  $\lambda/2$  dipole;
- radiation from a  $\lambda/4$  monopole;
- field strength related to power and distance;
- vertical and horizontal antennas above a perfectly conducting plane;
- radiation from a straight wire carrying a travelling wave;
- radiation from a Rhombic antenna;
- vertical and horizontal polar diagram of Rhombic;
- optimum dimensions for a Rhombic antenna;
- radiation resistance of a Rhombic antenna.

The various equations that have been derived are frequently used in the main text.

Symbols used:

- $\bar{A}$  = magnetic vector potential in webers/metre, the bar indicating a vector quantity.
- $a$  = charge density in coulombs/cubic metre.
- $B$  = magnetic flux density in webers/sq. metre.
- $D$  = displacement density in coulombs/sq. metre.
- $E$  = electric field strength in volts/metre.
- $G$  = gain over a  $\lambda/2$  free-space dipole in the equatorial plane (sometimes written  $G_H$ ) - also conductance in mhos/unit length.
- $G_o$  = gain over an isotropic radiator.
- $H$  = magnetic field strength in amps/metre.
- $\bar{i}$  = current density in amps/sq. metre.
- $o$  = used as a suffix to denote free-space values of  $\mu, \epsilon, \beta, \lambda, f, \omega, Z_o$ .
- $p$  = intrinsic propagation constant of medium.
- $\bar{s}$  = energy flow in watts/metre.

- - - - -



## APPENDIX A.

A. 1.0 Maxwell's field equations state the fundamental relations that must be satisfied in the solution of electromagnetic problems.

$$\nabla \cdot \vec{D} = \rho \quad (1.1)$$

$$\nabla \times \vec{E} + \frac{\partial \vec{B}}{\partial t} = 0 \quad (1.2)$$

$$\nabla \cdot \vec{B} = 0 \quad (1.3)$$

$$\nabla \times \vec{H} - \frac{\partial \vec{D}}{\partial t} = \vec{J} \quad (1.4)$$

The following constitutive equations concern the characteristics of the medium in which the field exists:

$$\vec{D} = \epsilon \vec{E} \quad (1.5)$$

$$\vec{B} = \mu \vec{H} \quad (1.6)$$

$$\vec{J} = \sigma \vec{E} \quad (1.7)$$

A. 2.0 d'Alembert's equations.

d'Alembert's equations are derived from the field equations and though the same end-result is achieved by Jordan<sup>(10)</sup> and Williams<sup>(7)</sup> it is proposed to follow a different, but preferred, method below:

Take the curl of eqn. (1.2) and make use of the identity that:

$$\nabla \times (\nabla \times \vec{E}) = \nabla \nabla \cdot \vec{E} - \nabla^2 \vec{E} \quad \text{giving:}$$

$$\nabla \nabla \cdot \vec{E} - \nabla^2 \vec{E} + \frac{\partial}{\partial t} \nabla \times \vec{B} = 0 \quad (2.1)$$

Substitute from (a),  $\vec{E} = \vec{D}/\epsilon$ , in (2.1)

$$\text{then } \nabla \nabla \cdot \frac{\vec{D}}{\epsilon} - \nabla^2 \frac{\vec{D}}{\epsilon} + \frac{\partial}{\partial t} \nabla \times \vec{B} = 0 \quad (2.3)$$

From (1.1),  $\nabla \cdot \vec{D} = \rho = 0$  in free space if medium has no static charges and from (1.6)  $\vec{B} = \mu \vec{H}$   
(2.3) now becomes:

$$-\nabla^2 \frac{\vec{D}}{\epsilon} + \frac{\partial}{\partial t} \nabla \times \mu \vec{H} = 0$$

But from (1.4) and (1.7)  $\nabla \times \vec{H} = \sigma \vec{E} + \frac{\partial \vec{D}}{\partial t} = \sigma \vec{E} + \epsilon \frac{\partial \vec{E}}{\partial t}$

$$\therefore -\nabla^2 \vec{E} + \mu \frac{\partial}{\partial t} (\sigma \vec{E} + \epsilon \frac{\partial \vec{E}}{\partial t}) = 0.$$

$$\therefore \nabla^2 \vec{E} - \mu \sigma \vec{E} - \mu \epsilon \frac{\partial^2 \vec{E}}{\partial t^2} = 0 \quad (2.4)$$

$$\text{Similarly } \nabla^2 \vec{H} - \mu \sigma \vec{H} - \mu \epsilon \frac{\partial^2 \vec{H}}{\partial t^2} = 0 \quad (2.5)$$

(2.4) and (2.5) are d'Alembert's equations.

A. 3.0 The wave equations.

These are a special application of free space conditions to (2.4) and (2.5). In a non-conducting medium,  $\sigma = 0$  giving the differential vector equations:

$$\nabla^2 \vec{E} - \mu \epsilon \frac{\partial^2 \vec{E}}{\partial t^2} = 0 \quad (3.1)$$

$$\nabla^2 \vec{H} - \mu \epsilon \frac{\partial^2 \vec{H}}{\partial t^2} = 0 \quad (3.2)$$

which are called the wave equations.

A. 4.0 Uniform plane waves in free space.

An example of a plane wave would be one in which  $\vec{E}$  and  $\vec{H}$  are functions of  $x$  and  $t$  only, varying sinusoidally with time

Then 
$$E_x = f(x, t) \quad (4.1)$$

$$E_y = f(x, t) \quad (4.2)$$

$$E_z = f(x, t) \quad (4.3)$$

and equation (3.1) becomes:

$$\frac{\partial^2}{\partial x^2} E_x = \mu \epsilon \ddot{E}_x \quad (4.4)$$

$$\frac{\partial^2}{\partial x^2} E_y = \mu \epsilon \ddot{E}_y \quad (4.5)$$

$$\frac{\partial^2}{\partial x^2} E_z = \mu \epsilon \ddot{E}_z \quad (4.6)$$

The general solution of 4.4, 4.5, 4.6 is of the form:

$$E_x = f_1 \left( t - x (\epsilon \mu)^{\frac{1}{2}} \right) + f_2 \left( t + x (\epsilon \mu)^{\frac{1}{2}} \right) \quad (4.7)$$

$$E_y = f_1 \left( t - x (\epsilon \mu)^{\frac{1}{2}} \right) + f_2 \left( t + x (\epsilon \mu)^{\frac{1}{2}} \right) \quad (4.8)$$

$$E_z = f_1 \left( t - x (\epsilon \mu)^{\frac{1}{2}} \right) + f_2 \left( t + x (\epsilon \mu)^{\frac{1}{2}} \right) \quad (4.9)$$

A similar general solution for  $\vec{H}$  from (3.2) will occur.

The retarded function,  $f_1 \left( t - x (\epsilon \mu)^{\frac{1}{2}} \right)$  refers to the incident wave and  $f_2 \left( t + x (\epsilon \mu)^{\frac{1}{2}} \right)$  to the reflected wave.

In a region where there is no charge density, from (1.1) and (1.5) putting  $\rho = 0$ :

$$\text{i.e.} \quad \nabla \cdot \vec{D} = \epsilon \nabla \cdot \vec{E} = 0 \quad (4.10)$$

As  $\vec{E}$  is a function of  $x$  and  $t$  only, the last two terms of 4.10 are zero and therefore:

$$\frac{\partial E_x}{\partial x} = 0 \quad (4.11)$$

This requires that  $E_x$  shall be zero for a wave progressing in the  $x$  direction. Similarly  $H_x$  is zero for this condition. Therefore  $\vec{E}$  and  $\vec{H}$  exist only in the plane at right angles to the direction of propagation.

On combining (1.2) and (1.6) it is clear that

$$\nabla \times \vec{E} = -\mu \dot{\vec{H}} \quad (4.12)$$

Therefore by definition of  $\nabla \times \vec{E}$ ,  $\vec{H}$  and  $\vec{E}$  are at right angles so that in the present example if  $\vec{E}$  is along the z-axis,  $\vec{H}$  is along the y-axis.

$$\text{Supposing } E = E_0 \cos \omega (t - x (\epsilon \mu)^{1/2}) \quad (4.13)$$

since  $x$  is a distance,  $(\frac{1}{\epsilon \mu})^{1/2}$  must represent the velocity of wave =  $v$ .

In free space this becomes  $(\frac{1}{\epsilon_0 \mu_0})^{1/2} = c =$  velocity of light  
 $= 3 \times 10^8$  m/sec.

Rearranging (4.13) :

$$\begin{aligned} E &= E_0 \cos(\omega t - \frac{\omega}{c} x) \\ &= E_0 \cos(\omega t - \frac{2\pi f}{\lambda f} x) \\ &= E_0 \cos(\omega t - \beta x) \end{aligned} \quad (4.14)$$

$$\text{where } \beta = \frac{2\pi}{\lambda} = \omega (\epsilon \mu)^{1/2} = \frac{\omega}{v} \quad (4.15)$$

#### A. 4.1 Intrinsic Impedance of a medium.

Assume a plane wave propagated in the  $x$  direction with  $\vec{E}$  and  $\vec{H}$  in the  $y$  and  $z$  directions respectively and varying as  $e^{j\omega t}$ . Then (1.4) and (1.2) simplify to:

$$\frac{\partial H_z}{\partial x} = -(\sigma + j \omega \epsilon) E_y \quad (4.16)$$

$$\frac{\partial E_y}{\partial x} = -j \omega \mu H_z \quad (4.17)$$

Substituting  $E_y = E e^{-j\beta x}$  and  $H_z = H e^{-j\beta x}$

in eqns(4.16) and (4.17) gives:

$$-j\beta H e^{-j\beta x} = -(\sigma + j \omega \epsilon) E e^{-j\beta x} \quad (4.18)$$

$$\text{and } -j\beta E e^{-j\beta x} = -j \omega \mu H e^{-j\beta x} \quad (4.19)$$

Thus from (4.18) and 4.19) :

$$\begin{aligned} \frac{E}{H} &= \frac{j\beta}{\sigma + j \omega \epsilon} = \frac{j \omega \mu}{j \beta} \\ \left( \frac{E}{H} \right)^2 &= \frac{j \omega \mu}{\sigma + j \omega \epsilon} \\ \frac{E}{H} &= \left( \frac{j \omega \mu}{\sigma + j \omega \epsilon} \right)^{1/2} = Z. \end{aligned} \quad (4.20)$$

where  $Z$  is the intrinsic impedance of the medium.

In the special case of free space  $\sigma = 0$ ,  $\mu = \mu_0 = 4 \pi \times 10^{-7}$  Henrys per metre, and  $\epsilon = \epsilon_0 = \frac{1}{36 \pi \times 10^9}$  Farads per metre. Then the intrinsic

impedance of free space,  $Z_{00}$  is given from eqn. (4.20) by

$$Z_{00} = \left( \frac{\mu_0}{\epsilon_0} \right)^{1/2} = 120 \pi = 377 \text{ ohms.} \quad (4.21)$$

### A. 5.0 Plane waves in a dielectric.

In a perfect dielectric  $\mu = \mu_0$  but  $\epsilon = \epsilon_0 \epsilon_r$

$$\therefore \beta = \omega (\epsilon \mu)^{\frac{1}{2}} = \omega (\epsilon_r)^{\frac{1}{2}} (\epsilon_0 \mu_0)^{\frac{1}{2}} \quad (5.1)$$

But  $\beta = \frac{\omega}{v}$  from (4.15)

$$\therefore v = \frac{\omega}{\beta} = \frac{1}{(\epsilon_r)^{\frac{1}{2}} (\epsilon_0 \mu_0)^{\frac{1}{2}}} = \frac{c}{(\epsilon_r)^{\frac{1}{2}}} \quad (5.2)$$

This is still approximately true even when medium is not perfectly non-conducting.

### A. 6.0 Plane waves in a conductor.

Williams<sup>(7)</sup> has pointed out that in transmission line theory, if R, L, G and C are series resistance, series inductance, shunt conductance and shunt capacitance respectively, per unit length, then I and V, varying harmonically with time are related by the equations:

$$\frac{\partial I}{\partial x} = - (G + j \omega C) V \quad (6.1)$$

$$\frac{\partial V}{\partial x} = - (R + j \omega L) I \quad (6.2)$$

where x is the direction of propagation.

There is a striking resemblance between these equations and (4.16) and (4.17).

The solution to the transmission line equations is found by differentiating (6.2) and then substituting for  $\frac{\partial I}{\partial x}$  from (6.1) giving:

$$\frac{\partial^2 V}{\partial x^2} = (R + j \omega L) (G + j \omega C) V \quad (6.3)$$

The solution of (6.3) is given by:

$$V = V_0 e^{-Px} \quad (6.4)$$

where P the propagation constant, is given by:

$$P = ((R + j \omega L) (G + j \omega C))^{\frac{1}{2}} \quad (6.5)$$

Similarly the solution of (4.16) and (4.17) is:

$$\vec{E} = \vec{E}_0 e^{-Px} \quad (6.6)$$

$$\text{where } p = (j \omega \mu (\sigma + j \omega \epsilon))^{\frac{1}{2}} \quad (6.7)$$

p may be called the "intrinsic propagation constant" of the medium,

$p = \alpha + j \beta$  where  $\alpha$  is the attenuation constant and

$\beta$  the phase constant of the medium.

Separating real and imaginary parts in (6.7):

$$\alpha^2 = \frac{1}{2} \omega \mu ((\sigma^2 + \omega^2 \epsilon^2)^{\frac{1}{2}} - \omega \epsilon) \quad (6.8)$$

$$\beta^2 = \frac{1}{2} \omega \mu ((\sigma^2 + \omega^2 \epsilon^2)^{\frac{1}{2}} + \omega \epsilon) \quad (6.9)$$



In a good conductor  $\sigma$  is much greater than  $\omega \epsilon$  :

$$\therefore \alpha = \beta = \left( \frac{1}{2} \omega \mu \sigma \right)^{\frac{1}{2}} = (\pi f \mu \sigma)^{\frac{1}{2}} \quad (6.10)$$

As in (4.17)

$$\frac{\partial E_y}{\partial x} = -j \omega \mu H_z$$

and as, from (6.6),

$$E_y = E_0 e^{-\alpha x}$$

and  $\alpha$  from (6.7) now is  $(j \omega \mu \sigma)^{\frac{1}{2}}$ ,

$$\frac{\partial E_y}{\partial x} = - (j \omega \mu \sigma)^{\frac{1}{2}} E_y = -j \omega \mu H_z \quad (6.11)$$

$$\text{and } \frac{E}{H} = \left( \frac{j \omega \mu}{\sigma} \right)^{\frac{1}{2}} = \left( \frac{\omega \mu}{\sigma} \right)^{\frac{1}{2}} \angle 45^\circ = Z_0 \text{ (metal)} \quad (6.12)$$

$$Z_m = R_m + jX_m$$

$$\text{and } R_m = X_m = \left( \frac{\omega \mu}{2 \sigma} \right)^{\frac{1}{2}} = \left( \frac{\pi f \mu}{\sigma} \right)^{\frac{1}{2}} \quad (6.13)$$

$$= \frac{\alpha}{\sigma} \text{ from (6.10)} \quad (6.14)$$

= the d.c. resistance of a plate of unit area, depth  $\frac{1}{\alpha}$  and conductivity  $\sigma$ .

At radio frequencies  $\frac{1}{\alpha}$  is known as the depth of penetration, "d".

$$"d" = \frac{1}{\alpha} = \frac{1}{\left( \frac{1}{2} \omega \mu \sigma \right)^{\frac{1}{2}}} \quad (6.15)$$

$$= \frac{1}{(\pi f \mu \sigma)^{\frac{1}{2}}} \text{ from (6.10) for a good conductor.} \quad (6.16)$$

$$\text{From (6.6) } \vec{E} = \vec{E}_0 e^{-\alpha x}$$

$$\text{At depth } x = \frac{1}{\alpha}, \vec{E} = \frac{\vec{E}_0}{e} = 0.368 \vec{E}_0 \quad (6.17)$$

#### A. 7.0. Reflection at a conducting surface.

When a wave, travelling in medium (A) reaches the boundary of medium (B) having constants that differ from those of (A), the wave, in general, will be partially transmitted and partially reflected.

This phenomenon is treated fully by such modern writers as Starr<sup>(8)</sup> Appendix 16; Booker<sup>(5)</sup>; and Jordan<sup>(10)</sup> but, as this Appendix has a more limited objective, a less general treatment is given, which is more akin to the method used by Williams<sup>(7)</sup>, noting in passing that his figures 3.4 and 3.6 of Vol. I should be transposed to be correct.

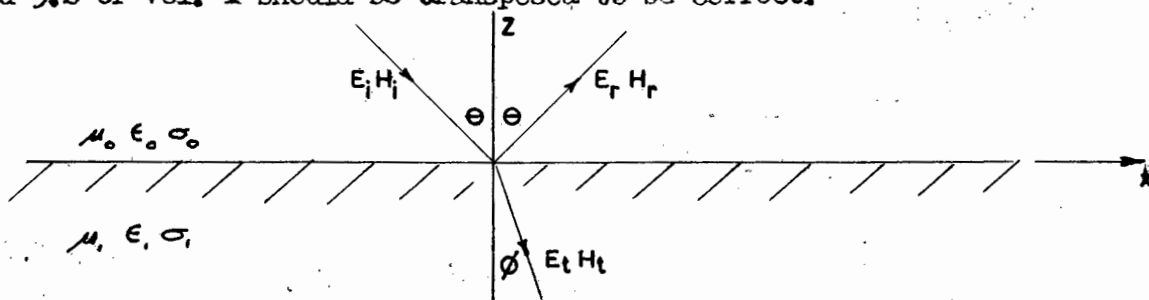


Fig. A. 7.0.1

As shown in (4.1)

$$\frac{E}{H} = \left( \frac{\mu}{\epsilon} \right)^{\frac{1}{2}} = Z_0$$

and the intensities vary as  $e^{j\omega t - ps}$

where  $s$  is the distance travelled by the wave.

In figure A. 7.0.1, resolving  $s$  into rectangular components, the expression  $e^{j\omega t - ps}$  becomes:

(a) for the incident wave:

$$e^{j\omega t - p_0 (x \sin \theta - z \cos \theta)} \quad (7.1)$$

(b) for the reflected wave:

$$e^{j\omega t - p_0 (x \sin \theta + z \cos \theta)} \quad (7.2)$$

(c) for the transmitted wave:

$$e^{j\omega t - p_1 (x \sin \phi - z \cos \phi)} \quad (7.3)$$

#### A. 7.1 Reflection of Vertically polarized waves.

Here  $\vec{E}_i$  is in the plane containing the ray and the normal at the point of reflection. Maxwell's equations (A.1.4) and (A. 1.2) require that at the boundary:

(a) the discontinuity in the tangential component of  $H$  equals the current density and,

(b) the tangential component of  $E$  is continuous across the surface boundary.

$$\text{From (b), } (E_i + E_r) \cos \theta = E_t \cos \phi \quad (7.4)$$

(NOTE: If  $\sigma_1$  were infinite (i.e for a perfect conductor)

$E_t \cos \phi$  would be zero and  $E_i = -E_r$ )

$$\text{From (a) } H_i - H_r = H_t \quad (7.5)$$

(NOTE: If  $\sigma_1$  were infinite, no energy could be transmitted in the conductor, making  $H_t$  zero and the incident and reflected energy must flow in opposite directions. For this to be the case, and knowing, from (7.4) that  $E_i = -E_r$ ,  $H_i$  must =  $H_r$

thus agreeing with (7.5) ).

Further the coefficients of the exponentials must be equal when  $z = 0$  in (7.2) and (7.3) giving  $p_0 \sin \theta = p_1 \sin \phi$  (7.6)

For most practical reflecting surfaces, such as land, water, copper sheet,  $\mu = \mu_0$  and  $\sigma$  is large compared with  $\omega \epsilon$

$$\begin{aligned} \frac{p_0}{p_1} &= \frac{(-\omega^2 \mu_0 \epsilon_0)^{\frac{1}{2}}}{(j \omega \mu_0 \sigma)^{\frac{1}{2}}} \\ &= \frac{\left( \frac{j \omega \mu_0}{\sigma} \right)^{\frac{1}{2}}}{\left( \frac{\mu_0}{\epsilon_0} \right)^{\frac{1}{2}}} = \frac{Z_0 \text{ of medium 1}}{Z_0 \text{ of air}} = \frac{Z_{01}}{Z_{00}} \end{aligned} \quad (7.7)$$

Applying (7.7) to (7.6) gives:

$$Z_{01} \sin \theta = Z_{00} \sin \phi \quad (7.8)$$

From (4.18)  $H_i = \frac{E_i}{Z_{00}}$

and (7.5) may be rewritten as:

$$\frac{Z_{01}}{Z_{00}} (E_i - E_r) = E_t$$

Substituting this value for  $E_t$ , and  $\frac{Z_{01}}{Z_{00}} = \frac{\sin \phi}{\sin \theta}$  from (7.8) in (7.4)

gives

$$(E_i + E_r) \cos \theta \sin \theta = (E_i - E_r) \cos \phi \sin \phi \quad (7.9)$$

Putting  $\sin \theta \cos \theta = 2 \sin 2 \theta$  (7.9) becomes  $(E_i + E_r) \sin 2 \theta$

$$= (E_i - E_r) \sin 2 \phi$$

Expanding and rearranging gives:

$$\frac{E_r}{E_i} = - \frac{\sin \theta \cos \theta - \sin \phi \cos \phi}{\sin \theta \cos \theta + \sin \phi \cos \phi} \quad (7.10)$$

From (7.6)  $\frac{P_1}{P_0} = \frac{\sin \theta}{\sin \phi}$

and since, on dividing throughout in (7.10) by  $\sin \phi$

$$\frac{E_r}{E_i} = - \frac{\frac{P_1}{P_0} \cos \theta - \cos \phi}{\frac{P_1}{P_0} \cos \theta + \cos \phi} = - \frac{\frac{P_1}{P_0} \cos \theta - (1 - \sin^2 \phi)^{\frac{1}{2}}}{\frac{P_1}{P_0} \cos \theta + (1 - \sin^2 \phi)^{\frac{1}{2}}}$$

giving: 
$$\frac{E_r}{E_i} = - \frac{(P_1^2/P_0^2) \cos \theta - ((P_1^2/P_0^2) - \sin^2 \theta)^{\frac{1}{2}}}{(P_1^2/P_0^2) \cos \theta + ((P_1^2/P_0^2) - \sin^2 \theta)^{\frac{1}{2}}} \quad (7.11)$$

From (6.7)  $\frac{P_1^2}{P_0^2} = \frac{\sigma_1 + j\omega\epsilon}{j\omega\epsilon_0}$

$$= \epsilon_{r1} - \frac{j \sigma_1}{\omega \epsilon_0} \quad (7.12)$$

where  $\epsilon_{r1}$  = relative permittivity of medium 1,  $\frac{\epsilon_1}{\epsilon_0}$

Now  $\omega = \frac{2\pi}{\lambda (\epsilon_0 \mu_0)^{\frac{1}{2}}}$

and  $\omega \epsilon_0 = \frac{2\pi}{\lambda} \left( \frac{\epsilon_0}{\mu_0} \right)^{\frac{1}{2}} = \frac{2\pi}{\lambda} \left( \frac{1}{120\pi} \right) = \frac{1}{60\lambda}$

and  $\frac{P_1^2}{P_0^2} = \epsilon_{r1} - j 60 \lambda \sigma \quad (7.13)$

Substituting in (7.11),  $R_v$ , the reflection coefficient (vertical polarization)

$$= \frac{E_r}{E_i} = - \frac{(\epsilon_{r1} - j 60 \lambda \sigma) \cos \theta - ((\epsilon_{r1} - j 60 \lambda \sigma) \sin^2 \theta)^{\frac{1}{2}}}{(\epsilon_{r1} - j 60 \lambda \sigma) \cos \theta + ((\epsilon_{r1} - j 60 \lambda \sigma) \sin^2 \theta)^{\frac{1}{2}}} \quad (7.14)$$

#### A. 7.2. Reflection of horizontally polarized waves.

Here the electric vector is at right angles to the plane containing the incident ray and the normal to the reflecting surface.

$R_h = \frac{E_r}{E_i}$  is derived in the same way as  $R_v$  was derived giving:

$$R_h = \frac{E_r}{E_i} = \frac{\cos \theta - ((\epsilon_{r1} - j 60 \lambda \sigma) \sin^2 \theta)^{\frac{1}{2}}}{\cos \theta + ((\epsilon_{r1} - j 60 \lambda \sigma) \sin^2 \theta)^{\frac{1}{2}}} \quad (7.15)$$

#### A. 8.0 Radiation.

The E.M. fields are best related to their sources by relating the potentials that produce the charges and currents respectively to  $\vec{E}$  and  $\vec{H}$ .

Maxwell's equations will be restated in terms of two potential functions, the two potentials being the electric scalar potential  $V$  which is related to  $\vec{E}$  (e.g. in electrostatics  $\vec{E} = -\nabla V$ ) and the magnetic vector potential  $\vec{A}$  which is related to  $\vec{H}$ .

$$\vec{A} \text{ is defined by the relationship: } \vec{B} = \nabla \times \vec{A} \quad (8.1)$$

Applying (8.1) to (1.2)

$$\nabla \times \vec{E} + \nabla \times \left( \frac{\partial \vec{A}}{\partial t} \right) = 0$$

$$\text{i.e. } \nabla \times (\vec{E} + \dot{\vec{A}}) = 0 \quad (8.2)$$

Now curl grad is always equal to zero

$\therefore \vec{E} + \dot{\vec{A}}$  can be expressed as a gradient.

$$\text{Put } \vec{E} + \dot{\vec{A}} = -\nabla V \quad (8.3)$$

This is in agreement with the relationship between  $\vec{E}$  and  $V$  for electrostatics, i.e. when  $\vec{A}$  is not changing and  $\dot{\vec{A}}$  is therefore zero.

Substitute for (8.3) in (1.1) modified by (1.5)

$$-\nabla \cdot \nabla V - \frac{\partial}{\partial t} (\nabla \cdot \vec{A}) = \frac{\rho}{\epsilon}$$

$$\text{Thus } -\nabla^2 V - \frac{\partial}{\partial t} (\nabla \cdot \vec{A}) = \frac{\rho}{\epsilon} \quad (8.4)$$

Equation (1.4) with (1.5) may be written:

$$\nabla \times \vec{H} = \epsilon \dot{\vec{E}} + \vec{i} \quad (8.5)$$

Substituting (8.1) and (8.3) in (8.5)

$$\nabla \times \nabla \times \vec{A} = \mu (\vec{i} - \epsilon \nabla \dot{V} - \epsilon \ddot{\vec{A}})$$

but  $\nabla \times \nabla \times \vec{A} = \nabla (\nabla \cdot \vec{A}) - \nabla^2 \vec{A}$

$$\text{Thus } \nabla (\nabla \cdot \vec{A}) - \nabla^2 \vec{A} = \mu (\vec{i} - \epsilon \nabla \dot{V} - \epsilon \ddot{\vec{A}}) \quad (8.6)$$

$\vec{A}$  and  $V$  may be related by assuming

$$\nabla \cdot \vec{A} = -\mu \epsilon \dot{V} \quad (8.7)$$

after noting that the equation of continuity is

$$\nabla \cdot \vec{i} = -\dot{a} \quad (8.8)$$

Combining (8.7) with (8.4) and (8.7) with (8.6) gives:

$$\nabla^2 V - \epsilon \mu \ddot{V} = -\frac{a}{\epsilon} \quad (8.9)$$

$$\nabla^2 \vec{A} - \epsilon \mu \ddot{\vec{A}} = -\mu \vec{i} \quad (8.10)$$

(8.9) and (8.10) are the wave equations (compare with (3.1) and (3.2))

for  $\vec{A}$  and  $V$  and relate the electric scalar potential ( $V$ ) and the mag-

netic vector potential  $\vec{A}$  at a point  $P$  distant  $r$  from an infinitesimally

short conductor carrying charge density  $a$  and impressed current density  $\vec{i}$

Eqs. (8.9) and (8.10), in conjunction with (4.13 ff), may be written (and in

this form are sometimes more convenient) as:

$$\nabla^2 V - \frac{\ddot{V}}{v^2} = -\frac{a}{\epsilon} \quad (8.11)$$

$$\text{and } \nabla^2 \vec{A} - \frac{\ddot{\vec{A}}}{v^2} = -\mu \vec{i} \quad (8.12)$$

where  $v = (\epsilon \mu)^{-\frac{1}{2}} =$  velocity of wave in the medium.

The solution to (8.9) or (8.11) is shown by Jordan<sup>(10)</sup> to be inferred from two limiting cases, (a) the static case and (b) the dynamic case,

taking pt.  $P$  to be outside the volume occupied by the charge density.

In (a),  $\dot{V} = 0$  giving:

$$\nabla^2 V = -\frac{a}{\epsilon} \quad (\text{Poisson's Eqn}) \quad (8.13)$$

From electrostatics the solution to (8.13), giving the potential at  $P$  distant  $r$  from a conductor carrying static charge density  $a$ , is

$$V_p = \frac{1}{4\pi\epsilon} \int_{\text{volume}} \frac{a}{r} dV \quad (8.14)$$

In (b)  $a = 0$ , therefore,

$$\nabla^2 V = \frac{\ddot{V}}{v^2} \quad (8.15)$$

A solution to this for harmonic variations would be of the form

$$V_P = \frac{K e^{j \omega (t - \frac{r}{v})}}{r} \quad (8.16)$$

i.e. the effect of a change in  $a$  in the conductor is felt at P distant  $r$  from the conductor only at a time  $\frac{r}{v}$  after the change took place, this being the time the radiated wave took to travel the distance  $r$  at velocity  $v$ . Jordan<sup>(10)</sup> and Williams<sup>(7)</sup>, using different methods, go on to show that the solution to (8.11) is a combination, reasonably so, of (8.16) and (8.14)

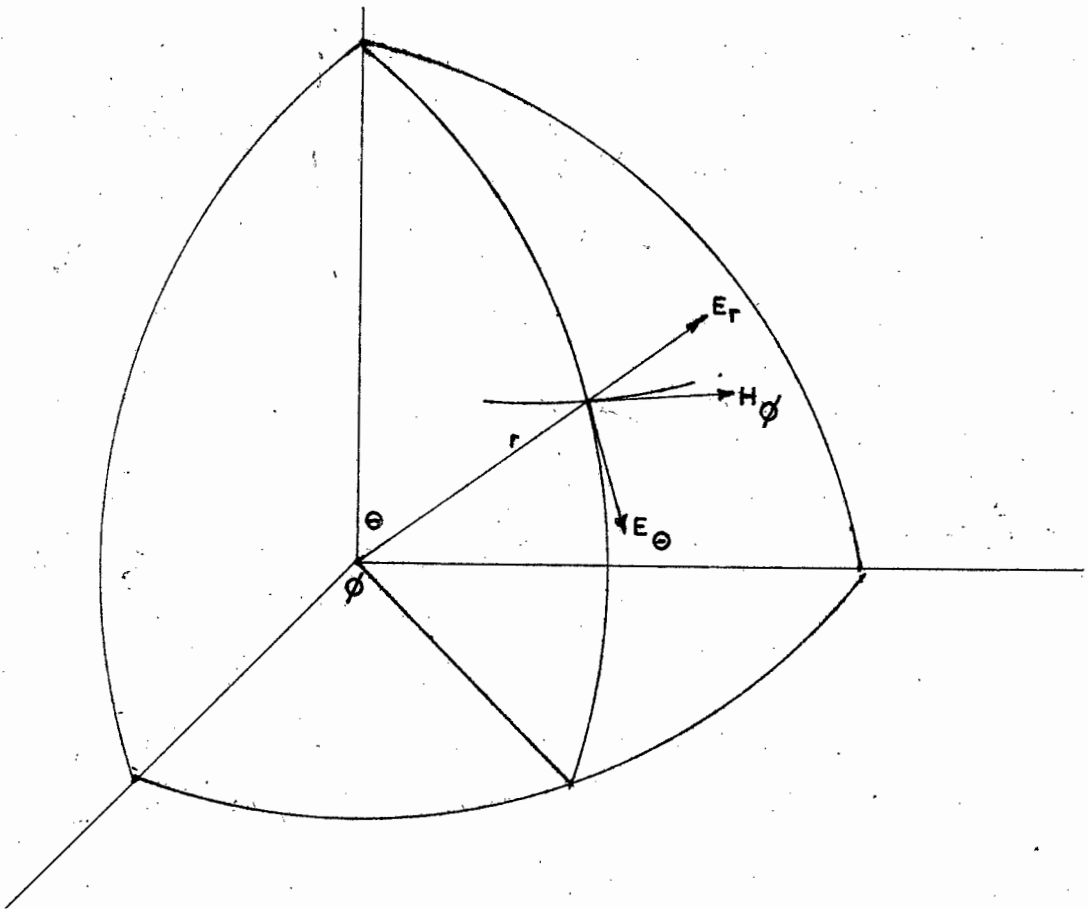
i.e.

$$V_P = \frac{1}{4 \pi \epsilon} \int_{\text{vol}} \frac{a e^{j \omega (t - \frac{r}{v})}}{r} d v. \quad (8.17)$$

and similarly

$$\bar{A}_P = -\frac{\mu}{4 \pi} \int_{\text{vol}} \frac{\bar{I} e^{j \omega (t - \frac{r}{v})}}{r} d v \quad (8.18)$$

These equations are sometimes combined to form the Hertzian vector potential but this is not required for the purpose of this work.



Field Components of a Doublet

The treatment given here is based on the writer's own notes on this subject, taken while at Cape Town University.

Assume doublet of length  $h$  lies at the origin in figure A.8.1. and points in the direction  $\theta = 0$ , i.e. along the  $z$  axis. ( $h$  is much smaller than  $\lambda$ .)

Assume  $i = i_m e^{j\omega t}$  and may be considered constant over length  $h$ .

$\vec{A}$  is in the direction  $\theta = 0$ .

$$A_z = \frac{\mu}{4\pi r} i h \exp. j (\omega t - \beta r) \quad \text{from eqn. 8.18} \quad (8.19)$$

$$\text{and } A_r = A_z \cos \theta \quad (8.20)$$

$$A_\theta = A_z \sin \theta \quad (8.21)$$

$$A_\phi = 0.$$

Therefore  $\mu H = B = \nabla \times \vec{A}$

$$\begin{aligned} &= \frac{1}{r \sin \theta} \left( \sin \theta A_\phi \right) - \frac{\partial A_\theta}{\partial \phi} \bar{1}_r \\ &+ \frac{1}{r} \left( \frac{1}{\sin \theta} \frac{\partial A_r}{\partial \phi} - \frac{\partial}{\partial r} (r A_\phi) \right) \bar{1}_\theta \\ &+ \frac{1}{r} \left( \frac{\partial}{\partial r} (r A_\theta) - \frac{\partial r}{\partial \theta} \right) \bar{1}_\phi. \end{aligned}$$

All terms, except the last, are equal to zero.

$$\text{Thus } H_\phi = \frac{i h \exp j (\omega t - \beta r)}{4 \pi} \left( \frac{j \beta}{r} + \frac{1}{r^2} \sin \theta \right) \quad (8.22)$$

The  $j\beta/r$  and  $1/r^2$  terms are in respect of the radiation field and the induction field respectively.

Similarly

$$E_r = \frac{i h \exp j (\omega t - \beta r)}{4 \pi \epsilon} \left( \frac{2 j \beta}{\omega r^2} + \frac{2}{j \omega r^3} \right) \cos \theta \quad (8.23)$$

$$E_\theta = \frac{i h \exp j (\omega t - \beta r)}{4 \pi \epsilon} \times \left( \frac{j \beta^2}{\omega r} + \frac{j \beta}{\omega r^2} + \frac{1}{j \omega r^3} \right) \sin \theta \quad (8.24)$$

$$E_\phi = 0 \quad (8.25)$$

(a) When  $r$  is small compared with  $\lambda$

$$H_\phi = \frac{i h \exp j \omega t}{4 \pi r^2} (\sin \theta) \quad (8.26)$$

$$E_r = \frac{2 i h \exp j \omega t}{j 4 \pi \omega \epsilon r^3} (\cos \theta) \quad (8.27)$$

$$E_\theta = \frac{i h \exp j \omega t}{j 4 \pi \omega \epsilon r^3} (\sin \theta) \quad (8.28)$$

(b) When  $r$  is large compared with  $\lambda$

$$H_\phi = \frac{j \beta i h \exp j (\omega t - \beta r)}{4 \pi r} (\sin \theta) \quad (8.29)$$

$$E_r = 0 \quad (8.30)$$

$$E_\theta = \frac{j \beta^2 i h \exp j (\omega t - \beta r)}{4 \pi r \epsilon \omega} (\sin \theta) \quad (8.31)$$

$\vec{E}$  and  $\vec{H}$  are in the plane of the wave front, are at right angles to each other, and their ratio is:

$$\frac{E}{H} = \frac{E_0}{H_0} = \frac{\beta}{\omega} = \left(\frac{\mu}{\epsilon}\right)^{\frac{1}{2}} = Z_{00} \quad (8.32)$$

$Z_{00}$  is the intrinsic impedance and its value agrees with (4.18).

The field impedance near the doublet is given by dividing (8.28) by (8.26)

$$\therefore Z_0 = \frac{1}{j \omega \epsilon r} = -j \frac{Z_{00}}{\beta r} \quad (8.33)$$

#### A. 9.0 Energy flow in a medium.

$$\vec{H} \cdot (\text{equation 1.2}) = \vec{H} \cdot \nabla \times \vec{E} + \vec{H} \cdot \dot{\vec{B}} = 0 \quad (9.1)$$

$$\vec{E} \cdot (\text{equation 1.4}) = \vec{E} \cdot \nabla \times \vec{H} - \vec{E} \cdot \dot{\vec{D}} = \vec{E} \cdot \vec{I} \quad (9.2)$$

Subtract (9.2) from (9.1) and apply the

identity that  $\nabla \cdot (\vec{E} \times \vec{H}) = \vec{H} \cdot \nabla \times \vec{E} - \vec{E} \cdot \nabla \times \vec{H}$

$$\text{Then } \nabla \cdot (\vec{E} \times \vec{H}) + \vec{E} \cdot \dot{\vec{D}} + \vec{H} \cdot \dot{\vec{B}} = -\vec{E} \cdot \vec{I} \quad (9.3)$$

This is Poynting's equation.

If there is an impressed current density  $\vec{I}_1$  (9.3) becomes:

$$\nabla \cdot (\vec{E} \times \vec{H}) + \vec{E} \cdot \dot{\vec{D}} + \vec{H} \cdot \dot{\vec{B}} = -\vec{E} \cdot \vec{I} - \vec{E} \cdot \vec{I}_1 \quad (9.4)$$

Integrating over a volume "v" bounded by a surface "a" (9.4) becomes:

$$\begin{aligned} \int_{\text{vol}} \nabla \cdot (\vec{E} \times \vec{H}) dv + \int_{\text{vol}} \vec{E} \cdot \epsilon \dot{\vec{E}} dv + \int_{\text{vol}} \vec{H} \cdot \dot{\vec{B}} dv = \\ - \int_{\text{vol}} \vec{E} \cdot \vec{I} dv - \int_{\text{vol}} \vec{E} \cdot \vec{I}_1 dv \end{aligned} \quad (9.5)$$

Gauss' Theorem states that

$$\int_{\text{vol}} \nabla \cdot \vec{E} dv = \int_{\text{area}} \vec{I}_n \cdot \vec{E} da.$$

$$\begin{aligned} \text{Therefore } \int_{\text{area}} (\vec{E} \times \vec{H}) \cdot \vec{I}_n da + \int_{\text{vol}} \vec{E} \cdot \epsilon \dot{\vec{E}} dv + \int_{\text{vol}} \frac{\vec{B}}{\mu} \cdot \dot{\vec{B}} dv \\ + \int_{\text{vol}} \vec{E} \cdot \vec{I} dv = - \int_{\text{vol}} \vec{E} \cdot \vec{I}_1 dv \end{aligned} \quad (9.6)$$

On the right hand side is the impressed energy ( $E I \cos \phi$ ). On the L.H.S. the first term is the flow of energy normal to the surface of the integration; the second and third terms represent the rate of change of the energy in the electric and magnetic fields; the fourth term is the energy dissipated as heat in the system.  $\vec{E} \times \vec{H} = \vec{S}$  is Poynting's Vector in watts/sq. metre.

#### A. 10.0 Radiated power and Radiation Resistance of a doublet antenna.

The power transmitted across a unit area at a radius r from the doublet is obtained by taking the time average of the Poynting Vector  $\vec{E} \times \vec{H} = \vec{S}$ .



Taking values for  $E_\theta$  and  $H_\phi$  from (8.31) and (8.29) the time average of  $\vec{S}$

$$= S_r = \frac{1}{2} |E_\theta| \cdot |H_\phi| \quad (10.1)$$

$$S_r = \frac{1}{2} \frac{\beta^3 I^2 h^2 \sin^2 \theta}{16 \pi^2 r^2 \epsilon \omega} \text{ watts/ unit area.} \quad (10.2)$$

To find the total energy radiated it is necessary to integrate over the whole sphere of radius  $r$

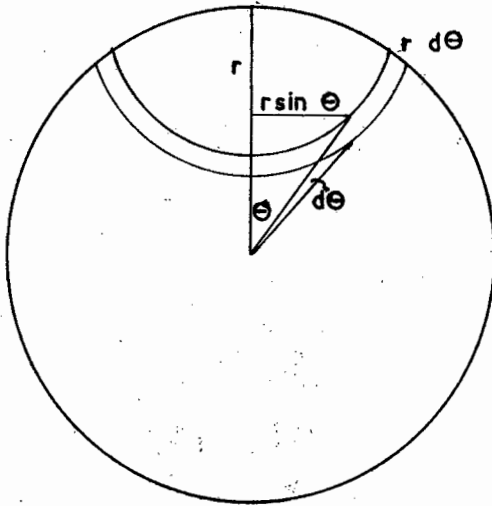


Fig. A. 10.1.1  
Element of area on a spherical surface.

$$\text{From fig. 10.1.1 } da = 2 \pi r^2 \sin \theta d\theta \quad (10.3)$$

$$\text{Thus } P_r = \int_{\text{area}} S_r da = \int_0^\pi S_r 2 \pi r^2 \sin \theta d\theta \quad (10.4)$$

$$= \frac{\beta^3 I^2 h^2}{16 \pi \epsilon \omega} \int_0^\pi \sin^3 \theta d\theta \quad (10.5)$$

$$= \frac{\beta^3 I^2 h^2}{16 \pi \epsilon \omega} \left[ \frac{-\cos \theta}{3} (\sin^2 \theta + 2) \right]_0^\pi$$

$$= \frac{\beta^3 I^2 h^2}{12 \pi \epsilon \omega} = \frac{\beta^2 I^2 h^2}{12 \pi} Z_{00} = 10 (\beta I h)^2 \text{ watts} \quad (10.6)$$

$$= \frac{1}{2} R_r I^2$$

where  $R_r$  is defined as the radiation resistance because  $I$  is the peak value of the current in the doublet.

$$\text{Thus } R_r = 20 (\beta h)^2 \quad (10.8)$$

But  $\beta = 2 \pi / \lambda$ .

$$\text{Therefore } R_r = 790 h^2 / \lambda^2 \quad (10.9)$$

$$\text{and power radiated} = 395 I^2 h^2 / \lambda^2 \text{ watts} \quad (10.10)$$

As this is for a doublet,  $h$  is small compared with  $\lambda$ .

Since  $P = 10 (\beta I h)^2$  from eqn (10.6) and

$$E_{rms} = \frac{.707 \beta^2 I h}{4 \pi r \epsilon \omega} = \frac{.707 \beta I h \times 120 \pi}{4 \pi r} = \frac{.707 \times 30}{(10)^{\frac{1}{2}}} \frac{(P)^{\frac{1}{2}}}{r} \quad (10.11)$$

A. 11. 1 Radiation from a half wave dipole.

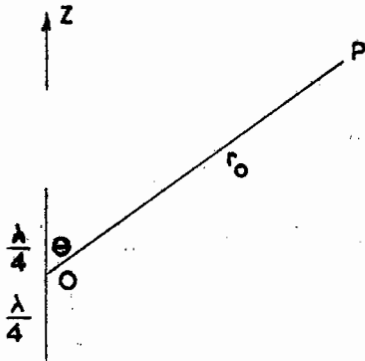


Fig. A. 11.1.1

P is far enough away from O for the distance r, from point P to any point on the dipole distant z from O, to be taken as  $r = r_0 - z \cos \theta$  (11.1)

Assume sinusoidal current distribution so that if  $I_0$  is peak current at O then the peak current at any point along the dipole, distant z from O will be  $I = I_0 \cos \beta z$  so that at  $z = \frac{\lambda}{4}$ ,  $I = 0$  (11.2)

An element of length dz will behave as a doublet. Therefore from (8.31) (radiation field)

$$E_\theta = \frac{-j \beta^2 I_0 \sin \theta}{4 \pi r \epsilon_0} \int_{-\lambda/4}^{\lambda/4} \cos \beta z e^{j(\omega t - \beta r_0 + \beta z \cos \theta)} dz. \quad (11.3)$$

$$= -\frac{j Z_0 I_0 \sin \theta}{4 \pi r} \int_{-\lambda/4}^{\lambda/4} \beta \cos \beta z e^{j(\omega t - \beta r_0 + \beta z \cos \theta)} dz \quad (11.4)$$

$$\text{But } \int e^{ax} \cos bx \, dx = \frac{e^{ax}}{a^2 + b^2} (a \cos bx + b \sin bx)$$

Therefore, integrating, and taking  $\frac{Z_0 I_0}{2 \pi} = 60$ ,

$$E_\theta = \frac{60 I_0}{r_0} e^{j(\omega t - \beta r_0)} \cos \frac{(\frac{\pi}{2} \cos \theta)}{\sin \theta} \quad (11.5)$$

Placing  $r_0$  for r in denominator, is permissible if  $r_0$  is large. If I is the r.m.s value of the current then the r.m.s. value of the field strength is given by

$$E = \frac{60 I}{r_0} \frac{\cos \frac{\pi}{2} \cos \theta}{\sin \theta} \quad (11.5 A)$$

The variable portion gives the polar diagram in the vertical plane and is a function of  $\theta$  given by:

$$F(\theta) = \frac{\cos(\frac{\pi}{2} \cos \theta)}{\sin \theta} \quad (11.6)$$

From (10.1)

$$S_r = \frac{Z_0 I_0^2}{8 \pi^2 r_0^2} \left( \frac{\cos(\frac{\pi}{2} \cos \theta)}{\sin \theta} \right)^2 \quad (11.7)$$

$$\text{and } P_r = \int_0^\pi S_r 2 \pi r^2 \sin \theta \, d\theta \text{ from (10.3)} \quad (11.8)$$

$$= \frac{Z_0 I_0^2}{4 \pi} \int_0^\pi F^2(\theta) \sin \theta \, d\theta \quad (11.9)$$

$$= 30 I_0^2 \int_0^\pi F^2(\theta) \sin \theta \, d\theta \quad (11.10)$$

and  $R_r$  referred, as usual, to the point where  $I$  is a maximum, from (10.7),

$$\text{is given by } R_r = 60 \int_0^\pi F^2(\theta) \sin \theta \, d\theta \quad (11.11)$$

$$= 60 \int_0^\pi \frac{\cos^2\left(\frac{\pi}{2} \cos \theta\right)}{\sin \theta} \, d\theta \quad (11.12)$$

(11.12) may be put into a form using tabulated integrals given by Jahnke and Emde<sup>(17)</sup> and  $R = 73$  ohms (approximately) (11.13)

Alternatively, following Jordan,<sup>(7)</sup> who appears to follow Pierce<sup>(18)</sup>:

Put  $\cos \theta = u$  then  $\frac{d\theta}{\sin \theta} = \frac{du}{1-u^2}$  and the integral becomes

$$\frac{1}{2} \int_{-1}^1 \frac{1 + \cos \pi u}{1 + u} \, du$$

Hence putting  $v = \pi(1+u)$

the integral becomes

$$\begin{aligned} & \frac{1}{2} \int_0^{2\pi} \left( \frac{v}{2!} - \frac{v^3}{4!} + \frac{v^5}{6!} \right) dv \\ &= \frac{1}{2} \left( \frac{v^2}{2 \cdot 2!} - \frac{v^4}{4 \cdot 4!} + \frac{v^6}{6 \cdot 6!} - \frac{v^8}{8 \cdot 8!} + \dots \right) \Big|_0^{2\pi} \end{aligned} \quad (11.14)$$

and since  $v = 2\pi = 6.2832$

the first term = 9.870

Using 8 terms the integral

$$\int_0^\pi \frac{\cos^2\left(\frac{\pi}{2} \cos \theta\right)}{\sin \theta} \, d\theta = 1.2186 \quad (11.15)$$

and  $R = 60 \times 1.2186$  for a  $\frac{\lambda}{2}$  dipole.

$$= 73.12 \text{ ohms as in (11.13)} \quad (11.16)$$

#### A. 11.1 Radiation from a $\frac{\lambda}{4}$ monopole (grounded).

In the case of a  $\frac{\lambda}{4}$  vertical rod the integral will be for a semi-spherical surface (limits are now 0 to  $\frac{\pi}{2}$ ) and

$$R_r = 60 \times .609 = 36.5 \text{ ohms.} \quad (11.17)$$

As would be expected, if  $I$  is the same in both cases the dipole radiates twice as much power as the monopole.

#### A. 11.2 Field strength related to power and distance.

If  $P_r = I^2 R_r = 1000$  watts, using R M S values for  $I$  and  $E$  then  $I_{\text{rms}} = \left(\frac{1000}{73}\right)^{\frac{1}{2}} = 3.7$  amps.

Then, from (11.5) one watt of radiated power will produce, at a point distant 1 metre in the equatorial plane ( $\theta = 90^\circ$ ), a field strength

$$E = \frac{60 \times 3.7}{(1000)^{\frac{1}{2}}} = 7 \text{ V/m}$$

$$\text{i.e. } Ed = 7 (P)^{\frac{1}{2}} \text{ for } \frac{\lambda}{2} \text{ dipole.} \quad (11.18)$$

At high frequencies a point distant 1 metre would probably be in the induction field making the case fictitious but the concept of  $P = 1$  watt,  $r = 1$  metre is useful in the M.K.S. system.

The field strength at one kilometre for  $P_r = 1$  kilowatt is given by:

$$E = 60 \times 3.7 \times 10^3 \text{ volts/metre.}$$

$$= 222 \text{ mV/m} \quad (11.19)$$

This is another useful concept.

Note that  $r$  is not expressed in wavelengths and therefore for a given radiated power, a  $\frac{\lambda}{2}$  dipole, for, say, 1 Mc/s, will produce the same field strength at one Km. as a  $\frac{\lambda}{2}$  dipole at 100 Mc/s.

### A. 11. 3.0 Influence of reflecting plane.

Assume the plane is a perfect conductor. Then the image would be as in fig. A. 11.3.0.1 (a) for a vertical element, (b) for a horizontal element and (c) for an inclined element.

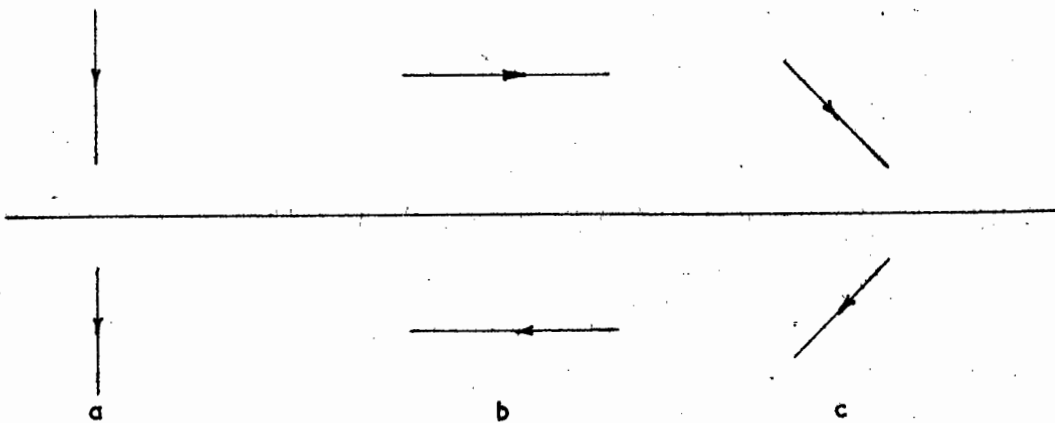


Fig. A. 11.3.0.1

The vertical radiator has an in-phase image; the horizontal radiator has an out-of-phase image.

The polar diagram is found by multiplying the polar pattern of a dipole in free space (equation 11.6) by that produced by two point sources situated at the centre of the dipole and at the centre of its image respectively. The point sources are in-phase for a vertical dipole and out-of-phase for one which is horizontal.

### A. 11.4.0 Vertical antenna above perfectly conducting plane.

Jordan<sup>(10)</sup> suggest that the multiplication referred to in 11.3.0 may be done qualitatively by inspection of the two polar diagrams to be multiplied.

It is proposed, however, to follow William's<sup>(7)</sup> method of deriving "height factors" which, when multiplied by equation (11.6) will produce a quantitative result.

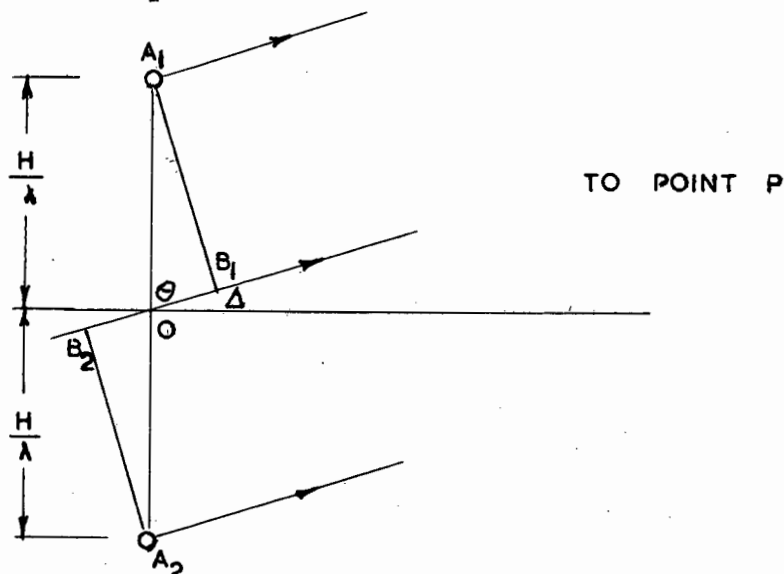


Fig. A. 11.4.0.1

Distance O P is so great that A<sub>1</sub> P; O P; A<sub>2</sub> P may be considered parallel.

$$O B_1 = \frac{H}{\lambda} \cos \theta = \beta H \cos \theta \text{ radians.}$$

Thus when  $\theta = 0$ , the phase of E<sub>1</sub> at P relative to reference pt. O due to A<sub>1</sub> will be  $\beta H$  radians whereas at  $\theta = 90^\circ$  it will be zero.

Similarly for A<sub>2</sub> the phase of E<sub>2</sub> at P relative to point O due to A<sub>2</sub> will be  $-\beta H$  radians.

The resultant field at P will be the vector sum of E<sub>1</sub> and E<sub>2</sub> taking into account any difference in phase in A<sub>1</sub> and A<sub>2</sub>.

Apply this to fig. A. 11. 3.0.1 (a). The currents in antenna and ground image are in phase. E at P due to antenna and image when

I<sub>1</sub> = antenna current and I<sub>2</sub> = image current is given by the equation:

$$E = k I_1 \text{ angle } (\beta H \cos \theta) + k I_2 \text{ angle } (-\beta H \cos \theta)$$

Assuming I<sub>1</sub> = I<sub>2</sub>

$$\bar{E} = k I_1 \text{ angle } (\beta H \cos \theta) + k I_1 \text{ angle } (-\beta H \cos \theta)$$

$$E = 2k I_1 \cos (\beta H \cos \theta) \quad (11.20)$$

$$= 2 k I_1 \cos (\beta H \sin \Delta) \quad (11.21)$$

$$= 2 k I_1 F_1 (H, \Delta)$$

where  $\Delta$  = angle between O P and the horizontal;  $\cos (\beta H \sin \Delta)$  is the height factor F<sub>1</sub> for positive images and is plotted graphically in figure A. 11.4.0.3.  $k I_1$  is the free-space value of the field (eqn. 11.5 A). The field strength, in the presence of a reflecting plane, is  $E = 2 \cos (\beta H \sin \Delta)$  times the free-space field strength.

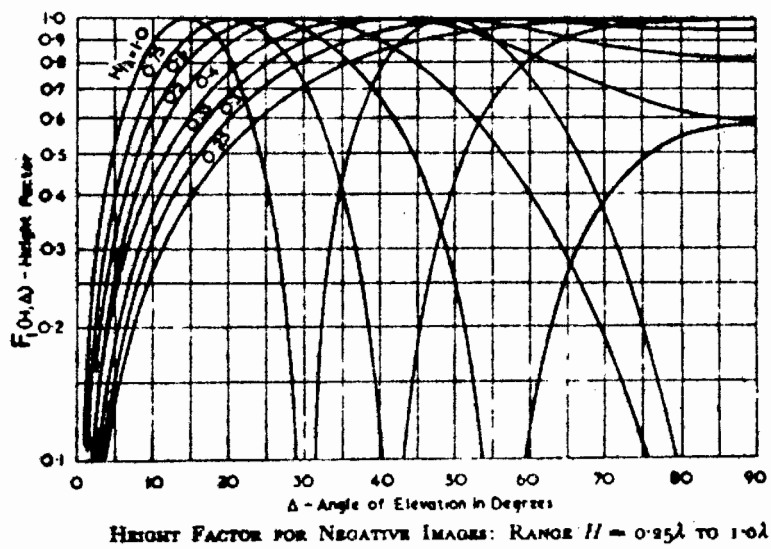


Figure A.11.4.0.2.

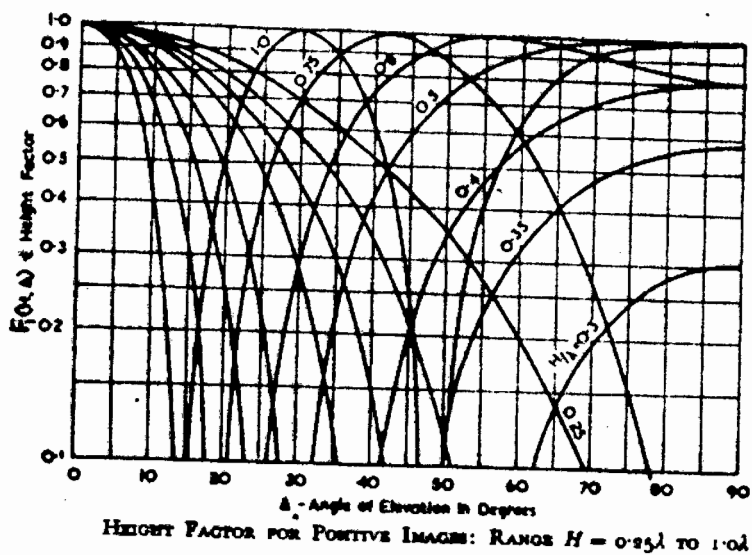


Figure A.11.4.0.3.

(7)

Both figures reproduced from Williams

A. 11. 5.0 Horizontal antenna above conducting plane.

Here the image current and the antenna current are in antiphase.

Therefore from fig. A.11.3.0.1 :

$$E_1 = k I_1 \sin \beta H \cos \theta \quad (11.23)$$

$$E_2 = -k I_1 \sin \beta H \cos (\theta + \pi)$$

Assuming  $I_1 = I_2$

$$\begin{aligned} E &= 2 k I_1 \sin (\beta H \cos \theta) \\ &= 2 k I_1 \sin (\beta H \sin \Delta) \end{aligned} \quad (11.24)$$

$F_1 \sin (\beta H \sin \Delta)$  is plotted graphically in fig. A.11.4.0.2 (11.25)

for  $H$  is  $\cdot 25 \lambda$  to  $1.0 \lambda$  for negative images. The field strength, in the presence of a reflecting plane, is  $E = 2 \sin (\beta H \sin \Delta)$  times the free space field.

A. 12. 0. Radiation from a straight wire carrying a travelling wave.

The sending peak current  $I_0$ , is related to the peak current at a point distant,  $z$  down the wire by the equation:

$$I_z = I_0 \exp (-j \beta z) \quad (12.1)$$

where  $I_z$  and  $I_0$  differ in phase but not in magnitude. They vary sinusoidally with time so that  $i_z = I_z \exp(-j \omega t)$  and  $i_0 = I_0 \exp(-j \omega t)$



Fig. A. 12. 0.1

Straight wire carrying travelling wave.

In fig. A.12. 0.1 a straight wire, length  $l$ , is centre fed. The instantaneous electric field at a distance  $r_0$  from  $0$  is given by equations (8.31) and (11.1)

$$\begin{aligned} E_\theta &= \frac{j \beta^2 \sin \theta}{4 \pi r_0 \omega} \int_{-\frac{l}{2}}^{+\frac{l}{2}} I_0 e^{-j \beta z} e^{j(\omega t - \beta r_0 + \beta z \cos \theta)} dz \\ &= \frac{j \beta^2 I_0}{4 \pi r_0 \omega} \sin \theta e^{j(\omega t - \beta r_0)} \int_{-\frac{l}{2}}^{+\frac{l}{2}} e^{j \beta z (1 - \cos \theta)} dz \end{aligned} \quad (12.2)$$

Dealing with effective values, i.e. dropping the phasing terms and putting  $\frac{I_0}{2 \pi} = 60$ , 12.2 becomes:

$$E_\theta = \frac{60 I_0}{2 r} \sin \theta \int_{-\frac{l}{2}}^{+\frac{l}{2}} e^{j \beta z (1 - \cos \theta)} dz \quad (12.3)$$

Putting  $\beta z (1 - \cos \theta) = x$

$$\beta (1 - \cos \theta) dz = dx$$

$$\text{and } dx = \frac{dz}{\beta (1 - \cos \theta)}$$

The integral then becomes

$$\int \frac{\beta}{\beta (1 - \cos \theta)} e^{-jx} = \left[ \frac{e^{-jx}}{-j (1 - \cos \theta)} \right]_{\beta \frac{1}{2} (1 - \cos \theta)}^{\beta \frac{1}{2} (1 - \cos \theta)}$$

$$= \frac{-j}{(1 - \cos \theta)} \left( e^{-j \beta \frac{1}{2} (1 - \cos \theta)} - e^{+j \beta \frac{1}{2} (1 - \cos \theta)} \right) \quad (12.4)$$

$$\text{Putting } \frac{\beta}{2} (1 - \cos \theta) = y.$$

$$= \frac{-j}{(1 - \cos \theta)} (\cos y - j \sin y - \cos y - j \sin y)$$

$$= \frac{2 \sin y}{(1 - \cos \theta)} = \frac{\sin \left( \beta \frac{1}{2} (1 - \cos \theta) \right)}{(1 - \cos \theta)} \quad (12.5)$$

From (12.3) and (12.5):

$$E_{\theta} = \frac{60 I_0 \sin \theta}{r (1 - \cos \theta)} \sin \left( \beta \frac{1}{2} (1 - \cos \theta) \right) \quad (12.6)$$

The polar diagram  $F(\theta)$  is a function of  $\theta$  such that

$$F(\theta) = \frac{\sin \theta \sin \left( \beta \frac{1}{2} (1 - \cos \theta) \right)}{(1 - \cos \theta)} \quad (12.7)$$

#### A.12. 1 Radiation from a Rhombic antenna.

Four straight wires, each carrying a travelling wave as in (12.0), and forming a diamond comprise a Rhombic antenna. Harper<sup>(9)</sup> has devoted a book to Rhombic antenna design; workers such as Cafferata<sup>(20)</sup> and Foster<sup>(21)</sup> have made significant contributions to the theory and the equations derived below were verified by Bruce<sup>(22)</sup> and Bruce, Beck and Lowry<sup>(19)</sup>. In 1953 the International Consultative Committee<sup>(11)</sup> published the valuable "Antenna Diagrams"<sup>(11)</sup> of which fig. F.4.4.3.1 is one and the qualitative signal strength diagrams have been verified by the British Post Office.

The treatment of the subject by such writers as Starr<sup>(8)</sup>, Jordan<sup>(10)</sup>, Terman<sup>(4)</sup> is fragmentary. It is better covered by Williams<sup>(7)</sup> who summarizes much of what has been written earlier and his approach is applied below to the special case of the field in the direction of propagation which is in the direction of the major axis and inclined at an angle  $\Delta$  to the horizontal, making an angle  $\theta$  to AB and AD. Only when  $\Delta = 0$  will the direction of propagation be in the plane containing A, B, C, D. (See fig. A. 12. 1.1 where  $\angle B = \angle C = \angle D = \angle A = 1$  )

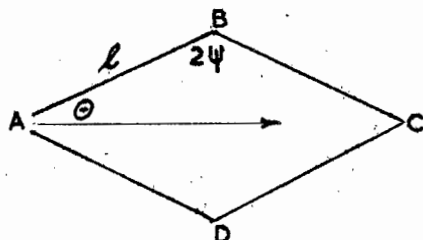


Fig. A. 12. 1.1.



From equation (12.6), but with the phasing terms in (12.2) re-introduced, the value of  $E_\theta$ , at P which lies in the direction of propagation, due to side A B referred to the current at A is given by:

$$E_\theta = \frac{j 60 I_0 \sin \theta}{r} e^{j(\omega t - \beta r)} \frac{\sin(\beta \frac{l}{2}(1 - \cos \theta))}{(1 - \cos \theta)} e^{-j\beta l/2(1 - \cos \theta)} \quad (12.8)$$

The last exponential term allows for referring the phase to A and for the phase difference along the wire.

The field due to side D C is the same as for A B except that there is a phase difference of  $\beta l \cos \theta$  radians (being the separation between the mid-points of A B and B C); a further phase difference between the currents at these points of  $\beta l$  radians due to the distance along the wire from the mid point of B C to that of D C; and a further phase difference of  $\pi$  radians due to the reversal in the sense of current between A B and D C.

The sum  $E_1$  of the fields in the direction of the major axis, from A B and C D, referred to the mid-point of A B, is given by:

$$E_1 = 2 E_\theta \cos \left( \frac{\beta l \cos \theta}{2} + \frac{\beta l}{2} + \frac{\pi}{2} \right) \\ = 2 E_\theta \sin \left( \beta \frac{l}{2} (1 - \cos \theta) \right) \quad (12.9)$$

This, as shown above, has a phase relationship with point A given by

$$e^{j\beta l/2(1 - \cos \theta)} \quad (12.10)$$

Thus, referred to current at A, from (12.9), (12.10), (12.8)

$$E_1 = \frac{j 120 I_0 \sin \theta \sin^2 \left( \frac{\beta l}{2} (1 - \cos \theta) \right)}{r (1 - \cos \theta)} e^{j(\omega t - \beta r)} e^{-2j\beta l/2(1 - \cos \theta)} \quad (12.11)$$

In like manner the sum  $E_2$  of the components from B C and D A are found to equal  $E_1$  in the direction of the major axis and the total field

$= E_1 + E_2$  in this direction.

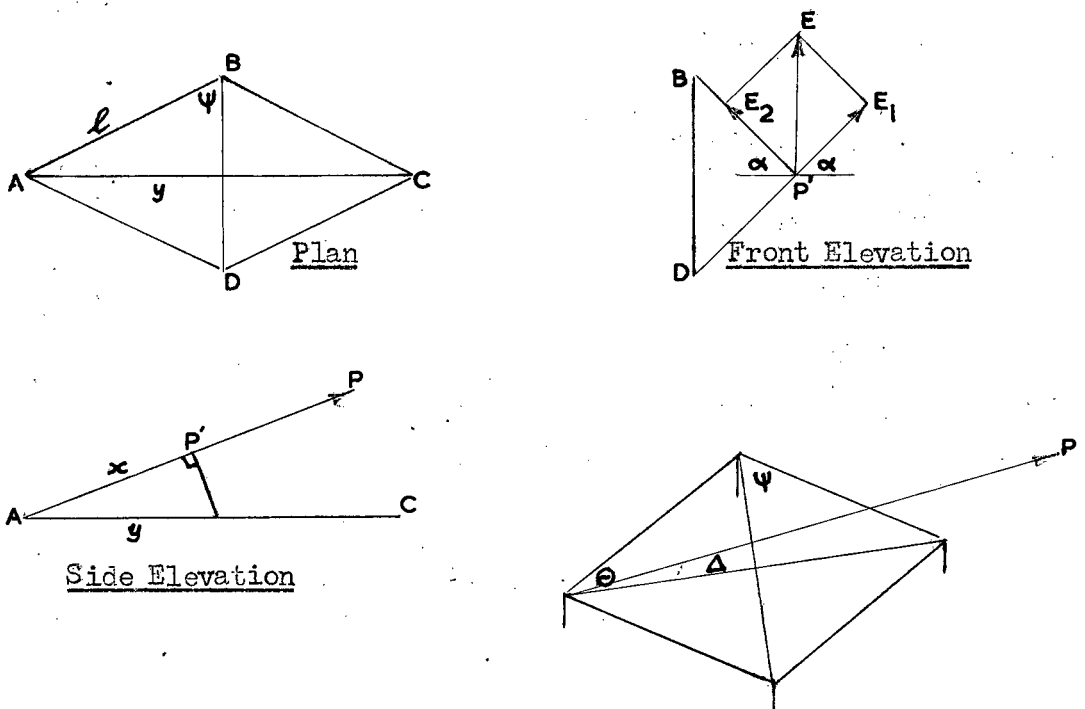


Fig. A. 12. 1.2

In fig. 12.1.2,  $\theta$  is the angle B A P

$$\cos \theta = \cos \Delta \sin \psi \quad (12.12)$$

$$E = 2 E_1 \sin \alpha = 2 E_1 \frac{\cos \psi}{\sin \theta} \quad (12.13)$$

Substituting for  $\cos \theta$  from (12.12) into (12.11) and then for  $E_1$  in (12.13), whilst dropping the time phasing terms, gives

$$E = \frac{240 I \cos \psi}{r (1 - \cos \Delta \sin \psi)} \sin^2 \left( \frac{\beta l}{2} (1 - \cos \Delta \sin \psi) \right) \quad (12.14)$$

where  $E$  and  $I$  are r.m.s values.

$$\text{Thus } E = \frac{240 I}{r} F_2 (\psi, \Delta) F_3 (1, \psi, \Delta) \quad (12.15)$$

$F_2$  is called the "asymmetry factor".

$F_3$  is called the "length factor".

If the input impedance = 600 ohms an input power of 1000 watts would produce a current of:

$$I = 1.29 \text{ amps and from (12.15)}$$

$$E = \frac{310 P^{\frac{1}{2}}}{r} F_2 F_3 \quad (12.16)$$

where  $E$  is in mV/metre

$r$  is in Km.

Comparing (12.16) with (11.19) the Rhombic antenna has a power gain,  $G_H$ , over a half wave dipole in free space such that

$$G_H = (1.396 F_2 F_3)^2$$

$$\text{say } G_H = (1.4 F_2 F_3) \quad (12.17)$$

Vertical Polar diagram. (Rhombic Antenna)

When a Rhombic antenna is mounted horizontally above the ground it may be considered to have a negative image below the ground as in fig. (A.11.1) and the combined field strength is double that given in (12.15) multiplied by the height factor  $F_1$ , for negative images. (Eqn. 11.25).

The power gain,  $G_H$ , of the Rhombic, situated above a conducting plane, over a dipole in free space, is therefore given by:

$$G_H = (2.8 F_1 F_2 F_3)^2 \quad (12.18)$$

$$\text{and } E = \frac{620 P^{\frac{1}{2}}}{r} F_1 F_2 F_3 \quad (12.19)$$

$$\text{or (from (12.15)) } E = \frac{480 I}{r} F_1 F_2 F_3 \quad (12.20)$$

where  $E$  is in mV/metre at pt P in direction of major axis.

$P$  is power in KW.

$r$  is distance of P from radiator in Km.

$F_1$  is given by equation (11.25)

$F_2, F_3$  are given by equations (12.14) and (12.15)

Horizontal polar diagram. (Rhombic Antenna ).

Starr<sup>(8)</sup> and Williams<sup>(7)</sup> quoting Bruce and his colleagues<sup>(22),(19)</sup>, extend  $F_2$ ,  $F_3$  to give a polar diagram for  $\Delta = \text{constant}$  in terms of an exploring azimuthal angle  $\phi$  so that

$$E = \frac{240 I}{r} F_4 (\Psi, \Delta, \phi) F_5 (1, \Psi, \Delta, \phi) \quad (12.21)$$

$$\text{where } F_4 = \frac{1}{2} \left( \frac{\cos (\Psi + \phi)}{1 - \cos \Delta \sin (\Psi + \phi)} + \frac{\cos (\Psi - \phi)}{1 - \cos \Delta \sin (\Psi - \phi)} \right) \quad (12.22)$$

$$\text{and } F_5 = \sin \left( \frac{\beta l}{2} (1 - \cos \Delta \sin (\Psi + \phi)) \right) \sin \left( \frac{\beta l}{2} (1 - \cos \Delta \sin (\Psi - \phi)) \right) \quad (12.23)$$

(Notice that  $F_4$  and  $F_5$  equal  $F_2$  and  $F_3$  in the special case when  $\phi = 0$ ).

Now, in free space, as in (12.16), (12.17)

$$E = \frac{310 (P)^{\frac{1}{2}}}{r} F_4 F_5 \quad (12.24)$$

$$G_H = (1.4 F_4 F_5)^2 \quad (12.25)$$

and when Rhombic is placed above a conducting plane, as in (12.19) and (12.18)

$$E = \frac{620 (P)^{\frac{1}{2}}}{r} F_1 F_4 F_5 \quad (12.26)$$

$$\text{or } E = \frac{480 I}{r} F_1 F_4 F_5 \quad (12.27)$$

where  $E$ ,  $P$  and  $r$  have the same units as in 12.19 and

$$G_H = (2.8 F_1 F_4 F_5) \quad (12.28)$$

Optimum dimensions of Rhombic Antenna.

To obtain maximum gain for a given value of  $\Delta$ , the functions  $F_1$ ,  $F_2$ ,  $F_3$  in eqn. (12.18) are differentiated with respect to  $\Delta$ . Williams<sup>(7)</sup> has shown that this leads to the following optimum dimensions:

$$H = \frac{\lambda}{4 \sin \Delta} \quad (12.29)$$

$$\Psi = 90 - \Delta \quad (12.30)$$

$$1 = \frac{\lambda}{2 \sin^2 \Delta} \quad (12.31)$$

But this gives a lobe maximum slightly below the chosen angle. In order to correct this  $\frac{dE}{d\Delta}$  from equation (12.20) must be put to zero.

$$\text{The maximum occurs at } 1 = \frac{.371 \lambda}{\sin^2 \Delta} \quad (12.32)$$

The signal strength in this direction is some 15% less than it is in the same direction for the maximum output design of eqn. (12.31). Eqs. (12.29)(12.30) and (12.34) are used to give optimum designs for transmitting antennas and eqns. (12.29), (12.30), (12.32) provide the optimum design for receiving antennas because no other part of the lobe is more sensitive than it is in the direction of the wanted signal.

Radiation Resistance of Rhombic antenna.

This is shown by Lewin<sup>(23)</sup> to be

$$R_r = 240 \left( \log_e \left( 4 \pi \frac{1}{\lambda} \cos^2 \psi \right) + 0.577 \right) \quad (12.34)$$

where  $R_r$  is in ohms.

-----

A P P E N D I X B.

H.F. PROPAGATION : LONDON - SALISBURY.

S U M M A R Y O F A P P E N D I X B.

H. F. propagation theory is developed and leads to the following results, which are used in the main text, assuming that the operating frequency is 21.47 Mc/s at noon, September, 1956, and that 100 kw is transmitted from London, using a Koomans H/4/4/1 antenna aligned on the great circle bearing of Salisbury from London:-

(a) Wave arrival angle ( $\Delta$ ) in Salisbury:	$8^{\circ} \pm 2^{\circ}$ .
(b) Mode of transmission:	3 hop F.
(c) Approximate height of trajectory:	255 km.
(d) Losses at reflection points:	8.6 db.
(e) Non-deviative absorption:	41.6 db.
(f) Deviative absorption:	2.2 db.
(g) Spatial attenuation.	75.0 db.
(h) Polarization and phasing loss (assumed):	4.6 db.
(i) Calculated received field strength:	12 db above $1\mu\text{V/m}$ i.e. $4\mu\text{V/m}$ .

Expected variations in signal strength are dealt with under the headings:-

- 1) Interference between signal components which are out of phase;
  - 2) Wave frequency approaching the value of path M.U.F.;
  - 3) Dellinger Fades (S.I.D.);
  - 4) Prolonged Ionospheric Disturbances (P.I.D.);
  - 5) Ionospheric Storms;
  - 6) Sporadic E Ionization;
  - 7) Winds and Tides in the Ionosphere;
  - 8) Scatter phenomena.
-

APPENDIX B.

H. F. PROPAGATION : LONDON - SALISBURY.

B.1.0 What must be known about the incoming signal.

When attempting to design a suitable receiving antenna for a high grade point-to-point circuit, a knowledge of the following is necessary:

- a) the mechanism by which the signal travels from transmitter to receiver;
- b) the expected wave arrival angle and bearing; (ignorance on this point could easily lead to the error of employing a high-gain antenna with maximum sensitivity in a direction other than that from which the signal is arriving);<sup>(214)</sup>
- c) the median value of the received signal strength;
- d) possible variations of (b) and (c) and the probable extent of the variations;
- e) polarization of the received signal.

By summarising the present knowledge on the propagation of radio waves, and the manner and extent of their attenuation from transmitter to receiver, it is possible to determine the parameters concerned.

B.1.0 The formation of an ionospheric layer.

Theories concerning the formation of ionized layers are summarized below.

Consider the earth as being enveloped by a gaseous element the density of which decreases exponentially upwards. The intensity of radiation from the sun decreases as the earth is approached because of absorption, by the gas particles, of this radiation as it penetrates the gaseous envelope. The absorbed radiation causes ionisation of the gas and the rate of ionization would therefore be expected to be a maximum at a certain level. In 1926 Pannekoek<sup>(66)</sup> developed Saha's<sup>(67)</sup> theory of thermal ionization as modified by Milne<sup>(69)</sup> and Woltjer<sup>(68)</sup> to take into account the continuous nature of the solar radiation but Chapman<sup>(51)</sup> produced a theory in 1931 that is simple, direct, and useful and takes into account diurnal and seasonal variations by specifying ionization in terms of the zenith angle  $X$  of the sun.

Due to absorption of the sun's radiation in the atmosphere the change in radiation intensity  $dI$  when the radiation passes through a layer of absorption coefficient  $A$  of atmosphere of thickness  $dh$  at height  $h$  is given by:-

$$dI = AI \, dh \sec X \, p_0 \exp(-h/H) \quad B.1.1.1$$

where  $p_0$  is the gas density at ground level and  $H$ , the scale height, is defined as:

$$H = \frac{kT}{mg} \quad B.1.1.2$$

where  $k$  = Boltzmann's Constant  $1.37 \times 10^{-16}$  erg/degree absolute.

$T$  = temperature at height  $h$  in degrees absolute.

$m$  = mean molecular mass of gas.

$g$  = acceleration, due to gravity, at height  $h$ .

On integration, eqn. (B.1.1.1) becomes:

$$I = I_0 \exp(-A p_0 H \sec X \exp(-h/H)) \text{ where } \quad B.1.1.3$$

$I_0$  = the intensity of radiation before it enters the atmosphere.

If  $\beta$  is the number of ions produced by absorption of unit quantity of radiation then the rate,  $q$ , of ion production per cc at height  $h$  is given by:-

$$q = \beta \frac{dI}{dh} \cos X. \quad B.1.1.4$$

Differentiating eqn. B.1.1.4 gives  $q$  as a maximum value of:

$$q_0 = \beta I_0 \cos X/H \exp 1 \quad B.1.1.5$$

and the height of this maximum rate of ion production is given by:

$$\exp(h/H) = A p_0 H \sec X \quad B.1.1.6$$

For the special case when the sun is vertically overhead,  $X = 0$  and eqns. B.1.1.5 and B.1.1.6 become:

$$q_0 = \beta I_0 / H \exp 1 \quad B.1.1.5a$$

$$h_m = H \log_e A p_0 H \quad B.1.1.6a$$

Now reckoning height from the reference level  $h_m$  in scale units and writing this height as " $z$  scale units from  $h_m$ " (where

$$z = \frac{h - h_m}{H} \text{ ),}$$

$$q = q_0 \exp(1 - z - \sec X \exp(-z)) \quad B.1.1.7$$

If  $N$  = number of electrons/cc at any instant  $t$  at height  $h$  and, assuming that the number of electrons lost per second due to recombination is  $\alpha N^2$ , then, for equilibrium conditions,

$$\frac{dN}{dt} = q - \alpha N^2 = 0 \quad B.1.1.8$$

$$\text{i.e. } q = \alpha N^2 \quad B.1.1.9$$

Substituting in eqn B.1.1.5

$$\alpha N^2 = \beta I_0 \cos X/H \exp 1$$

$$\text{and } N = \text{constant } (\cos X)^{\frac{1}{2}} \quad B.1.1.10$$

Substituting eqn. 2.1.1.9 in eqn 2.1.1.7 the distribution of N with height is given by:-

$$N = N_{\max} \exp \frac{1}{2} (1 - z - \sec X \exp (-3)) \quad \text{B.1.1.11}$$

where  $N_{\max} = (q_0 / \alpha)^{\frac{1}{2}}$  is the maximum electron density for  $X = 0$ .

In the region where  $z$  is small and for the case where  $X = 0$  Chapman<sup>(51)</sup> shows that eqn (B.1.1.11) approximates to:-

$$\begin{aligned} N &= N_{\max} (1 - z^2/4) \\ &= N_{\max} (1 - y^2/4 H^2) \end{aligned} \quad \text{B.1.1.12}$$

where  $y = h - h_m = z H$ .

Equation B.1.1.12 is that of a parabola and this parabolic distribution holds good to an accuracy of 95% within the region  $h_m \pm H$ . Such a region is commonly called a "Chapman Region".

## B.2.0

### Practical departures from the Chapman Theory.

The idealized assumptions of the theory, that (a) the atmosphere is isothermal (assuming  $H = kT/mg$  is constant), (b) that ionizing radiation is monochromatic and (c) that the recombination coefficient is constant with height, are not found in practice and this fact distorts the layer shape. Nicolet and Bossy<sup>(71)</sup> have investigated the effect on N when H is not assumed constant and Glidhill and Szendrei<sup>(72)</sup> have investigated the variation of N with h for a rising temperature gradient. However the deviation, in practice, from the Chapman layer, is not great in the E and F<sub>1</sub> layers.

## B.3.0

### The formation of a series of layers.

Mitra<sup>(73)</sup> has pointed out that Pannekoek's<sup>(66)</sup> calculations may be used to explain the origins of the various layers. Bahr<sup>(70)</sup> has calculated in great detail, the formation of layers using this method and the present theories may be summarised as:

## B.3.1

### The normal "D" region (60 km - 100 km).

The theory put forward by Mitra, Bhar and Ghosh<sup>(74)</sup>, in 1938, that this region is caused by ionization of O<sub>2</sub>, has given way to one proposed by Nicolet<sup>(75)</sup> as follows:-

- (a) The normal D ionization is due to ionization of O<sub>2</sub>,
- (b) Sometimes a sporadic layer is formed due to ionization of sodium, and
- (c) Sometimes extra ionization is produced during radio fade-outs due to ionization of NO by  $\lambda$  1300 giving



Mitra<sup>(76)</sup> supports this theory but Watanabe, Marmo, and Pressman<sup>(78)</sup> do not accept (a) and (b) and Gibbons and Waynick<sup>(76)</sup> favour (c) as the reason for normal D region ionization. It is hoped that the present scanty knowledge concerning the D region model will be assisted considerably by the space probe programme now in its infancy.



### B.3.2 The normal "E" region. (100 km. - 150 km.).

The under-boundary of this region is approximately 100 km. with  $N_{\max}$  at about 120 km. when the sun is vertically overhead. This is the transition region where  $O_2$  dissociates to form atomic oxygen. Bhar<sup>(70)</sup> has proposed that the layer is formed by the second ionization potential of  $O_2$ . Hoyle and Bates<sup>(79)</sup> theory that E ionization of O is due to emission from the solar corona (photon groups at 325Å) has received wider acceptance. Appleton<sup>(80)</sup> indicates that recent rocket soundings have demonstrated that E ionization is caused by soft X rays.

Appleton<sup>(80)</sup> has also drawn attention to the vertical transport of electrons in the E region pointing out that eqn. B.1.1.8 becomes:

$$\frac{dN}{dt} = q - \alpha N^2 - \text{div } N \quad \text{B.3.2.1}$$

where  $\text{div } N$  is the electron disappearance rate upwards per unit volume and this upward drift of electrons is responsible, according to Martyn<sup>(81)</sup>, for some of the perturbations in the F layer.

### B.3.3 The normal "F" region. (above 150 km.)

This is the region above about 150 km. and is usually subdivided to give the  $F_1$  layer and the  $F_2$  layer. Bhar's<sup>(70)</sup> proposal that  $F_1$  is due to ionization of molecular nitrogen and  $F_2$  to the ionization of atomic oxygen is not supported by Bates and Massey<sup>(83)</sup> who claim that  $F_1$  is due to ionization of atomic oxygen and this is supported by later workers. This region ( $F_1$ ) conforms to a normal Chapman layer and  $N$ , the electron density, near the maximum is given by the solution of the equation:

$$\frac{dN}{dt} = q - \alpha N^2 \quad \text{from eqn. B.1.1.8}$$

For equilibrium conditions ( $\frac{dN}{dt} = 0$ ) equations B.1.1.8,9,10 indicate that:

$$N = \text{const} \times (\cos X)^{\frac{1}{2}} \quad \text{as in (B.1.1.10)}$$

The  $F_2$  region, according to Mitra<sup>(76)</sup> is also produced by ionization of O by the following process:

As proposed by Bradbury<sup>(85)</sup> and favoured by Mohler<sup>(84)</sup> and Bates and Massey<sup>(83)</sup>, the effective recombination coefficient,  $\alpha$ , decreases with height so rapidly that a maximum occurs when equilibrium is reached at some height above  $F_1$ . Thus the F region has two maxima, one at  $F_1$  and one at  $F_2$ . Bradbury<sup>(85)</sup> suggests that in the  $F_2$  region the number of electrons lost per second =  $\beta N$  compared with the  $\alpha N^2$  in the E and  $F_1$  regions and therefore:

$$N_{\max} = \text{const} \times (\cos X) \quad \text{instead of } (\cos X)^{\frac{1}{2}}.$$

Martyn<sup>(86)</sup> agrees but maintains that Bradbury's theory<sup>(85)</sup> is not the whole story because  $N_{\max}$  ( $F_2$ ) varies with sunspot activity at a rate more than 3 times  $N_{\max}$  ( $F_1$ ) and has postulated the concept of ionization transport (See sec. D.3.2) so that in the  $F_2$  region:

$$\frac{dN}{dt} = q - \beta N - \text{div} (V N) \quad : \quad \text{D.3.3.1}$$

where  $N$  = number of electrons per cc.

$q$  = the production of ions per cc.

$\beta$  = coefficient of ionization decay =  $10^{-4} \exp(\frac{300-h}{50})$

$h$  = height in km.

$V$  = transport velocity of electrons (and ions).

The variation of  $N_{\max}$  with sunspot number has been investigated by Allen<sup>(87)(88)</sup> who has shown that the values at the equator at the equinoxes, during an epoch of sunspot number  $R$ , are given by:

$$F_1 \text{ layer, } N_{\max} = 2.5 \times 10^5 (1 + 0.0062 R) \quad : \quad \text{D.3.3.2}$$

$$F_2 \text{ layer, } N_{\max} = A \times 10^5 (1 + 0.02 R) \quad : \quad \text{D.3.3.3}$$

$$= f_c^2 \times 1.24 \times 10^4 \quad : \quad \text{D.3.3.4}$$

where  $f_c$  is the  $F_2$  critical freq. in Mc/s.

Martyn<sup>(86)</sup> has incorrectly stated eqn D.3.3.4 as " $N_{\max} = f_c^2 \times 1.24$  where  $f_c$  is in Mc/s")

By comparison with other data the value of  $A$  in eqn D.3.3.3 is considered to be about 4.5.

The collision frequency between an electron and ions,  $\nu_{ei}$ , and between an electron and neutral particles,  $\nu_{en}$ , may be calculated by formulae due to Chapman<sup>(89)</sup> as follows:

$$\nu_{ei} = (34 + 4.18 \log_{10} (T^3 / N)) N T^{-3/2} \quad : \quad \text{D.3.3.5}$$

$$\nu_{en} = 5.4 + 10^{-10} N_n T^{1/2} \quad : \quad \text{D.3.3.6}$$

where  $T$ , the absolute temperature, for various heights from 50 km to 100 km, is given by Nicolet<sup>(90)</sup>, Martyn<sup>(86)</sup> from satellite results quoted by Schilling and Sterne<sup>(96)</sup>, indicates that  $T$  rises fairly uniformly from  $560^\circ$  K at 160 km ( $F_1$ ) to about  $1400^\circ$  K at 300 km ( $F_2$ ).  $N_n$  = neutral particle number density/cc. The particle densities given by Terman<sup>(4)</sup> page 714 for various heights may be used for the values of  $N_n$  in eqn (D.3.3.6).

Martyn<sup>(86)</sup> indicates that the scale height  $H$  for this region is given by  $H = .039 T$  (km) at 300 km and  $H = .037 T$  at 160 km when  $T$  = absolute temperature, quoting Bales<sup>(173)</sup> for the assumption that the mean molecular weight in the  $F$  region is 23.8.

#### B.4.0

#### The Ionospheric Model of number density and total collision freq.

It is helpful to deduce the variation of  $N$  and  $\nu$  with height. This has been done for noon at the equator in September 1956 ( $X=0$ ) and the results are summarised in Figure F.D.2.4.0.1.

**B.4.1 Electron number density vs. height.**

Rocket soundings quoted by Friedman<sup>(79)</sup> and critical frequency soundings taken by Thomas<sup>(82)</sup> in July/August 1957 have been used as the basis of the model. These figures were adjusted so as to give the value of  $N_m$  for  $F_2$  as per equation B.3.3.4 taking noon  $f$  critical at the equator in September 1956 as 13 Mc/s<sup>(99)</sup> i.e.  $N_{max}$  for  $F_2 = 21 \times 10^5$  electrons/cc. (also see eqn. B.5.0.4).

The September noon curve for  $N$  versus height at the equator for any other year may be plotted approximately by multiplying the  $N$  curve in Figure F. B.4.0.1 by the ratio  $(f_o/13)^2$ .<sup>(99)</sup> The  $F_2$  critical frequency for which Fig. F.B.4.0.1 was constructed was 13 Mc/s and  $f_o$  is the  $F_2$  critical frequency in Mc/s at noon at the equator for the year in question. For other times of day and/or other seasons and/or other latitudes, find the solar zenith angle  $X$ : then the  $N$  curve is approximately  $(\cos X)^{0.5}$  times that obtained above for  $F_1$  region and  $(\cos X)$  times for the  $F_2$  region.

**B.4.2 Collision frequency. ( $v = v_{ei} + v_{en}$ ).**

The collision frequency for various heights was calculated as explained in B.3.3. Because of its very large range of values it has been plotted on a logarithmic base and reveals a linear variation, on this base, above and below the region of transition from  $O_2$  to  $O$ .

**B.4.3 The product  $Nv$ .**

This is the fundamental quantity that appears in the absorption formulae quoted by Piggott<sup>(56)</sup> and Appleton<sup>(57)</sup>. From figure F. B.4.0.1 it is a simple matter to obtain the average value of  $(Nv)$  for each 10 km. of path length.

There is still considerable difference of opinion between various authorities concerning the median values of  $v$  and  $N$ . When Mr. W.R. Piggott was asked<sup>(177)</sup> recently to comment on Fig. F.B.4.0.1, he replied<sup>(178)</sup> that he agreed that the important section of the  $v$  curve below 120 km. is correct but suggested values for  $v$  above 120 km. and for  $N$  below 110 km. that have resulted in the curves drawn in red. It is seen that a small change in the  $N$  curve below 110 km. has resulted in a large change in the  $Nv$  curve at these heights.

Piggott's suggested amendment<sup>(178)</sup> has been accepted because (a) the graphs by Thomas<sup>(82)</sup>, from which the original " $N$ " curve was deduced, are difficult to read with accuracy in the 70 to 100 km. region and (b), to quote Piggott<sup>(178)</sup>, " $v$ " values above 120 km. "are very controversial but the estimates are steadily falling with time, most of the losses seen experimentally being due to systematic defocus phenomena, the interpretation of rocket measurements being questionable".

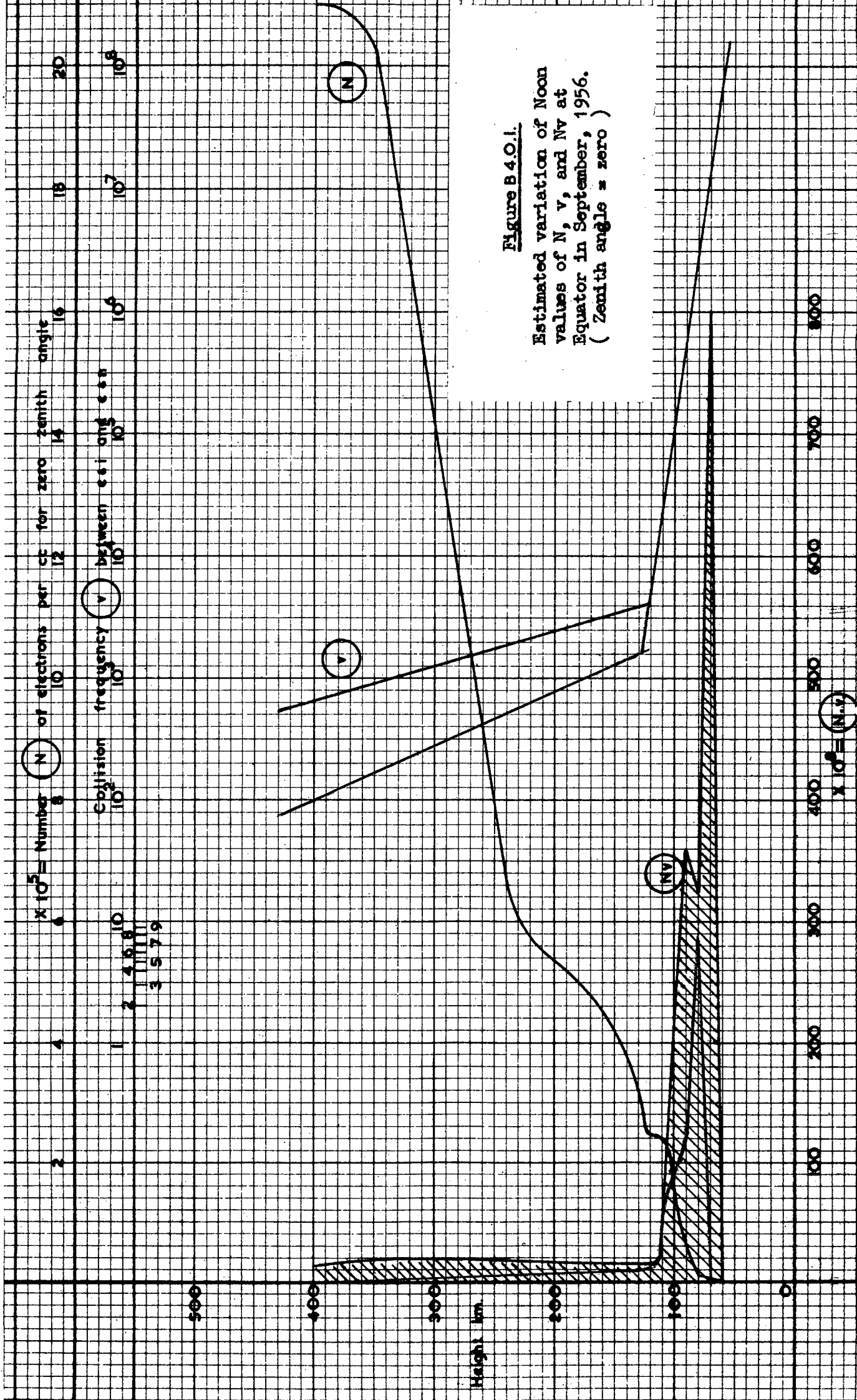


Figure B4.O.I.

Estimated variation of Noon values of N, v, and Nv at Equator in September, 1956. ( Zenith angle = zero )

B.5.0

PROPAGATION IN THE IONOSPHERE.

The refractive index when neglecting collisions and earth's field.

As pointed out by Eccles<sup>(91)</sup> in 1910 and developed by Larmor<sup>(92)</sup> in 1924, in what is regarded as the basic Eccles-Larmor theory of radio wave propagation in an ionized medium, and as supplemented by the Appleton-Hartree magneto-ionic theory,<sup>(47),(48),(49)</sup> neglecting collisions and the effect of the earth's magnetic field, the refractive index (n) of an ionized layer has been shown by Baker and Rice<sup>(37)</sup> to be given by the equation:

$$n = \left( 1 - \frac{81 N}{f^2} \right)^{\frac{1}{2}} \quad (\text{B.5.0.1})$$

where n = refractive index at the level of density N.

N = electron density in electrons/ cm<sup>3</sup>.

f = frequency of wave in kc/s.

If an ascending radio wave leaves the atmosphere (where n = 1) and enters a horizontally stratified ionized layer at an angle i to the vertical, then, by Snell's Law<sup>(4)</sup>, the angle,  $\theta_x$ , between the wave and the vertical at any point, x, where the refractive index =  $n_x$ , is governed by the equation:

$$n_x \sin \theta_x = \sin i. \quad (\text{B.5.0.2})$$

There will be total reflection at the height where  $\theta_x = 90^\circ$  where the wave is bent horizontal. At this point:

$$\sin i = n_x = \left( 1 - \frac{4 \pi N_0 e^2}{m \omega^2} \right)^{\frac{1}{2}}$$

$$\text{or } \sin i = n_x = \left( 1 - \frac{81 N_0}{f^2} \right)^{\frac{1}{2}} = \epsilon^2 \quad (\text{B.5.0.3})$$

where  $N_0$  is the density of electrons at the highest point of the trajectory of a wave, of frequency f kc/s, incident at the bottom of the layer at an angle i and  $\epsilon$  is the dielectric constant of the ionized medium.  $e$  = is charge on an electron.

For vertical incidence  $\sin i = 0$  and

$$f = 9 (N_0)^{\frac{1}{2}} \quad (\text{B.5.0.4})$$

where f is in kc/s.

The critical frequency,  $f_c$ , of a layer, is defined as the value of f in eqn (B.5.0.4) which corresponds to the maximum value,  $N_{\max}$ , for that layer, giving:

$$f_c = 9 (N_{\max})^{\frac{1}{2}} \quad (\text{B.5.0.5})$$

The maximum usable frequency (M.U.F.), sometimes referred to as "oblique incidence critical frequency",  $f_{ci}$ , is defined as the value of f in eqn (B.5.0.3) corresponding to the value of  $N_{\max}$  that applies to the F<sub>2</sub> layer. Thus:

$$\sin i = \left( 1 - \frac{81 N_{\max}}{f_{ci}^2} \right)^{\frac{1}{2}}$$

$$1 - \sin^2 i = \cos^2 i = \frac{81 N_{\max}}{f_{ci}^2} = \frac{f_c^2}{f_{ci}^2}$$

Thus  $f_{ci} = f_c \sec i.$

$$(\text{B.5.0.6})$$

From this relationship follows immediately a theorem (derived in a different way by Mitra<sup>(76)</sup>) and forming the basis of Martyn's absorption theorem<sup>(65)</sup> namely, that the height of trajectory of a wave of frequency  $f$ , incident at angle  $i$ , is the same as the trajectory height of a vertical incidence wave of frequency  $f'$  provided that:-

$$f' = f \cos i \quad (\text{B.5.0.7})$$

$f \cos i$  is called the "equivalent normal incidence frequency" corresponding to the "oblique incidence frequency",  $f$ .

The refractive index when neglecting collisions but taking account of the earth's field.

Appleton<sup>(91)</sup> has shown that when the earth's magnetic field is taken into account, the refractive index, when collisions are neglected, is given by:-

$$n^2 = 1 - \frac{2}{2y - \frac{x_T^2}{y-1} + \left( \frac{x_T^4}{(y-1)^2} + 4x_L^2 \right)^{\frac{1}{2}}} \quad (\text{B.5.0.8})$$

where  $y = \frac{m \omega^2}{4 \pi N e^2}$

$$x_L = \frac{m \omega \omega_1}{4 \pi N e^2}$$

$$x_T = \frac{m \omega \omega_2}{4 \pi N e^2}$$

where  $\omega_1$  = gyro magnetic angular frequency corresponding to  $H_L$

$\omega_2$  = ,, ,, ,, ,, ,, ,,  $H_T$

$H_L$  = magnetic field strength in direction of propagation.  
(in e.s.u.).

$H_T$  = Magnetic field strength at right angles to direction of propagation (in e.s.u.)

$e$  = electron charge (e.s.u.).

$\omega$  = angular frequency of the wave, radions/sec.

The upper sign gives rise to the ordinary ray and produces a value of  $n$  very similar to that of B.5.0.3 (identical to it when  $H_L = \text{zero}$ ) while the lower sign gives rise to the extraordinary ray. For propagation along the line of the field  $x_T$  is negligible and eqn (B.5.0.8) becomes:-

$$\begin{aligned} n^2 &= 1 - \frac{2}{2 \frac{m \omega^2}{4 \pi N e^2} - \frac{m \omega \omega_1}{4 \pi N e^2}} \\ &= 1 - \frac{4 \pi N e^2}{m \omega^2 \left( 1 + \frac{\omega_1}{\omega} \right)} \quad (\text{B.5.0.9}) \end{aligned}$$

When the wave frequency is large compared with the gyro-magnetic frequency the value of  $n$  in eqn (B.5.0.9) tends towards the "no-field" value of eqn (B.5.0.3).

Refractive index neglecting field and taking collisions into account.

In an expression for  $n$ , the refractive index for propagation along the line of the earth's magnetic field and when  $\omega$  is much greater than  $\omega_1$  (see eqn D.5.0.9), it is permissible to neglect the earth's field. Baker and Rice<sup>(37)</sup> have shown that if the earth's field is neglected the conductivity of the ionosphere is given by:-

$$\sigma = \frac{N e^2 v}{m (\omega^2 + v^2)} \quad (\text{B.5.0.9.A})$$

where  $\sigma$  = conductivity in e.s.u.

$v$  = collision frequency.

$m$  = electron mass (grams).

and it has an effective complex dielectric constant  $\epsilon^1$ , where

$$\epsilon^1 = \epsilon - j \frac{4 \pi \sigma}{\omega} \quad (\text{B.5.0.10})$$

where  $\epsilon$  is the dielectric constant of the medium  $= 1 - \frac{4 \pi N e^2}{m(\omega^2 + v^2)}$

It also has a complex refractive index  $n^1$  where:

$$(n^1)^2 = \epsilon^1 = \left( n - \frac{j c \alpha}{\omega} \right)^2 = n^2 - \left( \frac{c \alpha}{\omega} \right)^2 - \frac{j 2 n c \alpha}{\omega} \quad (\text{B.5.0.11})$$

where  $\alpha$  is the absorption per unit length of path.

Following Mitra<sup>(76)</sup> by equating real and imaginary parts of eqns (B.5.0.10) and (B.5.0.11) and substituting for  $\sigma$  from equation (B.5.0.9):

$$n^2 - \left( \frac{c \alpha}{\omega} \right)^2 = \epsilon = 1 - \frac{4 \pi N e^2}{m(\omega^2 + v^2)} \quad (\text{B.5.0.12})$$

$$\text{and } \frac{2 c \alpha n}{\omega} = \frac{4 \pi N e^2 v}{m \omega (\omega^2 + v^2)} \quad (\text{B.5.0.13})$$

If  $\alpha$ , the absorption, is small eqn. (B.5.0.12) can be written:

$$n^2 = 1 - \frac{4 \pi N e^2}{m(\omega^2 + v^2)} \quad (\text{B.5.0.14})$$

Thus only when the absorption may be neglected does  $n^2 = \epsilon$ .

From eqn (B.5.0.13):

$$\left( \frac{c \alpha}{\omega} \right)^2 = \left( \frac{2 \pi N e^2 v}{n m \omega (\omega^2 + v^2)} \right)^2 \quad (\text{B.5.0.15})$$

Adding eqns. (B.5.0.12) and (B.5.0.15):

$$n^2 = 1 - \frac{4 \pi N e^2}{m(\omega^2 + v^2)} + \left( \frac{2 \pi N e^2 v}{n m \omega (\omega^2 + v^2)} \right)^2 \quad (\text{B.5.0.16})$$

If  $v$  were to equal zero, i.e. if there were no collisions,  $n^2$  could equal zero for vertical incidence as required by equation (B.5.0.5) but owing to the presence of  $v$  in eqn. (B.5.0.16)  $n$  cannot become zero or negative but reaches a minimum value  $n_{\min}$ .

Therefore ~~there~~ cannot be total reflection of a vertical incidence wave. The ray theory has been used up to this point. In the ray theory there is no room for partial reflections: the wave will either be totally reflected or will penetrate the layer according as the frequency is below or above the critical frequency. Here, therefore, the ray theory breaks down and the wave theory must be invoked. The problem has been treated as being analogous to the crossing of potential barriers by fast particles in quantum mechanics<sup>(92)</sup> by Saha and Rai<sup>(93)</sup> for an isosceles-triangle profile and extended by Deb<sup>(94)</sup> to a parabolic profile such as a Chapman layer which has been shown in para B.1.1 to be the case near the maximum of the region. Deb<sup>(94)</sup> has determined the reflection coefficient near the critical frequency following Kemble's<sup>(95)</sup> analysis and found that:-

$$\text{Reflection coefficient, } R, = 1 - \frac{1}{1 + \exp.(-2Q)} \quad (\text{B.5.0.17})$$

$$\text{where } Q = \frac{4(\pi H/c)^{\frac{1}{2}} (f_c - f)}{f_c}$$

and H is the scale height  $= \frac{kT}{mg}$  as defined in (B.1.1.2)

When the frequency of the wave equals the critical frequency  $Q = 0$  and from eqn. (B.5.0.17) the reflection coefficient,  $R, = \frac{1}{2}$ .

R varies rapidly on either side of  $f_c$  tending to unity when  $f$  is less than  $f_c$  and zero when  $f$  is greater than  $f_c$ .

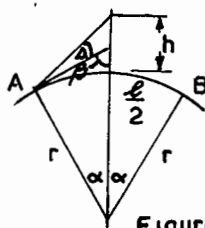
#### B.5.1 Wave arrival angle and its relation to distance over a curved earth.

If "virtual height" is taken to mean the height at which the refracted wave would have been reflected had the ionosphere behaved as a mirror, the "wave arrival angle" ( $\Delta$ ), (between the wave and the horizontal at the earth's surface), the virtual height ( $h$ ), the earth's radius ( $r$ ), and the great circle distance ( $l$ ), are related geometrically.

Terman<sup>(13)</sup> states, without proof, that:

$$\sin i = \frac{\cos \Delta}{1 + \frac{h}{r}} \quad (\text{B.5.1.1})$$

where  $i$  = angle of incidence, (i.e. angle between wave and the vertical) at height  $h$  in the ionosphere. (Terman<sup>(4)</sup> page 716 and <sup>(13)</sup> page 607 confuses the issue by referring to the complement of  $i$  as the "angle of incidence")



$$\begin{aligned} r &= 3960 \text{ miles} \\ &= 6370 \text{ km.} \end{aligned}$$

Figure B.5.1.1.



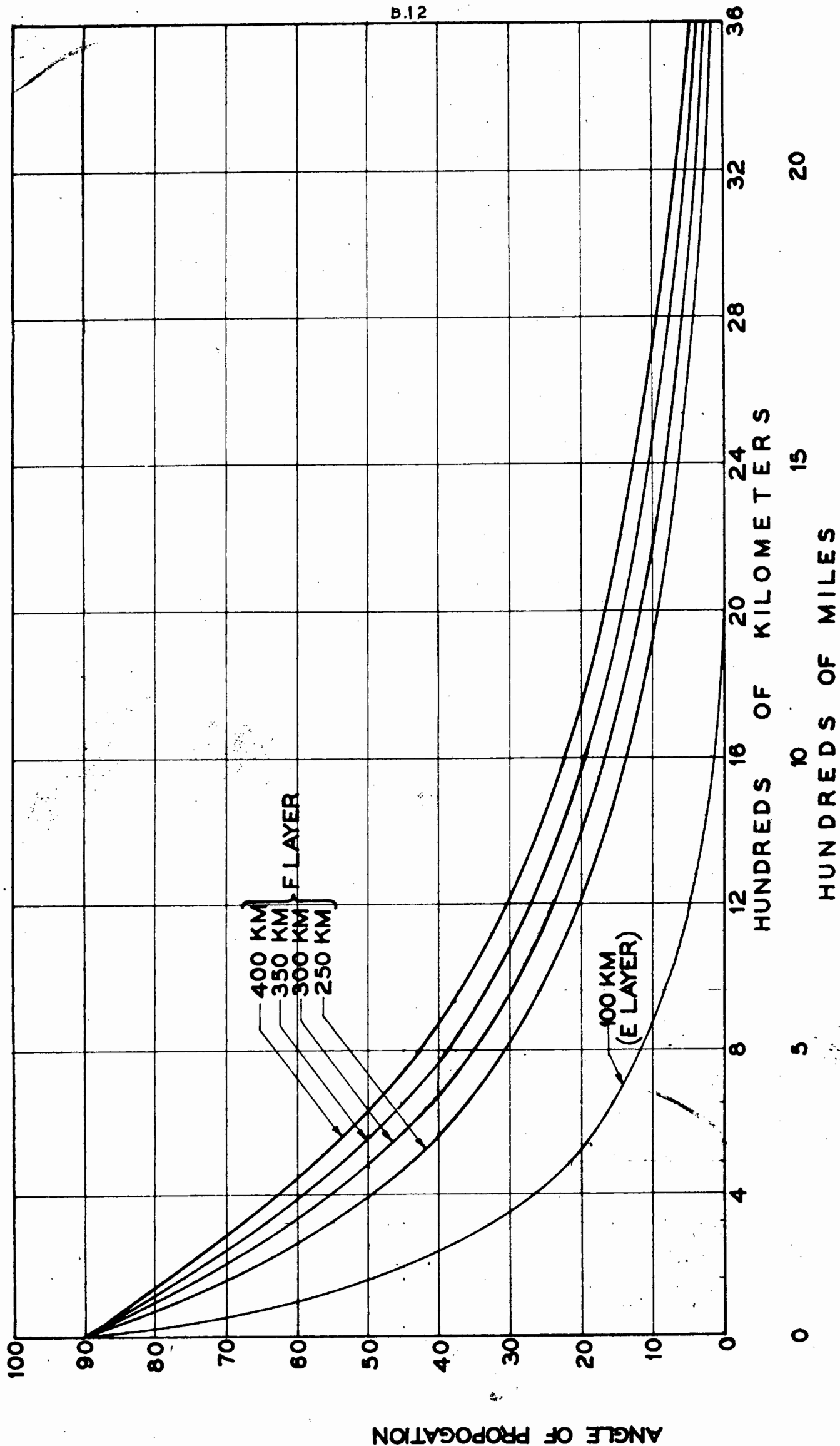


Figure B 5.1.2.

From B. 5.1.1 :

$$\beta = \Delta + i$$

$$\alpha = \frac{2\pi}{360} (90 - \Delta - i) \text{ radians if } \Delta \text{ and } i \text{ are in degrees.}$$

$$l = 2 r \alpha$$

$$= \frac{4\pi r}{360} (90 - \Delta - i) \quad (\text{B.5.1.2})$$

Terman's<sup>(13)</sup> equation B.5.1.1. is readily proved from Fig. B.5.1.1 as:

$$\sin\left(\frac{90 + \Delta}{r + h}\right) = \frac{\cos \Delta}{r + h} = \frac{\sin i}{r}$$

Therefore  $\sin i = \frac{\cos \Delta}{1 + \frac{h}{r}}$  as before.

Equations (B. 5.1.1) and (B. 5.1.2) combined are expressed graphically in Figure (F. B.5.1.2) giving " $\Delta$ " vs " $l$ " for various values of " $h$ ". For frequencies about  $0.85 \times \text{M.U.F.}$  the virtual height of reflection will be 300 - 400 km. The trajectory height will be approximately the height at which the value of  $N$  satisfies equation (B.5.0.3).

#### B. 5.2 The maximum distance for a single hop.

For  $\Delta = 0$  the maximum value of  $l$  (in Figure F. B.5.1.1) is 4400 km. (2740 miles) for  $h = 400$  km., and 3100 km. (1950 miles) for  $h = 200$  km. In practice ground absorption for values of  $\Delta$  less than  $5^\circ$  is prohibitive and Allcock<sup>(38)</sup> has shown recently in his observations on a North/South path (similar, in many respects, to the one at present under consideration) from Hawaii ( $20.8^\circ \text{ N}$ ,  $156.5^\circ \text{ W}$ ) transequatorially to Lower Hutt, New Zealand ( $41.2^\circ \text{ S}$ ,  $175.9^\circ \text{ E}$ ), that the practical limit of a single hop over this type of path is 3560 km. (2200 miles), the limit plotted in Figure B.5.1.2.

Observations by Shearman<sup>(39)</sup> and Allan<sup>(40)</sup> support this view.

#### B. 5.3 The great circle distance and bearing of London from Salisbury.

The spherical-trigonometrical formulae for these calculations vary considerably from text book to text book. One of the most popular versions is quoted in "Reference Data for Radio Engineers"<sup>(12)</sup> and these formulae appear to be based on Napier's Analogues. A preferred approach is to use spherical triangulation.<sup>(16)</sup>

$$\cos D_{AB} = \sin L_A \sin L_B + \cos L_A \cos L_B \cos IO_{AB} \quad (\text{B.5.3.1}).$$

where  $D_{AB}$  = great circle distance in degrees and minutes between points A and B. (1 minute = 1 nautical mile = 1.853 km.).  
= " $n$ " in Fig. B.5.3.1, measured in degrees and minutes.

$L_A, L_B$  = latitude of station A, B (positive for N and negative for S latitude).

$IO_{AB}$  = difference in longitude between A and B.

As a high order of accuracy is not necessary in this calculation the values for London are taken as  $52^{\circ}$  N,  $0^{\circ}$  and Salisbury as  $18^{\circ}$  S  $31^{\circ}$  E. giving:

$$D_{AB} = 75^{\circ}.$$

$$\text{Distance London/Salisbury} = 75 \times 69.09 = 5180 \text{ miles (8330 km) (B.5.3.2)}$$

The great circle bearing of London from Salisbury may be calculated from the following equation quoted by Williams<sup>(7)</sup> :-

$$\sin B_{AB} = \cos L_B \operatorname{cosec} D_{AB} \sin I_{OAB} \quad (\text{B.5.3.3})$$

where  $B_{AB}$  = the bearing of B from A.

Substitution in eqn. (B.5.5.3) gives:

$$\text{The bearing of London from Salisbury is } 19^{\circ} \text{ W of N.} \quad (\text{B.5.3.4}).$$

#### B.5.4 The number of hops Salisbury/London and wave arrival angle (vertical plane).

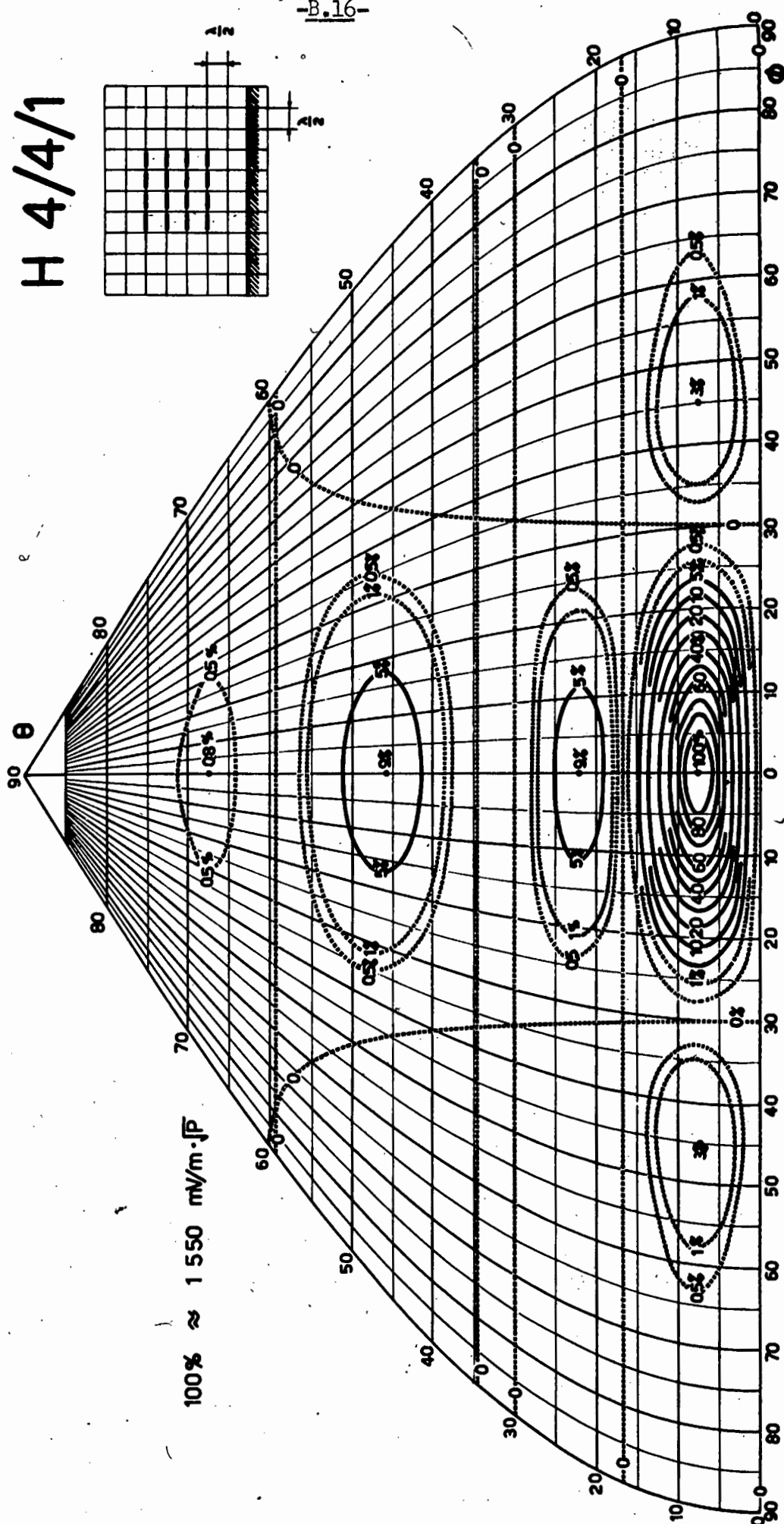
Referring to Figure (F B.5.1.2), bearing in mind the limitations imposed in sect. 2.5.2 on the distance of a single hop, it is clear that one hop of 5200 miles or two hops of 2600 miles each are out of the question and therefore the minimum number of hops is three where the average distance per hop will be about 1730 miles (2770 km).

The expected wave arrival angle, from Fig. (F B.5.1.2) is thus  $8^{\circ}$  with possible changes of  $\pm 2^{\circ}$  due to variations in virtual height.

It will be noted that the "average distance per hop" was referred to above. This is because the ionization gradient and the virtual layer height are not expected to be constant for the entire path length. It is well known that critical frequency and layer height vary, not only with the latitude, but also with the seasons. Summer in London corresponds with winter in Salisbury. Humby and Minnes<sup>(41)</sup> have shown that, on the London-Cape Town circuit in the period 1950-1954, the seasonal changes in performance on the outgoing and incoming circuits were exactly in opposition, the peaks occurring during local winter and the troughs during the local summer. We are concerned here not so much with performance, which is related to "in-time" and "out-time" of a circuit, as with the effect on  $\Delta$  of the "Maximum usable frequency" in any one hop. A radio wave of frequency  $f_1$  approaching the M.U.F. will penetrate the ionosphere to a much greater height than one of frequency  $f_2$  which is considerably less than M.U.F. The great circle distance travelled by  $F_1$  in a single reflection will be greater than that travelled by  $f_2$ . Thus, if the electron density, in, say, the  $F_2$  layer varies along the length of the path, causing the three heights  $h_1, h_2, h_3$  at which the reflections may be considered to take place, in the three hops, to be different, then the three hop distances  $l_1, l_2, l_3$  will be different and will vary according to the time of the year.

H 4/4/1

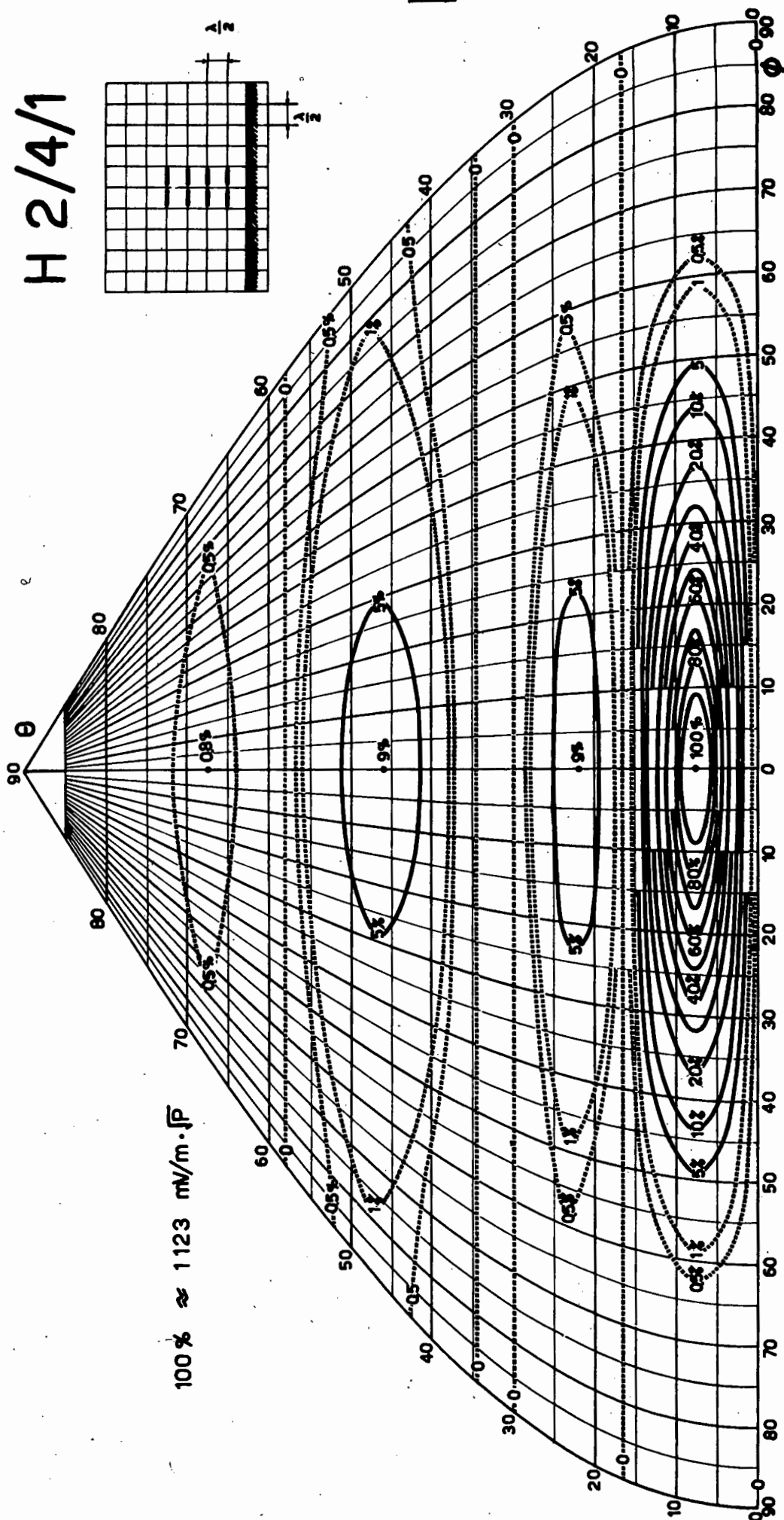
-B.16-



Power density diagram of Koomans H 4/4/1 Array.  
Reproduced from "Antenna Diagrams" (C.C.I.R.)<sup>(11)</sup>

Figure B 5.4.1.

H 2/4/1



Power density diagram of Koomans H 2/4/1 Array.

Reproduced from "Antenna Diagrams" (C.C.I.R.)<sup>(11)</sup>

Figure B 5.4.2.

Fortunately, as will be seen from Figure (B. 5.1.2) large variations in  $h$  and  $l$  will only cause small variations in  $\Delta$  at distances of about 2800 km. and the value of  $\Delta = 8^\circ \pm 2^\circ$  is expected to be fairly constant regardless of time of day, time of year, or even position in the 11 year sunspot cycle provided  $f$  is always not far below the M.U.F. of the path.

A cabled enquiry to the B.B.C., London, elicited the information that their 21.47 Mc/s transmitter, beamed on Central Africa at that time was feeding a Koomans H/4/4/1 array. Power density diagrams of an H/4/4/1 design and an H/2/4/1 design, reproduced from C.C.I.R. Antenna Diagrams<sup>(11)</sup>, are given in figures B.5.4.1/2. Both designs will produce a similar shape of vertical polar diagram with the lobe maximum occurring at  $\Delta = 8^\circ$ . The difference in gain is due to the difference in horizontal polar diagram. Although insufficient is known at present to be able to claim that, because most of the energy is launched at  $\Delta = 8^\circ$  it will therefore also arrive at  $\Delta = 8^\circ$ , it is clear that two independent calculations have led to the same conclusion, namely, that for this path there will be maximum energy transfer from transmitter to receiver if the transmitting and receiving antennas are designed for their lobe maxima to be at  $\Delta = 8^\circ$ .

#### B.5.5 The expected wave arrival angle (horizontal plane).

As calculated in section B.3, the receiving antenna in Salisbury should point in the direction  $19^\circ$  W of N.

However, Allcock,<sup>(38)</sup> in his observations on the Hawaii - New Zealand circuit, (a transequatorial path similar to the one under discussion), referred to in B.5.2, made some observations on the bearing angle, using a rotating interferometer developed by Whale<sup>(42)</sup> and found that the signal deviated horizontally by a maximum of  $3^\circ$  from the expected direction. As the layers are dependent, for their electron density, on ionizing radiation from the sun, it would be expected that in the morning, shortly before the M.U.F. on the great circle path rose to that value which would support transmission of the required frequency, the M.U.F. on a path slightly to the East of the great circle path would be able to support such transmission thus causing the observed deviation. Similar slight lateral deviations may be expected in the London-Salisbury circuit but as soon as the great circle path will support the transmission, the deviation should cease. The lateral deviation is thus not expected to present a problem.

#### B. 6.0 PATH LOSSES AND WAVE POLARIZATION.

##### B. 6.1 Losses at reflection points.

For the three-hop path referred to in B.5.4, the first ground reflection will occur in the Sahara desert, at roughly  $10^\circ$  E,  $28^\circ$  N.

The second ground reflection will occur in Equatorial Africa at roughly  $20^\circ$  E,  $5^\circ$  N.

In the desert the ground constants, quoting Starr,<sup>(8)</sup> are expected to be  $\epsilon_r = 10$  and  $\sigma = 2 \times 10^{-3}$  mho/metre, whilst in the jungle country of Equatorial Africa they are expected to be  $\epsilon_r = 14$ ,  $\sigma = 10^{-2}$  mho/metre. The ground-level angle of incidence  $= 90 - \Delta = 82^\circ$ .

Substituting these values in Appendix A equations 7.14 and 7.15, the reflection co-efficient may be calculated. Alternatively, convenient curves produced by Burrows<sup>(43)</sup> or McPetrie<sup>(44)</sup> may be used if  $\epsilon$  and  $\sigma$  are expressed in e.m.u.

Using either method the reflection coefficients for vertical and horizontal polarization are:

- (a) for the Sahara:  $R_v = .38$  (4.2db),  $R_H = .92$  (0.3 db).
- (b) for Equatorial Africa:  $R_v = .36$  (4.4 db),  $R_H = .93$  (0.3 db).

These figures are in respect of plane waves.

Day and Trolese<sup>(45)</sup> in their measurements of propagation over desert terrain at frequencies ranging from 25 Mc/s to 24,000 Mc/s concluded that the terrain may be considered as a flat, reflecting surface provided that:

$$H \cos \theta \text{ is much less than unity} \quad (\text{B.6.1.1})$$

where  $H$  = height of irregularities in wavelengths and  $\theta$  = angle of incidence.

They quote Ford and Oliver<sup>(46)</sup> as finding from measurement that when:

$H \cos \theta = .2\lambda$  6 db is added to the reflection loss and that when  $H \cos \theta = .5\lambda$  the extra loss increases to 20 db. Though Day and Trolese<sup>(45)</sup> discuss this in broad terms the figures probably refer more to U.H.F. than the frequencies at present under consideration.

The C.R.P.L.<sup>(101)</sup> usually assume a loss of 4 db for ground reflections and 1 db for sea reflections.

#### B.6.2.0 Absorption in the ionosphere.

Since the first publication of the Appleton-Hartree magneto-ionic theory<sup>(47),(48),(49)</sup> the theory of dissipative attenuation in the ionosphere has been discussed by many. A brief summary of present knowledge on the subject follows:

If an electron, set in vibration by a passing radio wave, collides with a gas molecule, its kinetic energy is partly transferred to the heavy gas molecule and partly radiated in a random manner. The energy thus dissipated is absorbed from the passing radio wave. The dissipation of energy in this way depends on:

- (a) the gas pressure, (b) electron density ( $N$ ) and (c) the velocity imparted to the electron by the wave.

(a) decreases with height and, up to a point (b) increases with height. For a given frequency, therefore, the greatest attenuation is suffered in the relatively thin "D" region, described in B.3.1 where  $N \times v$  is a maximum ( $v$  = collisional frequency). Radio waves only penetrate this region (thus making long-distance H.F. communication possible) because the electron density in the D region is low. Occasionally D ionization increases to an unusual degree due to solar radiation and results in a complete blackout of sky wave transmissions. This effect is sometimes referred to as the "Dellinger effect" described in more detail in section B.6.2.10.3.1.1. (c), the velocity imparted to an electron, depends (1) on the frequency of the wave, (being inversely proportional to frequency), and (2) on the earth's magnetic field, the action of which causes the electron movement to follow an elliptical path at high frequencies, a close-spaced spiral at low frequencies, and, at a certain resonance frequency called the "gyro-magnetic frequency", to follow an ever-increasing resonant spiral in which electron velocity is very large and attenuation correspondingly heavy.

This resonant frequency( $f_1$ ) is given as:

$$f_1 = \frac{B e}{2 \pi m} \quad (\text{B.6.2.0.1}).$$

where B is the earth's magnetic field, e = charge of particle, m = mass of particle.

Taking  $B = .5 \times 10^{-4}$  webers/sq m,  $e/m = 1.77 \times 10^{11}$  coulombs/kg for electrons,  $e/m = 10^8$  for hydrogen ions.

$f_1 = 1.4$  Mc/s for electrons,  $f_1 = 800$  c/s for hydrogen ions. Therefore only the electrons need be considered. The earth's magnetic field is responsible for the elliptical polarization associated with waves emerging from the ionosphere. It was also proposed by Nichols and Shelling<sup>(50)</sup> and Appleton<sup>(47)</sup> that it is responsible for the splitting of the wave into two components termed the "ordinary" and the "extraordinary" rays, "which follow different paths, have different phase velocities and suffer different attenuations".

The writer, while carrying out investigations in this connection at the War Office School of Signals, Catterick, in 1943/44, observed a consistent difference of about .6 Mc/s in the critical frequencies of the two rays when the critical frequency ( $f_c$ ) was approximately 4 Mc/s.

Terman<sup>(13)</sup> relates the two by the equation:

$$f_{cx}^2 = f_{co}^2 (f_{co}^2 + f_1^2) : \quad (\text{B.6.2.2})$$

where  $f_{co}$  and  $f_{cx}$  are the critical frequencies of the ordinary and the extraordinary rays and  $f_1$  is the gyro-magnetic frequency.



The absorption is defined as follows:

The relation between the field strength  $E$  of a wave after passing a distance  $l$  through the ionized medium, to the field strength  $E_n$  which would have obtained with no absorptions is:

$$E/E_n = \exp.(- \int \alpha dl) : \quad (B. 6.2.0.1)$$

$\int \alpha dl$  is, therefore, the absorption (expressed in nepers) suffered by the wave in the distance  $dl$  and  $8.68 \alpha dl$  will be the absorption expressed in db.  $\alpha$  varies along the path.

It is convenient to distinguish between "non-deviative absorption" which occurs at the lower levels of the ionosphere where ( $n$ , the refractive index, being approximately unity the deviation of the wave is negligible) and "deviative absorption" which occurs near the top of the trajectory where the absorption will be controlled mainly by  $n$  and will therefore be related to the amount of bending of the wave.

#### B.6.2.1. APPARENT OR VIRTUAL HEIGHT OF REFLECTION.

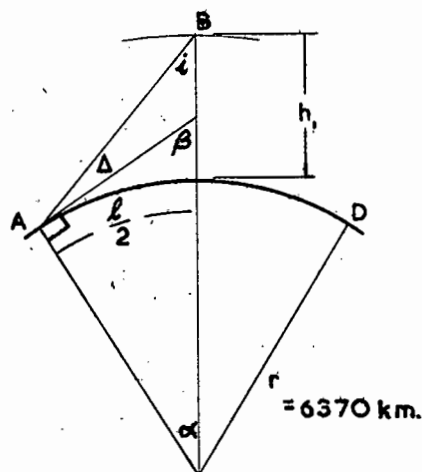


Fig. B.6.2.1.1

In calculating the wave arrival angle for a wave of frequency of the same order as the optimum frequency it was stated that the virtual height usually assumed for such conditions is about 350 km., the limits having been taken as 400 km. and 300 km. To the nearest degree  $\Delta$  was found to be  $8^\circ$  which actually corresponds to a virtual height of 360 km., as calculated below:-

In the case under consideration  $l = 2770$  km. (Sec sect.B.5.4).  
Therefore  $1385 = 6370 \alpha$  ( $\alpha$  in radians)

$$\text{and } \alpha = \frac{1385 \times 180}{6370 \times \pi} = 12.4 \text{ degrees.}$$

$$\beta = 90 - 12.4 = 77.6 \text{ degrees.}$$

$$\text{As } \Delta = 8 \text{ degrees (sect.B.5.4) } i = 77.6 - 8 = 69.6 \text{ degrees.}$$

$$\frac{6370 + h}{\sin 98} = \frac{6370}{\sin 69.6}$$

$$h_1 = 6370 \frac{\sin 82}{\sin 69.6} - 6370$$

$$= 360 \text{ km.}$$

B.6.2.2 The maximum height reached by the wave i.e. the height of the trajectory.

If it is assumed that the absorption per wavelength is small at the height of the trajectory equation B.5.0.12 simplifies to B.5.0.14 and from eqn. B.5.0.3 the refractive index,  $n$ , at the maximum height of the trajectory, must equal  $\sin i$  where  $i$  is the angle of incidence of the wave on the layer.

$$\text{Thus: } n = 1 - \frac{4\pi N e^2}{m(\omega^2 + \nu^2)} = \sin i. \quad \text{B.6.2.2.1}$$

Millington<sup>(97)</sup> has shown that when the earth cannot be assumed flat, i.e. for wave arrival angles which are small such as the long-distance transmission path considered here, the simple version of Snell's law requires modification. For convenience the law, quoted in B.5.0.2, is re-stated as follows: if the wave is incident on the under boundary of the layer at an angle " $i$ " then at any point  $x$ , in the layer where the refractive index is  $n_x$ , the angle between the wave and the vertical  $\theta_x$ , is governed by the equation:

$$n_x \sin \theta_x = \sin i.$$

For a curved earth of radius  $r$ , Millington<sup>(97)</sup> maintains the law should be written thus:

$$n_x (r + h_x) \sin \theta_x = (r + h) \sin i = r \cos \Delta. \quad (\text{B.6.2.2.2})$$

where  $h_x$  is the height of pt.  $x$  and  $h$  the height of the layer under-boundary above the earth and  $\Delta$  is the wave arrival angle. He goes on to indicate that the height of the trajectory where the wave becomes horizontal is therefore no longer given by  $n_x = \sin i$ , but depends somewhat upon the way  $n$ , (and hence  $M$ ) varies with height and, among other things, will vary with the time of the day. This undermines the important theorems of Martyn<sup>(65)</sup> and Breit and Tuve<sup>(98)</sup> and means that they require modification for long-distance application. The modification is difficult to apply. The value of  $n_x$  at the point where the wave becomes horizontal, instead of defining the height of the trajectory, is itself a function of that height:

$$n_x = \frac{r + h}{r + h_x} \sin i.$$

Furthermore, the height  $h$  of the under-boundary of the layer, and the corresponding value of  $i$ , are not easy to decide upon. It is submitted that probably the best solution, in practice, is to apply eqn. B.5.0.6 to the values of the optimum frequencies, quoted for the required month and required time of day in the frequency prediction charts, for zero distance and for the required range (in this case 2770 km).

Since  $f_{\text{optimum}} = .85 f_{\text{ci}}$  it will be seen from equation B.5.0.6 that  $f_{\text{optimum for 2770 km}} / f_{\text{optimum for zero distance}} = \sec i$  (B.6.2.2.3).

This will yield a sound practical value for  $i$  which, when used in equation B.5.0.3 and equation D.5.0.14, should lead to a result which has taken into account some of the errors at least.

The noon values at the Equator for September 1956 for the optimum frequencies for zero distance and 2770 km distance as given by the Radio Propagation Predictions<sup>(99)</sup> are 11.3 Mc/s and 29.0 Mc/s respectively, giving, from eqn D.6.2.2.3,

$$i = 67^\circ$$

Substitution in eqn D.6.2.2.1. gives:

$$.9205 = \left( 1 - \frac{81 N_0}{(21.47 \times 10^3)^2 + (0.5/2\pi)^2} \right)^{\frac{1}{2}}$$

from which

$$N_0 = 8.7 \times 10^5 \text{ electrons/cm}^3$$

This, from Fig. F.D.4.0.1, occurs at height 255 km.

Height of trajectory = 255 km.

#### D.6.2.3 Values of gyro-magnetic frequency. ( $f_1$ )

Referring to the three hop transmission path deduced in para 2.5.4 it was stated in para D.6.1 that the two reflection points will be approximately at ( $10^\circ$  E,  $28^\circ$  N) and ( $20^\circ$  E,  $5^\circ$  N). The mid-points  $A_1$ ,  $A_2$ ,  $A_3$  of the three hops are the ionosphere control points and are approximately at ( $6^\circ$  E,  $40^\circ$  N), and ( $16^\circ$  E,  $16^\circ$  N) and ( $26^\circ$  E,  $6^\circ$  S) respectively. The longitudinal component  $f_1$  of the gyro-magnetic frequency deduced in section D.6.2.9. is quoted in table below:

Locality	Function	Long. degrees.	Lat. degrees.	Longitudinal component ( $f_1$ ) of gyro-frequency (Mc/s)
London	Terminal.	0	52 N	0.67
Mediterranean (near Sardinia)	Contr.pt.3	6 E	40 N	
Libya(desert)	Refl.pt.	10 E	28 N	
near Lake Chad	Contr.Pt.2	16 E	16 N	0.79
Fr.Eq.Africa/Congo border near Mobaye.	Refl.pt.	20 E	5 N	
Belg.Congo(Kongelo)	Contr. pt.1	26 E	6 S	0.78
Salisbury.	Terminal.	31 E	18 S	

Table T.D.6.2.3.1.

#### D.6.2.4 Non-deviative absorption(from first principles).

In B.5.0 expressions were derived, neglecting the earth's field but taking collisions into account, for  $n$  and  $\frac{c}{\omega}$ . It was shown in eqn D.5.0.9 that in the circuit being considered the earth's field has negligible effect on  $n$  as the wave frequency (21.47 Mc/s) is much larger than the gyro-frequency, (0.67 Mc/s, 0.79 Mc/s and 0.78 Mc/s at the three control points).

Eqn. B.5.0.15, rearranged gives:

$$\alpha = \frac{2 \pi e^2 N v}{c n m (\omega^2 + v^2)} \quad : \quad \text{B.6.2.4.1}$$

where  $\alpha$  = absorption coefficient (nepers/cm if units used are in e.s.u.'s).

$$\begin{aligned} e &= \text{electron charge} = 1.59 \times 10^{-19} \text{ coulombs.} \\ &= 4.77 \times 10^{-10} \text{ e.s.u.} \\ &= 1.59 \times 10^{-20} \text{ e.m.u.} \end{aligned}$$

$$m = \text{electron mass} = 9.1 \times 10^{-28} \text{ grams.}$$

$$c = \text{velocity of light in vacuo} = 3 \times 10^{10} \text{ cm/sec.}$$

$$v = \text{collisions per sec.}$$

$$\omega = \text{angular frequency of wave} = 2 \pi f.$$

$$f = \text{in c/s.}$$

Though the magnetic field, in the circumstances, does not affect  $n$  it does affect  $\alpha$  and Piggott<sup>(56)</sup> following the magneto-ionic theory, proposes that eqn. B.6.2.4.1 be modified to give:

$$\alpha = \frac{2 \pi e^2}{m c} \frac{1}{n} \frac{N v}{v^2 + (\omega \pm \omega_1)^2} \quad : \quad \text{B.6.2.4.2}$$

where  $\omega_1$  is the angular gyro-frequency and the positive and negative signs are in respect of the ordinary and extraordinary rays respectively.

In the non-deviating region  $n = 1$  (approx) and therefore the total non-deviative absorption is given by:

$$\int \alpha \, dl = \frac{2 \pi e^2}{m c} \int_0^1 \frac{N v \, dl}{v^2 + (\omega \pm \omega_1)^2} \quad : \quad \text{B.6.2.4.3}$$

As is strikingly brought out in the curve for  $(N v)$  vs. height in fig. B.4.0.1 the noon non-deviative absorption is heavy between 70 and 110 km on normal days. Below 70 km it is usually zero because  $N$  is usually zero and above 110 km it is very small because of the small number of collisions/sec.

Appleton<sup>(57)</sup> has proposed a modification of eqn. B.6.2.4.3 on the assumption that the ionization is a simple Chapman layer (see B.1.1) formed in an atmosphere whose density is decreasing exponentially upwards and assuming that  $v$  is negligible compared with  $(\omega \pm \omega_1)$ . Appleton's<sup>(57)</sup> equation for non-deviative absorption in a layer is

$$\int \alpha \, dl = 4.13 \left( \frac{4 \pi e^2}{m c} \right) \frac{N_0 v_0 H}{(\omega \pm \omega_1)^2} (\cos X)^{1.5} \quad \text{B.6.2.4.4}$$

where  $N_0$  and  $v_0$  are the values of  $N$  and  $v$  at the height of the layer maximum when  $\cos x = 1$ .  $H$  is the scale height of the atmosphere for the region (see eqn B.1.1.2). The assumption made by Appleton<sup>(57)</sup> in eqn. B.6.2.4.4 was that the atmospheric density would decrease exponentially with height, the collisions between the electrons in the Chapman<sup>(51)</sup> layer with the gas particles causing the non-deviative absorption.  $X$  is the solar zenith angle.

An engineering application of eqn. B.6.2.4.4 would be to calculate  $\alpha$  for each of the Chapman layers, D, E and F but the value for H is elusive.

The value of H is dependent upon T. Koll and La Gow<sup>(61)</sup> claim that T increases with height above 85 km. Whipple<sup>(62)</sup>, in his studies of the deceleration of meteors, and Paton<sup>(63)</sup>, in<sup>(59)</sup> observations of extremely high clouds, confirm this view. Allcock assumes that the scale height (H) calculated from rocket data, increases almost linearly from a value of 6 km at an altitude of 85 km to 10 km at an altitude of 125 km and Nicolet<sup>(64)</sup> agrees that this is a reasonable assumption.

Martyn<sup>(86)</sup> postulates that T at 160 km = 560° K and quotes Schelling and Sterne's<sup>(96)</sup> report obtained from I G Y satellite data in 1958 that T at 300 km is about 1400° K. Thus Martyn<sup>(86)</sup> has calculated  $H = .039 T \text{ (km) at } 300 \text{ km} = 55 \text{ km (F}_2\text{)}$

and  $H = .037 T \text{ (km) at } 160 \text{ km} = 21 \text{ km (F}_1\text{)}$

However, the calculation of  $\alpha$  from eqn. B.6.2.4.4 is considered to be too approximate to be of much use.

Later work by Piggott<sup>(56)</sup> has taken into account more complex ionization equilibrium conditions and he has proposed that the absorption should be expressed as follows:

$$\int_0^1 \alpha \, dl = B \cos^x X \quad : \quad \text{B.6.2.4.5}$$

where B is a constant for a particular length of path, l, and x is quoted by Piggott<sup>(56)</sup> and Allcock<sup>(59)</sup> as averaging about .75. It will be recalled that in section B.3.3 the value of x was shown to be 0.5 for the F<sub>1</sub> region and 1.0 for the F<sub>2</sub> region as regards electron density and, assuming that the value of x has negligible effect on v, it would be expected that the value of x for waves suffering absorption in the D, E and F<sub>1</sub> regions would be .5 and that for waves suffering attenuation in the F<sub>2</sub> region it would be 1.0.

It is proposed to find the values of B for the ordinary ray at the three control points for X = 0 and then to deduce the absorption for other values of X.

The classical method of calculating the non-deviative absorption of a wave incident at an angle i at the lower boundary of the ionosphere (note the remarks in section B.6.2.2 concerning the complication introduced by earth curvature at long distances) is to invoke Martyn's<sup>(65)</sup> theorem which states that if the frequency of the oblique incidence wave is f then the absorption of this wave is equal to cos i of the absorption of a vertical incidence wave of frequency equal to (f cos i), so that

$$\alpha(f, i) = \cos i \alpha(f \cos i, 0) \quad : \quad \text{B.6.2.4.6}$$

In section B.6.2.2 the value of  $i$ , inferred from frequency prediction charts, is taken as  $67^\circ$  for noon at the equator in September, 1956. Therefore:

Oblique incidence frequency = 21.47 Mc/s

Equivalent vertical incidence freq. =  $f \cos i$

= 8.39 Mc/s.

Absorption at the Southern control point C.P.I. ( $26^\circ$  E,  $6^\circ$  S).

Conditions assumed: noon, September 1956.

Zenith angle ( $X$ ) at equator = zero; at C.P.I.,  $X = 6^\circ$ .

The absorption equation B.6.2.4.3 becomes:

$$f \alpha \, dl = \frac{2 \pi e^2 (\cos X)^{.75}}{m c} \int_0^1 \frac{N v \, dl}{v^2 + (\omega + \omega_1)^2} : \text{B.6.2.4.7.}$$

The values of  $N v$  and  $v$  for various heights are taken from fig. F.B.4.0.1 and the value of  $\omega_1 (= 2 \pi f_1)$ , in this case due to the vertical component of the earth's magnetic field at C.P.I.,  $= 2 \pi F_H \sin \alpha$  (where  $\alpha$  is angle of dip), is given in Fig. F.B.6.2.9.1.

If the equivalent vertical incidence frequency is used then the absorption may be calculated assuming a vertical ascent through each 10 km thickness of the layer up to 255 km (the height of trajectory calculated in section B.6.2.3) taking the average value of  $N v$  and  $v$  for each 10 km thickness.

In equation B.6.2.4.7 c.s.u. units used throughout yield the the absorption in nepers.

$e = 4.77 \times 10^{-10}$  c.s.u.

$m = 9.1 \times 10^{-28}$  grams.

$c = 3 \times 10^{10}$  cm/sec.

$f =$  in c/s

$X = 6^\circ$  for C.P.I.

Therefore  $\alpha$  for each 10 km vertically =

$$5.216 \times 10^4 \left( \frac{N v}{v^2 + (\omega + \omega_1)^2} \right) : \quad \text{B.6.2.4.8}$$

where  $N v$ ,  $v$  are the average values for that particular 10 km,  $f_1$  from Fig. F.B.6.2.9.1 = .75 Mc/s.  $f = 8.39$  Mc/s and  $v^2$  is negligible compared with  $(\omega + \omega_1)^2$ . Therefore equation B.6.2.4.8 simplifies to:

$\alpha$  for each 10 km vertically =  $1.58 \times 10^{11} \times$  average  $N v$ .

70-80 km .24 nepers.

80-90 km .33 nepers

90-100 km .17 nepers ( $v^2$  negligible c.f.  $(\omega + \omega_1)^2$ )

100-110 km .13 nepers (,, ,, ,, ,)

110-120 km .05 nepers (,, ,, ,, ,)

120-255 km .11 nepers ( $N v$  constant) )

Total(70-255 km  
upgoing) 1.03 nepers.

The absorption for the downcoming wave is the same so that at C.P.1 the value for eqn. (B.6.2.4.7) = 2.06 nepers.

Applying Martyn's theorem, eqn. (B.6.2.4.6), the total non-deviative absorption for C.P.1 at noon, September 1956 =

$$2.06 \cos i = 0.81 \text{ nepers.}$$

Recently Beynon<sup>(60)</sup> and Allcock<sup>(59)</sup> have quoted measured results on long-distance circuits and they both indicate that Martyn's theorem<sup>(65)</sup> yields results which are too low. They maintain that there is only close correlation between calculations employing Martyn's theorem and measured results when the  $\cos i$  term is omitted from the absorption, i.e. the absorption for C.P.1 would be nearer 2.06 than 0.8 nepers. In view of this doubt the absorption at C.P.1 will now be recalculated without applying Martyn's theorem to eqn. (B.6.2.4.7). Now for every 10 km ascended the distance travelled by the wave if incident at angle  $i$  will be  $10 \sec i$  km, where  $i$  for each layer is calculated from eqn. B.5.1.1. where:

$$\sin i = \cos \Delta / (1 + \frac{h}{r}) \quad \omega = 2\pi \times 21.47 \times 10^6$$

The other values are as before, except that  $f_1$  is the longitudinal component of the gyro-frequency = .78 Mc/s (See table T B.6.2.3.1).

For the upgoing wave the absorption per (sec  $i \times$  difference in height) from equation 2.6.2.4.7 is given by  $2.668 \times 10^{-12} N v \sec i$

70-80 km = .19 nepers ( $i$  at 75 km =  $78^\circ 6'$ )  
 80-90 km = .27 nepers ( $i$  at 85 km =  $77^\circ 54'$ )  
 90-100 km = .44 nepers ( $i$  at 95 km =  $77^\circ 20'$ )  
 100-110 km = .04 nepers ( $i$  at 105 km =  $77^\circ 0'$ )  
 110-120 km = .04 nepers ( $i$  at 115 km =  $76^\circ 39'$ )  
 120-255 km = .06 nepers ( $i$  at 190 km =  $71^\circ 30'$ )

Total: (60-255 km) = 0.74 nepers for upgoing wave.

$v$  is negligible compared with  $(\omega + \omega_1)^2$ .

The total non-deviative absorption for C.P. 1 is therefore 1.48 nepers (12.9 db) for noon, September 1956.

This is considered to be a more reliable figure than that obtained from Martyn's theorem.

Beynon<sup>(60)</sup> found that the measured absorption, in his experiments on a transatlantic path, was about three times the value calculated by Martyn's theorem<sup>(65)</sup>. Meadows<sup>(100)</sup> infers that the non-deviative absorption he measured between Slough and Inverness was about 2.5 times the value calculated by Martyn's theorem<sup>(65)</sup>. The ratio between the two results above  $1.48/0.81$  is 1.8.

Neither worker indicates how he chose the angle  $i$  for the calculation but it appears that it was taken as the angle of incidence at the virtual height of reflection. If this is the case it is probable that the method described above would have yielded a more realistic result, when applying Martyn's theorem<sup>(65)</sup>.

When the  $\cos i$  term in Martyn's theorem<sup>(65)</sup> is neglected the above results (  $2.06/1.48 = 1.4 / 1$  ) bear a similar relationship to one another as did Beynon's<sup>(60)</sup> calculated absorption (neglecting  $\cos i$  term) to measured absorption on a 14.59 Mc/s transatlantic path.

Allowing for the zenith angle of the sun (approx  $6^\circ$ ) the absorption at C.P.1 =  $1.48 \times (\cos 6) \cdot 75 = 1.48 \times .9959 = 1.48$  neper.

Absorption at the central control point, C.P.2. ( $16^\circ$  E,  $16^\circ$  N).

By taking into account the gyro frequency for C.P.2 as given in table T B.6.2.3.1 and making allowance for the fact that the zenith angle, when it is noon at the equator in September, 1956, is approximately  $22.5^\circ$ , giving a factor of  $(\cos 22.5) \cdot 75 = .9423$ , the total non-deviative absorption for C.P. 2, calculated as before (without invoking Martyn's theorem), is 1.39 neper.

Absorption at the northern control point C.P.3 ( $6^\circ$  E,  $40^\circ$  N).

Taking into account the gyro frequency and the zenith angle (about  $45^\circ$ ) for equator noon, September 1956, the total non-deviative absorption for C.P.3 is equal to  $1.48 \times 0.7781 = 1.15$  neper.

#### B.6.2.5 Deviative absorption (from first principles).

From eqn. B.6.2.4.2 the total attenuation is given by:

$$\int \alpha \, dl = \frac{2 \pi e^2}{n c} \int_0^1 \frac{1}{n} \frac{N v \, dl}{v^2 + (\omega \pm \omega_1)^2} : \text{B.3.2.5.1}$$

In the region where  $n$  is not unity but varies with  $N$ ,  $v$  and  $\omega$ , (approaching  $\sin i$  at the top of the trajectory for oblique incidence or zero for vertical incidence), the wave is continually bending and the absorption is referred to as the deviative absorption.

Imagine a wave transmitted vertically into the ionosphere. It travels into regions of increasing density and decreasing refractive index until the group velocity is reduced from a value equal to  $c$  before it enters the ionized region (where  $n = 1$ ), to zero at the reflection point, (where  $n = 0$ ). It then returns to earth.

A difficulty with equation B.6.2.5.1 is that if  $n$  becomes zero at the highest point reached by a wave incident vertically on the ionosphere (as required by eqn. B.5.0.4) the absorption must be infinite at that point and very high for those parts of the region where  $n$  is very small. When this difficulty was put to Sir Edward Appleton in a letter<sup>(174)</sup> he replied<sup>(175)</sup> to this effect:

"The answer to your point is that, although the absorption coefficient may become infinite, the path length over which this obtains is vanishingly small. So the overall absorption can be finite".



It will also be recalled that in equation B.5.0.16 and the discussion that follows it in section B.5.0) due to collisions,  $n$  cannot equal zero and, by changing from the ray theory, it was shown that for vertical incidence at the critical frequency the wave is only partially reflected, the reflection coefficient, from eqn. (B.5.0.17), being  $\frac{1}{2}$ .

From eqn. B.6.2.5.1 the absorption, in the deviating region is proportional to  $\frac{1}{n}$ . If a wave, projected into the ionosphere, takes  $t$  seconds to return then, regardless of what the actual group path may be, the equivalent path ( $P^1$ ) is equal to the distance  $c t$  metres that it would travel in vacuum.

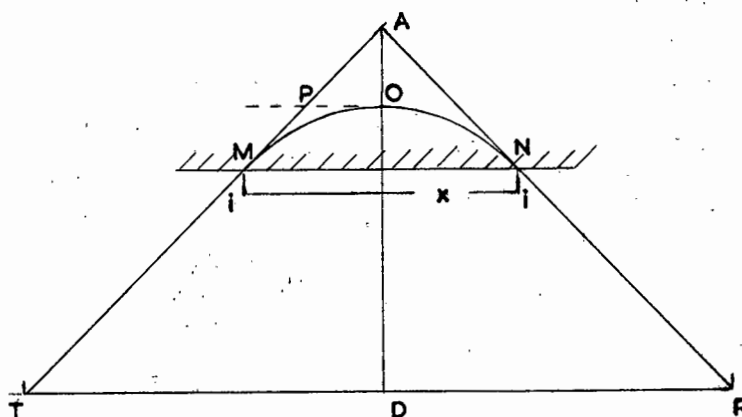


Fig. F. B.6.2.5.1.

Required next is the relationship between group path  $P$  (  $T O R$  in fig. F.B.6.2.5.1 ) and the equivalent path  $P^1$  which the wave would travel in vacuo in the same time as it took to travel  $P$ .

The velocity  $V$  of the group varies from  $c$  at  $M$  to  $c \sin i$  at  $O$ . Considering only the path in the ionosphere, the total time taken ( $t$ ) from  $M$  to  $N$  is given by:-

$$t = \int_{MON} \frac{dl}{v} \quad : \quad \text{B.6.2.5.3}$$

But if  $U$  is the phase velocity and  $n$  the refractive index,

$$V U = c^2, V = c n \text{ and } U = c/n.$$

$$\text{Therefore } t = \frac{1}{c} \int_{MON} \frac{dl}{n} \quad : \quad \text{B.6.2.5.4}$$

Assume the angle between direction of propagation and the vertical at any point on group path,  $\theta$ , and that the refractive index at that point is  $n_\theta$ . If  $dl$  is an element of path length then  $dx$ , the horizontal component of  $dl$ , is given by  $dx = dl \sin \theta$ .

$$\text{By Snell's Law }^{(13)} \quad n_\theta \sin \theta = \sin i$$

$$\text{hence } t = \frac{1}{c} \int_{MON} \frac{dl}{n_\theta} = \frac{1}{c} \int_0^x \frac{dx}{n_\theta \sin \theta} = \frac{1}{c} \int_0^x \frac{dx}{\sin i}$$

$$= \frac{1}{c} \left( \frac{x}{\sin i} \right) = \frac{1}{c} (\text{length } MAN) \quad : \quad \text{B.6.2.5.5}$$

i.e. the path T A R is the equivalent or effective path ( $P^1$ ) because a wave would take the same time to traverse path T A R in vacuo as it would take to traverse the path T O R in the ionized layer. This relationship was first suggested in the theorem of Breit and Tuve<sup>(98)</sup>.

The effect of this on eqn. B.6.2.5.1 is that due to the group retardation suffered at the top of the trajectory, the non-deviative absorption (calculated in section B.6.2.4 for the straight path T M P must have added to it a further term for the path length P A where  $N_v$  and  $v$  are those corresponding to the height D O (255 km). D A, as calculated in B.6.2.1 is 360 km. Taking into account the earth's curvature then, from the relationship  $\sin i = \cos \Delta / (1 + \frac{h}{r})$  (derived in section B.5.1); taking  $r$ , the radius of the earth, as 6370 km,  $i$  at 255 km = 72.2 degrees and  $i$  at 369 km = 69.6 degrees. It is sufficiently accurate, in this case, to use the average value of  $i = 70.9$  degrees.

Then the extra absorption due to the bending, over and above that calculated for the path T P, is given by:

$$\int \Delta dl = \frac{2 \pi e^2}{m c} \frac{N_o v_o 2x(\text{length OA}) \sec 70.9 (\cos X)}{v^2 + (\omega + \omega_1)^2} \quad \text{B.6.2.5.6.}$$

where the additional factor of 2 takes account of ascent and descent and  $X$  is the zenith angle of the sun at the control point. (The .75 index has been omitted for the reasons given in section B.3.3, as this is well up in the  $F_2$  region now.  $N_o v_o$  are the values at 255 km).

The extra absorption due to bending is

- .09 nepers at C P 1
- .09 nepers at C P 2
- .07 nepers at C P 3

Control Point.	Long.	Lat.	Absorption.		
			Non-deviative	Deviative	Total
C.P. 1	26 E	6 S	1.48	.09	1.57
C.F. 2	16 E	16 N	1.39	.09	1.48
C.P. 3	6 E	40 N	1.15	.07	1.22
Totals			4.02	.25	4.27

1 neper = 8.686 db.

Total path Absorption in ionosphere = 37.2 db.

B.6.2.6 Spatial attenuation.

In free space, the field strength at a distance  $r$  from a certain point at unit distance from the transmitter is equal to  $1/r$  of the field strength at that point.

Thus, given the field strength at 1 km., the attenuation ( $A_s$ ) introduced by spreading, which is additional to the attenuation discussed so far, is given by the relationship:

$$A_s = 20 \log \frac{E_1}{E_r} \quad : \quad \text{B.6.2.6.1}$$

where  $E_1$  and  $E_r$  represent the field strength at 1 km. and  $r$  km. from the transmitter, respectively. But  $E_r = E_1/r$ . Therefore  $E_r$  is  $20 \log r$  db less than  $E_1$ .

Referring to figure F.B.6.2.1.1 and assuming that the wave travels straight to the virtual height of reflection, the distance travelled per hop =  $2 (A B)$

$$\frac{A B}{\sin 12.4^\circ} = \frac{6370}{\sin 69.6^\circ}$$

Therefore  $A B = 1460$

Distance per hop is 2920 km.

Total distance (3 hops) = 8760 km.

The spatial attenuation is therefore:

$$20 \log 8760 = 78.9 \text{ db.}$$

From eqn. (11.19) in Appendix A,  $\frac{E_1 r}{\sqrt{P}} = 222 \text{ mV/m}$

for a dipole, where  $P$  is the radiated power in kilowatts.

In the case under consideration  $P = 100$  kilowatts. If this were radiated from a dipole  $E_1$  would be 2220 mV/m at 1 km. distance. The transmitting antenna is of the design (see section B.5.4) Kocmans H4/4/1. From the design data contained in Figure F.B.5.4.1 the signal gain, over a dipole, is calculated to be : 6.98, i.e. 16.88 db. at an angle of  $8^\circ$  to the horizontal i.e. in the maximum-radiation direction. Thus for the H 4/4/1 transmitting aerial  $E_1 = 15,500 \text{ mV/m}$  or 143.8 db above  $1 \mu \text{ V/m}$ .

For comparative purposes it is useful to express  $E_1$  for a dipole in space radiating 1 kilowatt. Here  $E_1 = 222 \text{ mV/m} = 106.9 \text{ db above } 1 \mu \text{ V/metre.}$

Gain due to  $P = 100 \text{ kw.} = 20.0 \text{ db.}$

Gain due to transmitting aerial directivity at  $8^\circ = 16.9 \text{ db.}$

### B.6.2.7 Polarization and phasing loss.

Part of the radiated energy is transmitted by the ordinary wave and part by the extraordinary wave. The latter is much more heavily absorbed than the former and they will be usually out of phase at the receiver (see eqn B.6.2.4.2. for example) with the result, according to Piggott<sup>(56)</sup> that, on a circuit, such as is being considered here, the combined amplitude at the receiver will be almost identical with the mean amplitude of the ordinary ray. On a circuit such as this it may be assumed that the wave emerging from the ionosphere is circularly polarized. As the receiving antenna is usually plane polarized the C.R.P.L.<sup>(101)</sup> allowance for polarization loss is 3 db and they also make an allowance for a further 1.6 db loss for destructive interference between the ordinary and extraordinary rays, giving a total polarization loss of 4.6 db.

### B.6.2.8 Estimated received field strength (from first principles).

- (a) Ground reflection losses at two reflection points ( $10^{\circ}$  E,  $28^{\circ}$  N) and ( $20^{\circ}$  E,  $5^{\circ}$  N) (see section B.6.1) = - 8.6 db.
- (b) Deviative and non-deviative absorption for the three control points ( $26^{\circ}$  E,  $6^{\circ}$  S), ( $16^{\circ}$  E,  $16^{\circ}$  N) and ( $6^{\circ}$  E,  $40^{\circ}$  N) (see sect. B.6.2.4/5) = - 37.2 db.
- (c) Polarization and phasing loss = - 4.6 db.
- (d) Spatial attenuation in travelling from a point 1 km. from transmitter to a point 8760 km. from transmitter (See Sect B.6.2.6). - 78.9 db.
- (e) Signal strength at 1 km. from transmitter radiating 1 kw from half wave dipole + 106.9 above  $1 \mu$  V/m. (See sect. B.6.2.6).
- (f) Power gain when 100 kw radiated instead of 1 kw assumed in (e) = + 20.0 db.
- (g) Directivity gain of transmitting aerial relative to half wave dipole in free space = + 16.9 db

Estimated signal strength at receiver = 14.5 db above  $1 \mu$  V/m.

Unfortunately this "first principles" calculation, instructive though it is, may be unreliable because (a) small errors in the assumed values of N lead to large changes in the values of Nv in the lower levels of the ionosphere and (b) the simple spreading assumed in calculating spatial attenuation is not likely to apply over a curved earth. Therefore empirical data, based on measurements, will now be used as a check.

### B.6.2.9.0 Estimation of received field strength from empirical data.

Recently (1959) Piggott<sup>(102)</sup> produced a method of estimating path loss which is based on measured results.

In correspondence with the writer, Piggott<sup>(176)</sup> has commented on the calculations contained in section B. 6.2.4 as follows:-

"In effect your numerical integration, if turned into decibels for the fictitious frequencies at which  $(\omega + \omega_1) = 2 \pi \text{ Mc/s}$ , is identical with my  $\alpha_2$  in the report".<sup>(102)</sup><sup>(176)</sup>

Piggott's method neglects deviative absorption at oblique incidence if  $f$  is much greater than  $f_0 E$ . In his letter Piggott<sup>(176)</sup> explains: "In general the only significant absorption on oblique incidence trajectory is that due to the non-deviative absorption in the E and D layers, and, in some cases, due to deviative absorption in passing through the E layer if the working frequency is not well above the E cut-off frequency". From the calculations in sections B. 6.2.4 and B. 6.2.5 it will be observed that the deviative absorption on this path is estimated as about 6% of the non-deviative absorption and is therefore apparently not negligible.

From the measured results collated by Piggott<sup>(102)</sup> and figures F B. 6.2.9.1/5 reproduced from his book<sup>(102)</sup>, it is possible to compute the expected field strength corresponding to a given set of circumstances. Applied to the present problem, figure F B. 6.2.9.1, the equatorial declination (shown on the left) indicates that the path of propagation is nearly in the same direction as the horizontal component of the earth's field and the difference may be neglected. The curves (shown on the right) for angle of dip and  $F_H$  (Mc/s) indicate that at control points 1, 2 and 3 the dip and gyrofrequency are as shown in the table below:

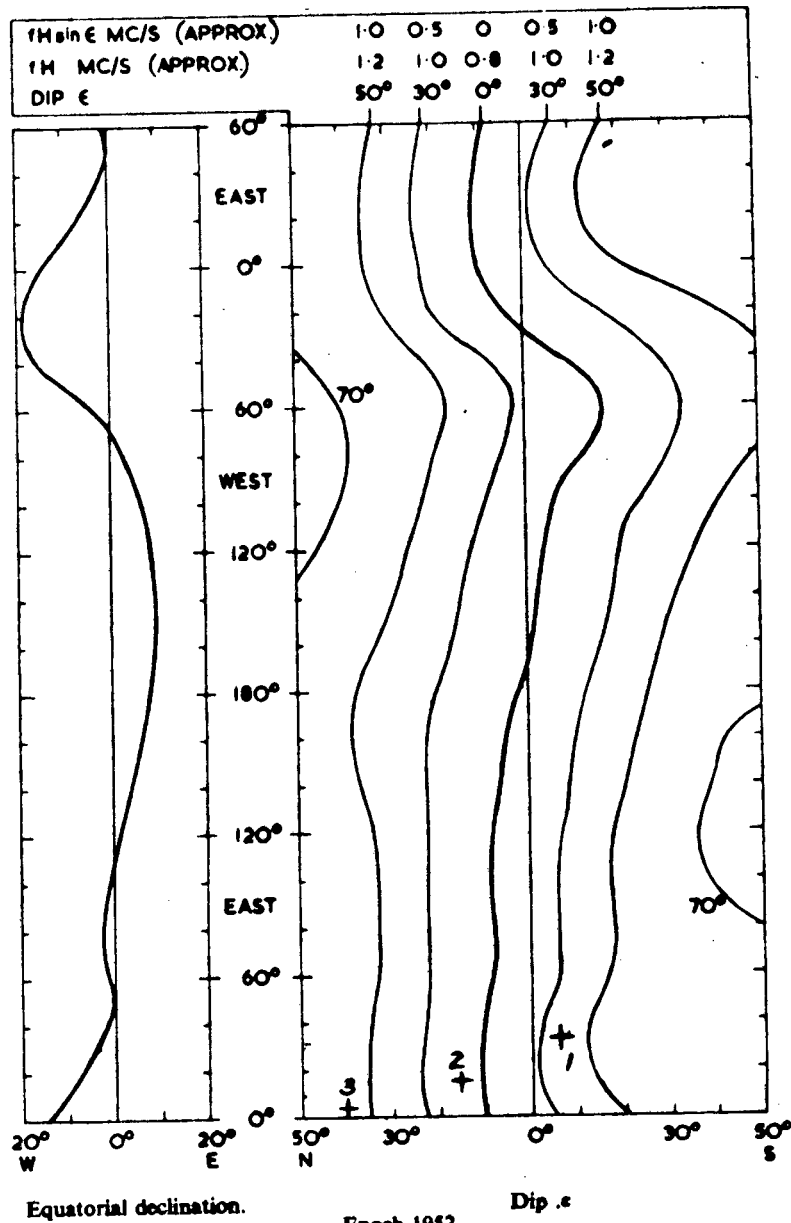
Control point.	Dip $\epsilon$	$f_H$ (Mc/s)	$f_a = f_H \cos \theta_a$	$f_b = f_H \cos \theta_b$	$f_0 = \frac{1}{2}(f_a + f_b)$	$f_1 \text{ Mc/s}$
3 (6 E, 40 N)	55	1.3	1.3 cos 63	1.3 cos 47	.74	.67
2 (16 E, 16 N)	12	.9	.9 cos 20	.9 cos 4	.87	.79
1 (26 E, 6 S)	38	1.1	1.1 cos 46	1.1 cos 30	.86	.78

Table T B. 6.2.9.0.1

If  $\theta$  is the angle between the direction of propagation and the direction of the earth's field then the gyro frequencies,  $f_a$  and  $f_b$ , for the up-going and down-coming waves respectively are given by:

$$f_a = f_H \cos \theta_a \text{ and } f_b = f_H \cos \theta_b$$

where  $\theta_a$  and  $\theta_b$  are the values of  $\theta$  for up-going and down-coming waves. In this case an angle of elevation of  $8^\circ$  is assumed, and the values of  $f_0$  taken as the average of  $f_a$  and  $f_b$  have been calculated and appear in the sixth column of the table above.



Equatorial declination.

Epoch 1952.

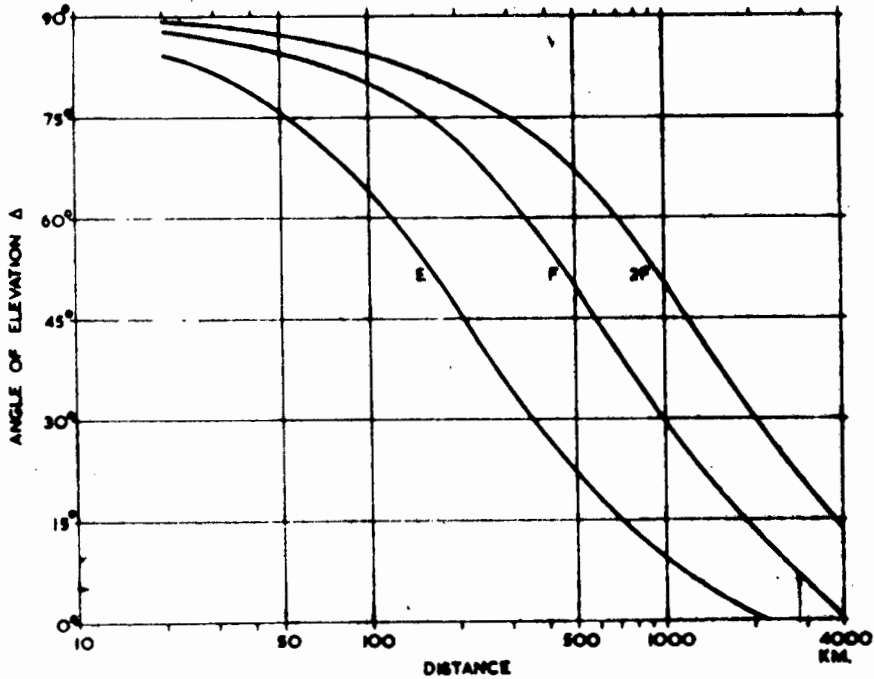
Note: for  $\epsilon < 30^\circ$  1° change in latitude alters  $\epsilon$  by 2°.

Dip and declination (variation) as a function of position in the equatorial zone.

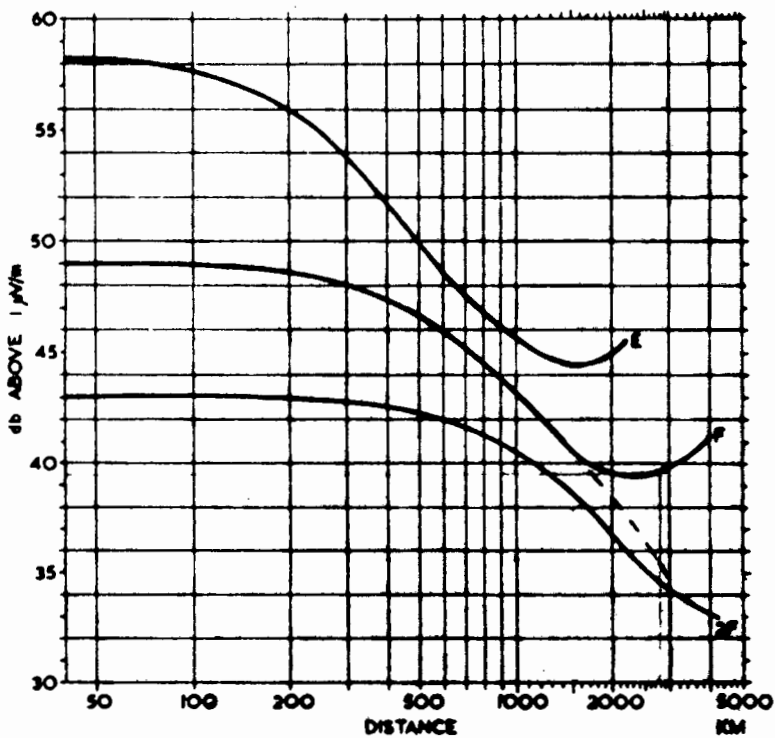
(102)

Reproduced from D.S.I.R. Report No 27.

Figure B 6.2.9.1.



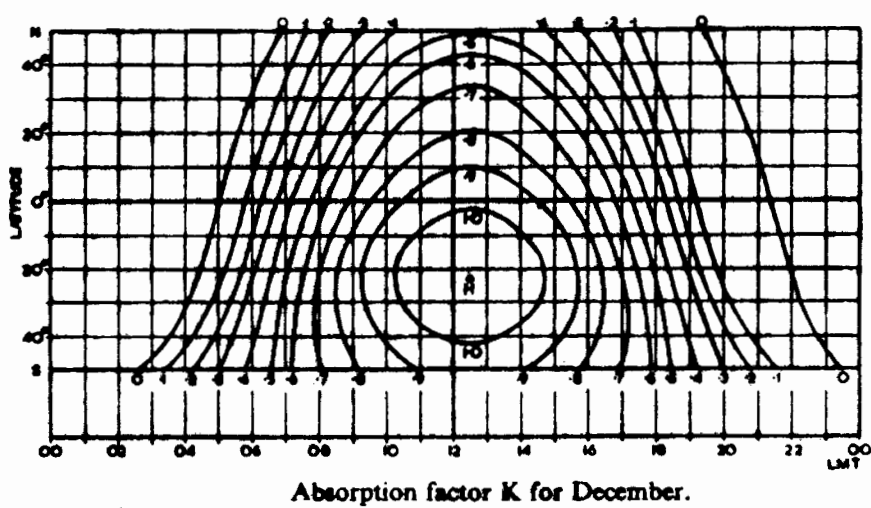
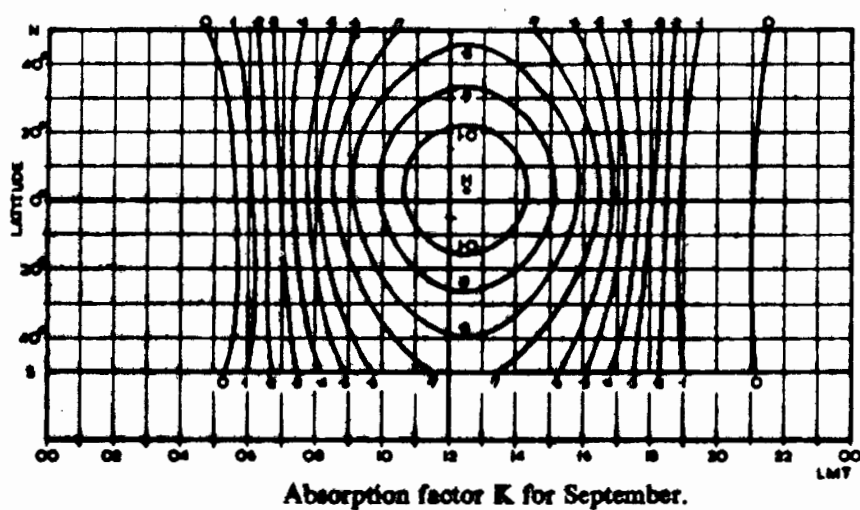
Angles of elevation for E, F, 2F modes.  
E at 105 km. F at 320 km.



Unabsorbed field strength for E reflection at 105 km, F  
at 320 km.

(102)  
Reproduced from D.S.I.R. Report No 27.

Figure B 6.2.9.2.



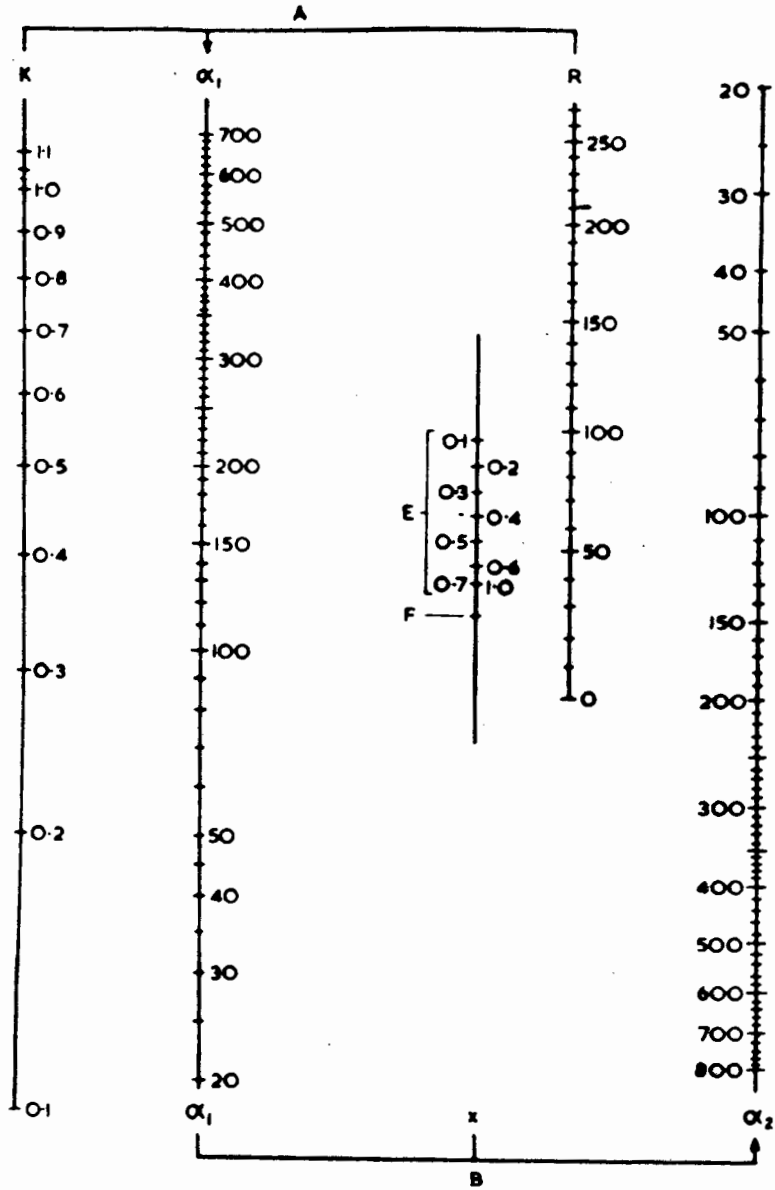
Absorption factor K plotted for September and December as a function of Latitude and Local Mean Time.

(102)  
Reproduced from D.S.I.R. Report No 27.

Figure B 6.2.9.3.

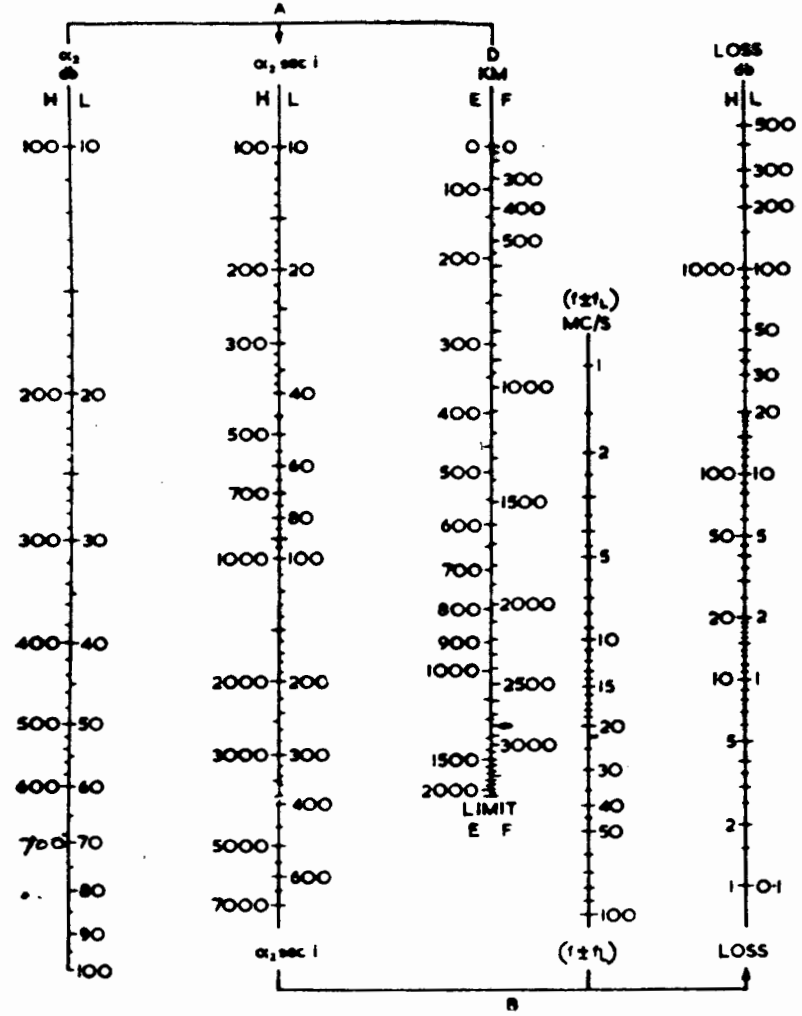


Figure B 6.2.9.4.



Nomogram for  $\alpha_1$  and  $\alpha_2$ .

Figure B 6.2.9.5.



Use H or L scales throughout

- A Line joining  $\alpha_1$  and D (use correct mode E or F) gives  $\alpha_1$  sec i.  
 B Line joining  $\alpha_1$  sec i and  $(f \pm f_L)$  gives absorption loss.

From this effective longitudinal component of the gyro frequency,  $f_1$ , for each control point, is calculated from the relation: (102)

$$f_1 = f_0 (1 - 2 f_0 / f)$$

where  $f$  is the wave frequency = 21.47 Mc/s in the present case.

$f_1$  appears in the 7th column in the above table. The information contained in figure FB.6.2.9.1 is for 1952 but it is assumed that it is applicable to the period under consideration, September 1956, with sufficient accuracy. Piggott<sup>(176)</sup> has supported this assumption.

#### B.6.2.9.1 The unabsorbed field (from empirical data).

Figure E.B.6.2.9.2 gives the unabsorbed field at distance 2800 km. for a single hop, using the F mode, as 39.5 db above 1  $\mu$  V/m. This assumes that the radiated power = 1 kilowatt fed into a short monopole touching a perfect earth and producing 300 mV/metre at 1 km. The curve allows -3 db for polarization loss and -1.6 db for fading, as recommended by the C.R.P.L.<sup>(101)</sup>. If it is assumed that the transmitter is radiating one kw from an antenna of H 4/4/1 design then, from the design data in figure FB.5.4.1, the field at 1 km for  $\Delta = 8^\circ$  and zero azimuth angle is 1550 mV/m. which represents a gain over the monopole of  $5.17 = 14.3$  db. Furthermore, as the radiated power from London is 100 kw, there is a power gain of 20 db and the unabsorbed field is therefore:

- (a) 1 kw radiated from earthed monopole, field at distance 2800 km., one F layer reflection, (from figure E.B.6.2.9.2) = 39.5 db above 1  $\mu$  V/m.
- (b) add directivity gain of transmitting antenna = + 14.3 db.
- (c) add power gain 100 kw/1 kw = + 20.0 db.
- (d) subtract  $20 \log 3$  to account for 3 hop path = - 9.5 db.

Therefore total unabsorbed field strength at Salisbury  
= 64.3 db above 1  $\mu$  V/m.

It would be expected that the same result would be obtained from the calculation from first principles by summing the results in section E.6.2.8 (c), (d), (e), (f), (g). This summation, in fact, comes to 60.3 db above 1  $\mu$  V/m.

Piggott<sup>(56)</sup> warns that the spatial attenuation will not follow the linear law because of a certain amount of focussing produced by the ionosphere at great distances. It will be observed from fig. FB.6.2.9.2 that the spatial attenuation for single F reflections decreases with increasing distance after about 2300 km. due to focussing. Had the curve continued to drop (as shown dotted) the field strength at 2800 km. would be 4 db lower than it is in reality. The difference between Piggott's method and the first principles method being 4 db the disparity is therefore completely accounted for by the focussing effect of the ionosphere at great distances.

B.6.2.9.2 The non-deviative absorption in the ionosphere (September 1956).

In figures ~~F~~B.6.2.9.3/4 the symbols used have the following meaning:-

$K$  = a constant depending on the variation of non-deviative absorption with position, local mean time, and season.

$f$  = the working frequency.

$f_L$  = the effective gyro frequency about the component of the earth's field which is parallel to the direction of propagation (referred to as  $f_1$  in the remainder of the text)

$i$  = angle of incidence at absorbing layer.

$R$  = solar activity factor expressed on the Wolf sunspot number scale ( $R = 210$  for September 1956)

At Control Point 1. ( $26^\circ \text{E}, 6^\circ \text{S}$ ).

1) From fig. ~~F~~B.6.2.9.3, for September noon,  $K = 1.05$

2) From fig. ~~F~~B.6.2.9.4, taking  $K = 1.05$ ,  $R = 210$  then:  
 $\alpha_1 = 580$  and  $\alpha_2 = 780$ .

3) From fig. ~~F~~B.6.2.9.5 using "H" scale and taking  $\alpha_2 = 780$ ,  
 $D_{km} = 2800$ ,  $f = 21.47$  and  $f_L = .72$  then:  
 $\alpha_2 \sec i = 4000$

and loss for ordinary ray ( $f + f_L = 22.25$ ) = 7.5 db.

Absorption for one hop at C.P.1 = 15.0 db.

At Control Point 2. ( $16^\circ \text{E}, 16^\circ \text{N}$ ).

Proceeding as for C.P.1.

1)  $K = 1.02$

2)  $\alpha_1 = 570$ ,  $\alpha_2 = 770$ .

3)  $\alpha_2 \sec i = 3950$

4)  $f + f_L = 22.26 \text{ Mc/s}$ , loss = 7.5 db.

Absorption for one hop at C.P. 2 = 15.0 db.

At Control Point 3. ( $6^\circ \text{E}, 40^\circ \text{N}$ ).

Proceeding as for C.P.1 and 2.

1)  $K = .83$

2)  $\alpha_1 = 460$ ,  $\alpha_2 = 600$ .

3)  $\alpha_2 \sec i = 3050$

4)  $f + f_1 = 22.14 \text{ Mc/s}$ , loss = 5.8 db.

Absorption for one hop = 11.6 db.

Piggott's method neglects deviative absorption for oblique incidence.

Total non-deviative absorption for the path: = 41.6 db.

**B.6.2.9.3 The deviative absorption in the ionosphere (September 1956).**

In 1948 Hacke<sup>(53)</sup> proposed a double parabola approximation to the Chapman<sup>(51)</sup> distribution described in section B.1.1 and also proposed a parabolic approximation for the product  $N v$  as a function of height. Using these approximations he produced graphs for normal incidence absorption which compared favourably with numerical results obtained by Pierce<sup>(54)</sup> and Jaeger<sup>(55)</sup>. Later the same year Hacke and Kelso<sup>(52)</sup> extended the theory to include deviative absorption at oblique incidence and fig. F B.6.2.9.6 provides an empirical method of calculating this. In the figure the meaning of the symbols is as follows:-

2 S is the total deviative absorption for the hop.

R = ratio of wave frequency to vertical-incidence critical frequency.

R<sup>1</sup> = ratio of wave frequency to oblique-incidence critical frequency.

H = scale height of the deviating region in the same units as c.

T = constant = 1.848.

K<sub>m</sub> =  $v_m / 2 c$ .

v<sub>m</sub> = collision frequency at the height of maximum density.

c = velocity of light in vacuo.

Frequency prediction charts<sup>(99)</sup> for September, 1956 at the equator give the optimum frequency for a hop length of 2800 km. as 29 Mc/s and for zero distance hop as 11.3 Mc/s, giving M.U.F's for the two cases as 34 Mc/s and 13.3 Mc/s respectively. (assuming "optimum frequency" = .85 "maximum usable frequency").

As the working frequency is 21.47 Mc/s

$$R = \frac{21.47}{13.3} = 1.62$$

$$R^1 = \frac{21.47}{34} = .63$$

H = 55 km. (approx) for F region according to Martyn<sup>(86)</sup>.

T = 1.848 as given by Hacke and Kelso<sup>(52)</sup>.

v<sub>m</sub> = 100 from figure F B.4.0.1.

$$c = 3 \times 10^5 \text{ km/sec.}$$

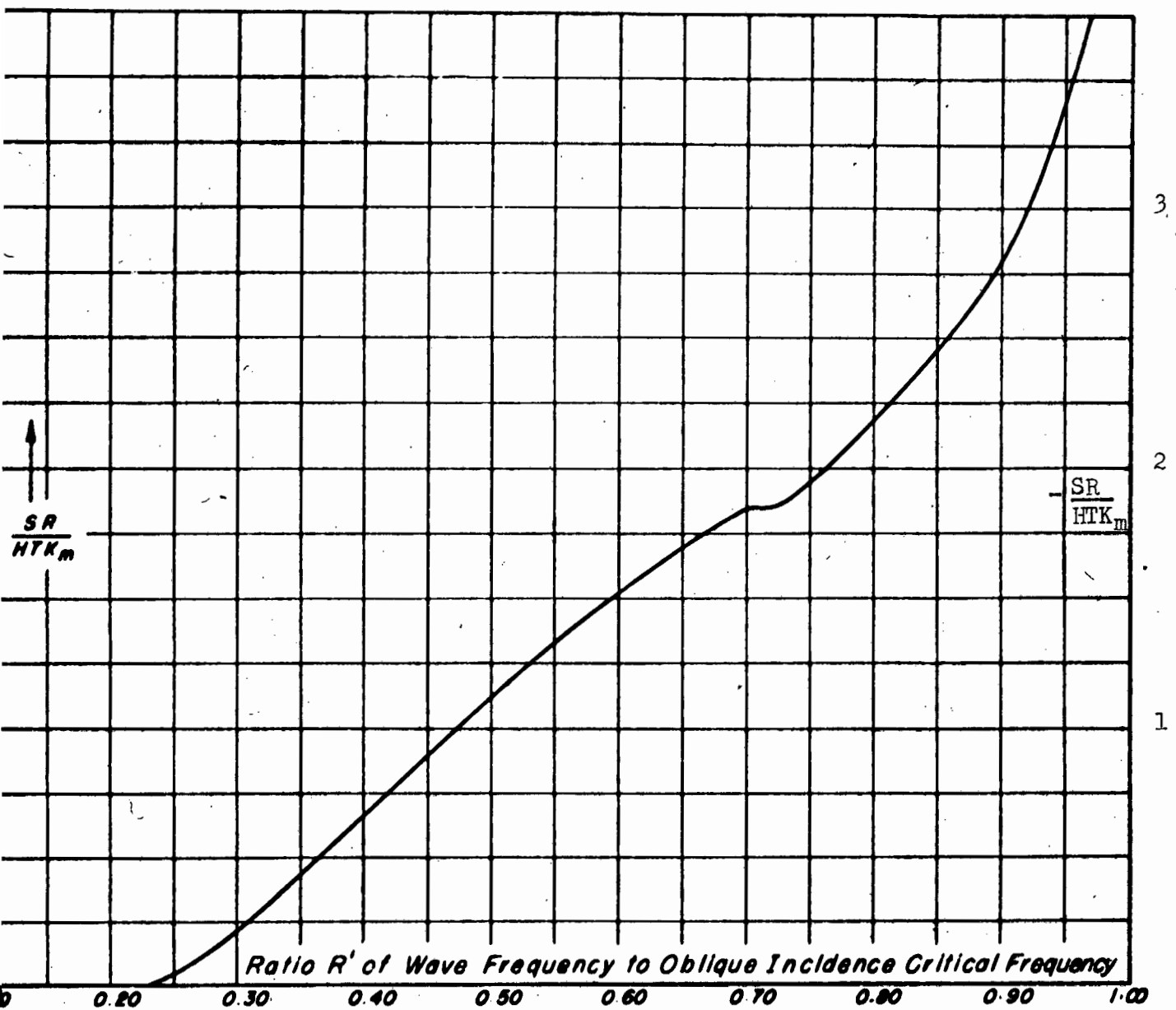
From fig. F B.6.2.9.6 :

$$\frac{S R}{H T K_m} = 1.7$$

Substituting the values given above:

$$S = .018 \text{ nepers} \\ = 0.154 \text{ db.}$$

The deviative absorption at the control points will be proportional to cos X for that point. The neon values are .30 db for C P.1; 0.29 db for C P.2; 0.28 for C P. 3.



-Absorption as a function of  $R'$ . The quantity plotted is  $-SR/(HTK_m)$ . See text for notation.

(52)

Reproduced from an article by Hacke and Kelso

Figure F 2.6.2.9.6.

Unfortunately the method of Hacke and Kelso<sup>(52)</sup>, used above for estimating the deviative absorption, relies, as does the "first principles" method, on the assumed values of the ionospheric model, fig. F B.4.0.1, and the value of  $v_m$  is controversial. Both the first-principles calculation and the method of Hacke and Kelso<sup>(52)</sup> produce a very small value for the deviative absorption and in this they are in line with an opinion expressed in letter Piggott to writer<sup>(178)</sup> that this type of absorption will be less than 1 db per hop for this path. As the model is based on information not available at the time Hacke and Kelso wrote their article<sup>(52)</sup> it is proposed to accept the deviative absorption figures calculated from first principles i.e. 0.25 nepers (2.2 db) for the whole path.

**B.6.2.9.4 Ground Reflection Losses.**

The C.R.P.L.<sup>(101)</sup> recommend that ground losses be taken as 4 db per reflection point. Since there are two reflection points on this path ground losses could be taken as 8 db. It would be more accurate to take the value of 8.6 db calculated in section B.6.1.

**B.6.2.9.5 Revised Estimate of field strength in Salisbury in September 1956.**

Unabsorbed field strength from section B.6.2.9.1 = + 64.3 db above 1  $\mu$  v/m.

Absorption in ionosphere (sections B.6.2.9.2/3 give 41.6 db for n.d. and 2.2 db for d.absorption) = - 43.8 db.

Ground reflection losses (section B.6.2.9.4) = - 8.6 db.

Therefore estimated field strength at receiver = 12 db above 1  $\mu$  v/m = 3.98  $\mu$  v/m; say 4  $\mu$  v/m.

**B.6.2.10.0 What variations in field strength and wave arrival angle are to be expected?**

The signal strength, the median value of which was calculated in section B.6.2.9, may vary due to the following causes:

**B.6.2.10.1 Interference between signal components which are out of phase.**

There will be a fairly rapid variation due to destructive interference between the ordinary ray and the weaker extraordinary ray. They are out of phase due to the difference in path which they follow and, if the gyro frequency is not fairly large, it will be seen from eqn. (B.6.2.4.2) that the difference in absorption between the two rays will not be great. The smaller the difference in signal strength between the two waves the greater will be the variation of the combined amplitude as they become, first, in phase and then, out of phase. However, for  $f_1$  greater than 0.5 Mc/s, the difference between the value of  $(\omega + \omega_1)^2$  and  $(\omega - \omega_1)^2$  is large enough for the interference between the two rays not to be unduly serious.

Similarly, interference occurs between energy arriving by a 3 hop mode and that arriving by 4 or more hops. This is particularly noticeable on antennas which are sensitive to both low- and high-angle radiation. A good receiving antenna must discriminate in favour of the dominant mode and thus reduce this interference (and distortion) to a negligible amount.

B.6.2.10.2 Wave frequency approaching the value of path M.U.F.

Deep fades will occur when the wave frequency approaches the M.U.F. of any of the control points. It should be borne in mind that the "layers" are varying in density all the time due to turbulence and electron drift in much the same way as the density of rain clouds is continually varying and the M.U.F. itself at a particular control point will vary continually by small amounts so that when the wave frequency is roughly the same as the M.U.F. the absorption varies from a value approaching infinity to a value equal to normal, according to whether the instantaneous value of the M.U.F. is just below or just above the frequency of the wave. When the wave frequency is less than 0.85 of the predicted M.U.F. for the entire path, fades of this kind should be very rare if they occur at all.

B.6.2.10.3.0 Fades due to abnormal ionospheric behaviour.

So much has been written about abnormalities such as Dellinger fades, magnetic storms, and enhanced auroral activity which accompany solar disturbances, that to discuss the various theories in detail would require much space. It should suffice to cover the effects, and theories about the causes, in brief outline:-

B.6.2.10.3.1.0 Solar disturbances.

Bright flares on the solar disc (sun spots) have been observed to have a profound effect on the electron number density of the ionosphere. The sun spot activity (and with it the value of the critical frequency) follows an 11 year cycle. In recent years maxima occurred in 1937 and 1948 and 1959.

B.6.2.10.3.1.1 Dellinger fades. ( Sudden Ionospheric Disturbances )

The main features of this effect were first ascertained by Mg<sup>103</sup> in 1930 and advanced by Dellinger<sup>(104,105)</sup> in 1935. Sudden and intense increase of ionization of the D region over the sun-lit hemisphere is found to occur simultaneously with the appearance of bright spots on the solar disc. The solar eruption must be large to cause an appreciable fade and most solar eruptions produce no noticeable change in D layer ionization. From fig. FB.4.0.1 it will be seen that in the D region (below 100 km.) the value of N<sub>v</sub> is large because the collisional frequency ( $\nu$ ) is large and this region accounts for nearly the whole of the non-deviative absorption (section B.6.2.4 makes this clear). If now N in this region were, for example, to be doubled due to a Sudden Ionospheric Disturbance (S.I.D), the estimated received signal strength, calculated in B.6.2.9, would be reduced by  $\frac{.60}{.74} \times 41.6 = 34$  db giving a signal 22-db below 1  $\mu$  v/metre instead of the normal 12 db above 1  $\mu$  v/metre. This fade would be so deep as virtually to destroy contact.

An H.F. radio fade of this sort usually lasts anything from a few minutes to a few hours. Long-wave transmissions on the other hand, employing, as they do, the earth and under-boundary of the ionosphere as a wave guide are, if anything, assisted by the greater conductivity of the D region due to S. I. D. as pointed out by Budden, Ratcliffe and Wilkes<sup>(106)</sup>. Bureau<sup>(107)</sup> has shown that quasi-periodic atmospheric noise, of low frequency and distant origin, will, for the same reason increase simultaneously with a Dellinger fade. The combined result is a doubly adverse effect on signal-to-noise ratio and causes even mild Dellinger fades to have a serious effect on the reliability of a circuit.

The smaller the zenith angle(X) the greater the Dellinger effect<sup>(107)</sup><sup>(108)</sup> and the path under consideration will therefore suffer considerably whenever a sudden large increase in D layer ionization occurs.

Modern ideas on the origin of ionization are summarised by Mitra<sup>(76)</sup> in stating that the solar radiation must be capable (a) of ionizing one or other of the atmospheric constituents in the 70-90 km. region and (b) of possessing a sufficiently small absorption coefficient to reach down to this region. It is almost certainly ultraviolet radiation emitted by those solar flares which appear on the disc, as distinct from those which appear on the limb of the sun ( i.e. in silhouette) and which, therefore, do not radiate much energy towards the earth. Very recently (1959) Bailey<sup>(109)</sup> has spoken of the great solar event of 23.2.56 in which the D region, even in the dark hemisphere, was heavily ionized due to the bombardment of gas molecules in the upper atmosphere by the sudden enhancement of solar cosmic rays( charged particles travelling at nearly the speed of light and having cosmic-ray energies) precipitated, due to the action of the earth's magnetic field, on both the light and the dark side of the earth. This effect, though, would only be expected in exceptional circumstances such as the great solar event referred to.

#### B.6.2.10.3.1.2 Prolonged Ionospheric Disturbance. (P.I.D).

The effect, described by such workers as Gilliland, Kirby, Smith and Reymer<sup>(110)</sup>, is similar, in cause and nature, to the S.I.D. but (a) it is usually not so severe, (b) it commences and ends more gradually and (c) it lasts a longer time. It is thought to be due to a great outpouring of ultra-violet radiation occurring over a long period, as distinct from the sudden burst of radiation causing the S.I.D. P.I.D.s occur most frequently when S.I.D.'s are numerous.

#### B.6.2.10.3.1.3 Ionospheric Storms.

Ionospheric storms and magnetic storms are closely linked as they stem from the same cause. Appleton and Piggott<sup>(111)</sup> maintain that ionospheric storms are the main cause of the general variability of the F<sub>2</sub> layer.



Bartels<sup>(112-116)</sup> has drawn attention to the fact that the incidence of magnetic and ionospheric storms follows sunspot activity very closely; Chapman<sup>(117)</sup> has shown that each year there is a maximum at each of the equinoxes; Chree<sup>(118)</sup> and Bartels<sup>(119)</sup> have pointed out that maxima have a tendency to recur every 27 days, i.e. after each rotation of the sun; there is a marked correlation between magnetic and ionospheric storms and increased auroral activity<sup>(120-125)</sup>. On magnetically quiet days the auroral activity is confined to belts  $20^{\circ} - 25^{\circ}$  from the poles but during storm periods the auroral activity spreads to lower latitudes.

About 20 hours after a large solar disc flare, the ionospheric storm begins with a "turbulent phase" in which F layer ionization is particularly affected in high altitudes and the intensity of the earth's magnetic field fluctuates. After about 2 hours the turbulent phase gives way to the "moderate phase" in which the virtual heights of  $F_1$  and  $F_2$  are abnormally high, the critical frequencies of  $F_1$  and  $F_2$  are abnormally low, and the deviative absorption increases. These effects are usually negligible at the magnetic equator and increase with increasing latitude. The "recovery phase", which follows the "moderate phase", is the period (usually several days) in which the ionosphere gradually returns to normal.

Several theories have been offered to explain the cause of ionospheric storms and related auroral effects but as indicated by Parker<sup>(126)</sup> recently (1959), it would appear that this is a much more complex phenomenon than any of our present theoretical models dream of because, to quote him, "our present ignorance of co-operative plasma dynamical processes".

Some of the more famous theories are summarized below:

(a) The Birkeland-Störmer theory: The sun occasionally sends out a beam of charged particles (of one sign only) which constitutes a current stream which, on approaching the earth, is deflected by the earth's magnetic field to form a ring of current circling the earth high above the equator with the charged particles spiralling along the magnetic lines of force to precipitate (and cause ionization of air particles) in the auroral zones. The theory was developed by Birkeland<sup>(127)</sup> and Störmer<sup>(128,129)</sup> but Schuster<sup>(130)</sup> has objected (i) that to produce the observed effects the number density of the particles would have to be very great and (ii) if the particles were all of one sign they would disperse, due to mutual repulsion, long before the stream reached earth. Therefore Lindemann<sup>(131)</sup> has proposed that the stream is composed of positive and negative particles, electrically balanced. This idea has been incorporated in:

(b) The Chapman - Ferraro Theory. (132,133,134).

A Lindemann<sup>(131)</sup> stream is considered to leave the sun at about  $10^8$  cm/sec. Since the wave front has a radius of about 5000 earth radii, it resembles the approach of a conducting plane. Interaction with the earth's field will cause currents to flow in a thin sheet of the wave front which will strengthen the earth's field on the side near the stream. This is characteristic of the first phase of the magnetic storm. The physical force exerted on that part of the stream carrying the current, due to interaction between the current and the earth's field, distorts the stream, forming a "shadow" or "hollow" on the far side of the earth. Also the electrons and ions in the stream are deflected in opposite directions by the earth's field and form positively and negatively charged layers on the opposite sides of the hollow. Ions will tend to flow across the gap under the influence of the electric field thus formed, producing a ring current round the earth with consequent world wide depression of H for the duration of the main phase of the storm. The theory has been extended by Martyn<sup>(135)</sup> as follows:-

(c) Martyn's extension <sup>(135)</sup> to Chapman-Ferraro theory.

This theory proposes that during the main phase of the storm the neutral stream completely encloses the hollow ("forbidden") space surrounding the earth, the ring current thus formed girdling the earth at a radius of about 5.5 earth radii. This is the elevation of those lines in the earth's field which cut the earth's surface at about  $25^\circ$  from the poles. Charged particles ejected from the ring current region spiral down the lines of force bombarding the earth's atmosphere in the auroral zone. This theory was acclaimed by Mitra<sup>(76)</sup> as the one which would survive but Parker<sup>(126)</sup> has objected to it on the grounds that Martyn's model predicts the wrong direction of drift of the aurora.

(d) Ultra-violet light theory.

Hulburt and Maris<sup>(136-138)</sup> have proposed that the charged particles come not from the sun but from the ionization of the upper-atmosphere by sudden bursts of ultra-violet radiation during a solar flare. Grave objections to the theory have been raised by Chapman<sup>(139)</sup> and make it unacceptable.

(e) Solar wind theory.

The most modern theory asserts that, because ionospheric storms, magnetic storms, and enhanced auroral activity commence about a day (and sometimes 2 days) after increased solar activity is visually observed, the storms are due to something emanating from the sun which travels at about 1000-2000 km/sec. Chamberlain,<sup>(140)</sup> in observing auroral protons, has suggested that solar corpuscular emission is the basic cause of storms. Biermann<sup>(141)</sup> has observed that gas, presumably ionized hydrogen, is streaming outwards from the sun in all directions at all times with a normal velocity of about 500 km/sec and density of 100 atoms/cm<sup>3</sup> at the orbit of the earth.

During a solar flare the velocity is said to increase in the direction normal to the disc to about 1500 km/sec or more and the density at the Earth's orbit to  $10^4$  or  $10^5 / \text{cm}^3$ . Parker<sup>(126)</sup> maintains that the presence of this "solar wind" streaming continuously past the earth is responsible for the daily auroral activity which occurs on magnetically quiet days and the increase in velocity and density of the solar wind produces the storms during enhanced solar activity.

Parker<sup>(142)</sup> points out that this tenuous, ionized, gas is a conducting medium and will push its way into the geomagnetic field until the magnetic pressure ( $B^2/8\pi$ ) becomes comparable with the impact pressure ( $N m U^2$ )

where  $B$  = flux density

$N$  = number density of ions, each of mass =  $m$ ,

$U$  = the wind velocity. There will not be a smooth interface where  $B^2/8\pi = N m U^2$  just as the surface of water is unstable to a strong blast of air.

The value of  $B$  at a point above the geomagnetic equator, distant  $r$  from the centre of the earth, taking  $B$  at the equator as 0.35 gauss, will be given by:

$$B = 0.35 (r_0 / r)^3$$

where  $r_0$  = radius of earth = 6370 km.

Then the maximum depth of penetration of the solar wind is to where  $r = R_1$  where

$$R_1 = r_0 (0.35/8\pi N m U^2)^{1/6} \quad (\text{approx}).$$

The everyday solar wind thus penetrates to about  $4.8 r_0$  (about 25,000 km. above the earth's surface) and the enhanced solar wind ( $U = 1500 \text{ km.}$ ,  $N = 10^4/\text{cm}^3$ ) to  $1.53 r_0$  (about 3500 km. above the surface).

The geomagnetic line of force which crosses the equatorial plane at a distance  $R_1$  comes down to earth an angular distance  $\theta$  from the poles such that :

$$\sin \theta = (r_0 / R_1)^{1/2}$$

The everyday solar wind therefore disturbs the lines of force originating within  $27^\circ$  of the pole. Here it is noted that Chapman<sup>(117)</sup> reports that within  $25^\circ$  of the magnetic pole there is unceasing agitation of the earth's field. As the protons and electrons are constrained to move along the geomagnetic lines of force the everyday auroral activity they produce is confined to an area within about  $25^\circ$  from the poles. The greater the solar activity the further will the solar wind penetrate the earth's field resulting in occasional auroral activity to within  $20^\circ$  of the magnetic equator.

Since observations indicate that the electrons and protons producing auroral displays are moving with velocities greater than their transit time from the sun would indicate, Chamberlain<sup>(140)</sup> concludes that they are accelerated near the Earth. Storey<sup>(143)</sup> indicates that the region occupied by the geomagnetic field beyond the outer fringe of the ionosphere is, like the solar wind, occupied by ionized hydrogen, producing a region of good conductivity around the Earth. Parker<sup>(126)</sup> admits that it is not easy to see how the necessary acceleration occurs but suggests that when the 1000 to 2000 km./sec solar wind collides with the ionized hydrogen ( of density about  $10^3/\text{cm}^3$  according to Storey<sup>(143)</sup>) enmeshed in the geomagnetic field, the interaction of the inter-penetrating, electrically neutral, streams of plasma<sup>(144)</sup> behaves rather like the inter-action of an electron stream and an ion cloud as described by Pierce<sup>(145)</sup> and the kinetic energy of the ions is converted into plasma oscillations of the electrons. Thus the initial 20 k eV energy of a 2000 km./sec hydrogen ion imparts 20 k eV energy to the electrons.

It is probable that this is nearer than the previous theories to the real explanation of the observed ionospheric and magnetic storms and auroral activity.

Because of the prevalence of ionospheric storms over polar regions, transmission paths which pass over or near the auroral belt are usually unsatisfactory. It is not expected that ionospheric storms will affect the circuit presently under consideration except at the northern control point (C P 3).

#### B.6.2.10.3.2 Sporadic E ionization ( $E_s$ ).

Patches of abnormally high ionization sometimes intrude into the body of the E layer. In equatorial regions  $E_s$  is weak but present throughout daylight hours, with a maximum at noon, according to Trenbelen and Cox<sup>(146)</sup>. In temperate and sub-tropical latitudes  $E_s$  occurs most frequently in the early morning and evening.  $E_s$  occurs more in local summer than at any other time of the year<sup>(146, 147)</sup> and it is not related to the sunspot cycle.

The origin of sporadic E is not yet known. It is known that meteors, rushing into the atmosphere produce trails of ionization and it has been suggested that this ionization causes the sporadic E patches. The findings of the following lend support to this theory: (a) Appleton and Naismith<sup>(147)</sup>, (b) Skellett<sup>(148)</sup>, (c) Schafer and Goodall<sup>(149)</sup>, (d) Mitra and Ghosh<sup>(150)</sup>, and (e) Bhar<sup>(151)</sup>. However, Pincus<sup>(152, 153)</sup> in analysing the data on meteor trail echoes recorded at the Central Radio Propagation Laboratory, National Bureau of Standards, U.S.A., maintains that  $E_s$  is not related to meteorite activity.

Workers such as Appleton and Ratcliffe<sup>(154)</sup> Bhar and Syam<sup>(155)</sup> and Appleton and Naismith<sup>(156)</sup> have suggested an association between thunder activity and  $E_s$  and a link between  $E_s$  and the isobaric situation

near the ground has been reported by Martyn and Pulley<sup>(157)</sup> and Ranzi<sup>(158)</sup>. A thundercloud charged positively above and negatively below contains an intense electric field capable, according to Schonland<sup>(159)</sup> of imparting  $5 \times 10^9$  e V to an electron within the cloud moving upwards. When a spark occurs which destroys the retarding field a spray of "run away" electrons moves upward with great speed and, if this is high enough, will increase the ionization of patches in the E region. Alternatively, as the electric moments of thunderclouds have been found to be  $3 \times 10^{16}$  e.s.u. in South Africa by Schonland,  $2 \times 10^{17}$  e.s.u. in England by Appleton, Watson, Watt and Herd<sup>(159)</sup> and are probably about  $5 \times 10^{18}$  e.s.u. in tropical regions,<sup>(76)</sup> the electric field at 80 km. will be about 6 volts/cm. Here the pressure is about  $10^{-2}$  m.m. and the mean free path about 3.2 cm. Mitra<sup>(76)</sup> has suggested that electrons will therefore gain 19 e V of energy at this level which is just sufficient to ionize the oxygen and nitrogen molecules present. Some electrons with free paths greater than the mean will acquire greater energy than that indicated above and could have moved in a weaker field to acquire the necessary minimum ionizing energy. A third possibility was advanced by Healey<sup>(160)</sup> in which it was claimed that the electromagnetic radiation produced by a lightning stroke could be sufficiently intense to produce  $E_s$  ionization in a patch of nearly E region if the collisional frequency is less than  $10^6$  per sec. From fig. FR.4.0.1 it will be seen that  $v$  is normally less than  $10^6$  above 85 km.

In polar regions it is probable that  $E_s$  is due to the same agency as causes the auroral effects discussed in section B.6.2.10.3.1.3.

The effect of  $E_s$  ionization on the London-Salisbury circuit will be that if the wave frequency ( $f$ ) approaches the oblique angle critical frequency of  $E_s$  the wave will suffer considerable bending in the E region and the deviative absorption will increase. If  $f$  is greater than the oblique angle critical frequency of a patch of  $E_s$  then if the wave encounters the  $E_s$  patch on the upward journey, the geometry of the path will be affected by the premature reflection that occurs and if the wave encounters an  $E_s$  patch on the last downward journey the re-radiated wave could be effectively prevented from reaching Salisbury receiving station. In both cases severe fades in received strength would occur but it will seldom be the case that the oblique angle critical frequency of  $E_s$  will be greater than the transmission frequency.

#### B.6.2.10.3.3 Winds and tides in the ionosphere.

Noctilucent clouds, situated between heights 72 and 92 km., and produced either by ice crystal formation or by cosmic dust, have been observed by such workers as Paton<sup>(161)</sup> and Manning, Villard and Peterson<sup>(162)</sup>.

The clouds were found to move from N.N.E with velocities between 44 and 55 m/sec. Meteor trails at 80-120 km. indicate high wind velocities at these heights according to Hey<sup>(163)</sup>. Echo patterns of E<sub>s</sub> patches have given the impression of travelling from one sounding station to the next<sup>(164),(165)</sup> at velocities of about 100 m/sec.

Workers such as Munro<sup>(166)</sup>, Beynen<sup>(167)</sup>, and Meek<sup>(165)</sup> have also reported motion in the F region of an oscillatory nature resembling lunar and solar tides and on these Martyn<sup>(168-171)</sup> has based his electro-dynamical theory in which he shows that at latitudes above about 35° there is an upward ionic drift and at latitudes below 35° there is a downward ionic drift. Because of its dependance on tide motion, the vertical drift velocity suffers a semi-diurnal and seasonal variation. This gives rise to Martyn's equilibrium equation quoted in section B. 3.3. and in this way he seeks to explain some of the complicated perturbations in the F<sub>2</sub> region and also the small departures of the E and F<sub>1</sub> layers from the simple Chapman region.

B. 6.2.10.4 Scatter Phenomena.

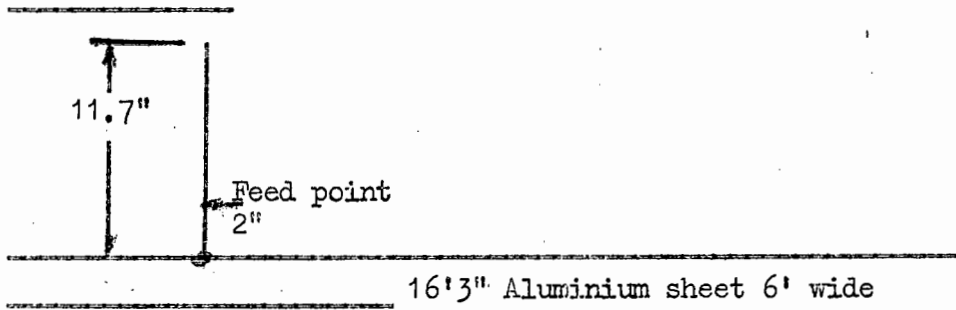
Osborne<sup>(205)</sup> has reported that in tropical regions the incidence of scattering is sufficiently common at certain epochs to be a significant feature of the normal diurnal propagation pattern. Piggott<sup>(102)</sup> indicates that sufficient data has not yet been collected to define the phenomenon adequately and, as it can cause large changes in the sky-wave field strength, its omission constitutes a serious limitation on the accuracy possible at the present time.

- - - - -

APPENDIX G.

RESULTS OF SCALE MODEL TESTS.

1) Single  $\frac{A}{A}$  rod.



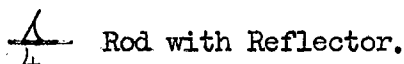
Using 0-50 uA (1000 Ohms) meter as receiving detector.  
 Freq. 243 Mc/s. Transmitter drive  $I_g$  final 1.9 mA,  $I_a$  final 170 mA.

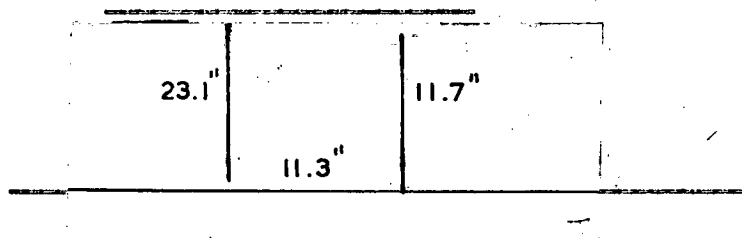
Mains voltage 218 Volts.

Vertical Angle. (Degrees).	Reading. (uA.)	Signal Voltage(From calibration curve.)(mV)
0	3.0	56
1	3.0	56
2	3.2	57
3	3.5	60
4	4.0	65
5	4.5	68
6	5.0	72
7	5.0	72
8	5.5	76
9	5.5	76
10	5.5	76
11	5.5	76
12	5.5	76
13	5.0	72
14	5.0	72
15	4.7	70
16	4.5	68
17	4.8	71
18	5.0	72
19	4.5	68
20	4.5	68
21	4.3	67
22	4.0	65
23	3.5	60
24	3.0	56
25	2.5	50
26	2.0	45
27	2.0	45
28	2.0	45
29	2.2	48
30	2.5	50
31	3.0	56
32	3.1	57
33	3.1	57
34	3.2	57
35	3.5	60
36	3.3	59
37	3.0	56
38	3.0	56
39	2.5	50
40	2.0	45
41	1.8	44
42	1.7	42
43	1.5	40
44	1.5	40
45	1.6	41

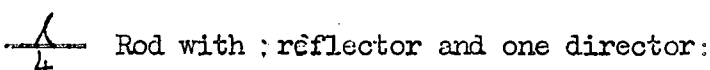
APPENDIX C.(continued).

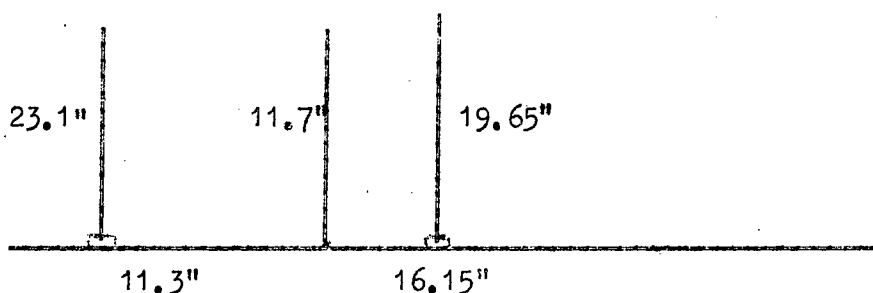
<u>Vertical Angle</u> (Degrees)	<u>Reading.</u> (uA)	<u>Signal voltage.</u> (From calibration curve) (mV)
46	1.5	40
50	.5	22
60	0.	0
70	.5	22
80	0.	0

- 2)  Rod with Reflector.

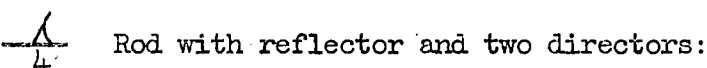


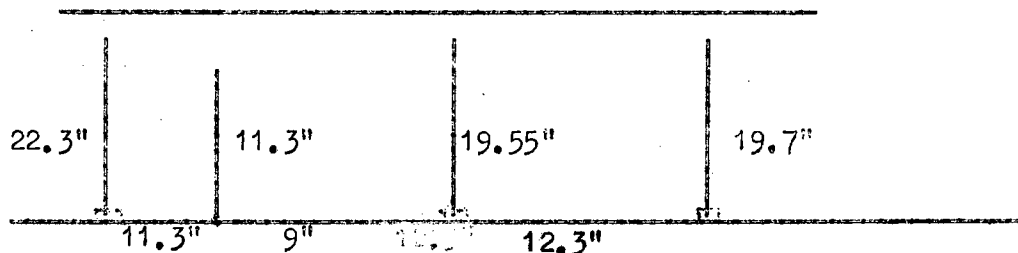
Using 0-100 uA (1000 Ohms) meter as a receiving detector.  
 Freq: 242 Mc/s Drive  $I_g = 1.9$  uA  $I_a = 170$  uA.  
 Mains voltage = 218 volts.  
 Signal measures at  $8\frac{1}{2}^\circ = 11.5$  uA.  
 Corresponding voltage from calibration curve = 103 mV.

- 3)  Rod with : reflector and one director:



Conditions same as in (2) above.  
 Signal measured at  $8\frac{1}{2}^\circ = 25$  uA. Corresponding voltage from cali-  
 bration curve = 148 mV.

- 4)  Rod with reflector and two directors:



Using 0-100 uA meter (1000 Ohms)  
 Freq. 243 Mc/s Drive  $I_g = 1.85$ ,  $I_a = 173$  mA.

<u>Vertical Angle.</u> (Degrees)	<u>Reading</u> (uA)	<u>Corresponding</u> <u>Voltage (mV).</u>
0	26	150
1	27	152
2	27	152
3	27	152
4	27	152
5	27.5	152.5
6	28	155
7	29	156
8	30	157



APPENDIX G. (continued)

<u>Vertical Angle.</u> <u>(Degrees)</u>	<u>Reading.</u> <u>(uA)</u>	<u>Corresponding</u> <u>Voltage. (mV)</u>
9	31	160
10	31.5	162
11	31	160
12	30	157
13	29	156
14	28	155
15	27	152
16	25.5	148
17	23	142
18	22	140
19	21	136
20	19	132
21	17	125
22	14	115
23	10	95
25	7	77
32	10	95
39	5	66
43	2	45
45-90	0	0

- 5)  $\frac{A}{4}$  Rod with Reflector and 3 directors:

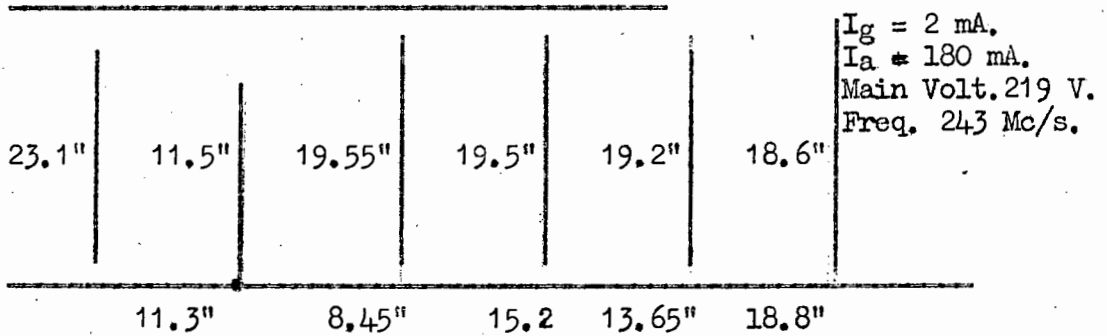
22.3"	11.5"	19.5"	19.43"	19.15"
	11.3"	9.1"	12.8"	15.1"

$I_g = 1.85 \text{ mA.}$   
 $I_a = 175 \text{ mA.}$   
 Mains voltage 217 V.  
 Frequency 243 Mc/s.

<u>Vertical Angle.</u> <u>(Degrees)</u>	<u>Reading:</u> <u>(uA)</u>	<u>Corresponding</u> <u>Voltage (mV)</u>
0	26	150
1	28.5	155
2	29	156
3	30	157
4	31	160
5	33.5	165
6	35	168
7	37	172
8	38.5	174
9	39.5	176
10	40	177
11	39	175
12	38	173
13	36	170
14	34.5	166
15	32.5	162
16	31.5	161
17	30	157
18	27	152
19	24.5	146
20	22	140
21	19.5	133
22	10.5	124
23	12.5	110
24	9	90
25	7	77
26	4	60
27	3	50
28	3	50
29	3	50
30	2	45
30-90°	0	0.

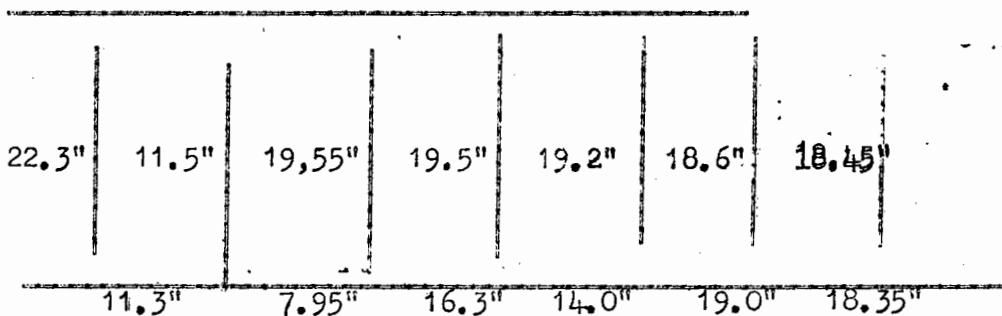
APPENDIX C.(continued)

- 6) 4 Rod met Reflector and 4 directors.



<u>Vertical Angle.</u> (Degrees)	<u>Reading:</u> ( $\mu\text{A}$ )	<u>Signal Voltage</u> ( From calibration curve) (mV)
0	38	173
1	44	184
2	45	186
3	47	188
4	49.5	194
5	52	198
6	55	205
7	56.5	206
8	58	208
9	59	210
10	59	210
11	57	207
12	55	205
13	53	200
14	51.5	197
15	48.5	192
16	45	186
17	42.5	182
18	40.5	178
19	37	172
20	34	166
21	30	158
22	26	150
23	22	148
24	18	129
25	14	115
30	9	95
35	6	79
40	2	45
45-90	0	0

- 7) 4 Rod with Reflector and 5 directors.



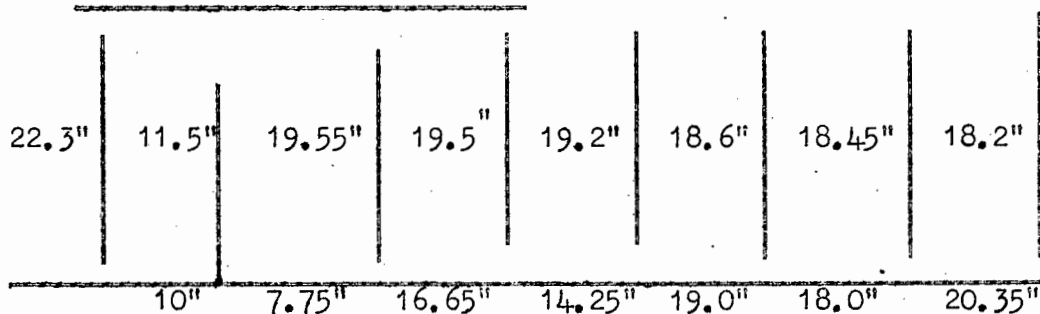
$I_g = 2 \text{ mA.}$   $I_a = 180 \text{ mA.}$  Main Voltage 219 Volts. Freq. 243 Mc/s.

<u>Vertical Angle:</u> (Degrees)	<u>Reading:</u> ( $\mu\text{A}$ )	<u>Signal Voltage.</u> (From Calibration Curve) (mV)
0	42	187
1	47.5	190
2	51	196
3	53	200

APPENDIX C.(continued)

<u>Vertical Angle</u> (Degrees)	<u>Reading:</u> (uA)	<u>Signal Voltage</u> (From calibration Curve) (mV)
4	56	205
5	59.5	211
6	61.5	214
7	63	217
8	64	219
9	64	219
10	62.5	216
11	60	212
12	57	207
13	54	202
14	51	196
15	48.5	192
16	45	186
17	42	181
18	39	175
19	35	167
20	30	158
25	9.5	97
30	4	65
35	3	56
40	2	45
45	1.5	40
50-90	0	0

8) 4 RoA with 6 directors:



$I_g = 2$  mA.  $I_a = 180$  mA. Mains voltage 219 Volts. Freq. 24s Mc/s.

<u>Vertical Angle.</u> (Degrees)	<u>Reading:</u> (uA)	<u>Signal Voltage.</u> (From Calibration Curve) (mV)
0	50	195
1	55	203
2	60	212
3	62	216
4	64	218
5	67	223
6	69	227
7	70	229
8	70.5	230
9	70	229
10	68	226
11	64	218
12	60	212
13	56	205
14	52	198
15	47	188
16	43	182
17	39	175
18	34	166
19	28	153
20	23	142
25	4	65
30	7	85

APPENDIX C.(continued)

<u>Vertical Angle.</u> (Degrees)	<u>Reading:</u> (uA)	<u>Signal Voltage.</u> (From Calibration Curve) (mV).
35	6	80
40	2	45
45	4	65
50	0	0
60	0	0
70	0	0
80	0	0
90	0	0

- 9) Comparison of three arrays erected in quick succession to ensure fair comparison.

Transmitter drive 2.0 mA.

Transmitter final anode current 180 mA.

- a) Four-director array : Max. at  $9.5^\circ$ , 56 uA ( 205 mV).
- b) Five-director array : Max. at  $8.5^\circ$ , 64 uA ( 218 mV).
- c) Six-director array : Max. at  $8^\circ$  , 70,5uA( 230 mV)

- 10) Horizontal Polar diagram for  $\frac{1}{4}$  rod with reflector and 4 directors:

<u>Angle from</u> <u>line of array:</u>	<u>Reading</u> (uA)	<u>Corresponding</u> <u>Voltage:</u>
$0^\circ$	40	177
$3^\circ$ , $357^\circ$	48	192
$5^\circ$ , $355^\circ$	40	177
$10^\circ$ , $350^\circ$	46	188
$15^\circ$ , $345^\circ$	36	170
$20^\circ$ , $340^\circ$	15	120
$25^\circ$ , $335^\circ$	18	128
$30^\circ$ , $330^\circ$	12	108
$35^\circ$ , $325^\circ$	4	65
$40^\circ - 180^\circ$ , $180^\circ - 320^\circ$	0	0.

-----

APPENDIX D.

RESULTS OF TESTS AT 21.47 Mc/s.

4 Rod with reflector and 4 directors.

21'9 $\frac{3}{8}$ " (.475 $\lambda$ )	10'10" (.237 $\lambda$ )	18'5 $\frac{1}{4}$ " (.402 $\lambda$ )	18'4 $\frac{5}{8}$ " (.401 $\lambda$ )	18'1 $\frac{3}{8}$ " (.395 $\lambda$ )	17'6 $\frac{1}{2}$ " (.383 $\lambda$ )
10'7 $\frac{7}{8}$ " (.233 $\lambda$ )	7'11 $\frac{5}{8}$ " (.174 $\lambda$ )	14'4" (.313 $\lambda$ )	12'10 $\frac{3}{8}$ " (.354 $\lambda$ )	17'8 $\frac{3}{4}$ " (.387 $\lambda$ )	

Earth mat 12 $\frac{1}{2}$  SWG copper at 12" centres; crossconnections at 2' centres. Total length 55 yards.

Array was used as a receiving aerial; signal fed to an Eddystone receiver via 50 Ohm co-axial feeder. Meter in A V C to give measure of signal strength. Sender - Marconi signal generator working from battery. Located 65 yards from receiver and capable of being raised 250 ft.

1) VERTICAL POLAR DIAGRAM:

<u>Vertical Angle.</u> <u>Degrees.</u>	<u>Reading:</u> <u>uA.</u>	<u>Signal.</u> <u>uV.</u>
1.75	52	310
1.9	44	255
2.3	41	235
2.9	40	228
3.5	39	221
4.4	40	228
5.0	41	235
5.8	42	242
6.6	43	248
7.6	43	248
8.2	44	255
9.0	45	260
9.9	45	260
10.7	45	260
11.4	44	258
12.1	44	258
12.9	43	248
13.0	40	228
20.0	36	205
23.7	29	160
27.6	21	108
34.7	14	62
37.0	9	30
40.0	8	0
45	8	0

2) HORIZONTAL POLAR DIAGRAM.

Signal generator moved round on a radius of 50 ft.

<u>Horizontal Angle</u> <u>(Degrees)</u>	<u>Reading.</u> <u>(uA)</u>	<u>Signal.</u> <u>(uV)</u>
0	55	345
1	54.5	339
2	55	345
3	52.5	316
4	52	312
5	52	312

APPENDIX D. (continued)

<u>Horizontal Angle.</u> (Degrees)	<u>Reading.</u> (uA)	<u>Signal.</u> (uV)
6	52	312
7	50.5	300
8	50	295
9	50	295
10	47	272
12	46	266
14	45	260
16	45	260
18	40	228
20	37	210
25	29	138
30	22	114
35	14.5	65
40	9	30
45	8+	15
50-180	8	0

3) Comparison between this array and a single ~~rod~~ <sup>rod.</sup>

<u>Vertical Angle</u> (Degrees)	<u>Reading (uA)</u>		<u>Signal. (uV)</u>		<u>Gain</u> db.
	<u>Array</u>	<u>Rod.</u>	<u>Array:</u>	<u>Rod.</u>	
1.75	54	21	335	108	9.8
9.00	47	15.5	270	70	11.7

4) Frequency Tolerance.

Signal Generator resting on ground.

	<u>Frequency (Mc/s.)</u>	<u>Reading. (uA)</u>	<u>Signal. (uV)</u>
	18.47	20	102
	19.47	35	196
	20.47	48	280
(Desing Freq)	21.47	55	345
	22.47	50	295
	22.97	37	210
	23.47	11	45
	23.97	8	10

APPENDIX E.

Frequency run on array of two, six-director arrays.

<u>Frequency</u> <u>Mc/s.</u>	<u>Set reading.</u>	<u>db above 1 <math>\mu</math>V</u> <u>from calibration curve.</u>
22.6	20	22.5
22.3	21	23.8
22	22	25
21.47	23.5	27
21	23.5	27
20.5	22	25
20	18	20
19	12	11

- - - - -

**A COMPACT SHORT-WAVE  
RECEIVING ANTENNA FOR USE IN  
HIGH-NOISE AREAS**

**SUMMARY FOLDER**





Ph.D. Thesis

UNIVERSITY OF CAPE TOWN

A COMPACT SHORT-WAVE RECEIVING ANTENNA

FOR USE IN HIGH-NOISE AREAS.

by

L.M. Muggleton.

CONTENTS OF SUMMARY FOLDER.

SUMMARY

THESIS CONTENTS PAGE

LIST OF DIAGRAMS AND PHOTOGRAPHS

POWER DENSITY DIAGRAM, DOUBLE 6-DIRECTOR ARRAY

PHOTOGRAPH, DOUBLE 6-DIRECTOR ARRAY

---

# A COMPACT SHORT-WAVE RECEIVING ANTENNA FOR USE IN HIGH-NOISE AREAS.

## SUMMARY

An antenna has been developed with a signal-to-noise performance that is better than that of a typical Rhombic antenna during local thunder storms. Although the design is of general application to the reception, in high-noise areas, of long distance transmissions, this work deals in particular with the London-Salisbury circuit, at September noon, 1956, on 21.47 Mc/s.

A basis of theoretical comparison between the performances of different antennas has been proposed. It relies on the technique of replacing a thunder storm by an "equivalent radio transmitter" set up on the frequency to which the receiver is tuned and for which the antenna is designed.

A V.H.F. scale model has been used to produce an optimum design for the proposed antenna which is an end-fire array of parasitic elements. The polar diagrams and signal-to-noise performance of the proposed design are derived for several different types of earth mat. The method used for these derivations is substantiated by correlation with practical sampling measurements.

A specification for the final configuration is given and its applicability is indicated by applying the design to the problem of improving the expected performance on the London-Salisbury transmissions from September to December, 1960.

Appendices A to E deal with the following :-

- Appendix A Antenna Theory, which includes the derivation of gain and polar equations for the  $\lambda/2$  dipole,  $\lambda/4$  monopole, the Rhombic antenna, and the mechanism of reflections.
  - Appendix B The Incoming Signal, which includes a summary of modern propagation theory, and details the calculations made in respect of the field strength and wave arrival angle of the incoming signal.
  - Appendix C The results of Scale Model tests.
  - Appendix D The results of tests at 21.47 Mc/s.
  - Appendix E A frequency run on an array of two, six-director designs.
-

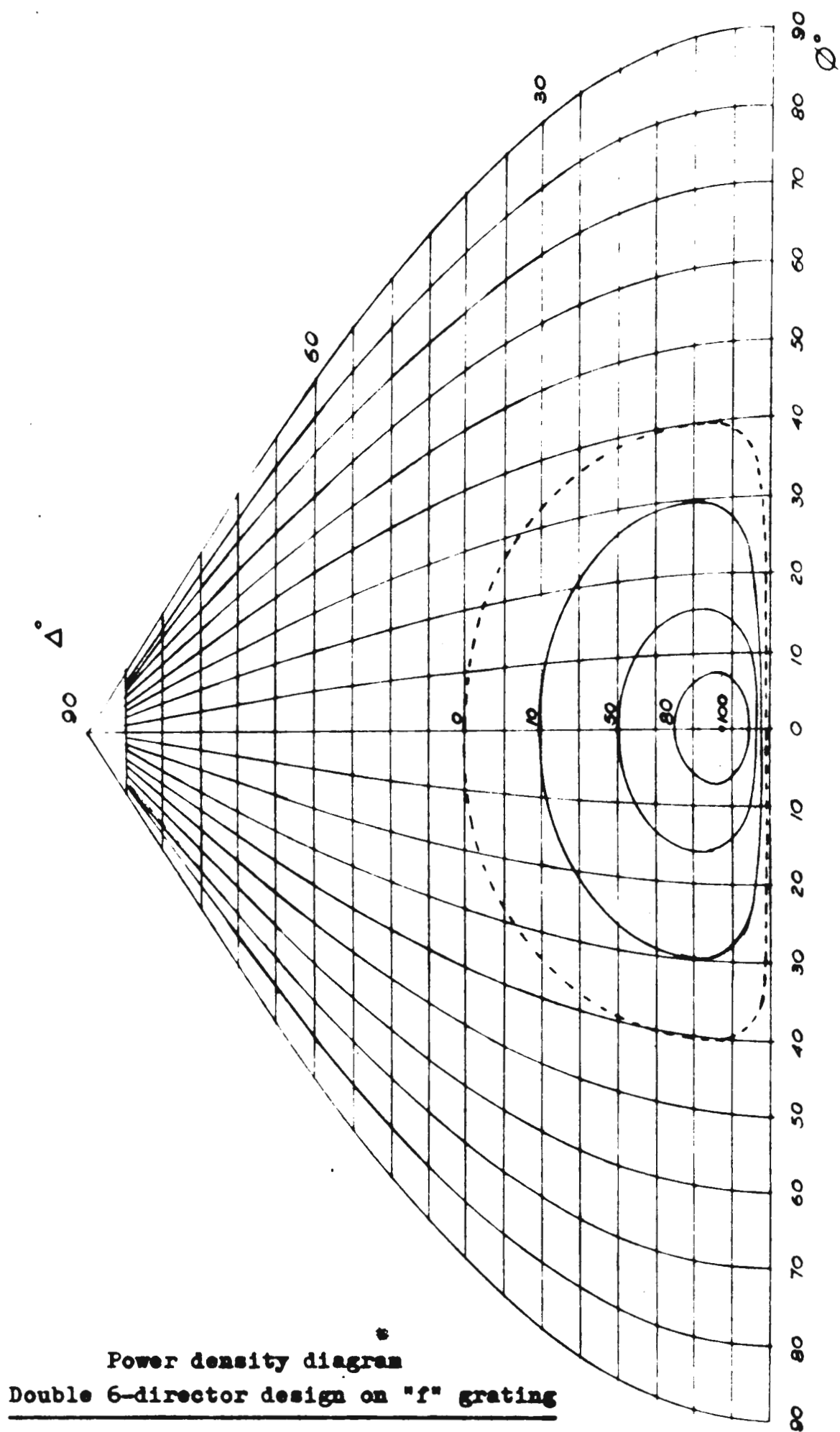
## C O N T E N T S.

List of diagrams and photographs.	F 1. to F 2.
Summary.	
Chapter 1 : Introduction to the problem and the proposed approach.	1.1.
Chapter 2 : The incoming signal from London at noon, September 1956, on 21.47 Mc/s.	2.1. to 2.10.
Chapter 3 : The minimum antenna gain necessary.	3.1. to 3.3.
Chapter 4 : Noise in short-wave circuits in tropical countries.	4.1. to 4.16.
Chapter 5 : Disadvantages of the Rhombic Receiving Antenna.	5.1. to 5.2.
Chapter 6 : The search for an improved design.	6.0. to 6.18.
Chapter 7 : The parasitic Antenna.	7.0. to 7.14.
Chapter 8 : The V.H.F. Scale Model.	8.0. to 8.22.
Chapter 9 : The 4-director test array at 21.47 Mc/s.	9.0. to 9.12.
Chapter 10 : The 6-director design.	10.0. to 10.29.
Chapter 11 : Indication of applicability.	11.1. to 11.6.
Acknowledgements.	
Bibliography.	1.to 8.
Appendix A : Antenna Theory.	A.0 to A.24.
Appendix B : The incoming signal : London - Salisbury	B.1 to B 50.
Appendix C : Results of scale model tests.	C.1. to C.6.
Appendix D : Results of tests at 21.47 Mc/s.	D.1. to D.2.
Appendix E : Frequency run on two, 6-director arrays.	E.1.

---

LIST OF DIAGRAMS AND PHOTOGRAPHS.

<u>Number</u>	<u>Subject</u>	<u>Page</u>
F 4.4.1.1.	Calculated noise field strength variation with $\Delta$ .	4.9.
F 4.4.1.2.	Noise Map, C.C.I.R. Noise predictions.	4.10.
F 4.4.3.1.	Power density diagram, Rhombic Antenna.	4.13.
F 4.4.3.2.	Power density diagram, Koomans H/4/4/1 Array.	4.14.
F 4.4.3.3.	Comparison curves, antenna signal-to-noise performance.	4.15.
F 6.3.3.1./2.	Polar diagrams, vertical monopole on perfect grnd.	6.4.
F 6.3.4.0.1.	Polar diagrams, $\lambda/2$ dipole grnd. of finite $\sigma$ .	6.7.
F 6.3.4.1.3.	Derived vertical polar diagrams at 21.47 Mc/s for various types of ground plane.	6.18.
F 7.1.1.	$Z_{12}$ and $\phi$ for $\lambda/2$ radiators in terms of spacing.	7.2.
F 7.1.2.	Reactance of parasitic radiators.	7.4.
F 7.2.1.	Yagi antenna, transmission line analogy.	7.5.
F 7.2.2.-4.	Spector's curves, phase vel., Q factor, beam width.	7.7.
F 7.3.2./1.	Reid's optimum "a" value for Yagi antennas.	7.11.
F 8.2.1.	Circuit diagram, V.H.F. transmitter.	8.2.
F 8.3.0.1.	Model antenna, micrometer screw adjustment of rod.	8.4.
F 8.3.0.2.	Model antenna, matching arrangements.	8.5.
F 8.3.1.1.	Shelkunoff's curves for $K_1$ and $R_1$ for cyl. dipole.	8.6.
F 8.3.3.1.	Model antenna, receiving loop.	8.8.
F 8.3.3.2.	Model antenna, control cabin.	8.9.
F 8.3.3.3.	Model antenna, method of measuring polar diagram.	8.10.
F 8.3.3.4.	Model antenna, calib. curve for VHF signal detect.	8.12.
F 8.3.5.1.1.	Polar diagrams, measured and expected, $\lambda/4$ monopole.	8.16.
F 8.3.5.2.1.	Array designs for one to six directors.	8.18.
F 8.3.5.3.1.1.	Measured and derived polar diagrams for 4-director and 6-director arrays.	8.21.
F 9.2.1.	Full-scale design, antenna matching unit.	9.2.
F 9.2.2.	Ditto.	9.3.
F 9.4.1.	Test transmitter for 21.47Mc/s experiments.	9.5.
F 9.4.2.	Measurement of vert. polar diag. at 21.47 Mc/s.	9.6.
F 9.5.1.	Calibration curve, Eddystone Receiver.	9.7.
F 9.6.1.	The 4-director Test array.	9.8.
F 9.6.2.	Polar diagram ( vertical plane) for Test array.	9.9.
F 9.6.3.	Polar diagram ( horizontal plane) for Test array.	9.10.
F 6.3.4.1.3.	Derived polar diagrams at 21.47 Mc/s.	10.4(a)
F 8.3.5.3.1.1.	Measured and derived polar diag.s for 4-director and 6-director arrays. (Repeated for convenience).	10.4(b)
F 10.2.1.1.	6-director array, derived polar diag.s for various ground planes.	10.5.
F 10.3.2.1.	Antenna performance curves, 6-dir. vs Rhombic and Koomans signal-to-noise performance.	10.12.
F 10.3.3.1.	Calibration curve, CR 88 Receiver.	10.14.
F 10.3.4.1.	R.F. Input vs. A.F. Output for large range of sig.	10.17.
F 10.4.0.1.	The double 6-director design ( photograph).	10.18.
F 10.4.1.1.	The phasing of the double 6-director antenna.	10.20.
F 10.5.1.1.1.	Practical details of parasitic elements.	10.24.
F 10.5.1.1.2.	Base of parasitic element.	10.25.
F 10.5.1.1.3.	Dismantled view of element.	10.26.
F 10.5.1.2.1.	Base design of driven element.	10.27.
F 10.5.1.2.2.	The driven element ( photograph).	10.28.
F 11.4.1.	Amplitude distribution for fading S.W. signals.	11.3.
F 11.5.1.1.	Power density diagram, 6-director design.	11.6.
A 7.0.1.	Mechanism of reflection at a discontinuity.	A.5.
A 8.1.	Field components of a doublet.	A.10.
A 10.1.1.	Element of area on a spherical surface.	A.13.
A 11.1.1.	Radiation from a $\lambda/2$ dipole.	A.14.
A 11.3.0.1.	Image antennas.	A.16.
A 11.4.0.1.	The phasing of two antennas.	A.17.
A 11.4.0.2./3.	Height factors for negative and positive images.	A.18.
A 12.0.1.	Straight wire carrying travelling wave.	A.19.
A 12.1.1.	Elements of the Rhombic Antenna.	A.20.
A 12.1.2.	Radiation from Rhombic Antenna.	A.21.



Power density diagram  
Double 6-director design on "f" grating



DOUBLE 6-DIRECTOR ARRAY AT HATCLIFFE, SALISBURY.